

5-1-2008

The effect of image size on the color appearance of image reproductions

Mahdi Nezamabadi

Follow this and additional works at: <http://scholarworks.rit.edu/theses>

Recommended Citation

Nezamabadi, Mahdi, "The effect of image size on the color appearance of image reproductions" (2008). Thesis. Rochester Institute of Technology. Accessed from

The Effect of Image Size on the Color Appearance of Image
Reproductions

by

Mahdi Nezamabadi

B.S., Amirkabir University of Technology
M.S., Amirkabir University of Technology

A dissertation submitted in partial fulfillment of the
requirements for the degree of Doctor of Philosophy
in the Chester F. Carlson Center for Imaging Science

Rochester Institute of Technology

May 20, 2008

Signature of the Author _____

Accepted by _____
Coordinator, Ph.D. Degree Program _____ Date _____

CHESTER F. CARLSON CENTER FOR IMAGING SCIENCE
ROCHESTER INSTITUTE OF TECHNOLOGY
ROCHESTER, NEW YORK

CERTIFICATE OF APPROVAL

Ph.D. DEGREE DISSERTATION

The Ph.D. Degree Dissertation of Mahdi Nezamabadi
has been examined and approved by the
dissertation committee as satisfactory for the
dissertation required for the
Ph.D. degree in Imaging Science

Dr. Roy S. Berns, dissertation Advisor

Dr. Mark D. Fairchild

Dr. Garrett M. Johnson

Dr. Tina Lent

Date

DISSERTATION RELEASE PERMISSION
ROCHESTER INSTITUTE OF TECHNOLOGY
CHESTER F. CARLSON CENTER FOR IMAGING SCIENCE

Title of Dissertation:

The Effect of Image Size on the Color Appearance of Image Reproductions

I, Mahdi Nezamabadi, hereby grant permission to Wallace Memorial Library of R.I.T. to reproduce my thesis in whole or in part. Any reproduction will not be for commercial use or profit.

Signature _____ Date _____

The Effect of Image Size on the Color Appearance of Image Reproductions

by

Mahdi Nezamabadi

Submitted to the
Chester F. Carlson Center for Imaging Science
in partial fulfillment of the requirements
for the Doctor of Philosophy Degree
at the Rochester Institute of Technology

Abstract

Original and reproduced art are usually viewed under quite different viewing conditions. One of the interesting differences in viewing condition is size difference. The main focus of this research was investigation of the effect of image size on color perception of rendered images. This research had several goals. The first goal was to develop an experimental paradigm for measuring the effect of image size on color appearance. The second goal was to identify the most affected image attributes for changes of image size. The final goal was to design and evaluate algorithms to compensate for the change of visual angle (size). To achieve the first goal, an exploratory experiment was performed using a colorimetrically characterized digital projector and LCD. The projector and LCD were light emitting devices and in this sense were similar soft-copy media. The physical sizes of the reproduced images on the LCD and projector screen could be very different. Additionally, one could benefit from flexibility of soft-copy reproduction devices such as real-time image rendering, which is essential for adjustment experiments. The capability of the experimental paradigm in revealing the change of appearance for a change of visual angle (size) was demonstrated by conducting a paired-comparison experiment. Through contrast matching experiments, achromatic and chromatic contrast and mean luminance of an image were identified as the most affected attributes for changes of

image size. Measurement of the extent and trend of changes for each attribute were measured using matching experiments. Proper algorithms to compensate for the image size effect were design and evaluated. The correction algorithms were tested versus traditional colorimetric image rendering using a paired-comparison technique. The paired-comparison results confirmed superiority of the algorithms over the traditional colorimetric image rendering for the size effect compensation.

ACKNOWLEDGEMENT

I would like to thank Dr. Roy S. Berns, my advisor, for his support and guidance.

I would like to thank Dr. Mark D. Fairchild, Dr. Ethan D. Montag, and Dr. Garrett M. Johnson for sharing their knowledge and constructive comments.

I would like to thank Dr. Tina Lent for accepting to chair my thesis committee.

I would like to thank Dr. David R. Wyble and Dr. Mitchell R. Rosen for their teaching and friendship.

My special thanks go to Lawrence A. Taplin who helped me a lot in this research.

I would like to thank Mrs. Val Hemink and Mrs. Colleen Desimone for their kindness and help during the last six years.

I would like to thank my colleagues at Munsell Color Science and Center for Imaging Science at RIT for their friendship, encouragement, and participation in my experiments.

I would like to thank Dr. Jalal Haddad and Dr. Farahnaz Mohammadi for their continuous support.

I would like to thank my wife and son for their love and patience.

I gratefully acknowledge the financial support of the National Gallery of Art in Washington, D.C., The museum of Modern Art in New York City, Institute of Museum and Library Services, Andrew W. Mellon Foundation, and Rochester Institute of Technology.

DEDICATION

This dissertation is dedicated to my parents, Mohammad and Eshrat Nezamabadi, my dearest wife, Mahnaz Mohammadi, and my lovely son, Navid.

Table of Contents

1 INTRODUCTION.....	1
1.1 Color Perception.....	3
1.2 Illumination.....	3
1.3 Materials	10
1.4 Human Visual System	11
1.5 Important Attributes of Visual Sensations.....	13
1.6 Color Appearance Phenomena	14
1.6.1 Simultaneous Contrast	15
1.6.2 Crispness	15
1.6.3 Spreading.....	16
1.6.4 Bezold-Brücke Hue Shift	17
1.6.5 Helmholtz-Kohlrausch Effect.....	18
1.6.6 Hunt Effect	19
1.6.7 Stevens Effect.....	19
1.6.8 Bartleson-Breneman Effect	21
1.6.9 Size Effect on the Color of Uniform Patches.....	22
1.7 Color Appearance Models	25
1.8 Image Appearance Model.....	28
1.9 IPT Color Space	32
1.10 Device-Independent Color Imaging System.....	33
1.11 Tone Reproduction	37
1.12 Single-scale Tone reproduction.....	41
1.13 Gamut Mapping.....	43
1.14 Visual Experiment Techniques	44
1.14.1 Threshold and Matching Experiments	45
1.14.2 Scaling Experiments	47
1.15 Conclusions	50
2 EXPLORATORY EXPERIMENT.....	56
2.1 Display Colorimetry	58
2.2 LCD Colorimetric Characterization	68
2.3 DLP Colorimetric Characterization.....	71
2.4 An Exploratory Visual Experiment	73
2.5 Image Processing.....	75
2.6 Results and Discussion	85
2.7 Conclusions	89

6	SUMMARY AND CONCLUSIONS.....	254
6.1	Scientific Contributions	267
6.2	Directions for Future Study.....	268
7	REFERENCES.....	269

List of Figures

Figure 1-1. Kruithof's curves present relationship between correlated color temperature, intensity, and the "pleasant" quality of an illumination source [Weintraub 2000].....	6
Figure 1-2. Color temperature of illuminant chosen to appear "neither warm nor cool". Solid lines shows mean setting for a group of eight observers and dotted lines present boundaries for ± 1 group standard deviation. The horizontal dashed line shows the overall mean choice [Scuello 2004B]......	8
Figure 1-3. An example demonstrating simultaneous contrast phenomenon. The gray patches on the gray background, (a), are physically identical to those on the white and black background, (b) [Fairchild 2005].	13
Figure 1-4. A: An example of crispening. The pairs of gray patches are physically identical on all three backgrounds. B: A demonstration of the difference between simultaneous contrast and spreading. The gray areas are physically identical but appear different depending on their spatial scale with respect to the red background [Fairchild 2005]......	16
Figure 1-5. Example data illustrating the Bezold-Brücke hue shift. Plot shows the wavelength shift required to maintain hue constant across a 10X reduction in luminance [Fairchild 2005].	17
Figure 1-6. Contours of constant brightness-to-luminance ratio illustrating the Helmholtz-Kohlrausch effect (adopted from Fairchild [2005])......	18
Figure 1-7. Changes in lightness contrast as a function of adapting luminance according to the Stevens effect [Fairchild 2005].....	20
Figure 1-8. Change in lightness contrast as a function of surround relative luminance according to the results of Bartleson and Breneman [Fairchild 2005].	22
Figure 1-9. Relationship between small and room size colors in CIELAB for lightness, chroma, and hue. [Xiao 2003].	24
Figure 1-10. Relationship between two samples with sizes of ($\sim 22^\circ$ indicated as 4) and ($\sim 50^\circ$ indicated as 6) for lightness, chroma, and hue. [Xiao 2004].....	25
Figure 1-11. The iCAM flow chart for simple stimulus (or a single pixel) [Fairchild 2002].....	30
Figure 1-12. The iCAM flow chart for spatially complex stimuli [Fairchild 2002].	31
Figure 1-13. A flowchart of conceptual process of device-independent color imaging [Fairchild 2005].....	35
Figure 1-14. Flowchart showing the International Color Consortium (ICC) approach for color management.....	36
Figure 1-15. Ideal tone reproduction process [Devlin 2002].....	38
Figure 1-16. A: The curve marked 'Actual system' shows the characteristic of a commercially successful system used for the production of color reflection prints. B: The curve marked as 'Actual film' shows the characteristic of a commercially successful reversal film used for the reproduction of color transparencies intended for projection [Hunt 1995].	42
Figure 1-17. An observer looking at a painting in a gallery. The same kites positioned at different locations of image are perceived to have different colors.....	52
Figure 1-18. The same observer is looking at a reproduction of the painting in a different illumination and viewing conditions from the gallery conditions.	53
Figure 1-19. Flowchart showing the modified version of the color management system.....	55
Figure 2-1. Normalized look-up tables, LUTs, for red, green, blue and white channels of the DLP projector.	61

<i>Figure 2-2. Histogram of ΔE_{00} color difference for the LCD colorimetric characterization between measured and estimated data for all 168 samples.....</i>	70
<i>Figure 2-3. Histogram of ΔE_{00} color difference for the projector colorimetric characterization between measured and estimated data for all 1000 samples.....</i>	72
<i>Figure 2-4. Arrangement of scene and equipment in the psychophysical experiment.....</i>	74
<i>Figure 2-5. General flowchart of test and reference image preparation.....</i>	75
<i>Figure 2-6. Histogram of lightness L^*, and chroma C^*_{ab} of colorimetric image.....</i>	76
<i>Figure 2-7. Transformation functions and corresponding histograms of linear rescaling of lightness with minimum lightness of $L^*=10, 15$, and 25.....</i>	79
<i>Figure 2-8. Transformation function and corresponding histogram of linear rescaling of chroma with minimum value of $C^*_{ab}=1$ and 5.....</i>	80
<i>Figure 2-9. Transformation functions and corresponding histograms of sigmoidal rescaling of lightness, L^*, with mean value of $L^*=40$ and standard deviation values of 30 and 50.....</i>	82
<i>Figure 2-10. Transformation function and corresponding histogram for the power law processing ($\gamma = 1.3$).</i>	83
<i>Figure 2-11. Interval scales and corresponding 95% confidence limits based on visual experiment.....</i>	87
<i>Figure 2-12. Bottom row: Colorimetric image of the painting (image1) and the linearly rescaled image for an increase in CIELAB lightness (image 6). Top: A three times larger version of the colorimetric image shown in the bottom left.</i>	91
<i>Figure 3-1. A Gabor image, H_g, was generated by multiplication of a sine-wave image and a radially symmetric Gaussian pattern.</i>	95
<i>Figure 3-2. An example of a Gabor pattern and its CIE L^* along the horizontal axis of symmetry (the axis of symmetry is shown by the solid black line in the image).....</i>	98
<i>Figure 3-3. Examples of Gabor patterns rendered for LCD display for $1X, 2/3X, 1/3X$, and $1/6X$ magnification levels. The Gabor patterns had minimum and maximum CIELAB lightness of 25 and 75, respectively.....</i>	99
<i>Figure 3-4. Gabor pattern rendered for DLP display with minimum and maximum CIELAB lightness of 25 and 75, respectively.....</i>	100
<i>Figure 3-5. Examples of histograms of CIEL*; A: original test pattern with CIEL* in the range of [25, 75] displayed on screen; B: Mean luminance was increased for 8 units of CIEL*; C: Five units of CIEL* was added to maximum and subtracted from the minimum lightness values to increase image contrast; D: combined effect of B and C.....</i>	101
<i>Figure 3-6. Observers could adjust mean luminance of test patterns by the outer knob of the dialer. In this example mean luminance was increased for 8 units.....</i>	104
<i>Figure 3-7. Adjusted Gabor pattern on the DLP display corresponding to the lightness-mapping curve, CD, shown in Figure 3-6.</i>	105
<i>Figure 3-8. Observers could adjust contrast of test patterns by the inner knob of the dialer. In this example 5 units of CIEL* was added to the maximum and subtracted from the minimum lightness values to increase image contrast.....</i>	107
<i>Figure 3-9. Adjusted Gabor pattern on the DLP display corresponding to the lightness-mapping curve, CD, shown in Figure 3-8.</i>	107
<i>Figure 3-10. An example of simultaneous adjustment of luminance and contrast. The contrast and mean luminance of the image on DLP display were increased.</i>	108
<i>Figure 3-11. Adjusted Gabor pattern on the DLP display corresponding to the lightness-mapping curve, CD, shown in Figure 3-10.</i>	109

<i>Figure 3-12. Arrangement of scene and equipment in the psychophysical experiment.</i>	110
<i>Figure 3-13. Mean of adjusted contrast of images projected on screen versus the size of images displayed on the LCD for three contrast levels. Solid blue line with circle: contrast = 0.97; solid red line with square: contrast = 0.84; solid magenta line with diamond: contrast = 0.3. Error bars present 95% confidence limits for mean values.</i>	112
<i>Figure 3-14. Mean of adjusted contrast of images displayed on the DLP projector versus contrast of the same images on the LCD display for different image sizes. Line with circle: size = 43.6 mm; line with square: size = 87.2 mm; line with triangle: size = 174.3 mm; line with diamond: size = 261.5 mm.</i>	113
<i>Figure 3-15. Mean luminance levels of adjusted images projected on screen versus size of images displayed on the LCD for three contrast levels. Solid blue line with circle is for contrast level of 0.97; solid red lines with square and solid magenta line with diamond are for contrasts of 0.84 and 0.3, respectively. The mean luminance level of 42.65 cd/m², corresponding to the CIE L* 50, is also shown by the dashed line. Error bars represent the 95% confidence intervals.</i>	114
<i>Figure 3-16. Top: the low contrast Gabor pattern, image numbered 10 from Table 1-1, rendered for DLP display; Bottom left: same pattern colorimetrically rendered for LCD; Bottom right: same pattern colorimetrically rendered and also adjusted for the effect of 1/3X magnification for the LCD display.</i>	116
<i>Figure 3-17. Frequency responses of octave filters centered at 0.5, 2, and 8 cycle-per-degree, (cpd), of visual angle. For frequencies lower than 0.5 cpd and higher than 8 cpd, filter responses were set to unity for filters centered at 0.5 and 8 cpd, respectively.</i>	121
<i>Figure 3-18. Octave cosine log filter centered at 2 cycles-per-deg. Response of the filter is plotted along its horizontal axis of symmetry.</i>	122
<i>Figure 3-19. Images corresponding to low, medium, and high frequency octave cosine log filters centered at 0.5, 2, and 8 (cpd), respectively. Top: low frequency; Bottom: high frequency; Middle: medium frequency. The center of each image corresponded to the zero frequency. Frequency range was [-35, 35] along the diagonal axis of each image.</i>	123
<i>Figure 3-20. White noise pattern and histogram of its pixel values.</i>	124
<i>Figure 3-21. Flowchart of stimuli generation.</i>	126
<i>Figure 3-22. Examples of the noise images. Top, middle, and bottom rows corresponded to images numbered 2, 5, and 7 in Table 3-3, respectively. Left, middle, and right columns corresponded to low, medium, and high frequency, respectively.</i>	128
<i>Figure 3-23. Histogram of the noise images presented in Figure 3-22.</i>	129
<i>Figure 3-24. Experimental setup in contrast matching experiment.</i>	132
<i>Figure 3-25. Examples of patterns displayed on the LCD. Medium frequency filtered pattern, image numbered 7 in Table 3-3, was displayed at magnification factors of 1X, 1/2X, and 1/3X on the LCD and compared to the image on the DLP screen (shown in Figure 3-26.)</i>	134
<i>Figure 3-26. An example of noise pattern displayed on the DLP screen. Medium frequency filtered pattern, image numbered 7 in Table 3-3, was compared to the same pattern displayed at magnification factors of 1X, 1/2X, and 1/3X on the LCD.</i>	135
<i>Figure 3-27. Top: original test image with CIEL* lightness of [15, 85]; middle: mean luminance was adjusted to CIEL* 45; bottom: contrast was decreased by adjustment of the CIEL*minimum and maximum to [30, 70].</i>	136
<i>Figure 3-28. Contrast adjustment of DLP images versus LCD images for 14 observers. Panels A, D, G correspond to low frequency noise patterns, centered at 0.5 cpd, and CIEL* values of 75, 50, and 25, respectively. Panels B, E, H correspond to medium frequency noise patterns. Panels C, F, I correspond to high frequency noise patterns, centered at 8 cpd. Dashed lines at each panel shows contrast of LCD images.</i>	138

<i>Figure 3-29. A band-pass filter in frequency domain similar to a contrast sensitivity function. Shift in frequency domain due to scaling down to smaller size for noise images of A: low frequency; B: medium frequency; C: high frequency.</i>	142
<i>Figure 3-30. Luminance adjustment results for DLP images versus LCD images for 14 observers. Panels A, D, G correspond to low frequency noise patterns, centered at 0.5 cpd, and three levels of contrast levels. Panels B, E, H correspond to medium frequency noise patterns, centered at 2 cpd. Panels C, F, I correspond to high frequency noise patterns, centered at 8 cpd. Dashed line at each panel shows mean luminance of LCD images.</i>	145
<i>Figure 3-31. Adjusted mean lightness of noise patterns on the projector screen versus the mean lightness of corresponding images on the LCD for three magnification factors of 1/3X, 1/2X, and 1X.</i>	147
<i>Figure 3-32. Top: low frequency noise pattern, image numbered 5 in Table 1-1, rendered for DLP display; Bottom left: same pattern colorimetrically rendered for LCD; Bottom right: same pattern colorimetrically rendered and also adjusted for the effect of 1/3X magnification for the LCD display.</i>	148
<i>Figure 3-33. Top: high frequency noise pattern, image numbered 5 in Table 1-1, rendered for DLP display; Bottom left: same pattern colorimetrically rendered for LCD; Bottom right: same pattern colorimetrically rendered and also adjusted for the effect of 1/3X magnification for the LCD display.</i>	149
<i>Figure 4-1. Forward model from RGB digital counts to IPT color coordinates.</i>	156
<i>Figure 4-2. IPT color coordinates of the selected five hues for the IBM display.</i>	158
<i>Figure 4-3. The red, green, blue, yellow, and magenta colors are tagged as R_1, G_1, B_1, Y_1, and M_1 at a lightness level of $I=0.25$. Symbols R_2, G_2, B_2, Y_2, and M_2 denote the same colors at a lightness level of $I=0.75$. The red color corresponding to digital counts of (255, 0, 0) is shown by 'R' symbol. The plane of constant hue for the red color encompassed the R_1, R_2, and R colors.</i>	161
<i>Figure 4-4. Lightness of the chromatic patch was adjusted to match the lightness of the achromatic patch. The instruction was: "Please adjust lightness of the color patch to the same lightness as of the gray patch using ShuttleXpress dialer. A clockwise turn increases lightness of the patch. You can decrease lightness by a counterclockwise turn."</i>	162
<i>Figure 4-5. Observers' responses for the Helmholtz-Kohlrausch effect. Lightness of the gray patches are shown by dashed lines at $I=0.25$ and $I=0.75$.</i>	164
<i>Figure 4-6. An example of perceived lightness reduction for the effect of Helmholtz-Kohlrausch for a red color denoted by A. Point A would be adjusted to A'.</i>	166
<i>Figure 4-7. Primary red color, R, was corrected for the Helmholtz-Kohlrausch effect and denoted by R'. Segment line KR' was assumed to have a constant hue and perceived lightness.</i>	167
<i>Figure 4-8. Color coordinates of the LCD and DLP primary colors projected on the P-T plane.</i>	168
<i>Figure 4-9. Color maps relating IPT to RGB values for LCD or DLP displays. All colors in a maps had the same hue and perceived lightness. A color map was generated for each hue. Chroma was zero for the first element and increased to the chroma of the primary color for the last element.</i>	170
<i>Figure 4-10. An example spatial contrast sensitivity functions for luminance and chromatic contrast of Human Visual System [Fairchild 2005].</i>	172
<i>Figure 4-11. Frequency responses of octave filters centered at 0.1875, 0.75, and 3.0 cycle-per-degree, (cpd), of visual angle. For frequencies lower than 0.1875 cpd and higher than 3.0 cpd, filter responses were set to unity for filters centered at 0.1875 and 3.0 cpd, respectively.</i>	173
<i>Figure 4-12. Octave cosine log filter centered at 0.75 cycles-per-deg. Response of the filter is plotted along its horizontal axis of symmetry.</i>	174
<i>Figure 4-13. Images corresponding to low, medium, and high frequency octave cosine log filters centered at 0.1875, 0.75, and 3 (cpd), respectively. Top: low frequency; Bottom: high frequency; Middle: medium frequency. The center of each image corresponded to the zero frequency. Frequency range was [-35, 35] along the diagonal axis of each image.</i>	175

<i>Figure 4-14. Low, medium, and high frequency noise images used to populate chromatic noise patterns at five hues. Pixel values were multiplied by 400 and used as indices to color map arrays.....</i>	177
<i>Figure 4-15. Low, medium, and high frequency noise patterns used in chromatic contrast matching. These noise patterns were populated based on the low, medium, and high frequency noise patterns presented in Figure 4-14.....</i>	178
<i>Figure 4-16. Top: original noise image; middle: 25% increase in chromatic contrast; bottom: 20% decrease in chromatic contrast. Histogram of the pixel values is plotted in the right column for each image. Pixel values were multiplied by 400 and used as indices to the corresponding color map.....</i>	182
<i>Figure 4-17. Contrast of a sample noise image was increased by adjusting the maximum value of the image to a higher value; so the indices to the color map would address a wider range of colors, In this example segment line AD map colors on the LCD from [0%, 70%] to a [0% 95%]. All values are expressed related to the chroma of the corresponding primary color.....</i>	183
<i>Figure 4-18. Contrast of a sample noise image was decreased by adjusting the maximum value of the image to a lower value.....</i>	184
<i>Figure 4-19. Adjusted chromatic contrast for red patterns displayed with different sizes on the LCD and compared to the DLP reproductions. Left: low frequency, Right: high frequency, Middle: Medium frequency. Dashed blue line is initial chroma of the images on the LCD.</i>	187
<i>Figure 4-20. Adjusted chromatic contrast for green patterns displayed with different sizes on the LCD and compared to the DLP reproductions. Left: low frequency, Right: high frequency, Middle: Medium frequency. Dashed blue line is initial chroma of the images on the LCD.</i>	188
<i>Figure 4-21. Adjusted chromatic contrast for blue patterns displayed with different sizes on the LCD and compared to the DLP reproductions. Left: low frequency, Right: high frequency, Middle: Medium frequency. Dashed blue line is initial chroma of the images on the LCD.</i>	189
<i>Figure 4-22. Adjusted chromatic contrast for yellow patterns displayed with different sizes on the LCD and compared to the DLP reproductions. Left: low frequency, Right: high frequency, Middle: Medium frequency. Dashed blue line is initial chroma of the images on the LCD.</i>	190
<i>Figure 4-23. Adjusted chromatic contrast for magenta patterns displayed with different sizes on the LCD and compared to the DLP reproductions. Left: low frequency, Right: high frequency, Middle: Medium frequency. Dashed blue line is initial chroma of the images on the LCD.</i>	191
<i>Figure 4-24. An example of spatial contrast sensitivity functions for luminance and chromatic contrast of Human Visual System [Fairchild 2005]. An image located in the frequency range 'A' would be shifted to range 'B' when scaled down to a smaller size.....</i>	193
<i>Figure 4-25. Adjusted chromatic contrast of the low frequency noise patterns on the DLP screen. The larger the polygon, the more chromatic corresponding images on the DLP screen. Dashed black line is initial chroma of the images on the LCD.</i>	194
<i>Figure 4-26. Adjusted chromatic contrast of the high frequency noise patterns on the DLP screen. The larger the polygon, the more chromatic corresponding images on the DLP screen. Dashed black line is initial chroma of images on the LCD.</i>	195
<i>Figure 4-27. Top: Low frequency noise pattern rendered for DLP display; Bottom left: same pattern colorimetrically rendered for LCD; Bottom right: same pattern colorimetrically rendered and also adjusted for the effect of 1/3X magnification for the LCD display.</i>	196
<i>Figure 4-28. Top: high frequency noise pattern rendered for DLP display; Bottom left: same pattern colorimetrically rendered for LCD; Bottom right: same pattern colorimetrically rendered and also adjusted for the effect of 1/3X magnification for the LCD display.</i>	197
<i>Figure 5-1. Histogram of CIE L* of the selected paintings. The red lines plot the cumulative distributions. A: Renoir; B: Seurat; C: Picasso; D: Rembrandt; E: Rousseau.</i>	203
<i>Figure 5-2. Lightness and five color separations of the Seurat painting.....</i>	204

<i>Figure 5-3. The circles show the DLP primary colors. The unit vectors along the five primary colors are represented by \vec{R}, \vec{G}, \vec{B}, \vec{Y}, and \vec{M}.....</i>	207
<i>Figure 5-4. Adjusted mean lightness of noise patterns on the projector screen versus the mean lightness of corresponding images on the LCD for three magnification factors of 1/3X, 1/2X, and 1X.....</i>	210
<i>Figure 5-5. Top: Colorimetric rendered image of Seurat painting for the LCD. Bottom left: 1/3X magnification of the top image. Bottom right: Same image colorimetrically rendered and also adjusted for the mean lightness.....</i>	211
<i>Figure 5-6. Samples of filter responses for different values of 'a', 'b', and 'c' parameters</i>	213
<i>Figure 5-7. Optimization of three parameters of the Movshon filter.....</i>	214
<i>Figure 5-8. Filter responses of three modeled achromatic filters for adjustment of lightness contrast. Filters are modeled from noise patterns with mean lightness of CIEL*=50 and Michelson contrast of 0.18.</i>	217
<i>Figure 5-9. Achromatic filters presented in Figure 5-8. Top left: 1/3X; Middle left: 1/2X; Bottom left: 1X. images in the left column are color mapped between black and white and shown in the right column to amplify differences, visually The center of each image corresponds to zero frequency.</i>	218
<i>Figure 5-10. Optimized filter for adjustment of lightness contrast of Seraut painting for a magnification of 1/3X. The computed 'a', 'b', and 'c' parameters were 119.5, 0.0072, and 0.0012, respectively</i>	220
<i>Figure 5-11. Top: Colorimetric rendered image of Seurat painting for the DLP. Bottom left: 1/3X magnification of the top image rendered for LCD. Bottom right: Same image colorimetrically rendered and also adjusted for achromatic contrast.....</i>	221
<i>Figure 5-12. Unadjusted and adjusted noise images at lightness level 'I_1' and 'I_2' were predicted from the original and adjusted noise images at a lightness level of 'I'.....</i>	224
<i>Figure 5-13. Optimized chromatic filters for Seurat painting image for a 1/3X magnification factor.</i>	225
<i>Figure 5-14. Top: Colorimetric rendered image of Seurat painting for the LCD. Bottom left: 1/3X magnification of the top image. Bottom right: Same image colorimetrically rendered and also adjusted for chromatic contrast.</i>	228
<i>Figure 5-15. Top: Colorimetric rendered image of Seurat painting for the LCD. Bottom left: 1/3X magnification of the top image. Bottom right: Same image colorimetrically rendered and also adjusted for the mean lightness and achromatic contrast.....</i>	230
<i>Figure 5-16. Top: Colorimetric rendered image of Seurat painting for the LCD. Bottom left: 1/3X magnification of the top image. Bottom right: Same image colorimetrically rendered and also adjusted for the mean lightness and chromatic contrast.....</i>	231
<i>Figure 5-17. Top: Colorimetric rendered image of Seurat painting for the LCD. Bottom left: 1/3X magnification of the top image. Bottom right: Same image colorimetrically rendered and also adjusted for achromatic and chromatic contrast.....</i>	232
<i>Figure 5-18. Top: Colorimetric rendered image of Seurat painting for the LCD. Bottom left: 1/3X magnification of the top image. Bottom right: Same image colorimetrically rendered and also adjusted for the mean lightness, chromatic and chromatic contrast.....</i>	233
<i>Figure 5-19. Arrangement of scene and equipment in the paired-comparison experiment, observers could not see both the LCD and screen at the same time and the paired-comparisons were based on short-term memory matching.</i>	236
<i>Figure 5-20. Overall results for different color rendering methods for the 1/3X magnification factor.....</i>	238
<i>Figure 5-21. Overall results for different color rendering methods for the 1/2X magnification factor.....</i>	240
<i>Figure 5-22. Overall results for different rendering methods for the 1X magnification factor.....</i>	241

<i>Figure 5-23. Interval scale values for different color rendering methods for the 1/3X magnification factor.</i>	243
<i>Figure 5-24. Interval scale values for different color rendering methods for the 1X magnification factor.</i>	247
<i>Figure 5-25. Interval scale values for different color rendering methods for the 1/2X magnification factor.</i>	250
<i>Figure 6-1. Interval scales and corresponding 95% confidence limits based on visual experiment.....</i>	257
<i>Figure 6-2. Contrast adjustment of DLP images versus LCD images for 14 observers. Panels A, D, G correspond to low frequency noise patterns, centered at 0.5 cpd, and CIEL* values of 75, 50, and 25, respectively. Panels B, E, H correspond to medium frequency noise patterns. Panels C, F, I correspond to high frequency noise patterns, centered at 8 cpd. Dashed lines at each panel shows contrast of LCD images.....</i>	259
<i>Figure 6-3. Luminance adjustment results for DLP images versus LCD images for 14 observers. Panels A, D, G correspond to low frequency noise patterns, centered at 0.5 cpd, and three levels of contrast levels. Panels B, E, H correspond to medium frequency noise patterns, centered at 2 cpd. Panels C, F, I correspond to high frequency noise patterns, centered at 8 cpd. Dashed line at each panel shows mean luminance of LCD images.....</i>	260
<i>Figure 6-4. Overall results for different color rendering methods for the 1/3X magnification factor.....</i>	263
<i>Figure 6-5. Overall results for different color rendering methods for the 1/2X magnification factor.....</i>	264
<i>Figure 6-6. Overall results for different rendering methods for the 1X magnification factor.....</i>	265

List of Tables

<i>Table 1-1. Tone Reproduction Operators, summary of attributes [Devlin 2002].....</i>	39
<i>Table 2-1. Summary of colorimetric characterization results for LCD display for the 1931 standard observer.....</i>	70
<i>Table 2-2. Summary of characterization results for DLP projector for the 1931 standard observer.....</i>	73
<i>Table 2-3. Summary of image processing algorithms.....</i>	84
<i>Table 2-4 continued: Summary of image processing algorithms.....</i>	85
<i>Table 3-1. Summary of specifications of the 12 images rendered for the LCD display. (Mc=Michelson Contrast.).....</i>	97
<i>Table 3-2. Summary of characterization results for LCD display and DLP projector for the 1931 standard observer.....</i>	102
<i>Table 3-3. Summary of specification of seven generated noise patterns for one of the frequency bands.....</i>	127
<i>Table 3-4. Summary of characterization results for the IBM T221 LCD display and ASK Proxima M1-DLP projector for the 1931 standard observer.....</i>	131
<i>Table 4-1. Tristimulus values, in cd/m², for the CIE 1931 standard observer and IPT color coordinate of the selected five primary colors.....</i>	158
<i>Table 4-2. Reduction of chroma for each primary color at selected lightness levels.....</i>	160
<i>Table 4-3. IPT color coordinates and tristimulus values, in cd/m², for the chromatic colors used in lightness adjustment.....</i>	160
<i>Table 4-4. Tristimulus values, in cd/m², of start and end of each hue line for the CIE 1931 standard observer.....</i>	169
<i>Table 4-5. IPT color coordinates of the start and end of each hue line for the tristimulus values listed in Table 4-4.....</i>	169
<i>Table 5-1. Mean CIE L* and calculated Michelson contrast for the five painting images.....</i>	202
<i>Table 5-2. Optimized parameters for the achromatic noise patterns at different contrast and lightness levels for three magnification factors of 1/3X, 1/2X, and IX. Contrast was calculated using Michelson formula and shown by Mc symbol.....</i>	216
<i>Table 5-3. Optimized parameters for the chromatic filters at five hues for the five selected paintings at three magnification factors of 1/3x, 1/2X, and IX.....</i>	226
<i>Table 5-4. Eight methods of image rendering used in preparation of painting images and corresponding abbreviations.....</i>	229
<i>Table 5-5. Summary of subtending visual angles and resolutions for reference and test images for the three magnification factors in the paired-comparison experiments.....</i>	235
<i>Table 6-1. Summary of colorimetric characterization results for LCD display for the 1931 standard observer.....</i>	255
<i>Table 6-2. Summary of characterization results for DLP projector for the 1931 standard observer.....</i>	255

1 INTRODUCTION

An ideal system of image reproduction includes two main subsystems, devices and software for data acquisition at the input side and devices and software for image display at the output side. The fidelity of the overall systems depends on the performance of each subsystem. Different techniques for spectral data acquisition have been developed and image reproduction of cultural heritage based on spectral imaging techniques has been an active research area in the last ten years [Berns 2005a, Berns 2005b, MCSL 2005]. The next important step is to render images and display them on different media like CRT, prints, and LCD displays. Since the reproduction images are usually viewed in a different viewing condition than the original scene, an image appearance model is required to account for these changes. In another approach, spectral color processing using an interim connection space has been proposed by Rosen, et al. [Rosen 2003]. Rosen and coworkers have also proposed useful investigating algorithms and a prototype data structure for performing color management within spectral imaging [Rosen 2000]. The colorimetric based Profile Connection Space (PCS) is not a suitable choice for rendering of spectral images. One proposed solution is creating a spectral based PCS [Rosen 2000]. However, in this approach the spatial and temporal aspects of color reproduction have not been accounted for and an image color appearance model is required.

Original and reproduced art are usually viewed under quite different viewing conditions. Suppose that we are going to simulate on a computer display, the perception of an observer at a museum looking at a large painting. When the observer is looking at the painting at very close distance he/she is adapted to a different surround, and the viewing condition is different from the case of looking at the painting from a far distance. The lighting geometry and painting surround also have a great effect on perceived appearance. Furthermore if the observer has been looking at a dark area and suddenly moved to look at some bright area his/her adaptation state is different from the case he/she has been already looking at in a bright area (adapted to bright light) and moved to look at the bright part of the painting. Therefore if the simulation software is zooming in to enlarge the image, it is also required to take into account the surround of that part of image in the rendering process. More sophisticated software may also keep track of previous locations that the observer has been looking at in order to calculate the temporal adaptation state. An image color appearance model (iCAM) can serve the task of spatial and temporal adaptation. The iCAM proposed by Johnson and Fairchild can be a suitable choice for this task [Fairchild 2002, Fairchild 2003].

Many art objects have a size much larger than their reproductions, whether displayed on a monitor or in print. The physical size or viewing angle of a stimulus is one of several factors affecting color perception. Differences in size or viewing distance leads to different surrounds and as shown by Bartleson and Breneman, the perceived contrasts will be different [Bartleson 1967]. Furthermore, images with the same content but

different sizes have the effect of a different adapting field, which in turn will produce different color perceptions. The goal of this dissertation was to develop a fundamental understanding of the effect of image size on color appearance.

1.1 Color Perception

A light source radiates energy in the form of visible radiant flux, which provides an external stimulus perceived by the human visual system. An object along the pathway of light can modify the radiant flux in different ways such as absorption, transmission, scattering, reflection, and fluorescence. In the following sections each of the three main elements of color perception, the light source, the object, and the human visual system (HVS), are briefly discussed.

1.2 Illumination

Conservation and aesthetic aspects of illuminating sources used in the display of artworks in museums and galleries are two important concerns of exhibitors and conservators [Berns 1987]. The influence of an illuminating light source on color appearance can be divided into three categories: spectral power distribution, geometry, and level of illumination. The relative spectral power distribution of a light source describes the amount of energy emitted at each wavelength. Conservators require sources with

minimum emission of ultraviolet radiation while exhibitors favor sources that are more pleasing to the viewer. On the other hand, a lighting differing from the original light source used by the artist results in a different color appearance of the artwork from the original appearance intended by the artist. The change of the human visual system (HVS) to compensate for the changes in relative spectral power distribution of the light source is known as chromatic adaptation [Berns 2000]. The color constancy of objects resulting from the chromatic adaptation ability of the human visual system is limited and one should be very careful in changing illumination conditions. In other words, the HVS cannot compensate for large changes in the spectral power distribution of a light source. Berns, *et al.* formed an experiment using eight artist's pigments under five different illuminants at several illumination levels to show the change of color appearance of color patches due to a change in illumination conditions [Berns 1987]. Large color appearance differences were observed for different illuminating environments. It was concluded that incandescent sources are not appropriate for accurate color rendition of artwork created under north-sky daylight. Furthermore, restoring a damaged area of a painting by visual matching of color under daylight may result in large appearance mismatch, if viewed under incandescent lighting. This phenomenon is referred to as metamerism [Berns 2000]. As many artworks were created prior to the advent of artificial lighting, the use of daylight sources was recommended. However, environments lit by daylight sources at low luminance level are psychologically uncomfortable, so the use of filtered

incandescent lamps, to obtain a correlated color temperature of about 4500 K, was suggested.

The correlated color temperature (CCT) of an illuminant is defined as the temperature of a black body radiator with the same (or nearly the same) color coordinates as the illuminant's color coordinates [Wyszecki 1982]. Kruithof investigated the relationship between correlated color temperature, intensity, and the "pleasant" quality of an illumination source [Kruithof 1941, Weintraub 2000]. The result of that research is summarized in a graph shown in Figure 1-1. An observer favors lightings with low CCT for low illuminance levels and prefers higher CCT when the light level is high. As an example, a room uniformly illuminated by a daylight source of CCT of 6000K with an intensity of 20 foot-candles (approximately 200 lx)*, appears overcast and gloomy, while the same space will appear comfortable and pleasant, if it is illuminated by a tungsten-halogen lamp with a CCT of 3000K at the same light intensity (20 foot-candles). Therefore, psychologically, it is not desirable to illuminate artwork created under daylight by a daylight source with the same CCT, but rather, at much lower luminance level. It should be noted that in the Kruithof's experiment the goal was to find the optimal illumination for a workplace assuming a light source neither warm nor cool is the best

* Each square meter, m^2 , is equal to $(3.084)^2 \approx 10.76$ square feet, f^2 ; hence each foot-candle (lumen/ f^2) is about 10.76 lx (lumen/ m^2).

choice and aesthetic issues, conservation considerations, and color consistency issues were not taken into account.

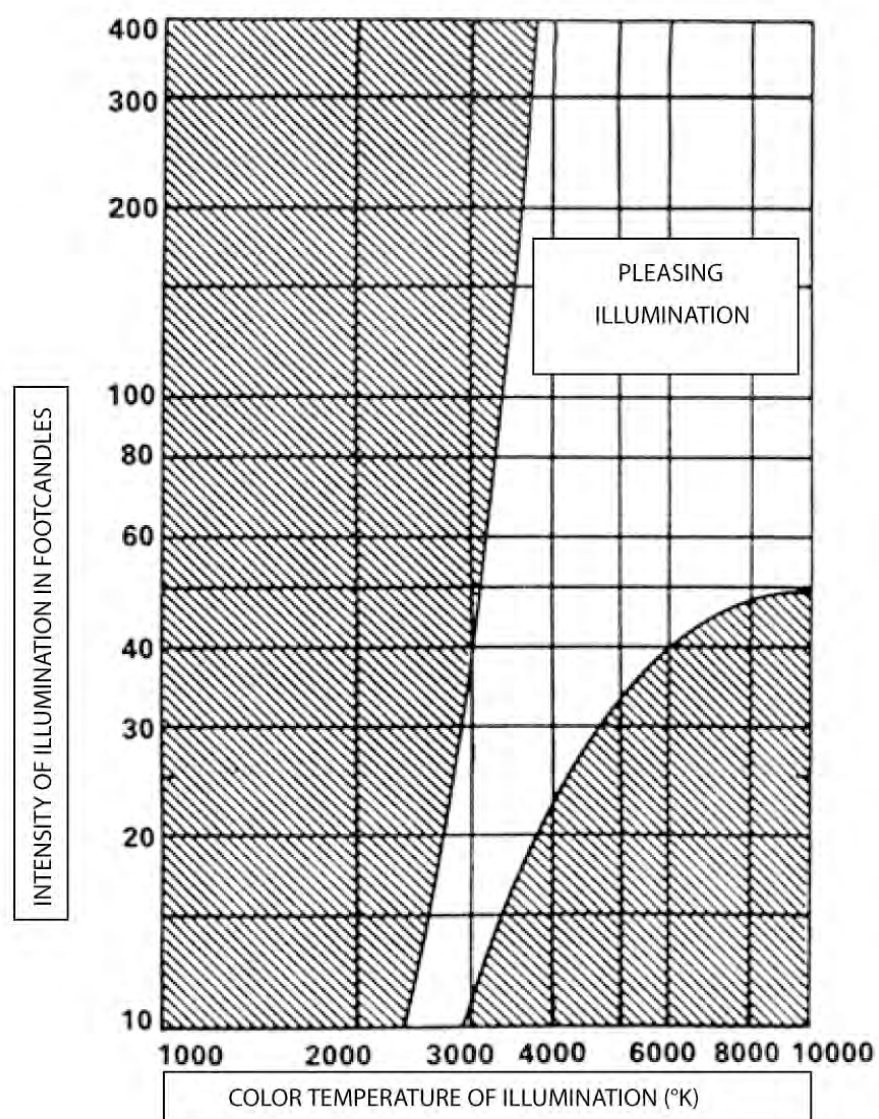


Figure 1-1. Kruithof's curves present relationship between correlated color temperature, intensity, and the "pleasant" quality of an illumination source [Weintraub 2000].

Scuello and coworkers conducted an experiment to compare the same “artwork” under different illumination conditions, utilizing side-by-side miniature museum rooms and printed postcards of artwork. Using a paired-comparison method, nine observers compared the same painting lit by two different illuminants, at a luminance of about 200 lux, which were selected randomly from a set of eleven daylight sources with correlated color temperatures ranging from 2500 K to 7000 K [Scuello 2004A]. Observers preferred lighting with a CCT of about 3600 K. It should be noted that the pigments that are used in printing inks are inherently more color constant than pigments used in real art, such as cobalt blue and ultramarine blue with reflectance tails in the long wavelength range.

More investigation using a broader set of pigments, as those used in artwork, are required. In another experiment each painting was viewed in a single simulated room lit by one of the illuminants and a preference score was assigned to it. The preference score was selected from an 11-point numeric scale, -5 to 0 to +5, where -5 and +5 denoted strong negative and positive responses respectively, and 0 denoted no opinion. The illuminant with the CCT of 3600 K was again preferred among the others. Scouello and coworker studied the relationship between the CCT of a light source and its intensity while it appears neither warm nor cool [Scuello 2004B]. A neutral white standard lit by a bank of lamps was observed at different luminance levels. Observers could adjust the combined CCT by adjustment of the voltage ratios of the lamps. In this way the total light intensity was kept approximately constant. The combination of lamps could generate a CCT in the range of 3000 K to 4000 K. Figure 1-2 presents the CCT versus the

illuminance level of the light sources adjusted in such a way that they were perceived neither warm nor cool. Scuello and coworkers suggested a preferred illuminant with a CCT of about 3700 K for viewing artwork [Scuello 2004B]. Because of the large variation of results shown in Figure 1-2, it is hard to select a preferred CCT and the results are inconclusive.

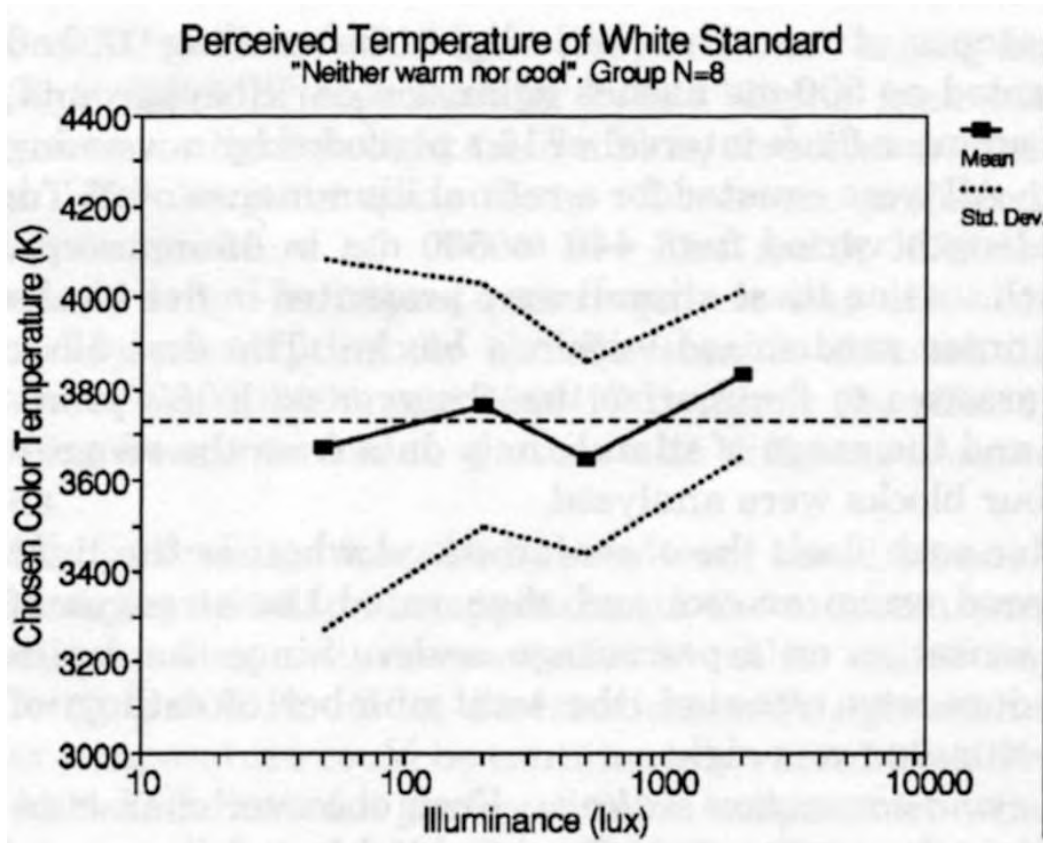


Figure 1-2. Color temperature of illuminant chosen to appear “neither warm nor cool”. Solid lines shows mean setting for a group of eight observers and dotted lines present boundaries for ± 1 group standard deviation. The horizontal dashed line shows the overall mean choice [Scuello 2004B].

In order to minimize photo degradation in museums, Thomson recommended an illuminance level of 150 lux [Thomson 1978]. Commercial environments are usually illuminated at levels between 500 lux and 1000 lux. The illuminance level in outdoors on a partly cloudy day and a clear summer day are 10,000 lux and 100,000 lux, respectively [Wandell 1995]. The human visual system normally adjusts for this wide range of illuminance, which is known as light adaptation [Berns 2000]. Light adaptation cannot fully compensate for changes in illumination level and there are some changes in perceived color. The Hunt effect [Hunt 1952] and the Stevens effect [Stevens 1963] are two phenomena that relate to different adaptation conditions. However, there is a general tendency of the color perception of an object to remain constant when the level and color of the illumination are changed. This phenomenon is known as color constancy [Berns 2000], but imprecise at best.

The geometry of illumination is another important factor in color appearance perception. A diffusely illuminated object appears lighter, flatter (two-dimensional) with a loss of colorfulness compared to the case of illumination by a point source [Evans 1948]. The spatial distribution of light on the object can enhance its texture appearance. By casting light across the surface of an artwork at very low angles, texture, irregularities, damages, and deformations can be highlighted [Padfield 2005]. Another aspect related to the illumination geometry is the amount of ambient light. More light is reflected from walls and ceiling onto the artworks for diffuse illumination compared to the spot illumination. Therefore the perceived color of an artwork is affected by the color

of the walls and other ambient objects; this occurs more for the diffuse illumination than illuminating the painting with a spot light source.

1.3 Colored Materials

An object along the pathway of light can modify the radiant flux in different ways such as absorption, transmission, scattering, reflection, and fluorescence. The result of the interaction of light and matter is not only a function of wavelength but also depends on the illumination geometry. There are a number of excellent classical texts and references available on this subject and reader is referred to the texts of Wyszecki [1982], Grum [1980], Judd [1975], Berns [2000], and Hunt [1995].

To fully quantify the geometric appearance effects, such as gloss and metallic and pearlescent effects, complete bidirectional reflectance distribution functions (BRDFs) should be measured for each possible combination of illumination and viewing angles at each wavelength. For most practical cases those measurements are expensive, time consuming, and difficult. There are a limited number of standard illumination and viewing geometries established for colorimetry by the CIE. Many techniques have been developed to compactly represent the BRDF of a surface. Linear basis functions such as spherical harmonics [Cabalal 1987, Sillion 1991, Wong 97], physically based analytical models like He [1991] and Stam [1999], and empirical models [Phong 1975, LaFortune 1997] are some examples.

1.4 Human Visual System

The external stimuli generated from the interaction of a light source and colored materials are perceived by the human visual system (HVS). In the human eye an image of the outside world is focused on the retina. The retina is a thin layer consisting of photoreceptors, photosensitive cells, and initial processing and transmission circuitry of the visual system. There are two types of photoreceptors, rods and cones, which transduce the optical image on the retina to chemical and electrical signals transmittable to the later stages of visual system. The signals generated in photoreceptors are processed through the network of retinal neurons (horizontal, bipolar, amacrine, and ganglion cells). The later visual processing in the thalamus and the cortex are extremely complex. In order to gain more details the reader is referred to some classical and general texts such as Boynton [1996], Wandell [1995], Backhaus [1998], Gegenfurtner [1999], and Palmer [1999]. There is also a very good review paper on the mechanism of color vision by Lennie and D’Zmura [Lennie 1988]. Another interesting book is an introductory text on vision by Livingstone, a neurophysiologist, focused on the scientific explanation of various visual phenomena in paintings [Livingstone 2002].

The modern opponent-colors theory was developed based on Hering’s opponent theory and a large amount of additional data from more recent studies. However the color processing of the human visual system should not be considered as a static ‘wiring diagram.’ There are dynamic mechanisms of adaptation that increase the performance of the HVS in different viewing environments. Three important adaptation mechanisms

related to color appearance are dark adaptation, light adaptation, and chromatic adaptation. Furthermore, there are cognitive visual mechanisms such as memory color, color constancy, discounting the color of the illuminant, and object recognition that impact color appearance [Fairchild 2005].

The specification of color by CIE XYZ is extremely useful but we should remember that it has limitations. Two samples with the same tristimulus values, XYZ, are perceived the same for an average observer if certain constraints and conditions hold. Some of these conditions are having the same surround, background, size, shape, surface characteristic, illumination geometry, retinal locus of stimulation, angular subtense, and luminance level [Fairchild 2005]. It is very likely that two samples will not match in color if any of above constraints is violated. However, in most color reproduction applications the above mentioned constraints are violated. Therefore it is necessary to enhance traditional colorimetry to include the influences of these variables. Such enhancements are known as color appearance models. Figure 1-3 shows one example where two samples with the same tristimulus values match in color because they have the same viewing condition, but if the same samples are placed on a different background they no longer match in appearance, although they still have the same tristimulus values, XYZ. This phenomenon is known as simultaneous contrast or induction [Fairchild 2005]. The constraint of equal background is violated in the Figure 1-3-b and a model to incorporate the background effect is needed. In section 1.6, some of the most important color appearance phenomena will be briefly described.

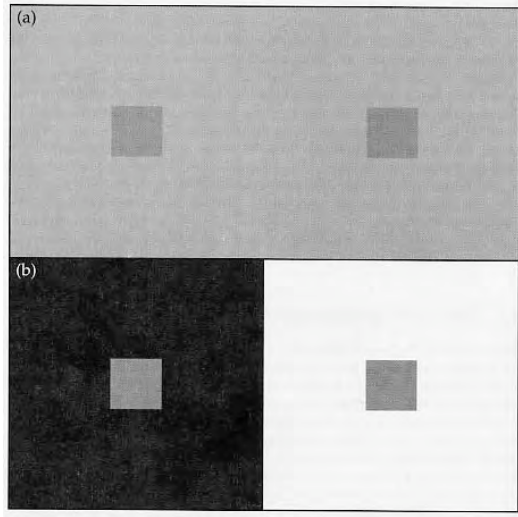


Figure 1-3. An example demonstrating simultaneous contrast phenomenon. The gray patches on the gray background, (a), are physically identical to those on the white and black background, (b) [Fairchild 2005].

1.5 Important Attributes of Visual Sensations

In this section some of the most important color attributes are defined for further reference in this chapter. These definitions are culled from three different sources by Fairchild and are quoted here [Fairchild 2005].

- Hue: Attribute of a visual sensation according to which an area appears to be similar to one of perceived colors: red, yellow, green, and blue, or to a combination of two of them. Using definition of hue, two groups of colors are defined as the following:
- Achromatic color: Perceived color devoid of hue.
- Chromatic color: Perceived color possessing hue.

- Brightness: Attribute of a visual sensation according to which an area appears to emit more or less light.
- Lightness: The brightness of an area judged relative to the brightness of a similarly illuminated area that appears to be white or highly transmitting. (Only related colors exhibit lightness.)
- Colorfulness: Attribute of a visual sensation according to which the perceived color of an area appears to be more or less chromatic.
- Chroma: Colorfulness of an area judged as a proportion of the brightness of a similarly illuminated area that appears white or highly transmitting.
- Saturation: Colorfulness of an area judged in proportion to its brightness.
- The chroma, saturation, and lightness can also be stated conceptually as:

$$\text{Chroma} = \frac{\text{Colorfulness}}{\text{Brightness(White)}} \quad \text{Lightness} = \frac{\text{Brightness}}{\text{Brightness(White)}}$$

$$\text{Saturation} = \frac{\text{Colorfulness}}{\text{Brightness}} = \frac{\text{Chroma}}{\text{Lightness}}$$

1.6 Color Appearance Phenomena

Some of the most important color appearance phenomena are briefly introduced in this section. Most of color appearance models are evaluated based on their accuracy in prediction of the following color appearance phenomena.

1.6.1 Simultaneous Contrast

As illustrated in Figure 1-3, a black background caused a shift in color appearance of the gray patch and made it to appear lighter. On the other hand the same patch appeared darker with a white background. In the same way a background of red induces green, yellow induces blue, green induces red, and blue induces yellow. These apparent shifts are induced in the opposite direction of background in the opponent color space. More details on this subject are explored in the classical textbooks such as Wandell [1995], Hurvich [1981], Boynton [1979], and Evans [1948].

1.6.2 Crispening

For two stimuli placed on the same background, the magnitude of perceived color difference between two stimuli increases if the background color is similar to the stimuli themselves. Crispening is a related phenomenon and an example of it is illustrated in Figure 1-4-A. A comprehensive study of the crispening effect was published by Semmelroth [1970].

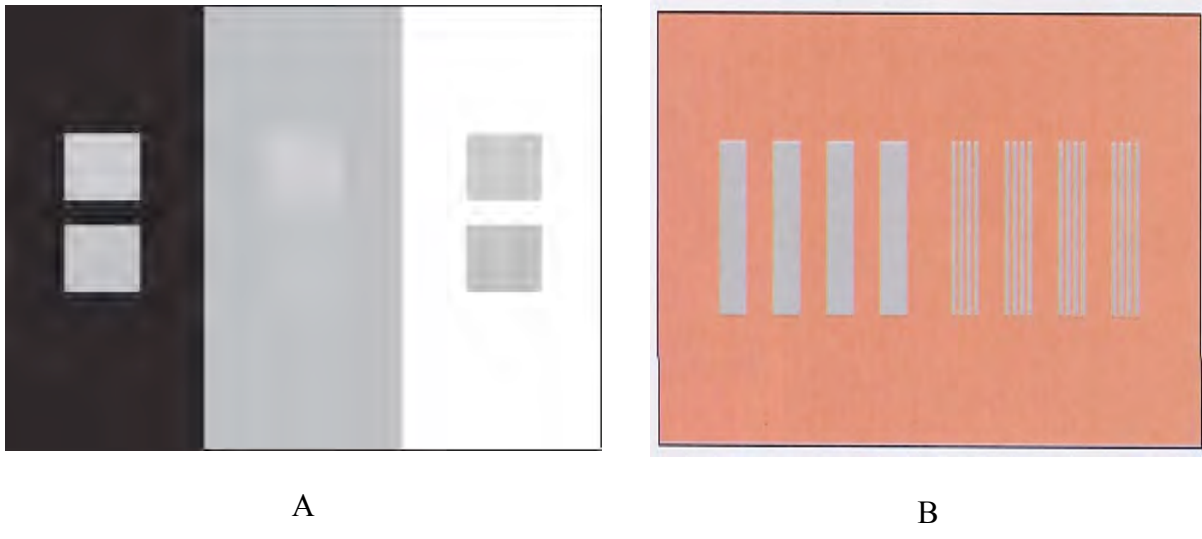


Figure 1-4. A: An example of crispening. The pairs of gray patches are physically identical on all three backgrounds. B: A demonstration of the difference between simultaneous contrast and spreading. The gray areas are physically identical but appear different depending on their spatial scale with respect to the red background [Fairchild 2005].

1.6.3 Spreading

Apparent mixture of a color stimulus with its surround is known as spreading. If spatial frequencies of stimuli are increased, the simultaneous contrast phenomenon is replaced by spreading and at the point of spatial fusion this effect is complete and the stimuli fuse into a single stimulus. For frequencies less than the fusion point, stimuli are not fused and are viewed as distinct stimuli, though colors blend to each other at some extent [Fairchild 2005]. Figure 1-4-B illustrates one example of spreading along one of the color dimensions.

1.6.4 Bezold-Brücke Hue Shift

If the luminance of a monochromatic stimulus is changed the perceived hue also changes.

The shift in hue with a change in luminance is known as the Bezold-Brücke hue shift.

Some of results of a typical experiment by Purdy are shown in Figure 1-5 [Purdy 1931].

The Bezold-Brücke hue shift suggests that there are some nonlinear processing in the visual system after the point of energy absorption in the cones but before the point that perception and judgments of the hue are made. It has been suggested by Hunt that the Bezold-Brücke hue shift does not occur for related colors [Hunt 1989].

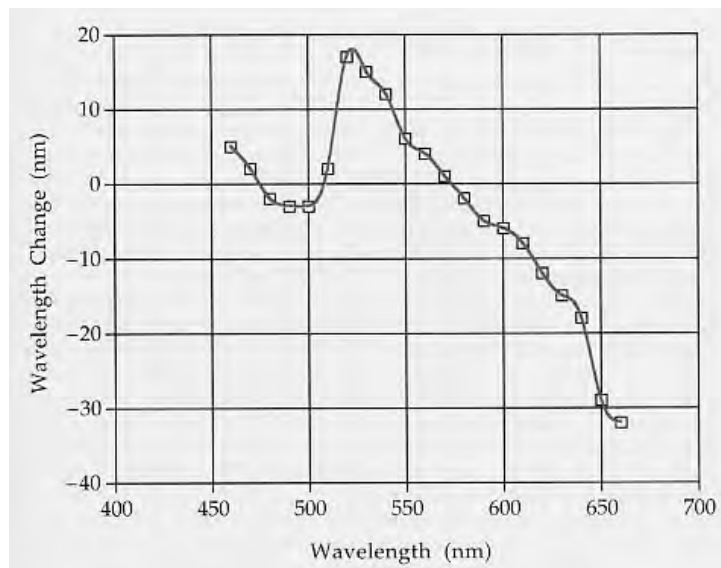


Figure 1-5. Example data illustrating the Bezold-Brücke hue shift. Plot shows the wavelength shift required to maintain hue constant across a 10X reduction in luminance [Fairchild 2005].

1.6.5 Helmholtz-Kohlrausch Effect

This is another interesting appearance phenomenon that is best illustrated by examining contours of constant brightness-to-luminance ratio as presented in Figure 1-6 adopted from Wyszecki and Stiles [1981]. As illustrated in Figure 1-6, at constant luminance, perceived brightness increase with increasing saturation and depends upon hue. In other words, brightness depends on luminance and chromaticity.

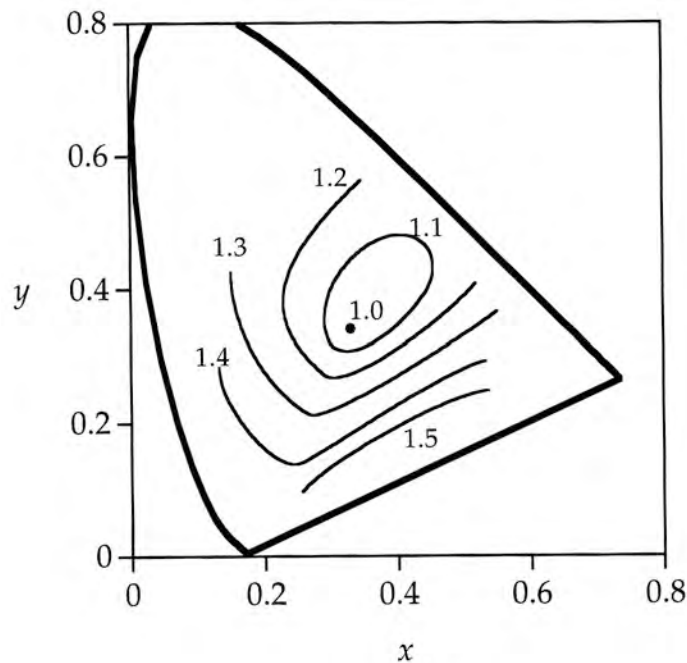


Figure 1-6. Contours of constant brightness-to-luminance ratio illustrating the Helmholtz-Kohlrausch effect (adopted from Fairchild [2005]).

One can witness this effect by examining Munsell chips of a given hue and value where higher chroma chips do appear brighter. The magnitude of the effect is dependent upon the selected hue and value [Fairchild 2005].

1.6.6 Hunt Effect

This effect obtains its name from the study of light and dark adaptation on color perception by Hunt in 1952 [Hunt 1952]. According to the Hunt study, the colorfulness of a given stimulus increases with an increase in luminance level. In other words a test stimulus of low colorimetric purity can match a reference stimulus with high colorimetric purity and low luminance level if the luminance of the test target is increased. As an example, objects observed in a bright summer afternoon appear more vivid than viewing them at dusk. An image viewed under a bright viewing condition appears more colorful than viewing it at a low luminance level.

1.6.7 Stevens Effect

Steven and Stevens in 1963 published a study in which observers were asked to perform magnitude estimations of the brightness of stimuli across different adapting conditions [Stevens 1963]. The results showed that there is a power relationship between perceived brightness and measured luminance. If the perceived brightness and measured luminance are plotted on a log-log scale, a straight line is obtained. Typical results from Stevens' experiments are presented in Figure 1-7 [Fairchild 2005].

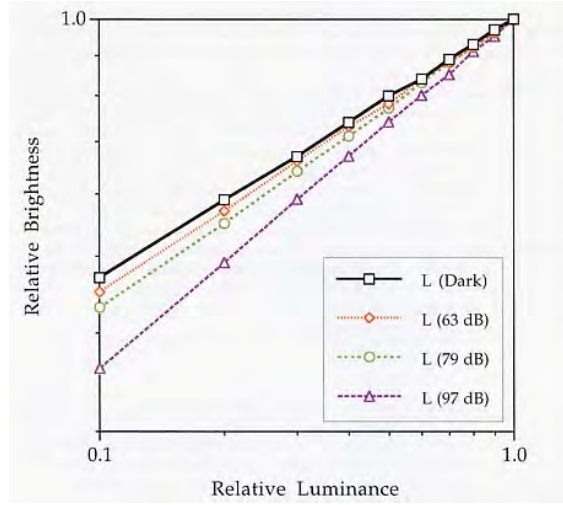


Figure 1-7. Changes in lightness contrast as a function of adapting luminance according to the Stevens effect [Fairchild 2005].

The Hunt effect refers to the increase of chromatic contrast with an increase in luminance while the Stevens effect refers to an increase in brightness (or lightness) contrast with an increase in luminance. A black-and-white image is a good example for explaining this effect. A black-and-white image has a low contrast at a low level of illumination (since white areas do not appear very bright and dark areas do not appear very dark). If the same image is viewed under a significantly brighter condition, then the white areas appear substantially brighter and dark areas appear darker and hence the perceived contrast increases.

1.6.8 Bartleson-Breneman Effect

The experimental results by Bartleson and Breneman, obtained by matching and scaling experiments, showed that the perceived contrast of an image increases with increase of the surround luminance [Bartleson 1967]. In other words, change of surround from dark to light increases images contrast. While the Stevens effect shows changes of perceived contrast with changes of luminance level, the Bartleson and Breneman experiments showed that changes in surround luminance also could cause changes of perceived contrast. Bartleson has published equations that predict their experimental results quite well [Bartleson 1975]. The experimental results by Bartleson and Breneman are consistent with historical requirements for optimum image tone reproduction for photographic transparencies viewed in the dark surround. Transparencies are made physically to a higher contrast in order to counteract the reduction of perceived contrast induced by the dark surround. Figure 1-8 illustrates the predictions of perceived lightness as a function of relative luminance for various surround luminance values [Fairchild 2005].

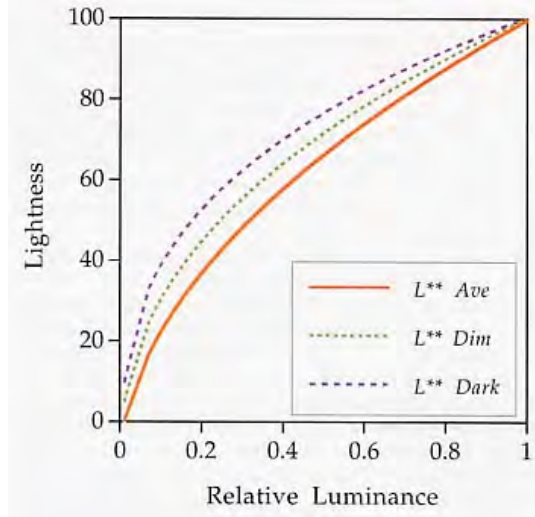


Figure 1-8. Change in lightness contrast as a function of surround relative luminance according to the results of Bartleson and Breneman [Fairchild 2005].

1.6.9 Size Effect on the Color of Uniform Patches

In architecture, a small sample, which is offered as an aid in selecting a paint color, does not exactly match the color appearance of the finished exterior and interior surfaces.

Anter [Anter 2000] has conducted outdoor observations to investigate the effect of size and viewing conditions on the color perception of facades. In an experiment by Xiao and coworkers [Xiao 2003], performed to specify the color appearance of a room, eleven colors were selected and used to paint all four walls of the room. Two light sources were used to illuminate the room, a D65 simulator and typical office lighting (CWF). For each light source, the color appearance of the target wall was matched with a calibrated CRT display and then measured by a spectroradiometer (referred to as CMM in Figure 1-9). In

a similar setup, small chips from an NCS Color Atlas were observed in a viewing cabinet (referred to as CMV in Figure 1-9). An increase of lightness and chroma were reported when the physical size changes from a small chip or a patch on the monitor to room size. Little or no effect on hue attribute was found. Figure 1-9 presents results of these experiments for lightness, chroma, and hue.

In another experiment by Xiao and coworkers [Xiao 2004], ten paint colors were selected to make samples of different sizes. Samples with sizes varying from 2° to 50° viewing fields were used in two viewing conditions to investigate the change of color appearance due to the size effect. Regardless of scaling techniques and viewing conditions used in the experiment, an increase of lightness and chroma, but no effect on hue, were reported for an increase in sample size. Figure 1-10 shows relationship between two samples with sizes of ($\sim 22^\circ$) and ($\sim 50^\circ$) for lightness, chroma, and hue.

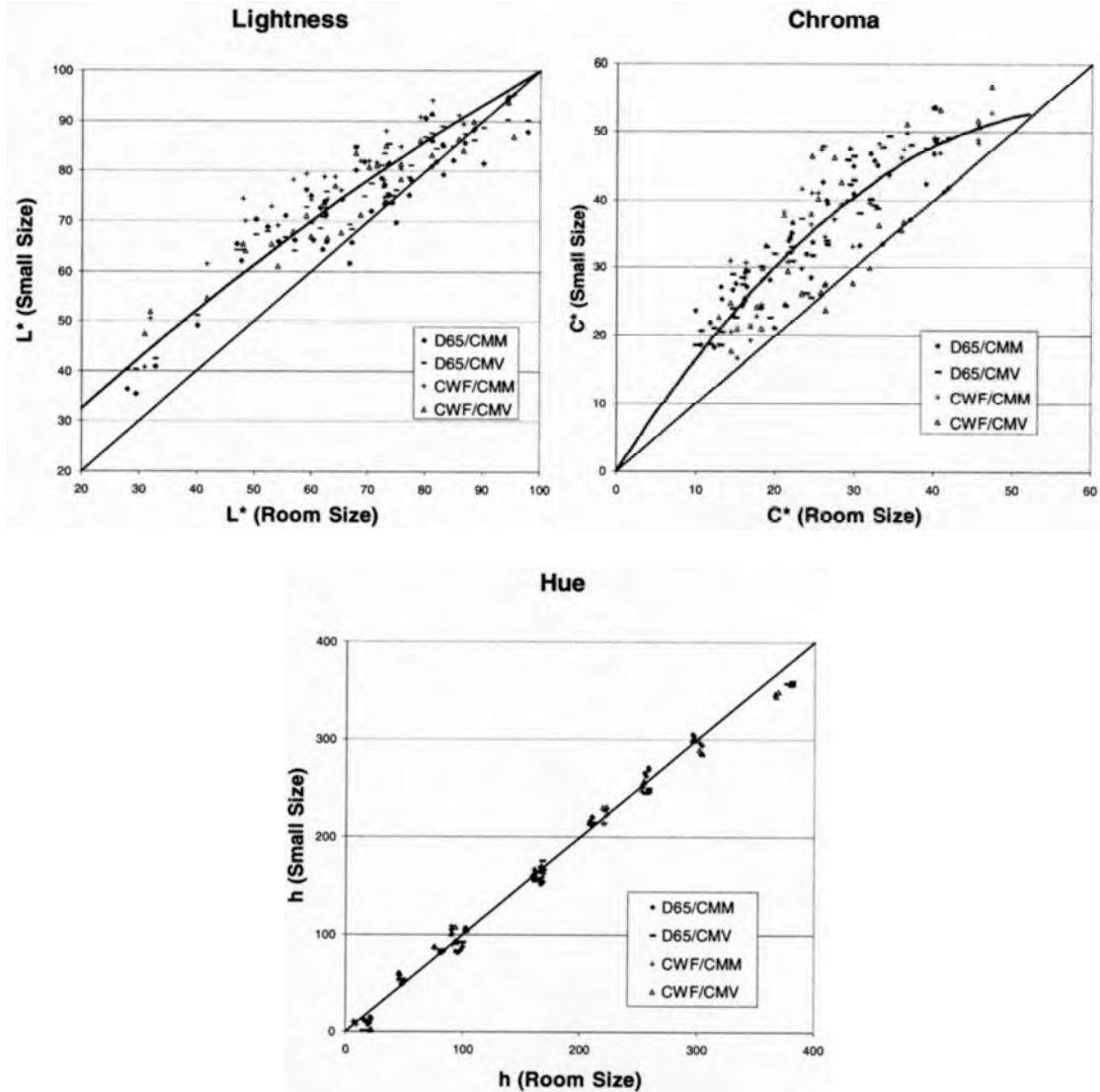


Figure 1-9. Relationship between small and room size colors in CIELAB for lightness, chroma, and hue. [Xiao 2003].

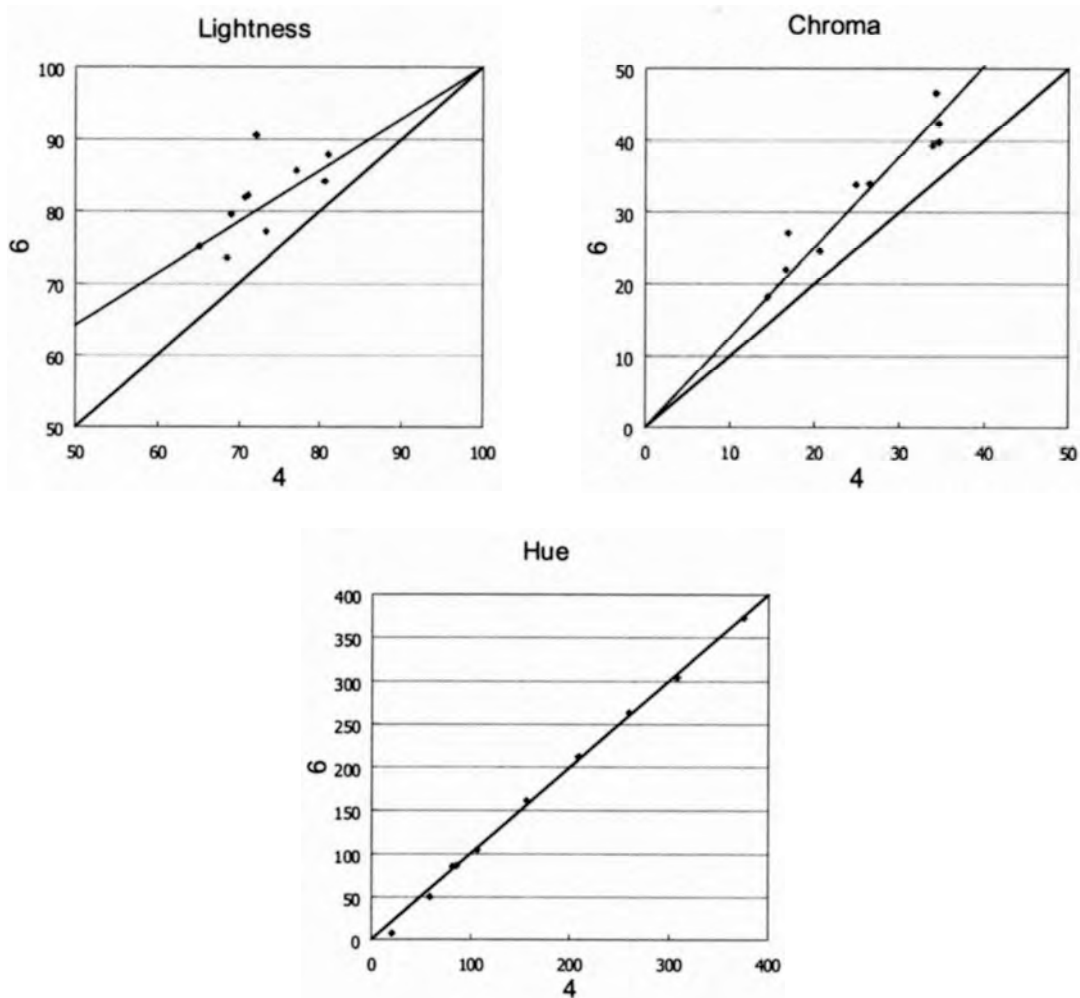


Figure 1-10. Relationship between two samples with sizes of (~22° indicated as 4) and (~50° indicated as 6) for lightness, chroma, and hue. [Xiao 2004].

1.7 Color Appearance Models

Color appearance models produce mathematical scales that correlate with the attributes of visual sensation, as defined in Section 1.5. These models extend CIE colorimetry by including information about viewing conditions such as illumination level, surround and

adaptation state. All color appearance models have a chromatic adaptation transformation and a perceptual color space. The chromatic adaptation transformation converts color coordinates of a stimulus, CIE XYZ, to some form of canonical tristimulus values after accounting for adaptation. The adaptation transform is used to calculate a corresponding color across changes in adaptation but for the prediction of appearance correlates we also need a color space component. The color space component of a color appearance model transforms the adapted cone signals into dimensions representing brightness, lightness, colorfulness, chroma, saturation, and hue.

The CIELAB color space is a very simple prototype example of a color appearance model. There are different varieties of color appearance model available and good reviews have been published [Fairchild 2005, Hunt 1995, Moroney 2002]. There have been CIE technical committees established to study, develop and recommend a color appearance model for digital color management. The CIECAM97s and CIECAM02 are two important examples of color appearance models proposed by CIE technical committees TC1-34 and TC8-01.

In summary, the CIECAM97s model converts input XYZ values to Bradford primaries and then a non-linear chromatic adaptation transform is applied to the data and the outputs are converted to Hunt-Pointer-Estevez cone signals. Perceptual attribute correlates are derived from the final responses and calculated by some hyperbolic non-linear post-adaptation response compression functions [Moroney 2002].

The CIECAM02 was designed to overcome three major drawbacks of CIECAM97s, which are over prediction of chroma for near neutral colors, poor prediction of saturation, and large variation of the predicted saturation for colors with different luminance factors but with the same chromaticity [Li 2002]. It was shown that the new CIECAM02 model overcomes the three drawbacks of the CIECAM97s model and has a performance as good as, or better than CIECAM97s [Li 2002].

Color appearance models have evolved for over 20 years and they are now capable of predicting appearance attributes of spatially simple stimuli; however for applications dealing with more spatially complex stimuli a new generation of color appearance models, indeed image appearance models, are needed. Traditional color appearance models deal with uniform color patches and do not account for spatial variation in the stimuli. The CIECAM97s and CIECAM02 are two examples of such models. On the other hand the vision models developed for image quality purposes largely ignore color [Daly 1993, Lubin 1993]. There are some exceptions such as the Retinex model [Land 1986, Land 1964, Land 1971, McCann 1976] and its derivatives [Funt 2000, Barnard 1997, Brainard 1986]. The spatial ATD model [Granger 1993] and the S-CIELAB model [Zhang 1996] also address spatial issues to some extent. The spatially variable mechanisms of chromatic adaptation and color constancy in the Retinex model serve the same purposes in image rendering applications that an image appearance model is intended to do. The iCAM model, developed for still images, integrates different research areas of image quality evaluation, image rendering, and image appearance

modeling into a single model [Fairchild 2005]. The iCAM model is explored in more detail in the following section.

1.8 Image Appearance Model

The iCAM model was developed with objectives of keeping capabilities of traditional color appearance models with additional considerations of spatial vision attributes and color difference metrics. The simplicity of the model was also one of the other considerations in its development.

Figure 1-11 presents a flow chart of iCAM for a simple stimulus. This flow chart is like the approach of traditional color appearance models. In the first step the tristimulus values, XYZ, of the stimulus and adapting white point are converted to RGB values by a (3x3) matrix multiplication. The RGB values are transformed to adapted signals using the von Kries adaptation transform embedded in CIECAM02 [CIE8-TC01]. Then the adapted signals are transformed to the IPT color space. The IPT color space has accurate constant hue contours and is discussed in the Section 1-9. The adapting and surround luminance information are used to calculate the F_L factors, which in turn are used to apply nonlinearity and response compression in the calculation of IPT coordinate values. Lightness, chroma, and hue predictors are computed by rectangular-to-cylindrical transformation of IPT coordinates. The adapting luminance is used to calculate colorfulness and brightness from lightness, chroma, and hue predictors,

Figure 1-12 presents the iCAM flowchart for more complex stimuli. In this version of iCAM, the stimulus is an image and the adapting stimulus is a low-pass image of the luminance channel of the original image. The degree of blurring of the adapting field image is dependent on application and desired results. In a very extreme case, this low-pass image can be the mean value of the pixels of the original image. The surround is a low-pass image of the luminance channel of a larger spatial extent.

Depending on the application, one can transform the adapted RGB values to linear IPT coordinates (before exponential transformation) and perform spatial filtering or apply contrast sensitivity functions to eliminate spatial frequencies that are too high to be perceived, and then back to the adapted RGB values. A set of exponential non-linearities is used in the calculation of IPT color coordinates. The exponents at this level can be modified by the adapting field image or the surround image. This is applied by multiplication of exponents by the computed F_L factors based on the surround and adapting field. The application of spatially varying exponents in the IPT space takes into account the spatial effects of surround and adapting field and enables the model to predict the Hunt, Stevens, and Bartleson-Breneman effects. The IPT coordinates are transformed to image-wise appearance correlates, lightness (J), chroma (C), and hue (h) by a transformation from a rectangular coordinate system to a cylindrical coordinate system. Colorfulness and brightness are calculated using J , C , h , and the adapting luminance information for each pixel of the image [Fairchild 2003, Fairchild 2005].

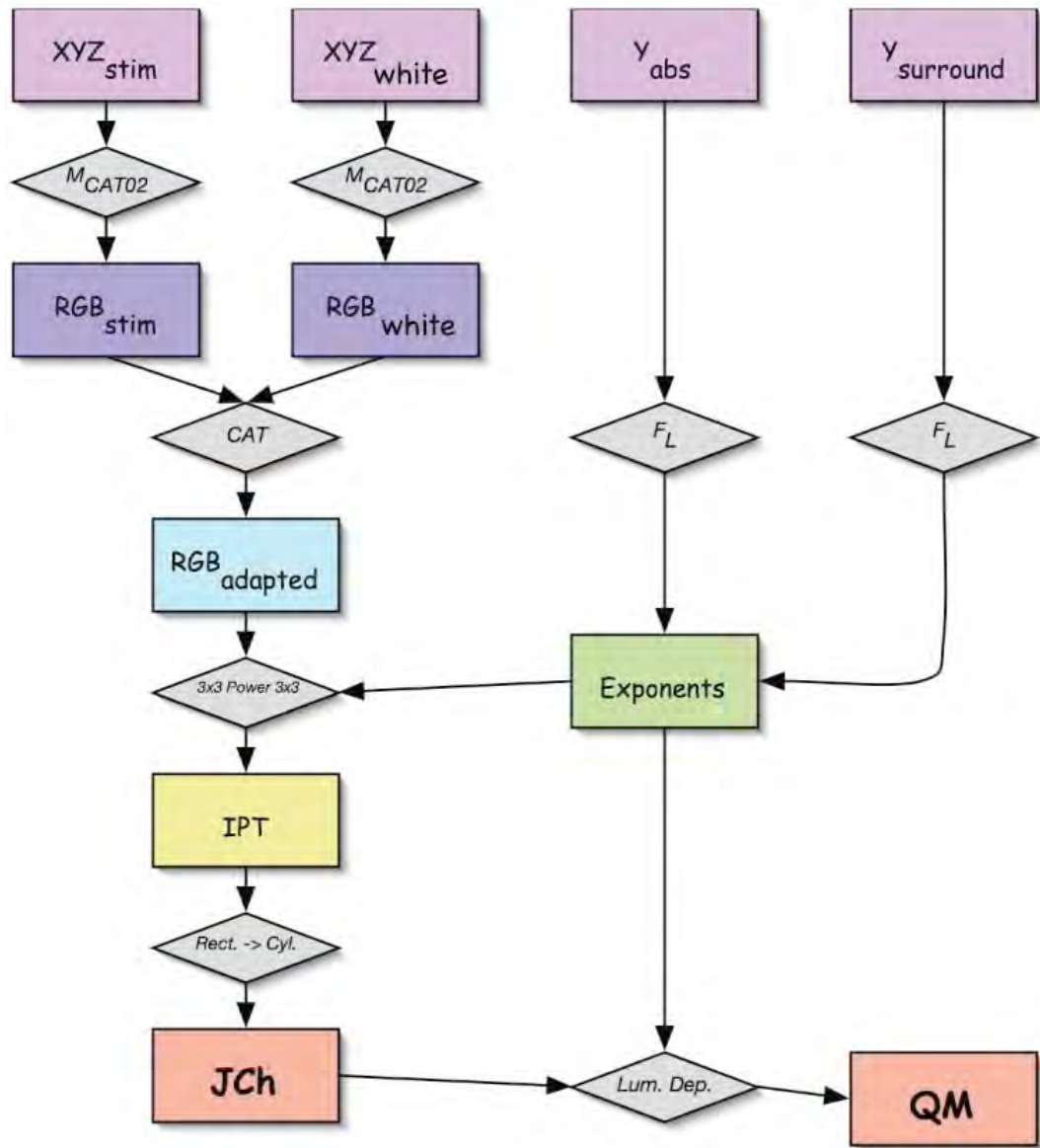


Figure 1-11. The iCAM flow chart for simple stimulus (or a single pixel) [Fairchild 2002].

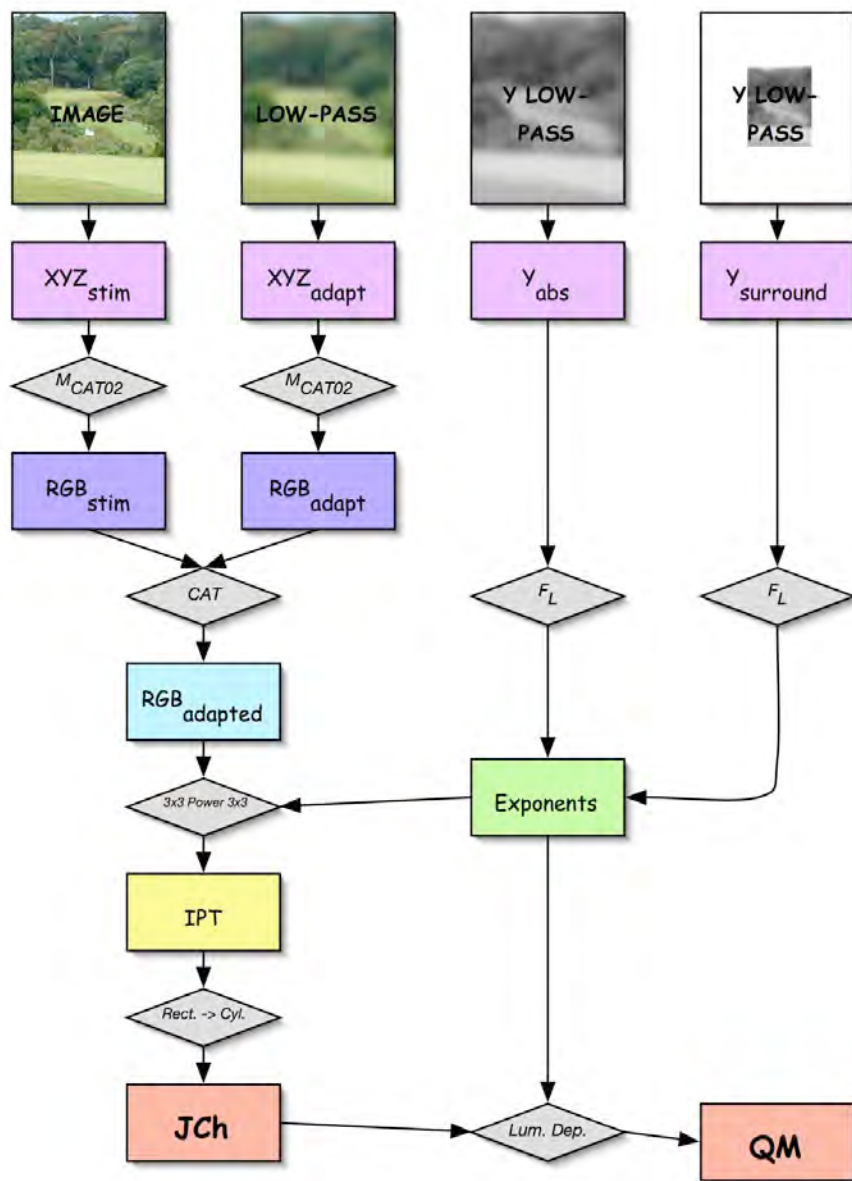


Figure 1-12. The iCAM flow chart for spatially complex stimuli [Fairchild 2002].

1.9 IPT Color Space

The input to this model is CIEXYZ values for the 1931 2-degree observer under D65 illuminant and the outputs are three IPT coordinates [Ebner 1998]. The name of IPT color space has some degree of relationship to the meaning of its dimensions: I was chosen for intensity, P was chosen for protan that is dominated by red for the red-green dimension. For blue-yellow dimension T was selected that is reminding of tritan.

The most important attribute of this color space is the linearity of constant hue lines. It is a simple model to implement and is invertible. The tristimulus values under D65 are the input to the model and are multiplied by a (3x3) matrix and transformed to the cone response space, LMS. Using exponential functions the LMS signals are properly compressed and the calculation is followed by another (3x3) matrix multiplication, which results in the I, P, and T coordinates. The parameters and computation process are shown in matrix form in equation set (1-1) to (1-8):

$$\begin{bmatrix} L \\ M \\ S \end{bmatrix} = \begin{bmatrix} 0.4002 & 0.7075 & -0.0807 \\ -0.2280 & 1.1500 & 0.0612 \\ 0.0 & 0.0 & 0.9184 \end{bmatrix} \begin{bmatrix} X_{D65} \\ Y_{D65} \\ Z_{D65} \end{bmatrix} \quad (1-1)$$

$$L' = L^{0.43}; L \geq 0 \quad (1-2)$$

$$L' = -(-L)^{0.43}; L \leq 0 \quad (1-3)$$

$$M' = M^{0.43}; M \geq 0 \quad (1-4)$$

$$M' = -(-M)^{0.43}; M \leq 0 \quad (1-5)$$

$$S' = S^{0.43}; S \geq 0 \quad (1-6)$$

$$S' = -(-S)^{0.43}; S \leq 0 \quad (1-7)$$

$$\begin{bmatrix} I \\ P \\ T \end{bmatrix} = \begin{bmatrix} 0.4000 & 0.4000 & 0.2000 \\ 4.4550 & -4.8510 & 0.3960 \\ 0.8056 & 0.3572 & -1.1628 \end{bmatrix} \begin{bmatrix} L' \\ M' \\ S' \end{bmatrix} \quad (1-8)$$

where L, M, and S are cone response and XD65, YD65, and ZD65 are input tristimulus values for CIE 1931 and illuminant D65. As can be seen from equation set (1-1) to (1-8), the exponent in the power function is almost identical to that of the RLAB color space model for average surround conditions [Fairchild 1996]. It has been shown that perceived hue in this color space is more uniform than other available color spaces at that time [Ebner 1998]. Since it is simple, invertible, and uniform, it is a suitable choice for imaging applications.

1.10 Device-Independent Color Imaging System

Figure 1-13 presents the conceptual process of a device-independent color imaging system [Fairchild 2005]. The process starts with the colorimetric characterization of an input device. The relationship between input parameters of a particular device, such as RGB digital counts in a CRT monitor, and the corresponding output in the intended color space, for example XYZ, is established in the characterization process. The mapping from input digital coordinates to colorimetric coordinates usually includes some linear and non-linear transformations that can be applied as lookup tables and rotation matrices.

The characterization process also includes some computations that are specific to the particular device such as black-level estimation in CRT displays and inclusion of the forth channel in digital light projectors. Berns has reviewed a generic approach to color modeling [Berns 1997]. There is an abundance of research in the characterization of different devices [MCSL 2005, Bala 2002].

The outputs from the device forward model, the color coordinates in the device-independent color space, are fed to the color appearance model. Indeed, the image appearance model is a better choice than the color appearance model as it also accounts for spatial and temporal aspects. Up to this stage, the initial input is transformed to an image in the viewing-condition-independent space. The image reproduction starts by gamut mapping and tone mapping, which reflect the limitations and capabilities of the reproduction device. Depending on the specifications of the output device, such as resolution and noise level, additional spatial processes are applied. In the reverse process, the image is pushed through the color appearance model to adjust for reproduction viewing conditions and then processed by the inverse model of the reproduction device to generate the output image.

The International Color Consortium (ICC) provides a standardized framework for the imaging industry and implements device-independent. Berns described the standardization of different components in a well color-managed open architecture system as the standardization of software, hardware, illuminating and viewing conditions, measurement geometries, a color appearance model, reference medium, encoding space,

and quality metrics [Berns 2000]. A flowchart of the ICC approach is shown in Figure 1-14. A profile connection space (PCS) is defined in ICC-based color management. A device profile transforms device-dependent encoding into the device-independent encoding in the PCS. The device profile includes three subsystems: device colorimetric characterization, color appearance modeling, and color gamut mapping.

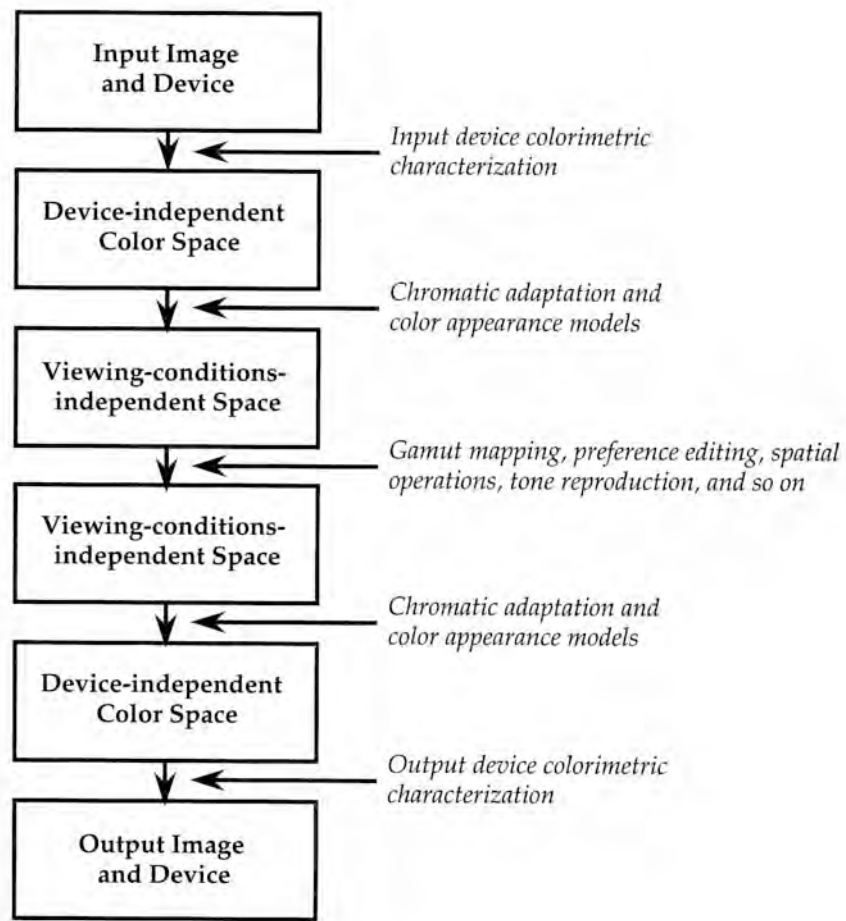


Figure 1-13. A flowchart of conceptual process of device-independent color imaging [Fairchild 2005].

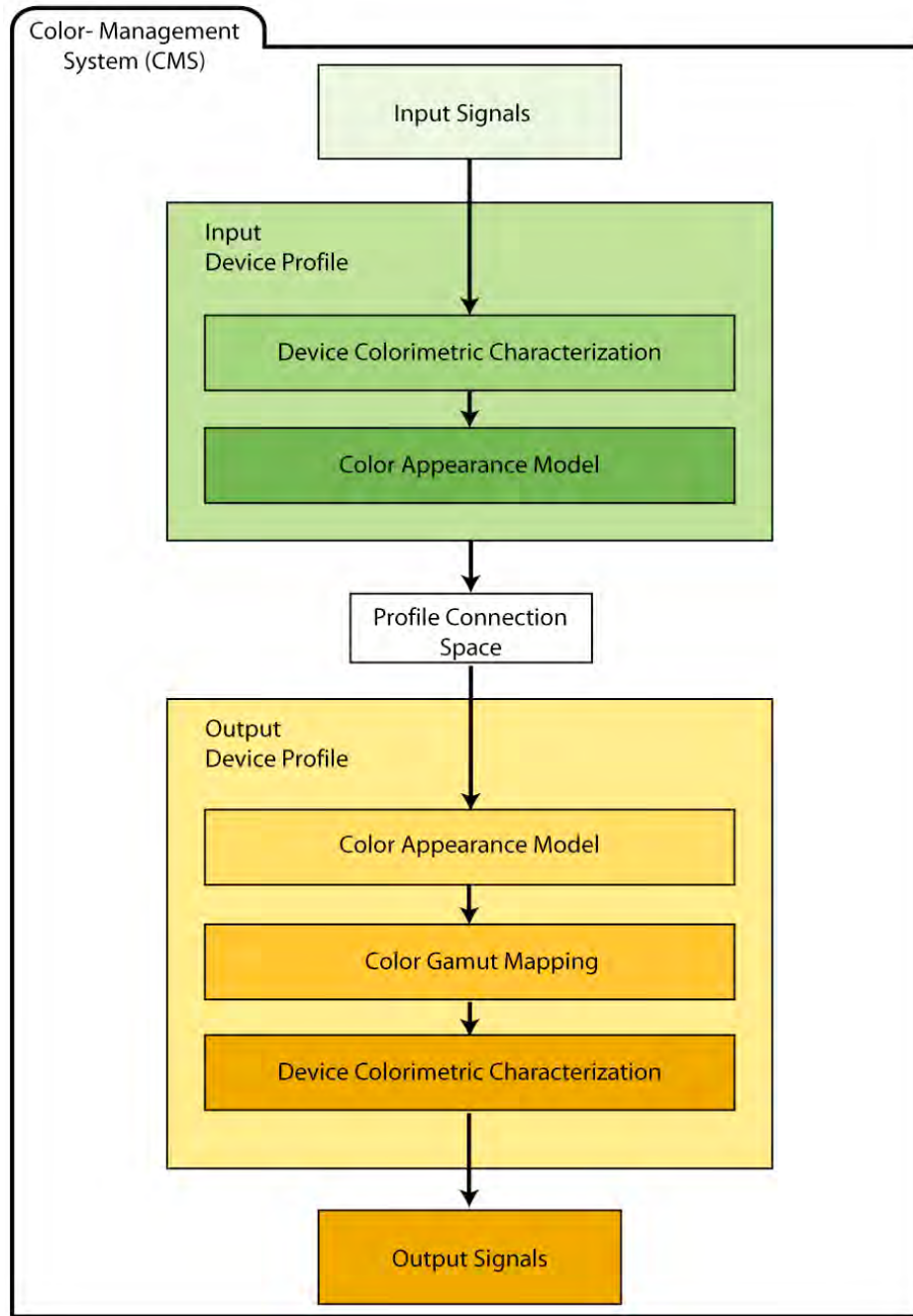


Figure 1-14. Flowchart showing the International Color Consortium (ICC) approach for color management.

Color appearance models and an image appearance model, iCAM, were described in previous sections; a short description of tone reproduction and gamut mapping is presented in the following sections.

1.11 Tone Reproduction

The final goal of a realistic tone reproduction system is to provoke the same response and sensation as an observer would have to an original scene. This idea is depicted in Figure 1-15. Two types of tone reproduction operators can be used in image rendering [Devlin 2002].

- Spatially uniform (also known as single-scale or global) operator: This type of operator applies the same transformation to every pixel of an image. The spatially uniform operator can also be a function of image content as long as it is applied to every pixel of image.
- Spatially varying (also known as multiscale or local) operator: This type of operator applies different scales to different parts of an image.

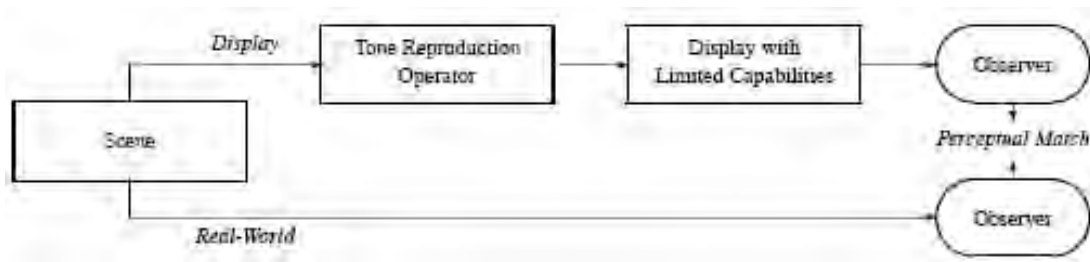


Figure 1-15. Ideal tone reproduction process [Devlin 2002].

There is another type of tone reproduction operator that accounts for temporal differences such as adaptation over time. These operators are classified as a separate category named "time dependent" tone reproduction operators. Table 1-1 presents the transformation type and a summary of some of the tone reproduction operators. In the following, more detail about single-scale tone reproduction is presented.

Table 1-1. Tone Reproduction Operators, summary of attributes [Devlin 2002].

Algorithm	Spatially			Attributes
	Uniform	Varying	Time dependent	
Oppenheim 1968		Yes		Attenuation of low frequency (HDR) data.
Stockham 1972		Yes		Extends Oppenheim, et al. Using a visual model.
Miller 1984	Yes			Uses perceptual data.
Upstill 1985	Yes			Uses perceptual model.
Tumblin 1993	Yes			Uses perceptual model. Preserves brightness. Does not preserve visibility or account for adaptation. Grey scale only.
Chiu 1993		Yes		Preserves local contrast. Ad hoc. Computationally demanding.
Ward 1994	Yes			Uses perceptual model. Preserves contrast - crucial for predictive lighting analysis. Clipping of very high and very low values. Does not consider complexities of typical workplace viewing.
Schlick 1994		Yes		Speed and simplification of uniform and varying operators.
Ferwerda 1996	Yes		Yes	Uses perceptual model. Accounts for changes in threshold visibility, color appearance, visual acuity and sensitivity over time. Useful for immersive displays.
Larson 1997	Yes			Uses perceptual model. Histogram adjustment. Preserves local contrast visibility. Uses models for glare, color sensitivity and visual acuity to increase perceptual realism.
Jobson 1997		Yes		Multi-scale retinex model - perceptually valid. Problems with monochrome scenes and maximum contrasts outside 24-bit RGB range.

Table 1-1 continued : Tone Reproduction Operators, summary of attributes.

Algorithm	Spatially			Time dependent	Attributes
	Uniform	Varying			
Pattanaik 1998		Yes			Multi-scale psychophysical representation of pattern, luminance and color processing resulting in increased perceptual fidelity.
Tumblin 1999a	Yes				Uses perceptual model. Layering method for static, synthetic images. Foveal method for interactive scenes.
Tumblin 1999b		Yes			LCIS method preserves subtle details.
Pattanaik 2000	Yes		Yes		Psychophysical operator with time-dependent adaptation and appearance models.
Scheel 2000	Yes				Interactive method using texturing hardware.
Durand 2000	Yes		Yes		Interactive method with time-dependent adaptation and simulation of visual acuity and chromatic adaptation.
Cohen 2001	Yes				Real-time method from HDR texture maps using graphics hardware.
Durand 2002		Yes			Uses edge-preserving filtering to decompose image, reduce contrast and preserve details.
Fattal 2002		Yes			Computationally efficient and simple operator that attenuates the magnitudes of large luminance gradients.
Reinhard 2002		Yes			Method analogous to photographic technique. Suits a wide variety of images; fast and computationally efficient.
Ashikhmin 2002		Yes			Uses simple functional perceptual model to preserve image details and absolute brightness information.

1.12 Single-scale Tone reproduction

If a scene and its reproduction are viewed under the same conditions then it is expected that they both should have the same physical tones, in other words, patches of gray colors in the reproduction should have the same luminance (amount of light) as the original scene [Hunt 1995]. Graphs of the log of the reproduced luminance plotted against the log of the original luminance are very useful in color reproduction. Since optical density (D) is widely used for reproduction and log of exposure (H) is used for the original scene, these graphs are referred as D- log H curves or characteristic curves. Such curves usually have some approximately linear section in the middle of curve and the slope or gradient of this linear part is known as gamma. There are two curved sections with a lower gradient at each side of the linear part. The curved section with lower density is known as the toe and that with higher density is referred to as the shoulder. If the reproduction is viewed in the same conditions as the original scene except for an overall shift in the level of illumination, then the reproduction density will have a linear relationship to the log of relative luminance of the scene (note that relative luminance is used instead of absolute luminance). Flare in imaging systems always has the effect of lowering gamma [Hunt 1995]. There are different sources of flare in imaging systems, for example, camera flare and viewing flare in dark tones and printer flare mostly in the light tones. In order to neutralize the effect of flare in tone reproduction, the photographic materials should have

characteristic curves that when measured without flare can counteract the decrease or increase of density caused by flare light. Figure 1-16-A illustrates an example of the characteristic curve of an actual system, which can partially counteract the effect of flare.

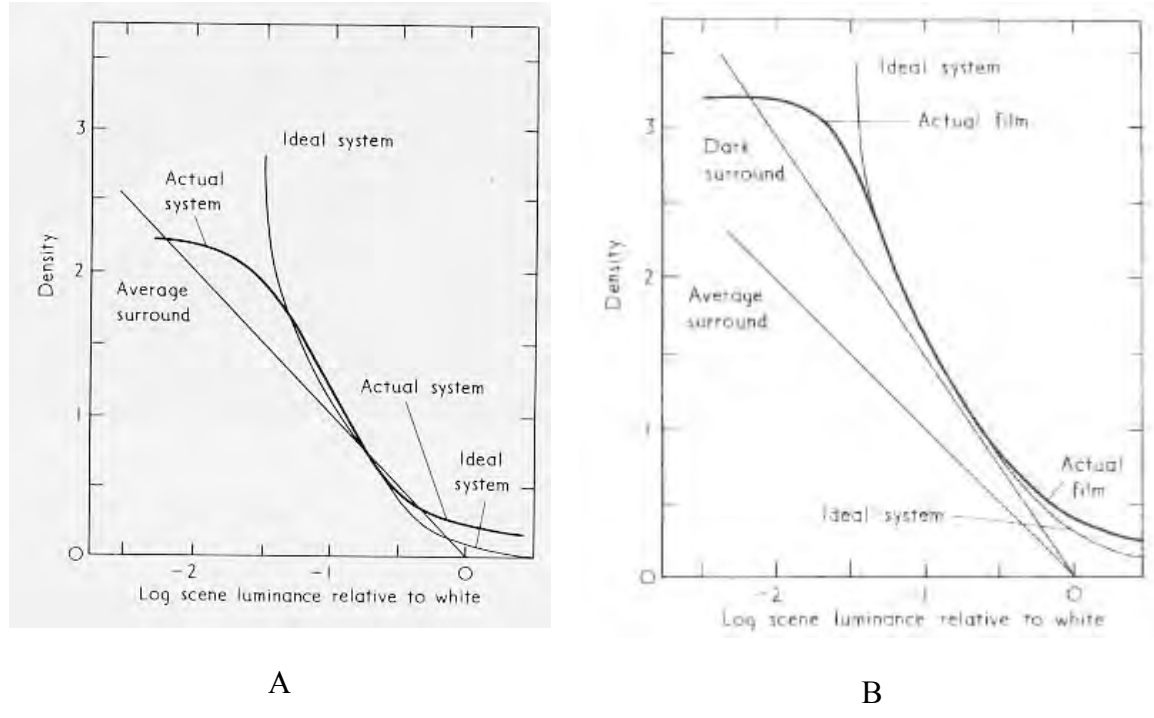


Figure 1-16. A: The curve marked ‘Actual system’ shows the characteristic of a commercially successful system used for the production of color reflection prints. B: The curve marked as ‘Actual film’ shows the characteristic of a commercially successful reversal film used for the reproduction of color transparencies intended for projection [Hunt 1995].

As mentioned in Section 1.6.8, the Bartleson and Breneman effect, the surround of an image can induce an increasing or a decreasing effect on image contrast. Transparencies projected in a dark room should have higher contrast to compensate for

the decreasing effect induced by the dark surround. Figure 1-16-B presents the characteristic curve of a photographic system that is designed for compensation of the dark surround effect on image contrast.

Television and cut-sheet transparencies have usually similar viewing conditions; both of them are viewed in a dim surround. Hence the gamma appropriate for them is less than the value recommended for dark surrounds ($\gamma=1.5$), and higher than the value of an average surround ($\gamma=1.0$). A gamma of 1.25 should be appropriate for these cases. In practice television signals are transmitted with a gamma of 1/2.2 and are displayed with a gamma of 2.8, which results in an overall gamma of approximately 1.25 [Hunt 1995].

1.13 Gamut Mapping

If all media could display the same set of colors and if there were not any image enhancement processes in the color reproduction chain then the image appearance and device characterizations would be sufficient for image reproduction [Morovic 2000]. This is not true for most of color reproduction cases, and media used in the reproduction chain have different obtainable colors.

Color gamut is defined as the range of colors produced by a coloration system [Berns 2000]. Gamut mapping, as its name denotes, is an algorithm for mapping between the gamuts of different media. Various color reproduction intents can be included in gamut mapping. The most generic reproduction intents are accuracy and pleasantness.

MacDonald [MacDonald 1993] has identified a number of the common goals in most gamut mapping algorithms. Some of those goals are the preservation of grey axis of the image, reducing the number of out-of-gamut colors, and minimization of hue shifts.

Gamut clipping and gamut compression are two major types of gamut mapping algorithms. In gamut clipping only colors outside of reproduction gamut are changed, while in gamut compression, all the colors are changed. The direction of mapping is another important feature of gamut mapping, which can be along the:

- lines of constant perceptual attributes such as lightness and hue,
- lines towards a single center-of-gravity,
- lines toward variable centers-of-gravity,
- lines towards the nearest color (minimum color difference).

For more details on gamut mapping one can review the publications of the CIE Division 8-TC03 [CIE8-TC03].

1.14 Visual Experiment Techniques

“Psychophysics” is defined as “the scientific study of the relationships between physical measurements of stimuli and the sensations and perceptions that those stimuli evoke” [Fairchild 2005]. The history of psychophysics goes back to the works of Weber, Fechner, and Stevens [Fechner 1966, Stevens 1966]. Vision is one of the human perceptions that are studied by the tools of psychophysics. The nominal, ordinal, interval,

and ratio scales are four key types of magnitude scales resulting from psychophysical experiments. The simplest type, the nominal scale, is just used to name items while ordinal scales are used to name and sort items in ascending or descending orders. The ordinal scales may or may not be spaced evenly. Logical operations such as greater-than, less-than, or equal-to can be performed with ordinal scales. The interval scale is an ordinal scale with equal intervals. There is no meaningful zero point on the interval scale. Logical operations, addition, and subtraction can be performed with interval scales. The ratio scales are interval scales with a meaningful zero point. All mathematical operations mentioned for previous scales can be performed with ratio scales. Furthermore, multiplication and division can be performed as well.

In order to minimize the influence of an observer's variability in judgment, experiments are designed in such a way that move as much control of results from the observers as possible. Two broad classes of visual experiments are presented very briefly in the following two sections. More detailed explanations can be found in Engeldrum [2000] and Fairchild [2005].

1.14.1 Threshold and Matching Experiments

These types of experiments are appropriate to measure visual sensitivity to small changes in stimuli, or sometimes referred to as a just-noticeable difference (JND). The just-noticeable change from no stimulus defines the absolute threshold. The relative or difference threshold is defined as the JND from a particular non-zero stimulus. Three

basic types of the threshold techniques are the method of adjustment, the method of limits, and the method of constant stimuli. More complex methods can be developed for specific applications [Engeldrum 2000].

In the method of adjustment, an observer adjusts the magnitude of a stimulus to a level of just perceptible or to a point that is just perceptibly different from an initial point. A major disadvantage of this method is the observer's control on the stimulus that can produce variability in the results among the observers. However, the method of adjustment is a simple and quick method and is a good choice to obtain a first estimate of a threshold.

In the method of limits, the experimenter has more control over the stimuli and presents them to the observer at predefined discrete intensity levels. The stimuli are presented in the ascending or descending levels of intensity. In an ascending series of stimuli, the experimenter begins with one stimulus that is certainly imperceptible to the observer and asks for the observer to respond (which will be "no" at the beginning). The stimuli are presented to the observer until the observer response changes from "no" to "yes". The experimenter starts with a clearly perceptible stimulus in a descending series of stimuli and continues until the observer response changes from "yes" to "no".

In the method of constant stimuli, about the intensity level of threshold, a number of levels (typically about 5 or 6) are selected. Stimuli at each of the selected levels are presented to the observer for multiple times in a random order. The frequency of perceived stimulus at each level is computed and a frequency-of-seeing curve, or

psychometric function is determined. The experiment can be performed in either a pass-fail or forced choice method. In the pass-fail or yes-no method, subjects respond “yes” if they perceive the stimulus and “no” if they do not. The threshold level is determined by the fifty percent “yes” responses. In the forced choice method, stimuli are presented in one of the two spatially or temporally separated intervals. Observers are forced to choose between two intervals and select one that has the stimulus in it. The percentage of correct responses versus the stimulus intensity is plotted (the psychometric function). The intensity level corresponding to the 75% correct responses is selected as the threshold level.

Matching techniques are designed to find the conditions when two stimuli are not perceptibly different. As an example, in the memory matching technique, an observer makes a match to a previously memorized color. Asymmetric matching is another example of a matching technique that is often used in the study of color appearance [Fairchild 2005]. In this method, a color match is made for different viewing conditions. The asymmetric matching is a common tool in study of chromatic adaptation.

1.14.2 Scaling Experiments

These types of experiment are designed to generate a relationship between the physical strength and the corresponding perceptual magnitude of a stimulus. Scaling methods can be divided into one-dimensional and multi-dimensional classes. Different scaling

techniques have been developed for the measurement of one-dimensional psychophysical scales. One-dimensional scaling experiments include the following:

Rank order: For a perceptual attribute (such as lightness), observers are asked to order a set of samples in an ascending or descending order. The collected data are averaged and an ordinal scale is derived.

Graphical rating: In the assessment of a particular attribute, observers assign to each of the presented stimulus a point on a one-dimensional graphical scale, which has defined endpoints. For example on a scale, with one end indicating black and the other end indicating white, a medium gray sample is assigned to a point in the middle of the scale. In the same way a dark gray is marked to a point closer to the black. The mean location of each stimulus on the graphical scale is taken as the interval scale for that stimulus.

Category scaling: Observers separate a large number of similar samples into various categories. The number of times that a sample is placed in each category is registered, then by using the law of categorical judgments interval scales are calculated [Thurston 1927]. The perceptual magnitudes are assumed to have a normal distribution.
Paired comparison experiment: For a small set of samples, all possible pairs of samples are made and presented to an observer. The observer is asked to select one sample in each pair that is judged greater in some attribute than the other. The proportional number of times that a sample is chosen versus the other samples is recorded. The law of

comparative judgments is used to calculate the interval scales from the proportional data [Thurston 1927, Engeldrum 2000].

Paired-Comparison: All possible pairwise combinations are presented to observers and the proportion of times that a particular sample was selected versus other samples is recorded. Thurston's Law of Comparative Judgments, Case V, are used to calculate the interval scales from the proportionality data. A 95% confidence limit can also be calculated for each interval scale. There are $n(n - 1)/2$ possible pairs for a group of n samples ($n(n - 1)/2 = \binom{n}{2} = \frac{n!}{2!(n - 2)!}$). The number of possible pairs increases rapidly as the number of sample, n , increased. Therefore, this method is suitable for a group with relatively small number of samples.

Magnitude estimation or production: In magnitude estimation observers assign a number to each sample according to the perceived magnitude of a particular attribute. In a production experiment a number is given to observers and they adjust a stimulus to have the same perceptual magnitude equal to the given number. These techniques are suitable to generate ratio scales.

Ratio estimation or production: The observers judge two or more samples and describe the ratios among them for perceptual magnitudes of an attribute. In a similar way, observers produce or select a sample that in comparison to some standards has a relative magnitude to equal to predefined ratios. This method is more complex than

magnitude estimation and because of difficulties in sample preparation and judgment, it is not suitable for practical visual experiments [Fairchild 2005].

A multi-dimensional map showing the perceptual relationship between the stimuli is generated using the multi-dimensional scaling technique. A more detailed description of this method can be found in Kruskal [1978] and Brog [1997].

1.15 Conclusions

Let us imagine an observer who is looking at a painting in a gallery as shown in Figure 1-17. Energy radiates in the form of visible radiant flux from the light source and interacts with the painting in different ways such as absorption, scattering, reflection, and fluorescence. These interactions provide external stimuli perceived by the observer's visual system. An image of the painting is focused on the observer's retina and signals generated in the photoreceptors of retina are processed through a series of neurons in the retina and other components of visual system such as the thalamus and the cortex. These extremely complex processes result in the color perception of the scene. Because of conservation and aesthetic considerations, as discussed in Section 1.2, galleries use illumination conditions that are different from the illumination conditions generally used in an office or an apartment. A color reproduction of the painting, for example a print, is usually viewed in a different viewing condition than the original conditions in the gallery. An example of such a case is shown in Figure 1-18 . Comparing Figure 1-17 and 1-18,

we can address differences in illumination conditions such as changes in spectral power distribution of light source, luminance level, and geometry of illumination. There are also changes in viewing angle (size) and surround of the painting in comparison to its reproduction. Furthermore, the painting has different surface properties than the printed reproduction. It is desired to have a color reproduction system such that its output image generates the same color perception for each pixel as the color perception of the original image. As mentioned in the previous sections, specification of the color of an image by CIEXYZ and matching tristimulus values between the original and reproduction image is very useful but it is not sufficient. There are color appearance phenomena, as presented in Section 1.6, that are not simply described by CIEXYZ. As it can be seen in Figure 1-17, color of the same kites look different due to different background, which points to the importance of the background of the stimulus. Changes in the color of the illumination (white point), illuminance level, and relative luminance of the surround are main concerns of color appearance models. Image appearance models have been evolved to include the spatial and temporal aspects of color perception. In the case of image reproduction with a size that differs from the original, for any fixation point, different backgrounds and surrounds are perceived, since the same viewing angle subtends different areas in the original and reproduction images (this is shown in Figures 1-17 and 1-18). Therefore an image appearance model that accounts for such spatial aspects is required. An example of such a model, iCAM, was described in Section 1.8.



Figure 1-17. An observer looking at a painting in a gallery. The same kites positioned at different locations of image are perceived to have different colors.

Limits and capabilities of devices used in the reproduction chain are also very important and reflected in the gamut mapping and tone reproduction processes. Depending on the specifications of the output device, such as resolution and noise level, additional spatial processes are also needed.

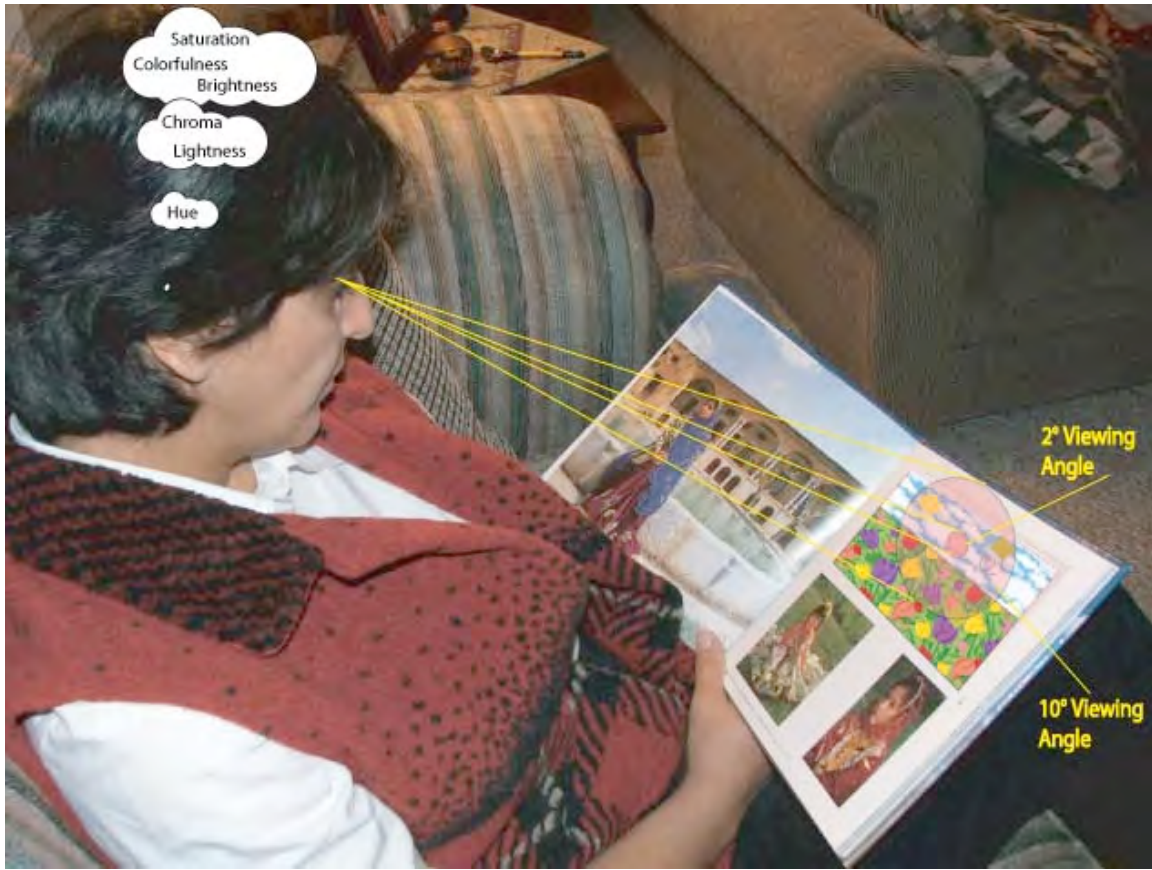


Figure 1-18. The same observer is looking at a reproduction of the painting in a different illumination and viewing conditions from the gallery conditions.

The ICC approach for device-independent color management was described in Section 1.10; we can adopt this approach and modify it as presented in Figure 1-19. In this modified version, an image appearance model replaces the color appearance model. Input signals from an input device are converted to tristimulus values for each pixel through device colorimetric characterization. The resulting values are fed to the image appearance module where localized adaptation and non-linear compression of the visual

response is applied to the image. As described in Sections 1.8 and 1.9 the iCAM model uses a uniform color space called IPT. By knowing the effect of the image size on the appearance of an image we can compensate for this effect by applying a proper transformation on each dimensions of the IPT space. The processed IPT values are pushed through the inverse image appearance model and the tristimulus values for each pixel in the output image are calculated. Color gamut mapping and other preference editing are performed in the next stage. The inverse model of device colorimetric characterization generates the output signals (digital counts for output image).

The main focus of this dissertation is to study the effect of size on the color appearance of an image and its reproduction. A series of visual experiments were performed to isolate the size effect from the other appearance phenomena and quantify its effect. The quantified effects of size were used in another series of experiments to render images with different sizes.

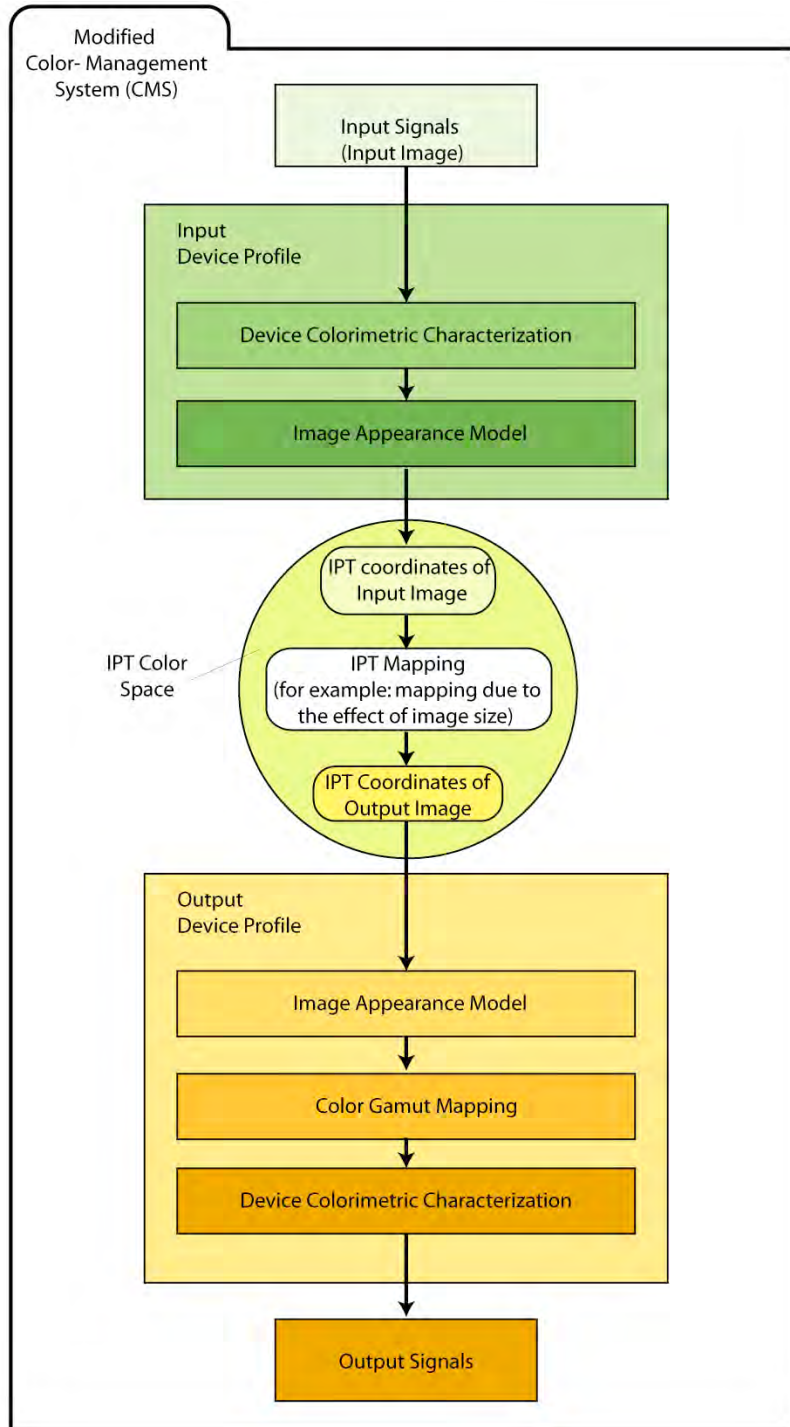


Figure 1-19. Flowchart showing the modified version of the color management system.

2 EXPLORATORY EXPERIMENT

One of the interesting differences in viewing condition is size difference. This leads to different surrounds and adaptation states. As already mentioned, in architecture, a small sample, which is offered as an aid in selecting a paint color, does not exactly match the color appearance of the finished exterior and interior surfaces. Anter has conducted outdoor observations to investigate the effect of size and viewing conditions on the color perception of facades [Anter 2000]. In an experiment by Xiao and coworkers, performed to specify the color appearance of a room, eleven colors were selected and used to paint all four walls of the room [Xiao 2003]. Two light sources were used to illuminate the room, a D65 simulator and typical office lighting. For each light source, the color appearance of the target wall was matched with a calibrated CRT display and then measured by a spectroradiometer. In a similar setup, small chips from an NCS Color Atlas were observed in a viewing cabinet. An increase of lightness and chroma were reported when the physical size changed from a small chip or a patch on the monitor to room size. Little or no effect on hue was found.

In another experiment by Xiao and coworkers [Xiao 2004], ten paint colors were selected to make samples of different sizes. Samples with sizes varying from 2° to 50° viewing fields were used in two viewing conditions to investigate the change of color appearance due to the size effect. Regardless of scaling techniques and viewing

conditions used in the experiment, an increase of lightness and chroma, but no effect on hue, were reported for an increase in sample size. Hannah made a series of paintings to demonstrate the color change due to change in observation distance [Hannah 1990, McCann 1990].

The majority of the above research has been done on uniform patches, but what are the size effects on the appearance of complex stimuli? How does size of a rendered image affect its appearance? In order to investigate the effect of size in color perception of rendered images, an exploratory visual experiment was conducted using a colorimetrically characterized digital projector and LCD. The projector and LCD are light emitting devices and in this sense are similar soft-copy media. The physical sizes of the reproduced images on the LCD and projector screen were very different. It was hypothesized that two images with the same colorimetric values for each pixel but having different physical sizes would have unequal color appearance. Thus, this experiment had several goals. The first was to evaluate how well one could control the colorimetric properties of an LCD and a DLP projector. The second goal was to develop an experimental paradigm for measuring the effect of image size on color appearance. The third goal was to test several algorithms that could compensate for image size.

2.1 Display Colorimetry

CRT, LCD, and projector displays are additive imaging systems. In theory,

$$L_\lambda = \sum_i S_i L_{\lambda,\max,i} \quad (2-1)$$

where, i counts the number of channels, L_λ is spectral radiance and S is a radiometric scalar. The ‘max’ subscript denotes the maximum output of each channel. This assumes the spectroradiometric property of each channel is scalable and each channel is independent. For a CRT display,

$$L_\lambda = RL_{\lambda,r\max} + GL_{\lambda,g\max} + BL_{\lambda,b\max} \quad (2-2)$$

where R , G , and B are radiometric scalars for the red, green, and blue channels, respectively. In colorimetric terms, Equation (2-2) reduces to:

$$\begin{bmatrix} X \\ Y \\ Z \end{bmatrix} = \begin{bmatrix} X_{r,\max} & X_{g,\max} & X_{b,\max} \\ Y_{r,\max} & Y_{g,\max} & Y_{b,\max} \\ Z_{r,\max} & Z_{g,\max} & Z_{b,\max} \end{bmatrix} \begin{bmatrix} R \\ G \\ B \end{bmatrix} \quad (2-3)$$

where X_{\max} , Y_{\max} , and Z_{\max} are the tristimulus values of each channel at maximum output. For displays that emit light when R , G , and B are at zero, Equation (2-3) becomes:

$$\begin{bmatrix} X \\ Y \\ Z \end{bmatrix} = \begin{bmatrix} X_{r,\max} - X_k & X_{g,\max} - X_k & X_{b,\max} - X_k & X_k \\ Y_{r,\max} - Y_k & Y_{g,\max} - Y_k & Y_{b,\max} - Y_k & Y_k \\ Z_{r,\max} - Z_k & Z_{g,\max} - Z_k & Z_{b,\max} - Z_k & Z_k \end{bmatrix} \begin{bmatrix} R \\ G \\ B \\ 1 \end{bmatrix} \quad (2-4)$$

where the ‘k’ subscripts represents the black-level output. This occurs commonly for CRTs set with a positive gun-amplifier offset and for devices that cannot achieve zero

emittance such as LCD's and DLP projectors. For clarity, Equation (2-4) is rewritten as Equation (2-5),

$$\begin{bmatrix} X \\ Y \\ Z \end{bmatrix} = \begin{bmatrix} X_K \\ Y_K \\ Z_K \end{bmatrix} + \begin{bmatrix} X_R^c & X_G^c & X_B^c \\ Y_R^c & Y_G^c & Y_B^c \\ Z_R^c & Z_G^c & Z_B^c \end{bmatrix} \begin{bmatrix} R \\ G \\ B \end{bmatrix} \quad (2-5)$$

where $X_R^c = X_{r,\max} - X_K$, $Y_R^c = Y_{r,\max} - Y_K$, and $Z_R^c = Z_{r,\max} - Z_K$. For many applications, displays are output devices and it is necessary to calculate the radiometric scalars for a requested tristimulus values, XYZ , shown in Equation (2-6).

$$\begin{bmatrix} R \\ G \\ B \end{bmatrix} = \begin{bmatrix} X_R^c & X_G^c & X_B^c \\ Y_R^c & Y_G^c & Y_B^c \\ Z_R^c & Z_G^c & Z_B^c \end{bmatrix}^{-1} \begin{bmatrix} X - X_k \\ Y - Y_k \\ Z - Z_k \end{bmatrix} \quad (2-6)$$

The relationship between digital signals and radiometric scalars are usually non-linear, known as devices' optoelectronic conversion function or OECF [CCIR 709]. Several models exist for CRT displays [Berns 1996, Berns 1997, Katoh 2001a, Katoh 2001b]. Models require monotonic behavior that may not occur for LCDs, consequently, lookup tables (LUTs) are created based on sub-sampling and either linear or non-linear interpolation, shown in Equation (2-7).

$$\begin{aligned} R &= \text{LUT}(d_r) \\ G &= \text{LUT}(d_g) \\ B &= \text{LUT}(d_b) \\ 0 \leq R, G, B \leq 1 \end{aligned} \quad (2-7)$$

where d denotes digital signal. For CRT and LCDs, Equation (2-6) can be used to calculate radiometric scalars [Fairchild 1998, Gibson 2000]. In this fashion, one can use

three primary ramps or an equal-digital-signal ramp (i.e., neutrals). For displays with more than three primaries, such as a DLP projector, each channel is independently measured using a photometer or one arbitrary colorimetric channel, for example

$R = (X - X_K) / X_R^c$. In practice, displays exhibit minor channel interaction, as well as theoretical limitation is each channel's chromaticity invariance with drive level. Using non-linear optimization to estimate the matrix coefficients and LUTs, one can improve performance [Berns 2003, Day 2004].

Some DLP projectors are four channel devices, Equation (2-5) becomes Equation (2-8),

$$\begin{bmatrix} X \\ Y \\ Z \end{bmatrix} = \begin{bmatrix} X_K \\ Y_K \\ Z_K \end{bmatrix} + \begin{bmatrix} X_R^c & X_G^c & X_B^c & X_W^c \\ Y_R^c & Y_G^c & Y_B^c & Y_W^c \\ Z_R^c & Z_G^c & Z_B^c & Z_W^c \end{bmatrix} \begin{bmatrix} R \\ G \\ B \\ W \end{bmatrix} \quad (2-8)$$

where W represents the white channel. Despite the four channels, DLP projectors are considered “RGB” devices since there are three input signals. Internal, and often proprietary, signal processing converts the three signals to four drive signals. Wyble and coworkers [2003, 2004] have described general signal processing, Equation (2-9).

$$\begin{aligned} R &= \text{LUT}(d_r) \\ G &= \text{LUT}(d_g) \\ B &= \text{LUT}(d_b) \\ d_w &= \min\{d_r, d_g, d_b\} \\ W &= \text{LUT}(d_w) \\ 0 \leq R, G, B, W &\leq 1 \end{aligned} \quad (2-9)$$

White is added depending on the minimum red, green, or blue signals. Wyble [2003] has shown that white is added gradually beyond a minimum signal shown in Figure 2-1 for the DLP projector used in this experiment.

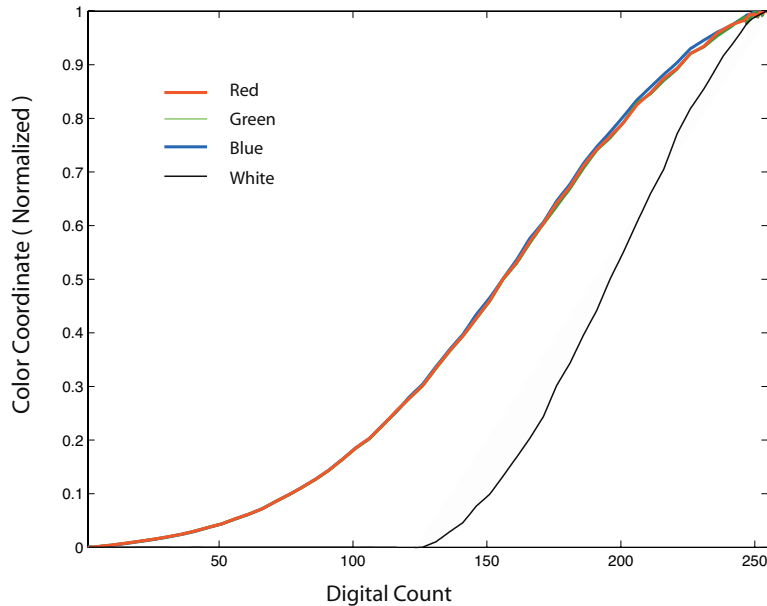


Figure 2-1. Normalized look-up tables, LUTs, for red, green, blue and white channels of the DLP projector.

Assuming that the maximum input level, $d_r=d_g=d_b=255$, is an addition of all four channels, the tristimulus values of white are calculated using Equation (2-10).

$$\begin{bmatrix} X_W^c \\ Y_W^c \\ Z_W^c \end{bmatrix} = \begin{bmatrix} X_{255,255,255}^c - (X_R^c + X_G^c + X_B^c) \\ Y_{255,255,255}^c - (Y_R^c + Y_G^c + Y_B^c) \\ Z_{255,255,255}^c - (Z_R^c + Z_G^c + Z_B^c) \end{bmatrix} \quad (2-10)$$

Unlike CRT and LCDs, the DLP projector model is not directly invertible. The DLP projector inverse model relates the requested tristimulus values to the corresponding

digital counts. At the first step, shown by Equation (2-11), requested tristimulus values, XYZ , indicated by the ‘request’ subscript, are transformed to a set of theoretical radiometric scalars, RGB , denoted by subscript ‘theo’ through a rotation matrix. The rotation matrix is the inverse of the matrix consisting of dark-corrected tristimulus values for the red, green, and blue primaries.

$$\begin{bmatrix} R \\ G \\ B \end{bmatrix}_{\text{theo}} = \begin{bmatrix} X_R^c & X_G^c & X_B^c \\ Y_R^c & Y_G^c & Y_B^c \\ Z_R^c & Z_G^c & Z_B^c \end{bmatrix}^{-1} \begin{bmatrix} X_{\text{request}} - X_K \\ Y_{\text{request}} - Y_K \\ Z_{\text{request}} - Z_K \end{bmatrix} \quad (2-11)$$

The radiometric scalars, RGB_{theo} , are called theoretical because they can exceed unity (since we were not considering any white addition up to this stage). In the next step the minimum value among the three theoretical scalars is assigned to a temporary scalar, W' , as shown in Equation (2-12).

$$W' = \min\{R_{\text{theo}}, G_{\text{theo}}, B_{\text{theo}}\} \quad (2-12)$$

This temporary scalar is mapped to the white radiometric scalar using one of the three look-up tables $wLUT_r$, $wLUT_g$, or $wLUT_b$ depending on the minimum value of the theoretical scalar determined in Equation (2-12). For example, if the green channel has the lowest theoretical radiometric scalar value among the R_{theo} , G_{theo} , and B_{theo} then $wLUT_g$, corresponding to green channel, would be used. Equation (2-13) presents look-up tables used to map the W' to the white radiometric scalar, W ,

$$W = wLUT_j(W') \quad (2-13)$$

where j is r, g, or b. The final red, green, and blue radiometric scalars are calculated from the R_{theo} , G_{theo} , and B_{theo} and white radiometric scalar, W , shown in Equation (2-14)

$$\begin{bmatrix} R \\ G \\ B \end{bmatrix} = \begin{bmatrix} R \\ G \\ B \end{bmatrix}_{theo} - \begin{bmatrix} X_R^c & X_G^c & X_B^c \\ Y_R^c & Y_G^c & Y_B^c \\ Z_R^c & Z_G^c & Z_B^c \end{bmatrix}^{-1} \begin{bmatrix} X_w^c \\ Y_w^c \\ Z_w^c \end{bmatrix} \cdot W \quad (2-14)$$

where subscript ‘R’, ‘G’, ‘B’, and ‘W’ indicate red, green, blue, and white, respectively and the ‘c’ superscript denotes dark-corrected. The computed radiometric scalars, R , G , and B are converted to digital counts using the forward look-up tables earlier described in equation (2-8) in the reverse direction.

The following steps were suggested by Wyble *et al* [2004], for creating wLUT_r look up table while green and blue were set on full and red channel was increase from 0 to 255.

1. Select a digital count, d_r , from the range of 0 to 255.
2. Calculate XYZ for the color corresponding to triplet $(d_r, 255, 255)$ using forward model, Equations (2-8) and (2-9). Maintain white radiometric scalar, W .
3. Compute theoretical radiometric values, $(RGB)_{theo}$, by substituting XYZ values from step 2 into $XYZ_{request}$ in Equation (2-11).

Repeat steps 1-3 for all digital counts in the range of [0, 255].

Construct wLUT_r using R_{theo} as the input and W as the output.

The same steps were applied to construct the wLUT_g and wLUT_b. The construction process of wLUT_r, relating R_{theo} to W , is independent of the values of d_g and d_b as long as

d_r is the minimum among the three digital counts, (d_r , d_g , d_b). A proof for this statement is as the following:

In the above procedure the d_g and d_b were set to 255 to ensure that d_r was always the minimum among the three digital counts; therefore d_w was always equal to d_r , since $d_w = \min \{d_r, d_g, d_b\}$. Scalars R and W only depended on d_r as expressed in Equation (2-8). It should be demonstrated that R_{theo} was also dependent only on R and W . Matrices \mathbf{M} , \mathbf{N} , and \mathbf{F} are defined as presented in Equation (2-15).

$$M = \begin{bmatrix} X_R^c & X_G^c & X_B^c \\ Y_R^c & Y_G^c & Y_B^c \\ Z_R^c & Z_G^c & Z_B^c \end{bmatrix} \quad N = \begin{bmatrix} X_R^c & X_G^c & X_B^c & X_W^c & X_K \\ Y_R^c & Y_G^c & Y_B^c & Y_W^c & Y_K \\ Z_R^c & Z_G^c & Z_B^c & Z_W^c & Z_K \end{bmatrix} \quad F = \begin{bmatrix} X_K \\ Y_K \\ Z_K \end{bmatrix} \quad (2-15)$$

In steps 1 through 3 using Equation (2-8), radiometric scalars, R , G , B , and W were calculated and substituted into Equation (2-9), to compute theoretical scalars, RGB_{theo} . It would be shown that calculation of R_{theo} was independent of G and B and only depended on R and W radiometric scalars. These steps combined together are expressed in matrix notation using matrices \mathbf{M} , \mathbf{N} , and \mathbf{F} in Equation (2-16).

$$\begin{bmatrix} R \\ G \\ B \end{bmatrix}_{theo} = M^{-1} \left(N \begin{bmatrix} R \\ G \\ B \\ W \\ 1 \end{bmatrix} - F \right) \quad (2-16)$$

The \mathbf{M} is a 3×3 matrix such that its inverse, \mathbf{M}^{-1} , transforms tristimulus values to theoretical radiometric scalars as described in Equation (2-12). Another way of presenting matrix \mathbf{M}^{-1} is shown in Equation (2-17),

$$\begin{aligned}
\mathbf{M}^{-1} &= \begin{bmatrix} X_R^c & X_G^c & X_B^c \\ Y_R^c & Y_G^c & Y_B^c \\ Z_R^c & Z_G^c & Z_B^c \end{bmatrix}^{-1} = \begin{bmatrix} R_X^c & R_Y^c & R_Z^c \\ G_X^c & G_Y^c & G_z^c \\ B_X^c & B_Y^c & B_Z^c \end{bmatrix} \\
\mathbf{M}\mathbf{M}^{-1} &= \begin{bmatrix} X_R^c & X_G^c & X_B^c & R_X^c & R_Y^c & R_Z^c \\ Y_R^c & Y_G^c & Y_B^c & G_X^c & G_Y^c & G_z^c \\ Z_R^c & Z_G^c & Z_B^c & B_X^c & B_Y^c & B_Z^c \end{bmatrix} \\
\mathbf{M}^{-1}\mathbf{M} &= \begin{bmatrix} R_X^c & R_Y^c & R_Z^c \\ G_X^c & G_Y^c & G_z^c \\ B_X^c & B_Y^c & B_Z^c \end{bmatrix} \begin{bmatrix} X_R^c & X_G^c & X_B^c \\ Y_R^c & Y_G^c & Y_B^c \\ Z_R^c & Z_G^c & Z_B^c \end{bmatrix} = \begin{bmatrix} 1 & 0 & 0 \\ 0 & 1 & 0 \\ 0 & 0 & 1 \end{bmatrix}
\end{aligned} \tag{2-17}$$

where R_X^c , R_Y^c , and R_Z^c are contributions of dark-corrected tristimulus values to theoretical radiometric scalar for red channel. In the same manner, (G_X^c, G_Y^c, G_z^c) and (B_X^c, B_Y^c, B_Z^c) are contributions to green and blue channels, respectively. From Equation (2-16) by distribution of \mathbf{M}^{-1} into parenthesis:

$$\begin{bmatrix} R \\ G \\ B \end{bmatrix}_{theo} = \mathbf{M}^{-1} \mathbf{N} \begin{bmatrix} R \\ G \\ B \\ W \\ 1 \end{bmatrix} - \mathbf{M}^{-1} \mathbf{F} \tag{2-18}$$

The $\mathbf{M}^{-1}\mathbf{F}$ in Equation (2-18) is a 3×1 constant matrix, which is computed from tristimulus values of black (or flare), \mathbf{F} , and inverse of rotation matrix, \mathbf{M} . The product of matrices \mathbf{M}^{-1} , \mathbf{N} , and radiometric scalars is shown in Equations (2-19) to (2-21).

$$\mathbf{M}^{-1}\mathbf{N} \begin{bmatrix} R \\ G \\ B \\ W \\ 1 \end{bmatrix} = \begin{bmatrix} X_R^c & X_G^c & X_B^c \\ Y_R^c & Y_G^c & Y_B^c \\ Z_R^c & Z_G^c & Z_B^c \end{bmatrix}^{-1} \begin{bmatrix} X_R^c & X_G^c & X_B^c & X_W^c & X_K \\ Y_R^c & Y_G^c & Y_B^c & Y_W^c & Y_K \\ Z_R^c & Z_G^c & Z_B^c & Z_W^c & Z_K \end{bmatrix} \begin{bmatrix} R \\ G \\ B \\ W \\ 1 \end{bmatrix} \quad (2-19)$$

$$\mathbf{M}^{-1}\mathbf{F} = \begin{bmatrix} X_R^c & X_G^c & X_B^c \\ Y_R^c & Y_G^c & Y_B^c \\ Z_R^c & Z_G^c & Z_B^c \end{bmatrix}^{-1} \begin{bmatrix} X_K \\ Y_K \\ Z_K \end{bmatrix} = \begin{bmatrix} R_X^c & R_Y^c & R_Z^c \\ G_X^c & G_Y^c & G_Z^c \\ B_X^c & B_Y^c & B_Z^c \end{bmatrix} \begin{bmatrix} X_K \\ Y_K \\ Z_K \end{bmatrix} = \begin{bmatrix} (R_X^c X_K + R_Y^c Y_K + R_Z^c Z_K) \\ (G_X^c X_K + G_Y^c Y_K + G_Z^c Z_K) \\ (B_X^c X_K + B_Y^c Y_K + B_Z^c Z_K) \end{bmatrix}$$

$$\mathbf{M}^{-1}\mathbf{N} \begin{bmatrix} R \\ G \\ B \\ W \\ 1 \end{bmatrix} = \begin{bmatrix} R_X^c & R_Y^c & R_Z^c \\ G_X^c & G_Y^c & G_Z^c \\ B_X^c & B_Y^c & B_Z^c \end{bmatrix} \begin{bmatrix} X_R^c & X_G^c & X_B^c & X_W^c & X_K \\ Y_R^c & Y_G^c & Y_B^c & Y_W^c & Y_K \\ Z_R^c & Z_G^c & Z_B^c & Z_W^c & Z_K \end{bmatrix} \begin{bmatrix} R \\ G \\ B \\ W \\ 1 \end{bmatrix} \quad (2-20)$$

Note that the first three columns of matrix \mathbf{N} are identical to the matrix \mathbf{M} . Therefore we

get a 3×3 identity matrix in the first three columns of the product of \mathbf{M}^{-1} and \mathbf{N} :

$$\begin{aligned} \mathbf{M}^{-1}\mathbf{N} \begin{bmatrix} R \\ G \\ B \\ W \\ 1 \end{bmatrix} &= \begin{bmatrix} 1 & 0 & 0 & R_X^c X_W^c + R_Y^c Y_W^c + R_Z^c Z_W^c & R_X^c X_K + R_Y^c Y_K + R_Z^c Z_K \\ 0 & 1 & 0 & G_X^c X_W^c + G_Y^c Y_W^c + G_Z^c Z_W^c & G_X^c X_K + G_Y^c Y_K + G_Z^c Z_K \\ 0 & 0 & 1 & B_X^c X_W^c + B_Y^c Y_W^c + B_Z^c Z_W^c & B_X^c X_K + B_Y^c Y_K + B_Z^c Z_K \end{bmatrix} \begin{bmatrix} R \\ G \\ B \\ W \\ 1 \end{bmatrix} \quad (2-21) \\ &= \begin{bmatrix} R + 0 + 0 + W(R_X^c X_W^c + R_Y^c Y_W^c + R_Z^c Z_W^c) + (R_X^c X_K + R_Y^c Y_K + R_Z^c Z_K) \\ 0 + G + 0 + W(G_X^c X_W^c + G_Y^c Y_W^c + G_Z^c Z_W^c) + (G_X^c X_K + G_Y^c Y_K + G_Z^c Z_K) \\ 0 + 0 + B + W(B_X^c X_W^c + B_Y^c Y_W^c + B_Z^c Z_W^c) + (B_X^c X_K + B_Y^c Y_K + B_Z^c Z_K) \end{bmatrix} \end{aligned}$$

Substituting Equation (2-21) into Equation (2-18) one could get Equation (2-22).

$$\begin{aligned}
\begin{bmatrix} R \\ G \\ B \end{bmatrix}_{\text{theo}} &= \begin{bmatrix} 1 & 0 & 0 & R_X^c X_W^c + R_Y^c Y_W^c + R_Z^c Z_W^c & R_X^c X_K + R_Y^c Y_K + R_Z^c Z_K \\ 0 & 1 & 0 & G_X^c X_W^c + G_Y^c Y_W^c + G_Z^c Z_W^c & G_X^c X_K + G_Y^c Y_K + G_Z^c Z_K \\ 0 & 0 & 1 & B_X^c X_W^c + B_Y^c Y_W^c + B_Z^c Z_W^c & B_X^c X_K + B_Y^c Y_K + B_Z^c Z_K \end{bmatrix} \begin{bmatrix} R \\ G \\ B \\ W \\ 1 \end{bmatrix} - \begin{bmatrix} R_X^c & R_Y^c & R_Z^c \\ G_X^c & G_Y^c & G_Z^c \\ B_X^c & B_Y^c & B_Z^c \end{bmatrix} \begin{bmatrix} X_K \\ Y_K \\ Z_K \end{bmatrix} \\
&= \begin{bmatrix} R + 0 + 0 + W(R_X^c X_W^c + R_Y^c Y_W^c + R_Z^c Z_W^c) + (R_X^c X_K + R_Y^c Y_K + R_Z^c Z_K) \\ 0 + G + 0 + W(G_X^c X_W^c + G_Y^c Y_W^c + G_Z^c Z_W^c) + (G_X^c X_K + G_Y^c Y_K + G_Z^c Z_K) \\ 0 + 0 + B + W(B_X^c X_W^c + B_Y^c Y_W^c + B_Z^c Z_W^c) + (B_X^c X_K + B_Y^c Y_K + B_Z^c Z_K) \end{bmatrix} - \begin{bmatrix} (R_X^c X_K + R_Y^c Y_K + R_Z^c Z_K) \\ (G_X^c X_K + G_Y^c Y_K + G_Z^c Z_K) \\ (B_X^c X_K + B_Y^c Y_K + B_Z^c Z_K) \end{bmatrix} \\
&= \begin{bmatrix} R + W(R_X^c X_W^c + R_Y^c Y_W^c + R_Z^c Z_W^c) + (R_X^c X_K + R_Y^c Y_K + R_Z^c Z_K) - (R_X^c X_K + R_Y^c Y_K + R_Z^c Z_K) \\ G + W(G_X^c X_W^c + G_Y^c Y_W^c + G_Z^c Z_W^c) + (G_X^c X_K + G_Y^c Y_K + G_Z^c Z_K) - (G_X^c X_K + G_Y^c Y_K + G_Z^c Z_K) \\ B + W(B_X^c X_W^c + B_Y^c Y_W^c + B_Z^c Z_W^c) + (B_X^c X_K + B_Y^c Y_K + B_Z^c Z_K) - (B_X^c X_K + B_Y^c Y_K + B_Z^c Z_K) \end{bmatrix} \\
&= \begin{bmatrix} R + W(R_X^c X_W^c + R_Y^c Y_W^c + R_Z^c Z_W^c) \\ G + W(G_X^c X_W^c + G_Y^c Y_W^c + G_Z^c Z_W^c) \\ B + W(B_X^c X_W^c + B_Y^c Y_W^c + B_Z^c Z_W^c) \end{bmatrix}
\end{aligned}$$

(2-22)

As it can be seen from Equation (2-22), the theoretical radiometric scalar for red channel, R_{theo} , was calculated from subtraction of a constant from the product of multiplication of the first row of the 3×5 matrix by elements of a vector matrix consisted of R , G , B , W , and unity; since G and B were multiplied by zero in this computation, the R_{theo} was only dependent on R and W . It has been demonstrated that the R_{theo} was independent of values of G and B and consequently independent of d_g and d_b .

2.2 LCD Colorimetric Characterization

An IBM T221 LCD having a resolution of 3840x2400 pixels and driven by a Dual 2GHz PowerPC G5 Apple computer was characterized in a dark room and used in the visual experiment in this research. Two sets of input digital counts were generated. The first set consisted of three individual red, green, and blue channel ramps. There were 11 steps, equally spaced from 0 to 255, for each channel. The first set also included 11 neutral samples made by an equal combination of the three channels with the same interval spacing as the individual primary ramps. A second set, a grid of 125 samples, 5x5x5, was generated by regular sampling from the digital count space.

As will be described in the visual experiment, a pair of images, each 125mm × 87mm, with a 75mm gap between them, was displayed on the LCD on a black background in a paired-comparison experiment. A pair of uniform patches, with color corresponding to each element of the two sample sets, with the same size and orientation as the pair of images used in the visual experiment was displayed on a black background. Both patches were measured and averaged using a Photo Research PR650 spectroradiometer in a dark environment. The tristimulus values of red, green, and blue ramps for the 1931 standard observer were calculated from measured spectral radiance values. These tristimulus values, XYZ , were converted to radiometric scalars, RGB , using Equation (2-6). The radiometric scalars of the three ramps and corresponding digital counts were used to build three one-dimensional look-up tables, described in Equation (2-7), using linear interpolation. In the next step, digital counts of all samples (in both

data sets) were mapped to radiometric scalars using the generated look-up tables. Mapped radiometric scalars were transformed to tristimulus values as stated by Equation (2-4). The average ΔE_{00} color difference between calculated and measured tristimulus values was computed. Coefficients of the 3×4 transformation matrix of Equation (2-4) were adjusted through a nonlinear optimization process aimed to minimize the average ΔE_{00} color difference between the measured and computed tristimulus values [Berns 2003, Day 2004]. After each adjustment to the transformation matrix of Equation (2-4), the three look up tables were also updated. The radiometric scalars were constrained between zero and unity during the optimization process.

Table 2-1 lists the colorimetric results from the LCD characterization model for the identical dataset used by Day, *et al.* [Day 2004]. The colorimetric characterizations had excellent performance; the average ΔE_{00} color difference for the primary ramps was 0.4 with a maximum of 0.8 and comparable to the results reported by Day, *et al* [Day 2004]. The average ΔE_{00} color difference for all 168 samples was 0.9. The relatively small values of the 90th percentile, 0.6, and maximum ΔE_{00} color difference, 0.8, shown in Table 2-1, are evidence of an acceptable characterization process. Figure 2-2 presents the color differences histogram. It should be stated that because of the excellent forward model results and past experiences using this display in visual experiments, the inverse model was not evaluated.

Table 2-1. Summary of colorimetric characterization results for LCD display for the 1931 standard observer.

	Mean ΔE_{00}	Max ΔE_{00}	90th percentile ΔE_{00}
All Samples	0.9	2.4	1.6
Primary ramps	0.4	0.8	0.6

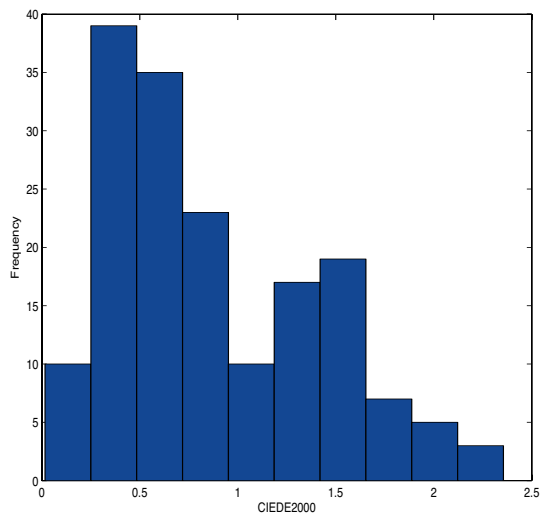


Figure 2-2. Histogram of ΔE_{00} color difference for the LCD colorimetric characterization between measured and estimated data for all 168 samples.

2.3 DLP Colorimetric Characterization

A Plus Data Projector U4-232 from Plus Vision Corp., driven by a Dual 2GHz PowerPC G5 Apple computer, was used to project a rendered version of the original colorimetric image on the screen. This projector uses Digital Light Processing (DLP) technology and had a resolution of 1024x768. We will call this projector the DLP projector through the rest of this article. The DLP projector has four primaries: red, green, blue, and white. The fourth primary has been added to increase the luminous output of this display device. It was set to its “standard mode” during both the characterization and visual experiment. Primary ramps of red, green, blue, and gray (i.e. $d_r=d_g=d_b$) were sampled with an interval of five digital counts in the range of 10 to 245 and sampling intervals of one digital count at the two ends (less than 10 and greater than 245). For each sample, a rectangular uniform patch with a size of 615x470 pixels (about 60% of screen size) was displayed on the center of the screen in the dark room and measured by a Photo Research PR650 spectroradiometer. The remainder of the screen was set to black. In addition to the primary ramps, a set of 1000 samples was similarly projected and measured. Similar to LCDs, the OECFs of the DLP projector were modeled by look-up tables; there were three look-up tables, LUTs, for red, green, and blue channels and an additional LUT for the white channel (Equation 2-9). The spectral radiance of the red, green, and blue ramps and the maximum outputs of each channel were used to calculate tristimulus values and radiometric scalars, for example $R = (X - X_K) / X_R^c$. Similar to the LCD, the radiometric

scalars were constrained between zero and unity. Analogous to LCD characterization, linear interpolation was utilized in populating the look-up tables.

The color differences, ΔE_{00} , for the 1000 samples from the projector forward model for the 1931 standard observer were calculated and Table (2-2) presents corresponding mean, maximum, and 90th percentile values. Computed mean color difference was about unity. Although the maximum color difference was 8.4, the 90th percentile value of 1.6 shows that most of the color difference values were relatively small compared to the maximum value. Figure 2-3 presents a histogram of color difference values. More inspection revealed that there were 10 samples with color difference values greater than 5 units. Because of small value of the mean color difference for the forward model the inverse model was not evaluated.

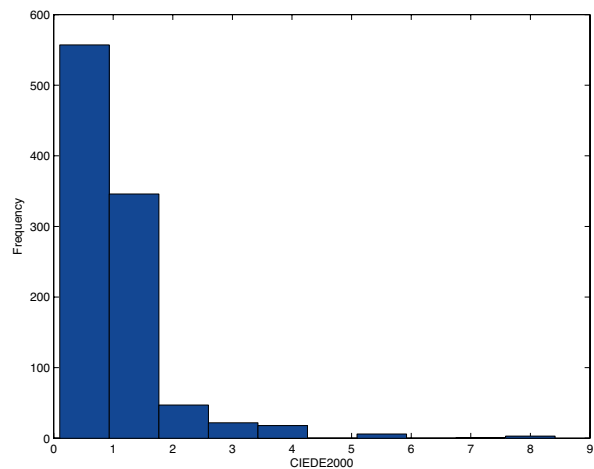


Figure 2-3. Histogram of ΔE_{00} color difference for the projector colorimetric characterization between measured and estimated data for all 1000 samples.

Table 2-2. Summary of characterization results for DLP projector for the 1931 standard observer.

Display	Mean ΔE_{00}	Max ΔE_{00}	90th percentile ΔE_{00}
Plus Data Projector U4-232	1.0	8.4	1.6

2.4 An Exploratory Visual Experiment

A colorimetric image of Georges Seurat's, "Sunday Afternoon on the Island of La Grande Jatte – 1884," was used as the experimental stimulus [Berns 2004]. It was selected because of its large size (206 cm × 305 cm), low contrast, and its spatial characteristics. The image was cropped so when projected, had the same size as the actual painting. Using the inverse models described above, the colorimetric image of the painting was rendered for the DLP display and projected on the screen in a dark environment, forming the reference image. The background and surround of the reference image were set to black. The DLP projector had more luminous power than the LCD. In order to keep the same luminance level on the LCD and projector screen, all renderings were performed using the white point of the LCD (otherwise there would be colors that the projector could generate but the LCD could not display). The physical size and resolution of the projected image on the screen were 150cm X 100cm and 1024x768 pixels, respectively. The LCD and DLP screen were positioned at a 180° angle from one

another as shown in Figure 2-4. The observer was standing 50cm from the LCD display and about 200 cm from the screen. A pair of images, each 125mm X 87mm, was displayed on the LCD with a black background. Each image consisted of 1000x700 pixels and there was a 75mm gap between the two images. As will be described in the image processing section, 10 images were prepared and all different pairs consisting of these 10 images, a total number of 45 pairs, $(10 \times 9)/2 = 45$, were generated. All pairs were presented to the observers in a random order and the observer task was to select one of the images in each pair that best matched the reference projected image. Due to the specific experimental arrangement, an observer could not see both the LCD and screen at the same time and the selection of the image was based on short-term memory matching.

Twenty observers participated in the experiment.

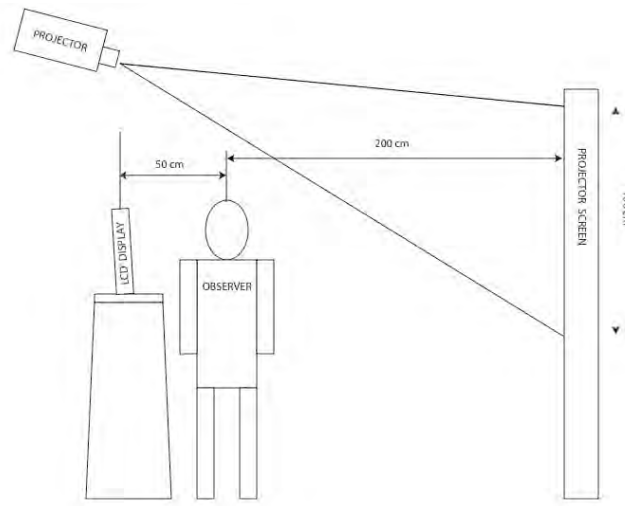


Figure 2-4. Arrangement of scene and equipment in the psychophysical experiment.

2.5 Image Processing

The original colorimetric image was encoded as 16-bit LAB TIFF. As described in the introduction section, Xiao and coworkers have reported an increase of lightness and chroma, but no effect on hue, for an increase in sample size for uniform patches [Xiao 2003, 2004]. Hence, two image attributes, lightness and chroma, were selected for further processing. The LCD white point was selected for all image rendering to maintain the same luminance level on both LCD and DLP output. Figure 2-5 presents the general flowchart of test and reference image preparation.

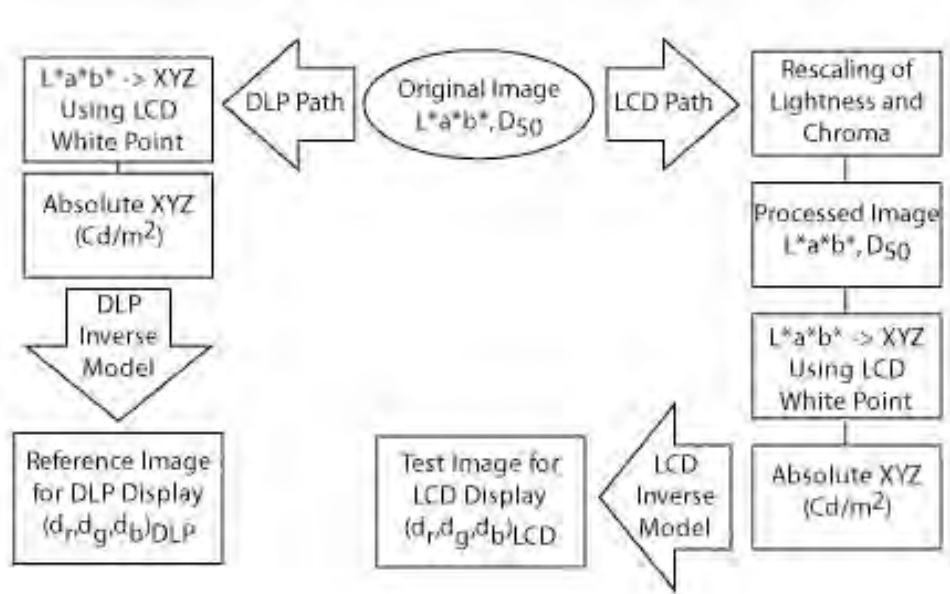


Figure 2-5. General flowchart of test and reference image preparation.

The original LAB image was converted to tristimulus values using the LCD white point. The absolute tristimulus values were transformed to digital signals through the

projector inverse model. This image was stored as the reference image and projected. For the LCD, lightness and chroma of the original LAB image were rescaled. The new images generated from the modification of lightness or chroma were converted to absolute tristimulus values and the inverse LCD model was used to calculate digital signals. Figure 2-6 shows histograms of lightness and chroma of the original colorimetric image.

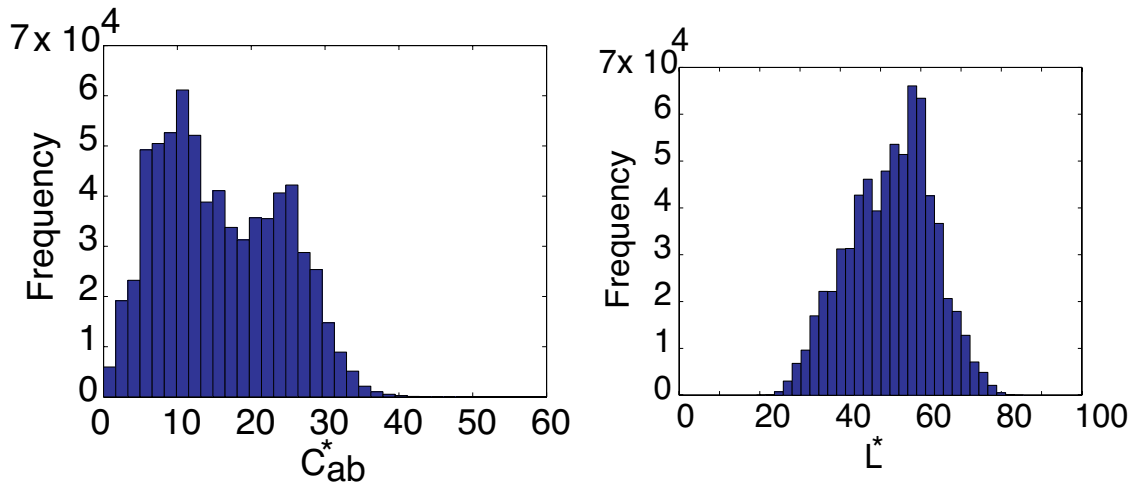


Figure 2-6. Histogram of lightness L^* , and chroma C_{ab}^* of colorimetric image.

Lightness is one of the most important attributes of an image. Linear rescaling of lightness is a simple and fast algorithm that maps input CIELAB lightness values to new output values through the following linear equation:

$$L_{out} = \frac{L_{in} - L_{mi}}{100 - L_{mi}}(100 - L_{mo}) + L_{mo} \quad (2-23)$$

where L_{in} is lightness of the input for each pixel and L_{out} is mapped lightness for the output image. (The “*” superscript is omitted for clarity.) The L_{mi} and L_{mo} are minimum lightness in the input and output images, respectively. In other words, the input range of $\{L_{mi}, 100\}$ in the source image was rescaled to the range of $\{L_{mo}, 100\}$ for the output image. For this experiment, L_{mo} was assigned to values of 10, 15, and 25, and then based on equation (2-15), three images with the same chroma and hue but different lightness values were generated. Figure 2-7 presents the transformation functions for linear rescaling of lightness and the corresponding histograms of the output images. As can be seen, the linear rescaling functions with L_{mo} equal to 10 and 15 results in images darker than the original image while the transformation with L_{mo} equal to 25 produced an image lighter than the original image.

Linear rescaling was also employed to transform chroma of the original image. In this way equation (2-15) was modified for CIELAB chroma, shown in equation (2-16):

$$C_{out} = \frac{C_{in} - C_{mi}}{C_{mxi} - C_{mi}}(C_{mxi} - C_{mo}) + C_{mo} \quad (2-24)$$

where C_{in} is CIELAB chroma values for each pixel of the original image and C_{out} is the linearly rescaled chroma. (The “ab” subscript and “*” superscript are omitted for clarity.) The C_{mi} and C_{mxi} are minimum and maximum values of chroma in the original image, respectively. The desired minimum value of chroma in the output image was assigned to the C_{mo} . The linear rescaling presented by equation (2-16) remaps the input chroma $\{C_{mi}, C_{mxi}\}$ to output range of $\{C_{mo}, C_{mxi}\}$. Figure 2-8 presents two linear rescaling

transformation functions and the resulting histograms for minimum chroma values of $C_{mo} = 1$ and $C_{mo} = 5$. As it can be seen from Figure 2-8, both linear rescaling functions increased chroma values compared to the original image.

Sigmoidal lightness rescaling is another lightness remapping strategy [Braun 1999]. This transformation function is derived from a discrete cumulative normal function as shown in equation (2-17):

$$S_i = \sum_{n=0}^{n=i} \frac{1}{\sqrt{2\pi}\sigma} e^{-\frac{(L_n - L_0)^2}{2\sigma^2}} \quad (2-25)$$

where L_0 and σ are mean and standard deviations of the normal distribution. The shape of the function is controlled by mean L_0 and standard deviation σ . The L_0 controls centering of the sigmoid and σ controls the slope of the sigmoid curve. Figure 2-9 shows two sigmoidal transformation functions and corresponding histograms with L_0 equal to 40 and σ assigned to 30 and 50. As seen from Figure 2-9, the sigmoidal rescaling with σ value of 50 remaps lightness of the original image to higher values in the output image. The sigmoidal function with σ of 30, increases L^* values between 30 and 85, while it decreases lightness for values less than 30.

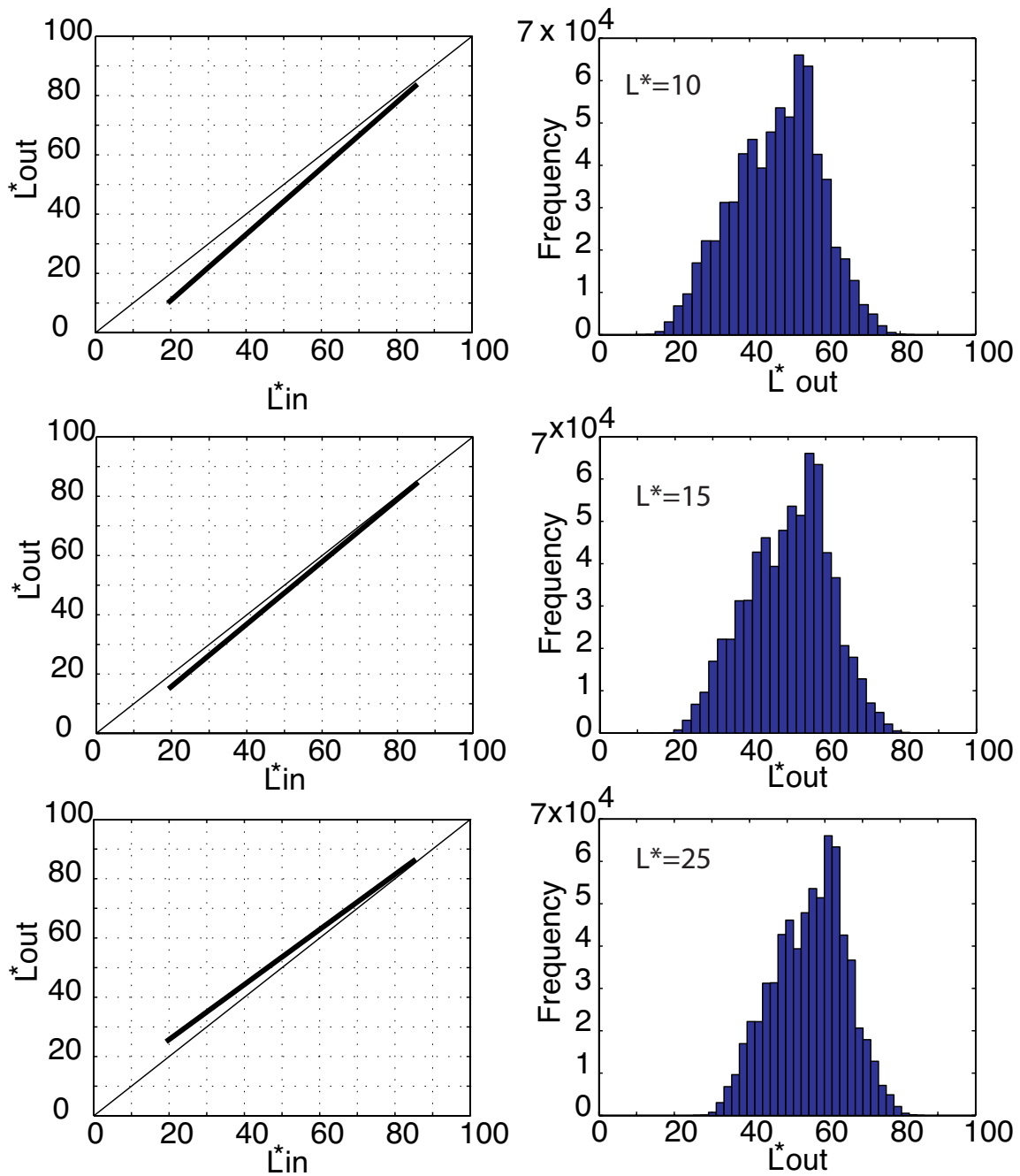


Figure 2-7. Transformation functions and corresponding histograms of linear rescaling of lightness with minimum lightness of $L^=10$, 15, and 25.*

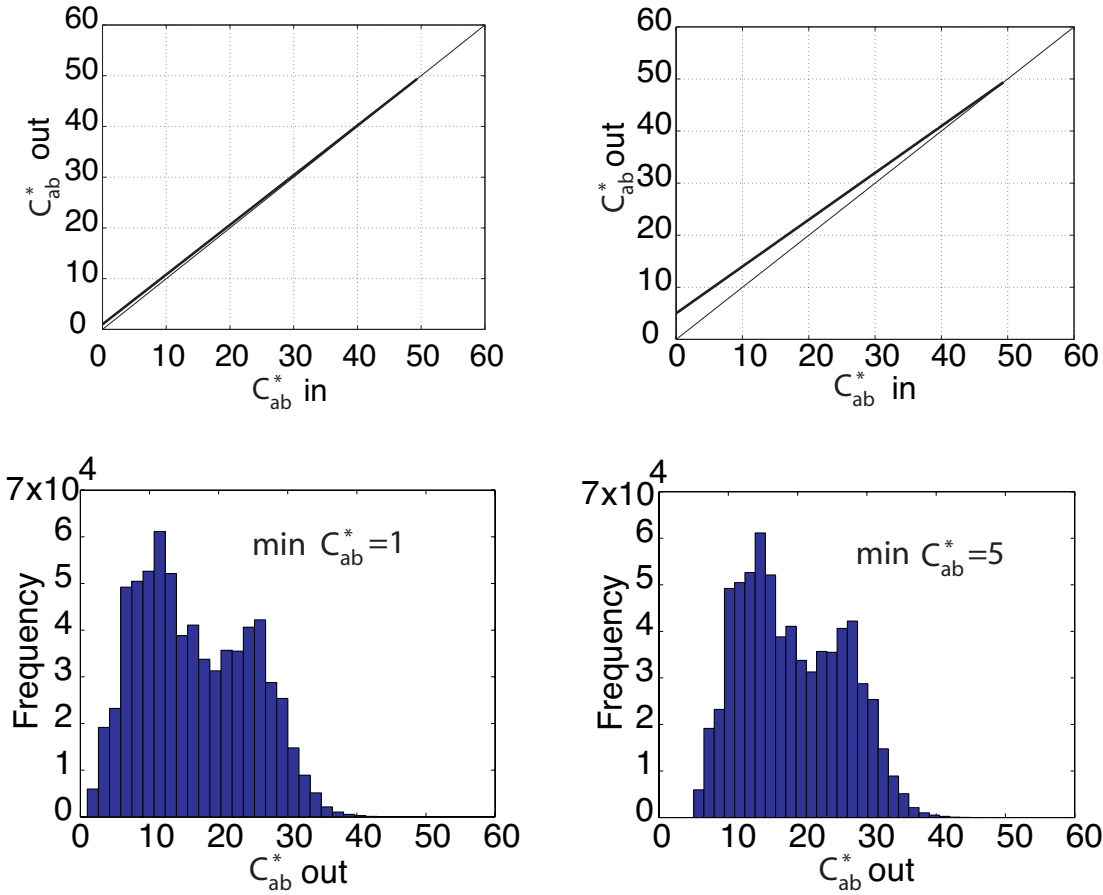


Figure 2-8. Transformation function and corresponding histogram of linear rescaling of chroma with minimum value of $C_{ab}^ = 1$ and 5.*

The CIELAB data of the original image were converted to tristimulus values (X, Y, Z) using the LCD white point. The Y values were scaled in a way that the maximum values of Y could be equal to unity and then followed by processing through a power law as shown in equation (2-18):

$$Y_o = Y_{o,\max} \left(\frac{Y_i}{Y_{i,\max}} \right)^\gamma \quad (18)$$

where Y_i and Y_o are luminance factors of input and processed images, respectively (the ‘max’ subscript denotes for the maximum). The γ is a power factor which was set to a value of 1.3 to see the effect of a nonlinear decrease of Y on the image appearance. The modified tristimulus values were converted back to CIE L*, a*, b*. Figure 2-10 shows the corresponding transformation in terms of CIE L* and the resulting histogram. This transformation had a darkening effect on the processed image. This effect was more pronounced in the lower values of lightness.

A spatial filtering was applied to the original image using Adobe Photoshop CS version 8.0. The crystallize filter with a cell size of 3 was applied to the image to produce an output image with less resolution and larger pixels. It is important to note that no color processing such as lightness or chroma rescaling were applied to this image. Therefore this image had the basic colorimetric nature as the reference image.

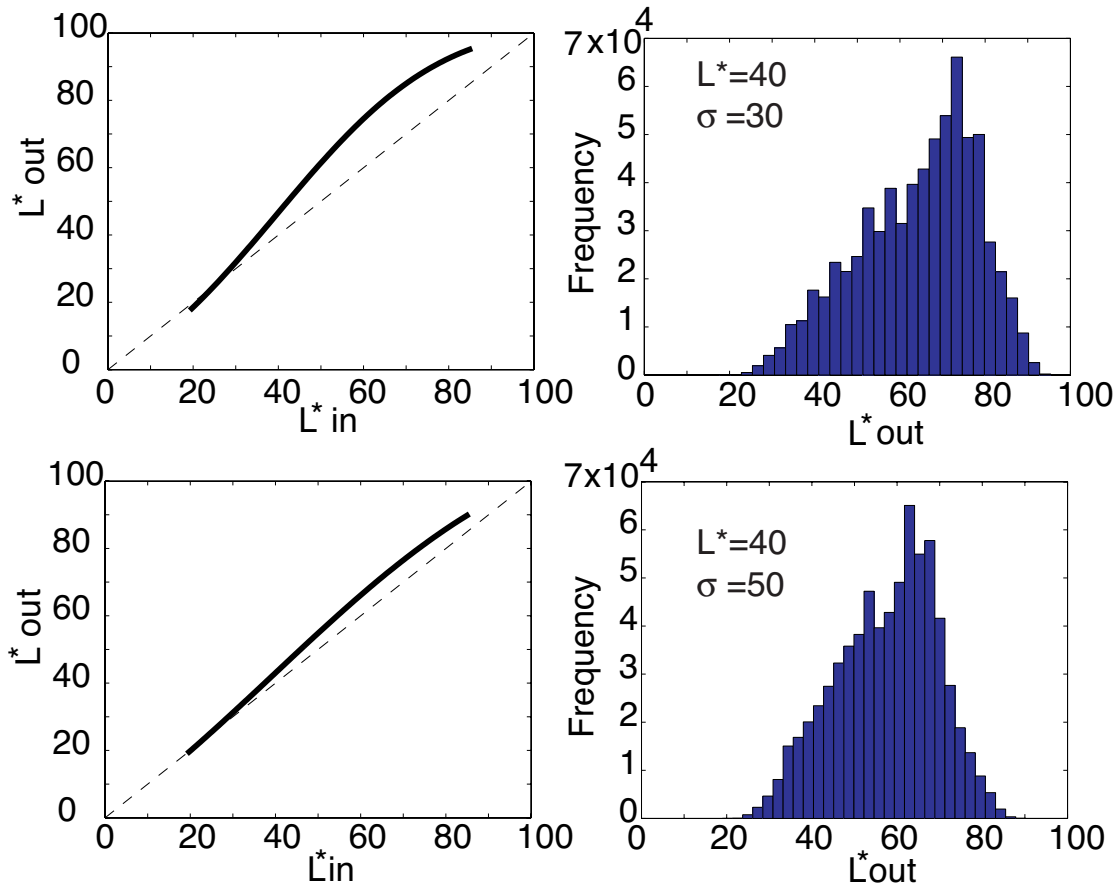


Figure 2-9. Transformation functions and corresponding histograms of sigmoidal rescaling of lightness, L^ , with mean value of $L^* = 40$ and standard deviation values of 30 and 50.*

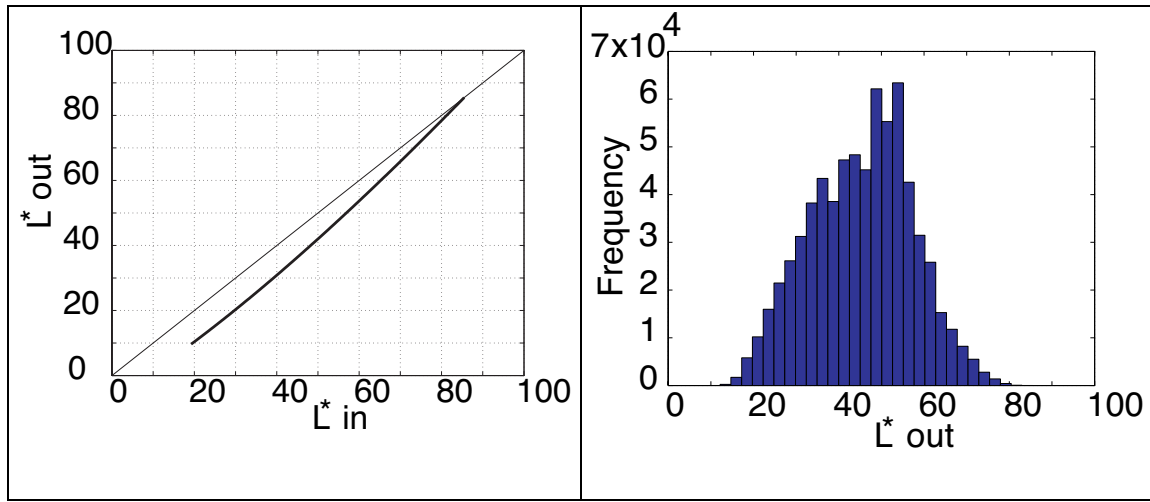


Figure 2-10. Transformation function and corresponding histogram for the power law processing ($\gamma = 1.3$).

Table 2-3 summarizes the image processing algorithms used in this research.

Images 1 through 10 will be referred in the rest of this article as described in Table 2-3.

In order to present the effect of each processing algorithm, a portion of images processed by the different algorithms are shown in Table 2-3.

Table 2-3. Summary of image processing algorithms.

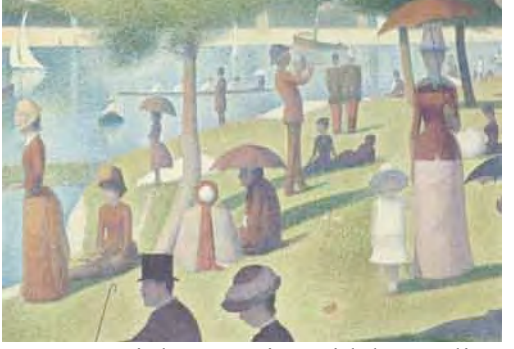
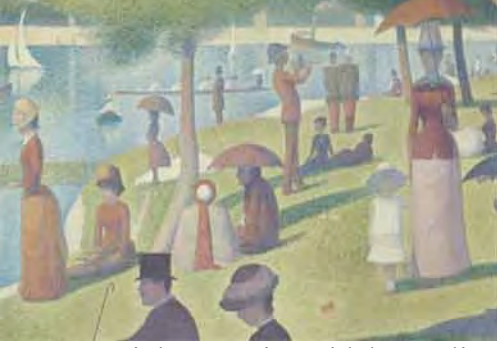
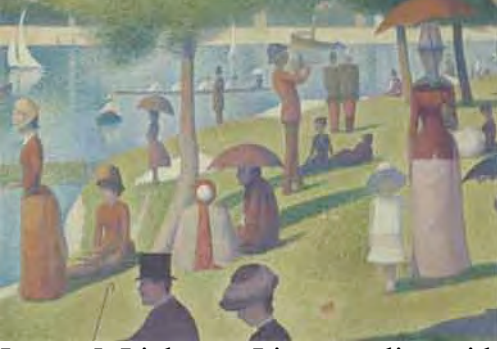
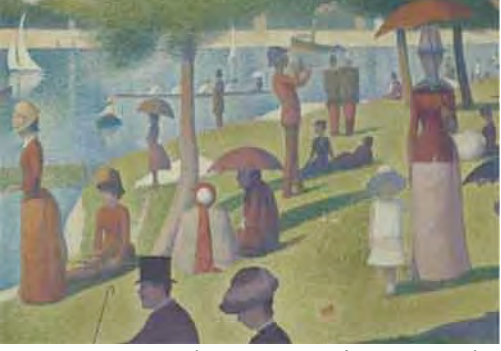
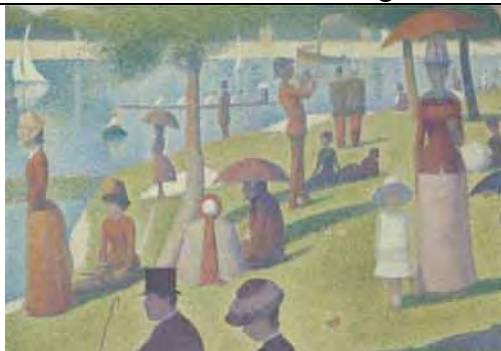
 <p>Image 1. No image processing, just colorimetric rendering.</p>	 <p>Image 2. Lightness Sigmoidal rescaling, $L^*=40$, $\sigma=30$, followed by colorimetric rendering.</p>
 <p>Image 3. Lightness Sigmoidal rescaling, $L^*=40$, $\sigma=50$, followed by colorimetric rendering.</p>	 <p>Image 4. Lightness Linear scaling with minimum $L^*=10$ then followed by colorimetric rendering.</p>
 <p>Image 5. Lightness Linear scaling with minimum $L^*=15$ then followed by colorimetric rendering.</p>	 <p>Image 6. Lightness Linear scaling with minimum $L^*=25$ then followed by colorimetric rendering.</p>

Table 2-4 continued: Summary of image processing algorithms.

 Image 7. Power law processing on Y then followed by colorimetric rendering.	 Image 8. Chroma Linear scaling with minimum $C_{ab}^*=1$ then followed by colorimetric rendering.
 Image 9. Chroma Linear scaling with minimum $C_{ab}^*=5$ then followed by colorimetric rendering.	 Image 10. Photoshop crystallize command then followed by colorimetric rendering.

2.6 Results and Discussion

Vision is one of the human perceptions that are studied by the tools of psychophysics. As discussed in Chapter 1, the nominal, ordinal, interval, and ratio scales are four key types of magnitude scales resulting from psychophysical experiments [Engeldrum 2000]. The simplest type, the nominal scale, is just used to name items while ordinal scales are used

to name and sort items in ascending or descending orders. The ordinal scales may or may not be spaced evenly. Logical operations such as greater-than, less-than, or equal-to can be performed with ordinal scales. The interval scale is an ordinal scale with equal intervals. There is no meaningful zero point on the interval scale. Logical operations, addition, and subtraction can be performed with interval scales. The ratio scales are interval scales with a meaningful zero point. All mathematical operations mentioned for previous scales can be performed with ratio scales. Furthermore, multiplication and division can be performed as well. In the paired-comparison method, used in this experiment, a one-dimensional interval scale was developed.

All possible pairs of test images, 45 pairs, were presented to the observers on the LCD display. The observers were asked to select one image in each pair that was judged as a better match to the reference image on the screen. The proportional number of times that an image was chosen versus the other images was recorded. Thurston's Law of Comparative Judgments, Case V, was used to calculate the interval scales from the proportionality data [Engeldrum 2000]. A 95% confidence limit was also calculated for each image [Montag 2004]. Figure 2-11 presents the interval scales and corresponding 95% confidence limits for the 10 images used in the experiment: the larger the interval scale value, the closer the match to the reference image. For example, image 3 was selected as a closer match to the reference image and had a larger interval scale value than image 4. The interval scale values of test images were in the range of -1 to 0.6. This range was large enough that one could differentiate between interval scale values. In

other words, observers could distinguish the quality of appearance-matching of test images to the reference image. Therefore the technique used in this experiment was successful in generating an interval scale correlated to the appearance-matching of test images to the reference image. The image made using the Photoshop crystallize command was not statistically different from the colorimetric version of the reference image; both had the same interval scale value. This implies that the difference in resolution was not an important factor in this experiment.

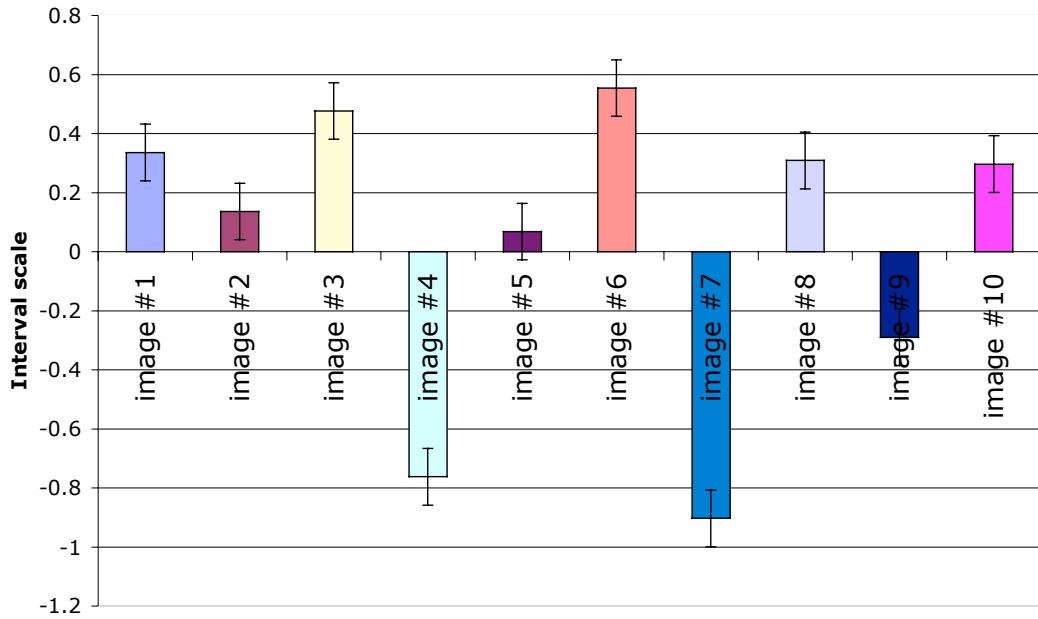


Figure 2-11. Interval scales and corresponding 95% confidence limits based on visual experiment.

The lightness linear rescaling with minimum L* value of 25 had a higher scale value than the others. This image was also statistically different from the original

colorimetric rendered image since the 95% confidence limits were not overlapping. Therefore this image was selected as a closer match to the original image on the screen than the colorimetric version. A trend of increasing interval scales with an increase of minimum L* value was seen for linear lightness rescaling (images 4, 5, and 6). The image generated based on minimum L* value of 10 (image 4) had the smallest scale value and that with minimum L* value of 25 (image 6) had the largest interval scale value within the linear rescaling set. The image rendered based on power function processing on luminance factor was selected less than all the other images and had the smallest interval values among all the other values. Since the power function darkened the image as shown in Figure 2-10, the results were not surprising and was consistent with Xiao [2004]. In a general sense, an increase in lightness on test images generated a better appearance match to the reference image. Linear rescaling of chroma with minimum $C_{mo} = 1$ (image 8) was not statistically different from the colorimetric rendered image of the target. The extra increase in the minimum chroma produced a poorer matching image to the projected image on the screen and hence the interval scale for the image rendered with $C_{mo} = 5$ (image 9) was reduced. Therefore an increase in lightness but not chroma could generate a closer match to the reference image.

2.7 Conclusions

The experimental approach proved successful in evaluating the effect of image size on color appearance. Both displays had good colorimetric characterization accuracy. The short-term memory matching did not result in excessively large confidence limits. In fact, by having 20 observers performing the experiment, the limits were typical of paired-comparison experiments using a single display and adjacent images. There was sufficient difference between interval scale values that one could differentiate among them. The observers found that colorimetrically matching images of different size could be made to more closely match in appearance by image manipulation. In particular, changes in lightness in which lightness was linearly increased and rescaled were preferred over other tested algorithms. This result was consistent with previous experiments comparing small paint chips with painted walls. In both cases, size enlargement caused an increase in perceived lightness.

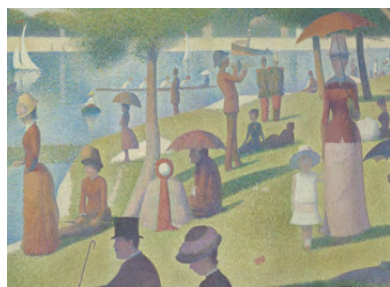
It is a common practice to render an image of a large painting to a smaller size. In such cases, a colorimetric reproduction of a large painting should be remapped such that the minimum lightness is increased when reproduced on display in a smaller size.

The most selected image, the linearly rescaled image for the increase of CIELAB lightness (image 6), as well as the original colorimetric image of the painting (image 1) are presented in Figure 2-12. A three times larger version of the colorimetric image is also presented in Figure 2-12.

In the next sections achromatic and chromatic contrast matching of images with different size, contrast and mean luminance levels were explored to further the study of the effect of size on the lightness and chroma. In this way one could collect observer responses and establish a relationship between image size, lightness, and chroma of an image. Ultimately, the goal is to develop a fundamental understanding of the effect of image size on color appearance.



Colorimetric (3X)



Colorimetric



Linear increase of CIELAB lightness

Figure 2-12. Bottom row: Colorimetric image of the painting (image1) and the linearly rescaled image for an increase in CIELAB lightness (image 6). Top: A three times larger version of the colorimetric image shown in the bottom left.

3 ACHROMATIC CONTRAST MATCHING AND ADJUSTMENT OF MEAN LUMINACE

In order to develop a better understanding of the effect of image size on color appearance, a digital projector and LCD display were colorimetrically characterized and used in a series of contrast matching experiments. Two set of images, Gabor and noise patterns, were rendered for both displays and observers adjusted the mean luminance level and contrast of images on the projector screen to match the images displayed on the LCD. This chapter details visual experiments performed to study the effect of image size on mean luminance and contrasts of achromatic patterns.

3.1 Matching Experiment using Gabor Patterns

Perceived contrast is one of the perceptual attributes of an image. Michelson contrast, Weber fraction, and root-mean-square contrast are examples of metrics proposed for quantifying this perceptual attribute [Peli 1990]. Sinusoid patterns at suprathreshold have been studied for their apparent contrast. It has been reported that two suprathreshold patterns generally match in apparent contrast if their physical contrast are equal, even when they have large differences in their contrast thresholds. This phenomenon is termed “contrast constancy.” [Georgeson 1975] In other words, if a test and a standard with

different spatial frequencies have equal physical contrast and mean luminance, then their apparent contrast will match.

3.1.1 Stimuli Generation

A sine wave pattern is a traditional stimulus used in experiments of contrast matching and visual sensitivity measurements [Georgeson 1990, Kelly 1994]. The Gabor pattern is a variation of the sinusoid pattern, which is a modulation of the sine wave pattern by a radially symmetric Gaussian function. In this way the sine wave pattern fades from its maximum and minimum values to its mean value.

A Gabor image with a resolution of 3300x3300 was computed by multiplication of a sine-wave image and a radially symmetric Gaussian function. There were 30 full sinusoid cycles in the sine-wave image. The Gaussian image was generated using Matlab low-pass filter function, '*fspecial*', with parameters of 3300 and 528 for the filter-window size and standard deviation, respectively. Pixel values, $g(n_1, n_2)$, within a filter-window were calculated based on Equations (3-1) and (3-2):

$$f(n_1, n_2) = e^{-(n_1^2 + n_2^2)/(2\sigma^2)} \quad (3-1)$$

$$g(n_1, n_2) = \frac{f(n_1, n_2)}{\sum_{n_1} \sum_{n_2} f(n_1, n_2)} \quad (3-2)$$

where n_1 and n_2 were filter-window sizes and σ was the standard deviation. A square window was used in this experiment ($n_1=n_2=3300$ and $\sigma=528$.) The resulting

Gaussian image was normalized to its maximum value to generate an image in the range of [0, 1]. Therefore the Gabor image, H_g , had values in the range of [-1, +1]. The Gabor, sine-wave, and Gaussian images are shown in Figure 3-1. One could normalize the Gabor pattern to a specific range of values using Equation (3-3):

$$G_{test} = H_g \frac{(L_{max} - L_{min})}{2} + \frac{(L_{max} + L_{min})}{2} \quad (3-3)$$

where L_{min} and L_{max} were desired minimum and maximum values, respectively.

Contrast of a periodic pattern such as sinusoidal grating can be measured by the Michelson formula [Kelly 1994], which is expressed in Equation (3-4):

$$M_c = \frac{L_{max} - L_{min}}{L_{max} + L_{min}} \quad (3-4)$$

where M_c is Michelson contrast and L_{min} and L_{max} are minimum and maximum luminance value, in the pattern, respectively. Three Gabor patterns corresponding to three ranges of CIELAB lightness of [25, 75], [10, 90], and [47.5, 62.5] were computed based on the H_g using Equation (3-3). The three Gabor images had contrast levels of 0.97, 0.84, and 0.30 and were rendered for LCD display using the LCD inverse model. It is important to note that reported contrast values were based on calculations using luminance levels in units of (cd/m^2).

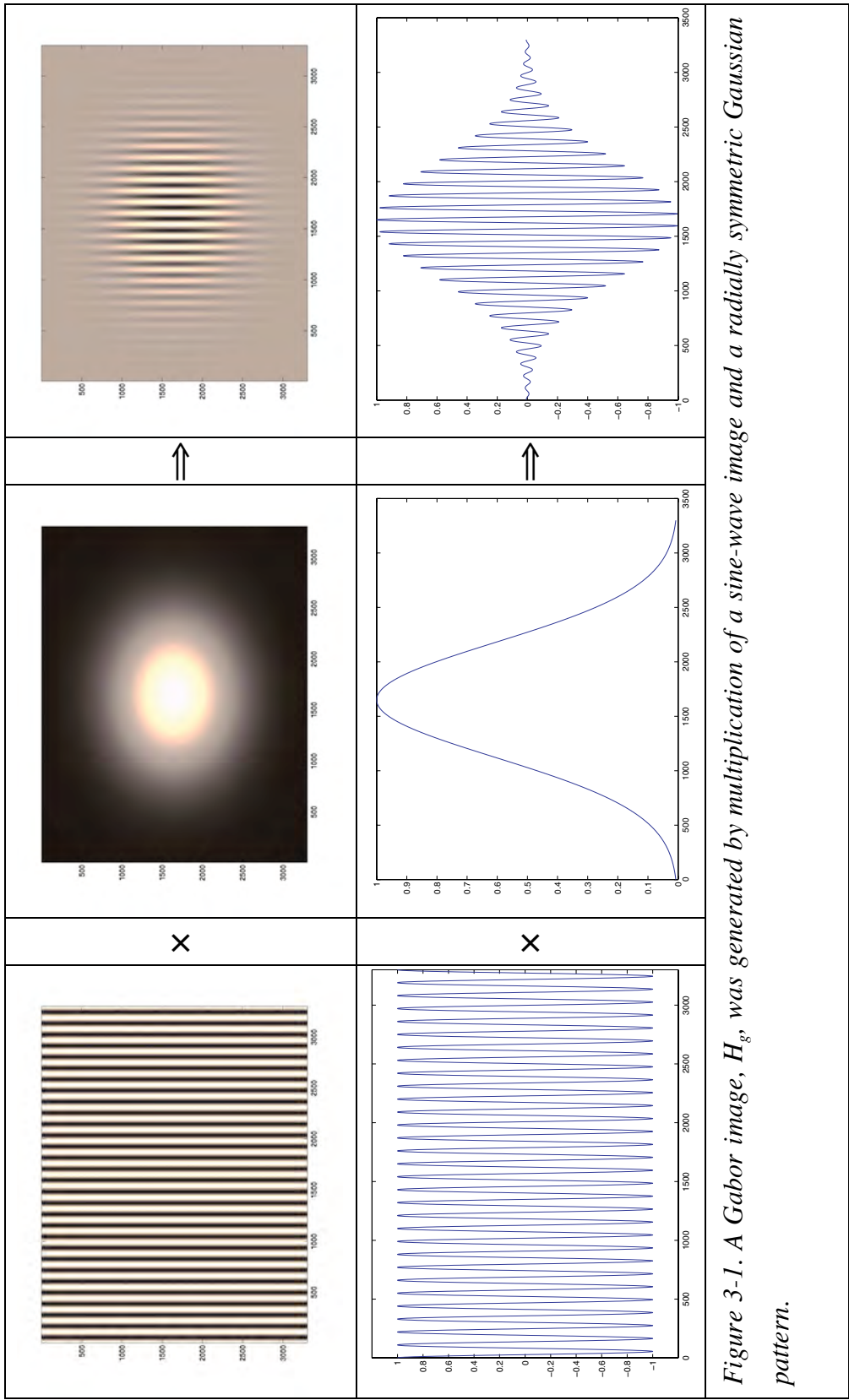


Figure 3-1. A Gabor image, H_g , was generated by multiplication of a sine-wave image and a radially symmetric Gaussian pattern.

For each contrast level, using the nearest-neighbor interpolation technique, applied by the Matlab '*imresize*' function, four images at resolutions of 350x350, 700x700, 1400x1400, and 2100x2100 pixels were populated. These corresponded to retinal subtenses of approximately 5, 10, 20, and 29 degrees of visual angle, although strict viewing distances were not fixed in order to approximate the natural viewing conditions in a museum setting. In this way a total of 12 images were prepared. Table 3-1 summarizes specifications of the 12 images rendered for the LCD display. An example of a Gabor pattern rendered for LCD display with a resolution of 700x700 with a minimum and maximum CIELAB lightness of 25 and 75 is presented in Figure 3-2. The lightness values of this example, in CIEL*, along the horizontal axis of symmetry are also plotted in Figure 3-2.

Using the LCD white point and inverse model of the digital projector (described below), images numbered 2, 6, and 10, from Table 3-1, were also rendered for the projector display. Therefore, for each image on the screen, four images with the same contrast but with different sizes were rendered and displayed on the LCD display. Images on the screen had a fixed physical size of 100cm X 100cm that corresponded to a visual angle of about 28 degree. Therefore, the LCD images had approximate magnifications 1X, 2/3X, 1/3X, and 1/6X compared to the screen images. Sample images of patterns rendered for LCD display with a CIEL* range of [25, 75], images numbered 5 to 8, from Table 3-1, are presented in Figure 3-3. Corresponding Gabor pattern rendered for DLP display is shown in Figure 3-4. The distribution of CIEL* for this pattern is presented in

Figure 3-5-A. It should be noted that the white point of the LCD display was used in the renderings of all images to equalize maximum luminance level for both LCD and DLP displays.

*Table 3-1. Summary of specifications of the 12 images rendered for the LCD display.
(Mc=Michelson Contrast.)*

No	Resolution (Pixels)	Size (mm)	Luminance Range (cd/m ²)	Range of CIE L*	Mc
1	350x350	43.6	2.1 - 165.8	10 – 90	0.97
2	700x700	87.2	2.1 - 165.8	10 – 90	0.97
3	1400x1400	174.3	2.1 - 165.8	10 – 90	0.97
4	2100x2100	261.5	2.1 - 165.8	10 – 90	0.97
5	350x350	43.6	9.6 - 107.3	25 – 75	0.84
6	700x700	87.2	9.6 - 107.3	25 – 75	0.84
7	1400x1400	174.3	9.6 - 107.3	25 – 75	0.84
8	2100x2100	261.5	9.6 - 107.3	25 – 75	0.84
9	350x350	43.6	38.3 - 70.4	47.5 - 62.5	0.30
10	700x700	87.2	38.3 - 70.4	47.5 - 62.5	0.30
11	1400x1400	174.3	38.3 - 70.4	47.5 - 62.5	0.30
12	2100x2100	261.5	38.3 - 70.4	47.5 - 62.5	0.30

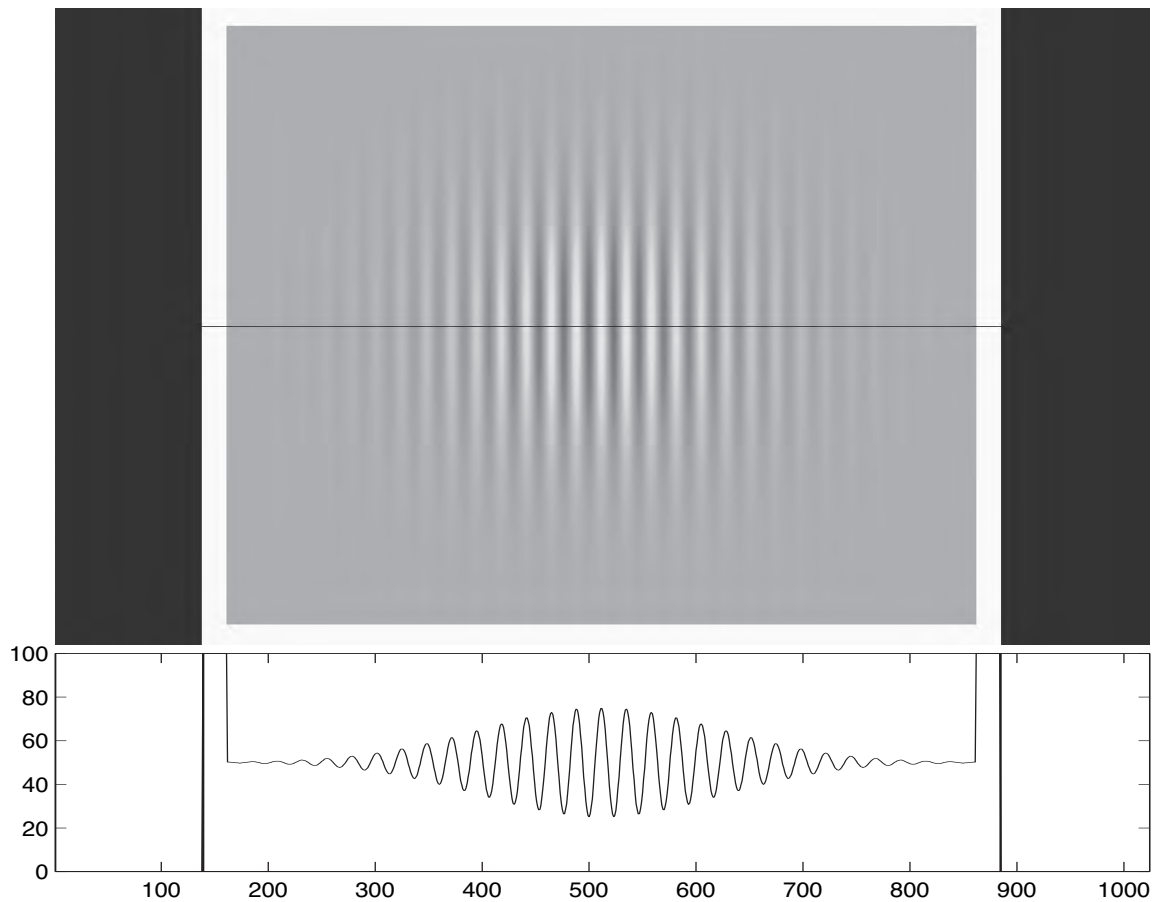


Figure 3-2. An example of a Gabor pattern and its CIE L^ along the horizontal axis of symmetry (the axis of symmetry is shown by the solid black line in the image).*

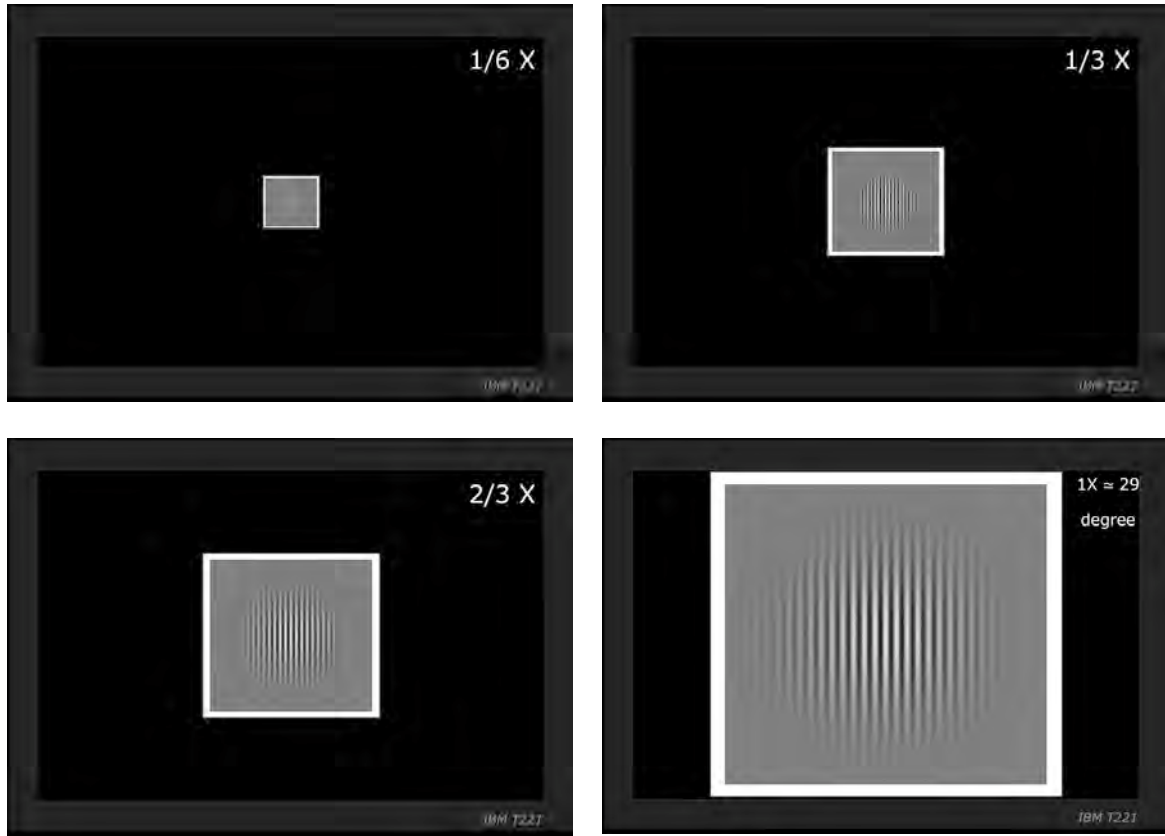


Figure 3-3. Examples of Gabor patterns rendered for LCD display for 1X, 2/3X, 1/3X, and 1/6X magnification levels. The Gabor patterns had minimum and maximum CIELAB lightness of 25 and 75, respectively.

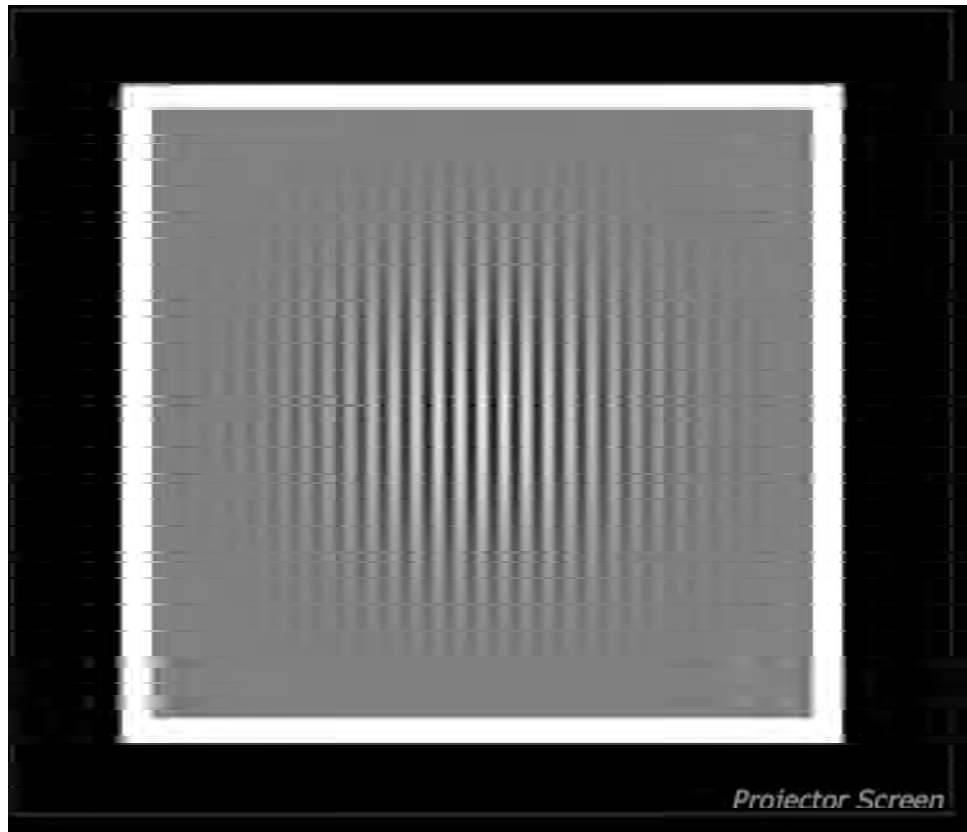


Figure 3-4. Gabor pattern rendered for DLP display with minimum and maximum CIELAB lightness of 25 and 75, respectively.

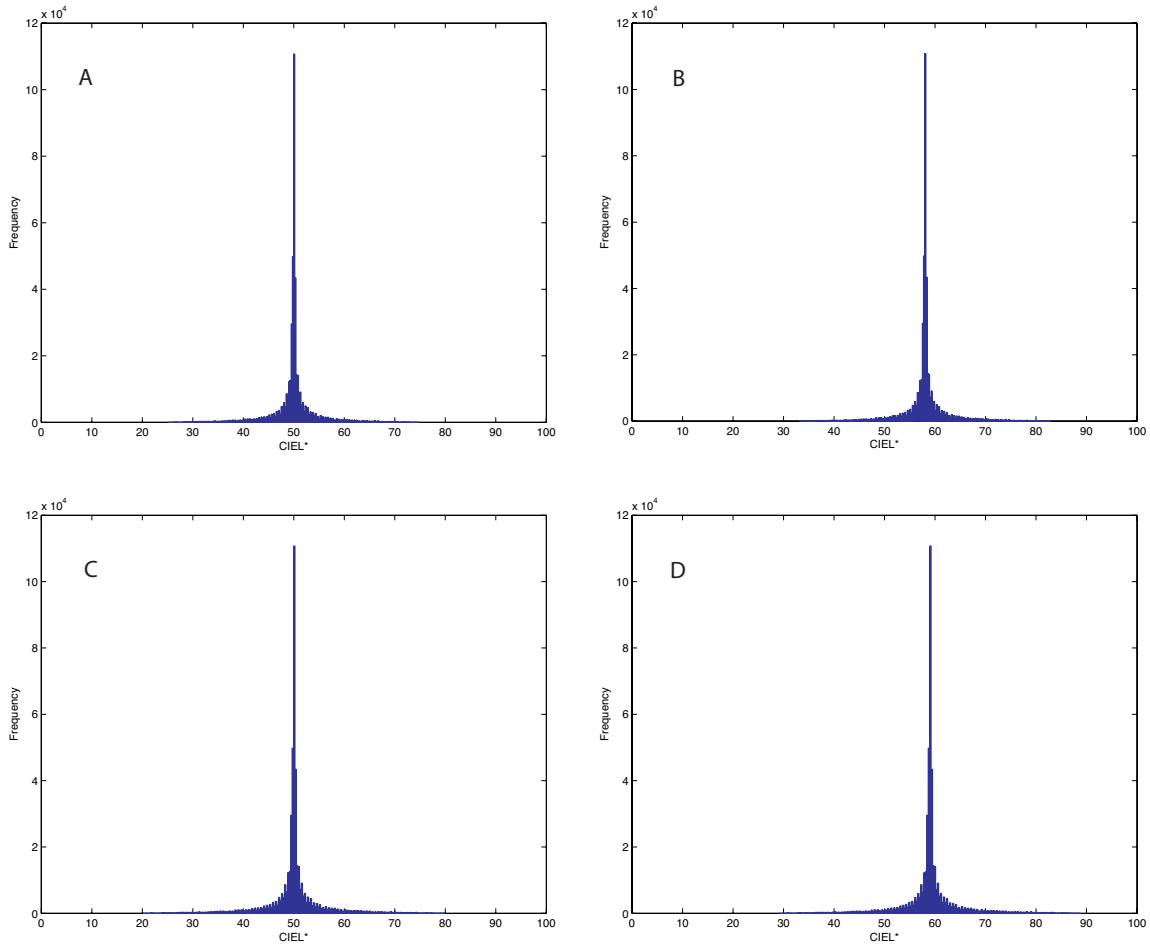


Figure 3-5. Examples of histograms of CIEL; A: original test pattern with CIEL* in the range of [25, 75] displayed on screen; B: Mean luminance was increased for 8 units of CIEL*; C: Five units of CIEL* was added to maximum and subtracted from the minimum lightness values to increase image contrast; D: combined effect of B and C.*

3.1.2 Characterization of Devices

The same LCD and DLP displays utilized in the exploratory experiment, an IBM T221LCD and a Plus Data Projector U4-232, were used in this experiment. The same

characterization as described in Sections 2.2 and 2.3 was performed. The DLP projector was set to its factory standard mode during the experiment. Table 3-2 lists colorimetric results for the LCD and DLP displays. As it can be seen from Table 3-2, both colorimetric characterizations of the DLP and LCD had good performance.

Table 3-2. Summary of characterization results for LCD display and DLP projector for the 1931 standard observer.

Display	Mean ΔE_{00}	Max ΔE_{00}	90 percentile ΔE_{00}
LCD Display	0.9	2.4	1.6
DLP Projector	1.0	8.4	1.6

3.1.3 Psychophysical Experiment

Twenty observers participated in the experiment. Using the method of adjustment, a contrast matching experiment was performed in a dark environment. The three Gabor patterns at contrast levels of 0.97, 0.84, and 0.30 were rendered and projected on a screen by the DLP projector. Each observer adjusted 12 images on the screen to match the corresponding LCD images. For example an image with a contrast value of 0.84 on the screen was compared and adjusted to four images of the same contrast but with sizes of 43.6, 87.2, 174.3, and 261.5 mm on the LCD display. Observers were asked to match the

appearance of images on the LCD and screen by adjusting the mean luminance level and contrast of the image displayed on the screen using a ShuttleXpress dialer.

The ShuttleXpress dialer had two knobs on it. By turning the outer knob in clockwise or counter clockwise direction, observers could increase or decrease mean luminance of the test patterns on the DLP display. An example of CIEL* mapping from LCD to DLP screen for an image pattern with CIEL* in the range of [25, 75] is presented in Figure 3-6. If there was no adjustment then all CIEL* values on DLP and LCD would have the same values and mapping curve from LCD to DLP display would be a straight line such as the segment line AB. Points A and B in Figure 3-6 corresponded to the minimum and maximum lightness values of the test pattern. In this example, by turning the outer dialer in clockwise direction, an intercept of 8 units of CIEL* was added to both A and B. Therefore, the new mapping curve, segment CD, could easily be calculated:

$$\begin{aligned} L_C &= L_A + \Delta L \\ L_D &= L_B + \Delta L \end{aligned} \tag{3-5}$$

where L_A and L_B are minimum and maximum CIEL* lightness values before adjustment and L_C and L_D are corresponding adjusted values. The ΔL is the increment or decrement applied on CIEL* lightness which in this example was equal to +8. The ΔL could be positive or negative, depending on turning direction of the knob, with a step size of 0.2 unit of CIEL*. In this way any lightness value such as L_i was mapped to L_o as stated in Equation (3-6):

$$L_o = (L_i - L_A) \cdot \frac{(L_D - L_C)}{(L_B - L_A)} + L_C \quad (3-6)$$

The resulting image in this example, the linearly rescaled Gabor pattern, is presented in Figure 3-7 and its CIEL* histogram is shown in Figure 3-5-B. Comparing histograms in Figure 3-5-A and 3-5-B, one can see that an increase in mean luminance of the pattern caused a horizontal shift in its histogram. The histogram was shifted for 8 units to the right in this example covering the range of [33, 83].

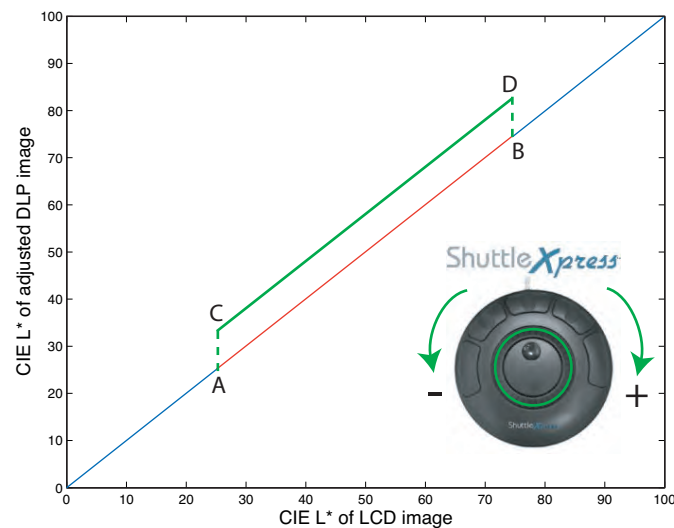


Figure 3-6. Observers could adjust mean luminance of test patterns by the outer knob of the dialer. In this example mean luminance was increased for 8 units.

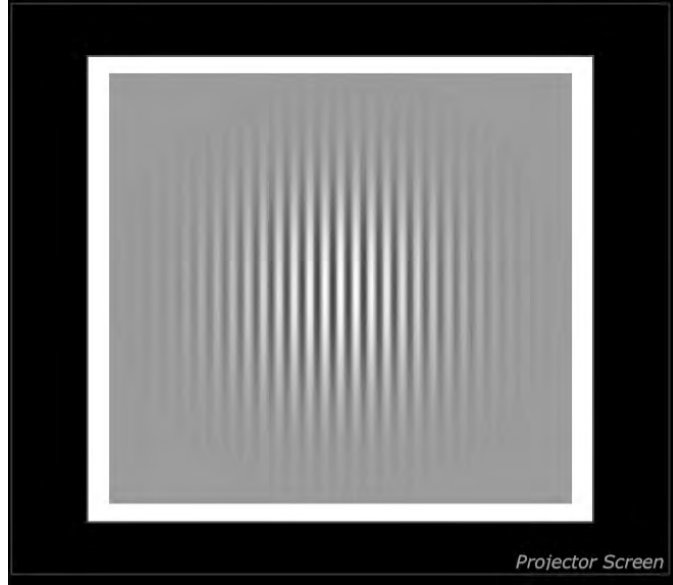


Figure 3-7. Adjusted Gabor pattern on the DLP display corresponding to the lightness-mapping curve, CD, shown in Figure 3-6.

Observers could change contrast of a test image on the DLP display by adjustment of the inner knob on the ShuttleXpress dialer. By turning the inner knob in clockwise direction one could add a ΔL to the maximum CIEL* lightness of the test pattern and subtracted the same ΔL from the minimum. This is stated in Equation (3-7):

$$\begin{aligned} L_C &= L_A - \Delta L \\ L_D &= L_B + \Delta L \end{aligned} \quad (3-7)$$

where L_A and L_B are minimum and maximum CIEL* lightness values before adjustment and L_C and L_D are corresponding adjusted values. Conversely a counterclockwise turn would subtract a ΔL from the maximum and add the same ΔL to the minimum.

For an increment of ΔL , Michelson contrast of the pattern would change by an amount of $\frac{2\Delta L}{(L_B + L_A)}$ as described in Equations (3-8) to (3-10):

$$Mc_{AB} = \frac{(L_B - L_A)}{(L_B + L_A)} \quad (3-8)$$

$$Mc_{CD} = \frac{(L_D - L_C)}{(L_D + L_C)} \quad (3-9)$$

substituting L_C and L_D from Equation (3-7) into (3-9):

$$Mc_{CD} = \frac{(L_D - L_C)}{(L_D + L_C)} = \frac{(L_B + \Delta L - L_A + \Delta L)}{(L_B + \Delta L + L_A - \Delta L)} = Mc_{AB} + \frac{2\Delta L}{(L_B + L_A)} \quad (3-10)$$

where Mc_{AB} and Mc_{CD} are Michelson contrast before and after adjustment, respectively.

In this way a clockwise turn, positive ΔL , would increase contrast and a counterclockwise, negative ΔL , would decrease contrast. The ΔL had a step size of 0.2 units of CIEL*. In the example presented in Figure 3-8, contrast of a test pattern was increased by turning the inner knob in clockwise direction to make a ΔL of +5 units of CIEL*. The new mapping curve, segment CD, had a higher slope. In other words, the resulting image had a higher contrast. The corresponding modified image and its CIEL* histogram are shown in Figure 3-9 and 3-5-C, respectively. The histogram was extended from the range of [25, 75] to a range of [20, 80] but had the same mean value ($L^*=50$.)

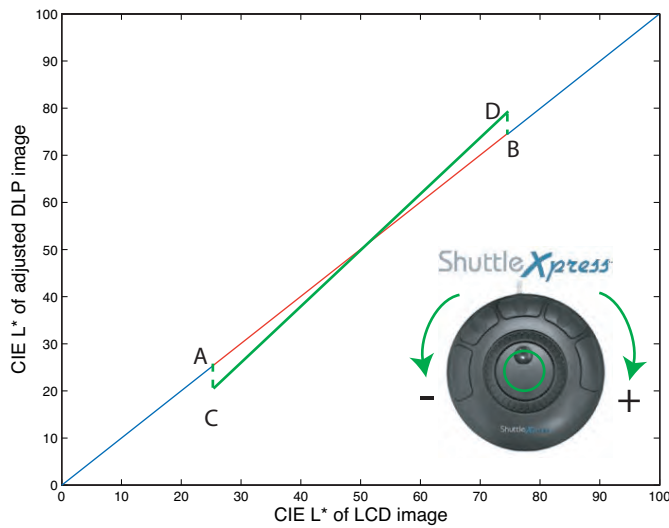


Figure 3-8. Observers could adjust contrast of test patterns by the inner knob of the dialer. In this example 5 units of CIEL was added to the maximum and subtracted from the minimum lightness values to increase image contrast.*

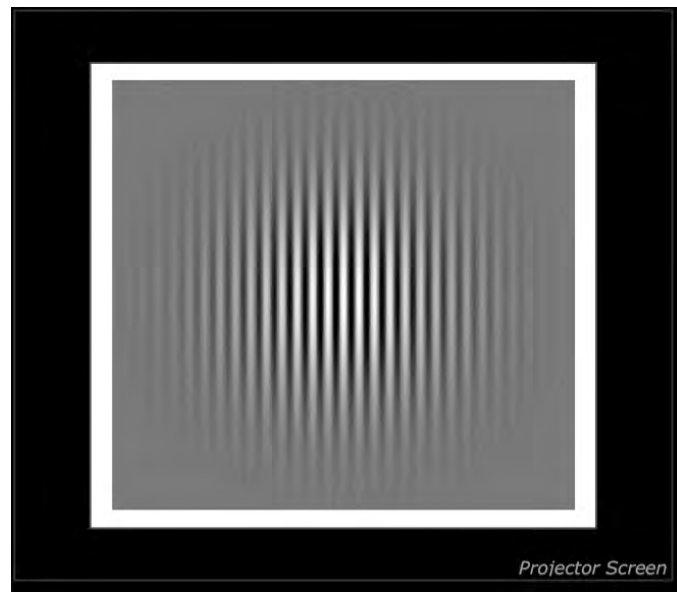


Figure 3-9. Adjusted Gabor pattern on the DLP display corresponding to the lightness-mapping curve, CD, shown in Figure 3-8.

A simultaneous change of mean luminance and contrast is demonstrated in Figure 3-10 where the test image, shown in Figure 3-4, with a mean luminance of 50 and a range of lightness of [25, 75] was adjusted to a higher mean luminance and contrast. Five units of CIEL* was added to the maximum and subtracted from the minimum lightness values to increase image contrast and then an intercept of 8 units of CIEL* was added to all pixel values to make the image brighter. The new mapping curve, segment CD, is plotted in Figure 3-10. The processed image and corresponding CIEL* histogram are presented in Figures 3-10 and 3-5-D. In comparison to the histogram of the original image, plotted in Figure 3-5-A, the histogram of the adjusted image shifted to right and covered a wider range of CIEL*.

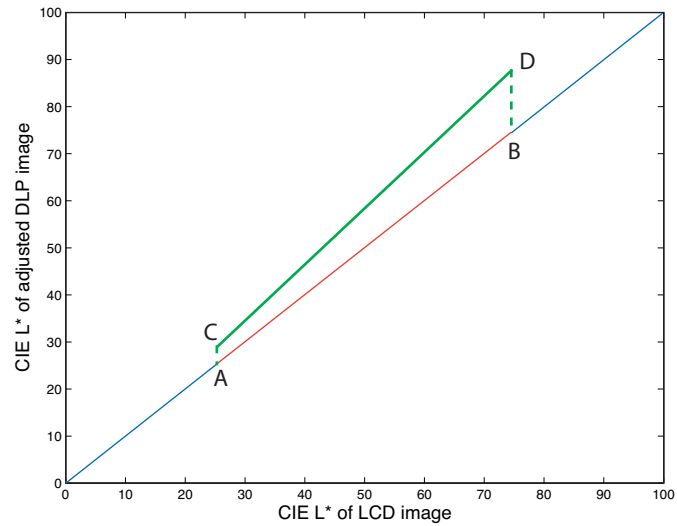


Figure 3-10. An example of simultaneous adjustment of luminance and contrast. The contrast and mean luminance of the image on DLP display were increased.

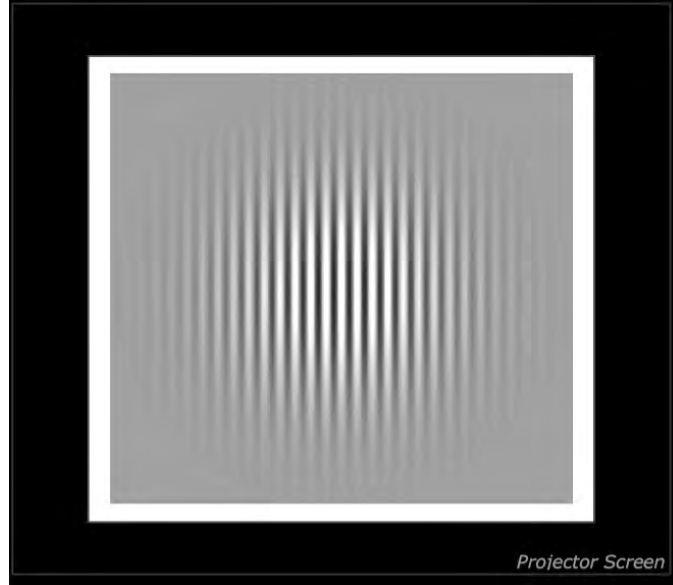


Figure 3-11. Adjusted Gabor pattern on the DLP display corresponding to the lightness-mapping curve, CD, shown in Figure 3-10.

Each observer adjusted 12 images on the screen to match the corresponding LCD images. Pairs were selected in a random order from the available 12 pairs. Furthermore, the test image on the screen had an initial contrast and mean luminance level selected from a uniform random distribution in the range of [-20%, +20%] of the original values. There was an interval of 10 seconds between each adjustment, which was controlled by the data collection software. Observers were asked to ignore artifacts caused by aliasing. All images on the LCD display and screen had a white margin as shown in Figure 3-3 and 3-4. The background and surround of the images on the screen and LCD display were set to a black color. The LCD display and DLP screen were positioned at a 180° angle from one another shown in Figure 3-12. The observer was standing 50 cm from the LCD

display and about 200 cm from the screen. Observer responses were saved as data files and used to redisplay and measure the minimum, maximum, and mean luminance values with the PR650 spectroradiometer.

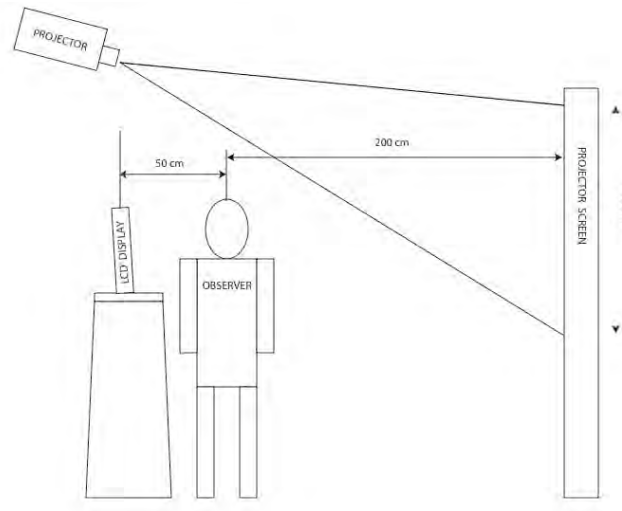


Figure 3-12. Arrangement of scene and equipment in the psychophysical experiment.

3.1.4 Results and Discussion

The minimum and maximum luminance values measured from observer responses were used to calculate contrast according to Equation (3-4) for adjusted images (projected on screen). The mean of adjusted contrasts was calculated for each image size. For a Simple Random Sample (SRS) of size n , one can construct a confidence interval of $(1-\alpha)$ as stated in Equation (3-11):

$$\bar{x} \pm \frac{s}{\sqrt{n}} \cdot t_{(1-\alpha)/2} \quad (3-11)$$

where \bar{x} and s are mean and standard deviation of the sample, respectively. The $t_{(1-\alpha)/2}$ is the $(1-\alpha)/2$ critical value of the t-distribution function for $(n-1)$ degree of freedom [Anderson 1999]. In this way a 95% confidence interval, $\alpha = 0.05$, was computed for each mean value. Figure 3-13 shows the mean of the adjusted contrast and corresponding 95% confidence limits for the projected images versus size of the images displayed on the LCD for three contrast levels.

As seen in Figure 3-13, for contrast values of 0.84 and 0.3, there was an increase of contrast for adjusted images when image size was decreased on the LCD display. The smaller the image on the LCD, the higher the adjusted contrast for images on the screen. However, a significant increase for adjusted contrast was not observed for the high contrast images. Figure 3-14 presents the same data in another way, the adjusted contrast of images on the screen versus contrast of the corresponding images on the LCD display. For contrast values of less than 0.85, the contrast of images with different sizes displayed on the LCD were mapped to different contrast values for images on the screen but were mapped to the same value as the contrast level is increased.

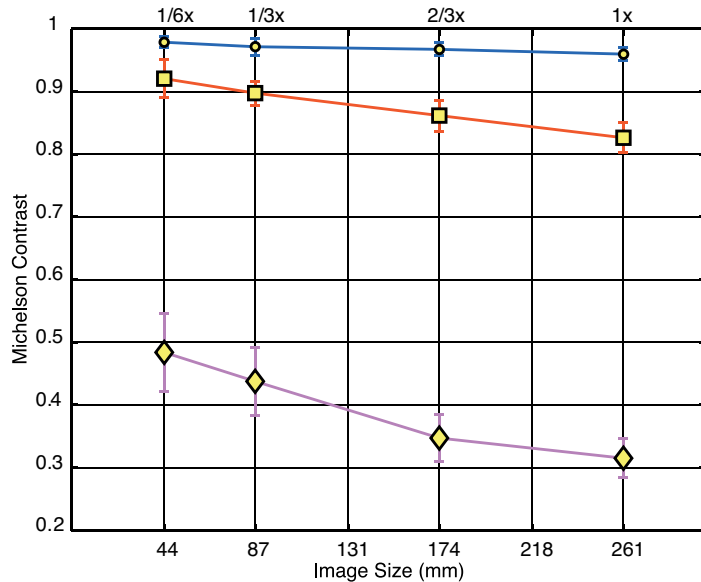


Figure 3-13. Mean of adjusted contrast of images projected on screen versus the size of images displayed on the LCD for three contrast levels. Solid blue line with circle: contrast = 0.97; solid red line with square: contrast = 0.84; solid magenta line with diamond: contrast = 0.3. Error bars present 95% confidence limits for mean values.

Figure 3-15 shows the mean luminance levels of the adjusted images on the screen versus the size of the corresponding images displayed on the LCD for the three contrast levels. The mean luminance level of the images displayed on the LCD, 42.65 cd/m² corresponding to the CIE L* 50, is also shown as a dashed line. For each mean value, a 95% confidence interval was computed and shown as error-bars in Figure 3-15.

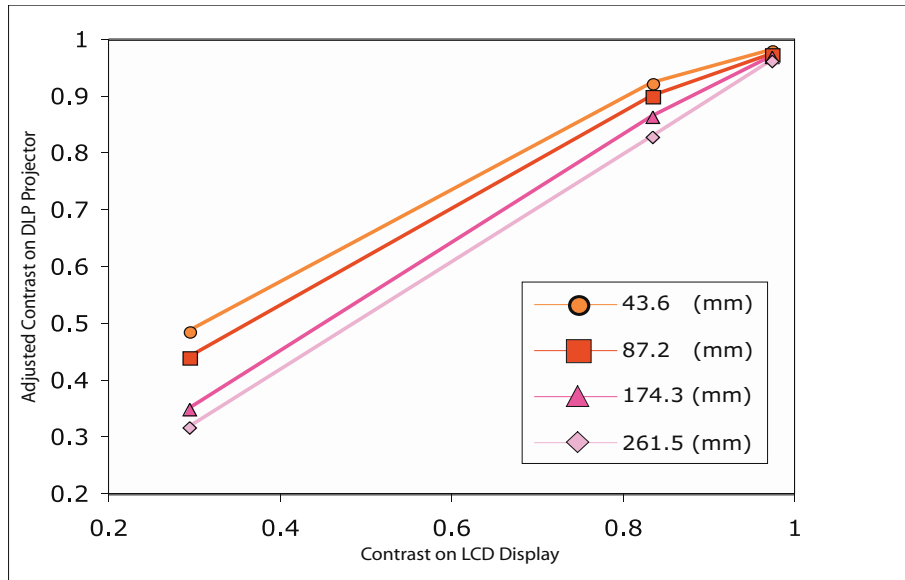


Figure 3-14. Mean of adjusted contrast of images displayed on the DLP projector versus contrast of the same images on the LCD display for different image sizes. Line with circle: size = 43.6 mm; line with square: size = 87.2 mm; line with triangle: size = 174.3 mm; line with diamond: size = 261.5 mm.

For images of contrast values of 0.97 and 0.84, the mean luminance values of the projected images were reduced compared to displayed images on the LCD. This decrease in mean luminance value was more pronounced in the case of smaller images on the LCD. For low contrast images, contrast value of 0.30, the same trend was seen for adjusted images compared to LCD images with size of 1/6X and 1/3X, but the mean luminance values of the adjusted images were not statistically different from corresponding values of images on the LCD with a size of 2/3X and 1X (confidence intervals overlap with the dashed line). In the experiment described in chapter 2, [Nezamabadi 2005], the lightness of the image on the LCD was increased compared to

the image on screen which is in agreement with the decrease in luminance level in the adjusted image on screen in this experiment. Xiao and coworkers, also have reported an increase of lightness for an increase in sample size for uniform patches [Xiao 2003, 2004].

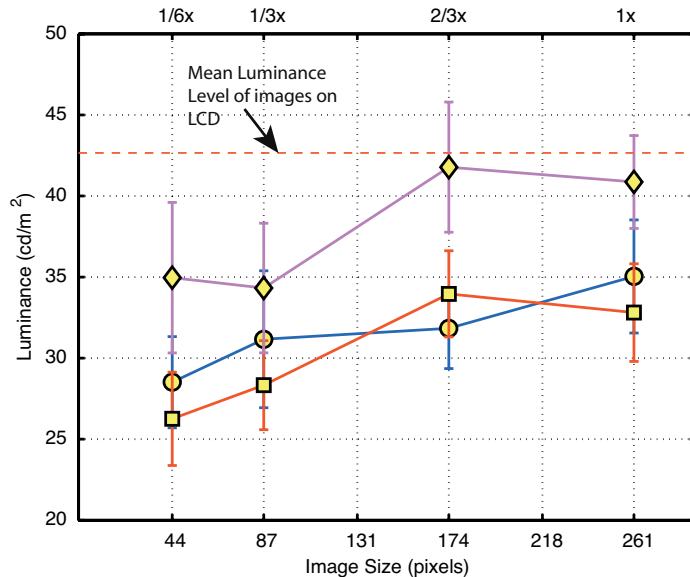


Figure 3-15. Mean luminance levels of adjusted images projected on screen versus size of images displayed on the LCD for three contrast levels. Solid blue line with circle is for contrast level of 0.97; solid red lines with square and solid magenta line with diamond are for contrasts of 0.84 and 0.3, respectively. The mean luminance level of 42.65 cd/m², corresponding to the CIE L 50, is also shown by the dashed line. Error bars represent the 95% confidence intervals.*

For this experiment an increase of physical contrast on projector screen images was needed to achieve an equally perceived contrast on both displays and contrast

constancy did not occur. However, the curves in Figure 3-13 flattened for higher contrast values and for the highest contrast values, the images were almost contrast constant.

It is a common practice to render an image of a large painting to a smaller size. A Gabor pattern, image numbered 10 in Table 1-1, rendered for projection on the DLP screen is shown in the top row of Figure 3-16. The same pattern colorimetrically rendered for LCD display is shown in bottom left. Results of this experiment suggested that a colorimetric reproduction of the Gabor pattern for LCD display should be remapped such that the mean luminance is increased and contrast is decreased. Such an image was rendered for LCD and is presented at the bottom left of Figure 3-16.

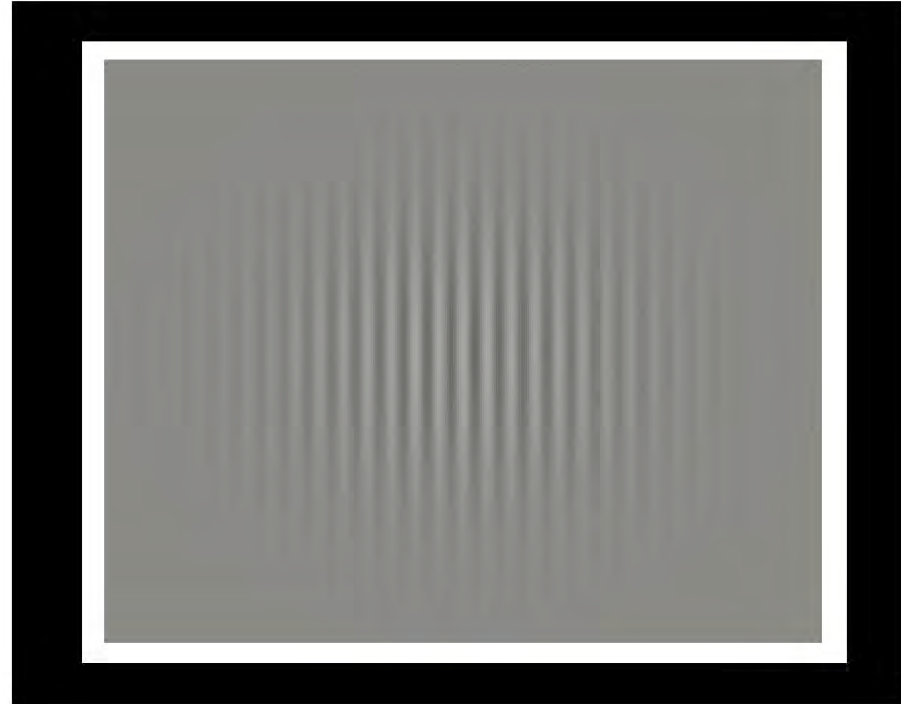


Image on DLP

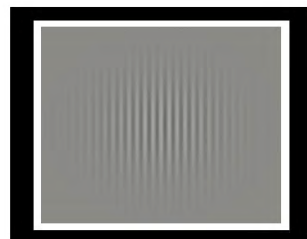


Image on LCD



Adjusted image rendered for LCD

Figure 3-16. Top: the low contrast Gabor pattern, image numbered 10 from Table 1-1, rendered for DLP display; Bottom left: same pattern colorimetrically rendered for LCD; Bottom right: same pattern colorimetrically rendered and also adjusted for the effect of 1/3X magnification for the LCD display.

3.1.5 Conclusions

Both displays had good colorimetric characterization accuracy. It was shown that both mean luminance level and contrast were affected by image size and hence image size should be considered in softcopy reproduction. The method of adjustment utilized in this experiment successfully showed a trend of the increase of contrast in adjusted images versus the decrease of image size on the LCD display. For high contrast images this increase in contrast was insignificant.

Compared to the mean luminance level of the LCD images, a reduction of the mean luminance level of the adjusted images was observed. This decrease was more pronounced for smaller images. Low contrast images with a size of 2/3X and 1X and corresponding adjusted images on screen had the same mean luminance values. The decrease in luminance level in the adjusted images on the projector screen is in agreement with the result described experiment in which the lightness of the image on the LCD had increased in order to make a match [Nezamabadi 2005].

Complete contrast constancy was not observed in this experiment. An increase of physical contrast on screen images was needed to achieve an equal perceived contrast on both displays. However, for the highest contrast images the required increase in contrast was lower. The higher contrast the greater the degree of contrast constancy.

3.2 Contrast Matching Experiments Using Noise Patterns

In the exploratory experiment using a paired-comparison method, Chapter 2, it was shown that a linear increase in lightness of a small image on a LCD display resulted in a closer match to a large image projected on screen compared with the original colorimetric rendered image, and was perceived as a more accurate reproduction than the majority of algorithms tested.

In the previous experiment, using Gabor patterns, the contrasts of the larger images for the projector were boosted while their mean luminance values were decreased relative to the smaller images on the LCD. In the following section a similar visual experiment is described, where band-pass noise patterns were generated using three cosine log filters and used in a contrast matching experiment. The main goal of this experiment was to investigate the effect of image size on appearance for images with different frequency contents. In this manner one can use the results of the experiment to develop a multiscale model for image size compensation.

3.2.1 Multiscale model of visual system

In building a model accounting for the effect of image size difference on color images it is necessary to consider both achromatic and chromatic attributes of an image. Furthermore, a systematic way to collect data and incorporate them into a proper image model is needed. A literature review on contrast and mechanisms of contrast perception

addressed to the early works on spatial selectivity of human cells and the existence of selectively sensitive spatial frequency neurons in the human visual system by Campbell [1968] and Blakemore [1968]. In an approach by Maffei and Fiorentini [Maffei 1973], the visual cortex was considered as a spatial frequency analyzer. The measured contrast sensitivity function was considered as the envelope to multiple mechanisms whose response characteristics were band-pass in the frequency domain [Wilson 1991, Losada 1994]. These mechanisms also changed with the level of illumination, which was reflected in the change of contrast sensitivity with the change of illumination [Nes 1967]. Performing contrast matching using relatively simple stimuli such as band-pass noise patterns in a controlled condition could provide information on the effect of image size on mechanisms of the human visual system.

3.2.2 Cosine log filters

In image processing, Gaussian filters are attractive because of their mathematical convenience in the transformation from the frequency to spatial domains. However, they have several shortcomings, described by Watson [1987] and Field [1987]. Cosine log filters are symmetric on a log frequency axis and are good approximations for Gaussian filters. Furthermore, an image filtered by a bank of cosine log filters can be reconstructed from its segments by a simple addition process [Peli 1990].

Response of an octave cosine log filter is stated in Equation (3-12):

$$F_{resp} = \frac{1}{2} + \frac{1}{2} \cdot \cos\left(\frac{\pi}{2} \cdot \log_2 \frac{f}{\phi}\right) \quad (3-12)$$

where F_{resp} is response of a filter centered at ϕ for the frequency range of f . Octave cosine log filters were generated at center frequencies of 0.5, 2, and 8 cycles-per-degree (cpd) for a range of 0 to 35 cycles-per-degree. An octave filter has half-width at the half and double of the center frequency. For example, an octave filter centered at 2 cycles-per-degree, shown by solid green line in Figure 3-17, has a half-width at 1 and 4 cycles-per-degree. The filter response at frequencies lower than 0.5 cpd were set to unity for the cosine log filter centered at 0.5. In a similar way, filter responses at frequencies higher than 8 cpd were set to unity for filter centered at 8 cpd. In this way, the addition of three filters at each frequency results in unity; in other words, the addition of the filtered images results in the original image.

The filters centered at 0.5, 2, and 8 (cpd) are called low, medium, and high frequency filters through the rest of this chapter. Using the one-dimensional filter the corresponding radially symmetric two-dimensional filter was constructed. The center of the two-dimensional filter corresponded to the zero frequency. As an example, the image of an octave cosine log filter, centered at 2 cycles-per-degree, is presented in Figure 3-17. Pixel by pixel multiplication of this image with the Fourier transfer of a test image would result in a band-pass filtered image of the test sample in the frequency domain. Images

corresponding to the octave filters centered at 0.5, 2, and 8 cpd are presented in Figure 3-19.

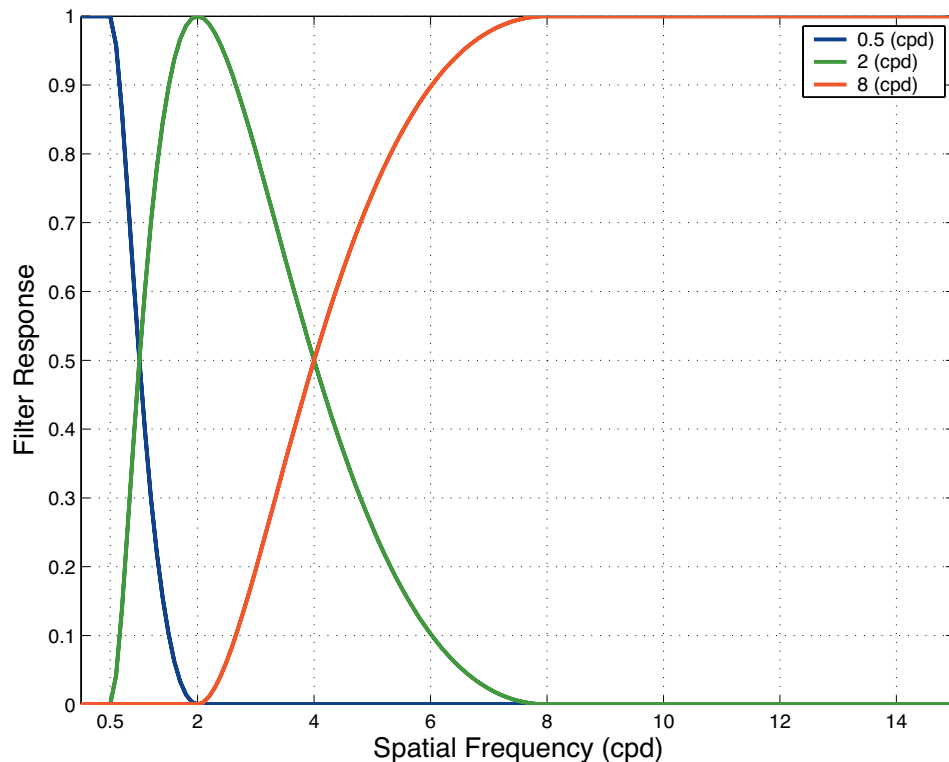


Figure 3-17. Frequency responses of octave filters centered at 0.5, 2, and 8 cycle-per-degree, (cpd), of visual angle. For frequencies lower than 0.5 cpd and higher than 8 cpd, filter responses were set to unity for filters centered at 0.5 and 8 cpd, respectively.

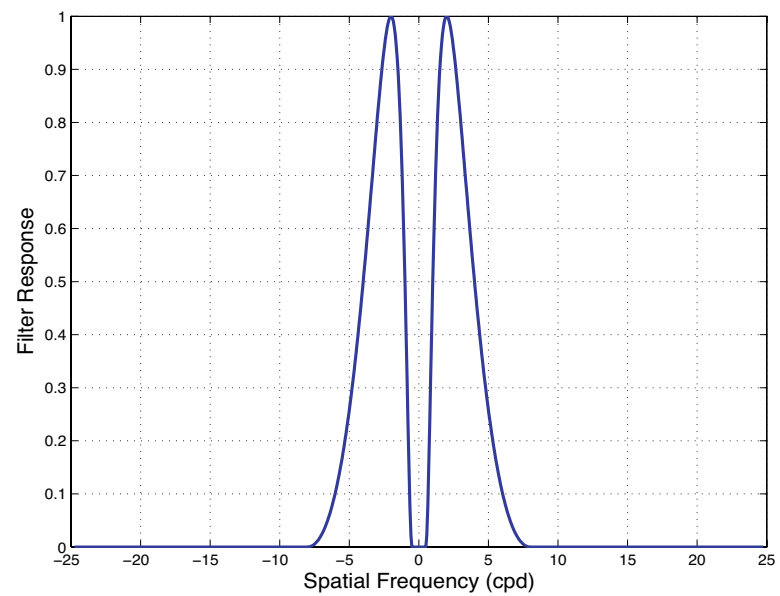
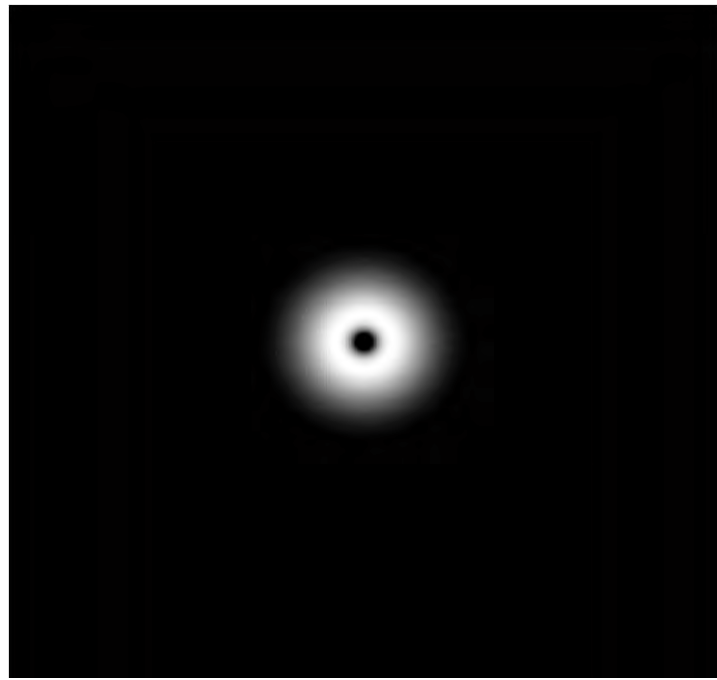


Figure 3-18. Octave cosine log filter centered at 2 cycles-per-deg. Response of the filter is plotted along its horizontal axis of symmetry.

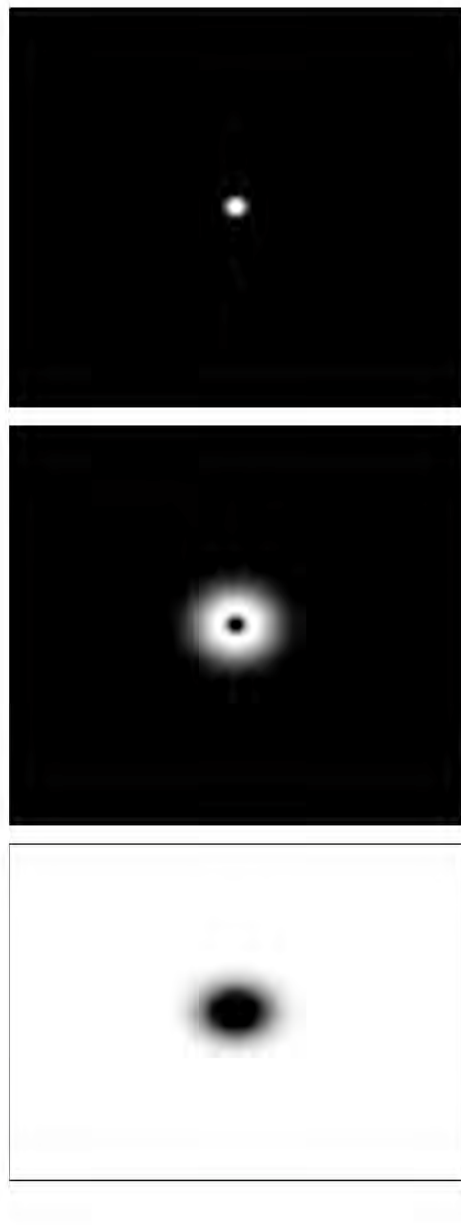


Figure 3-19. Images corresponding to low, medium, and high frequency octave cosine log filters centered at 0.5, 2, and 8 (cpd), respectively. Top: low frequency; Bottom: high frequency; Middle: medium frequency. The center of each image corresponded to the zero frequency. Frequency range was [-35, 35] along the diagonal axis of each image.

3.2.3 Noise pattern generation

Pixel values of an image with a resolution of 701×701 were assigned from a uniform random distribution in the range of $[0,1]$. This noise image is called “white noise pattern” in the rest of this chapter and denoted by matrix \mathbf{N} . The white noise pattern and its histogram are presented in Figure 3-20.

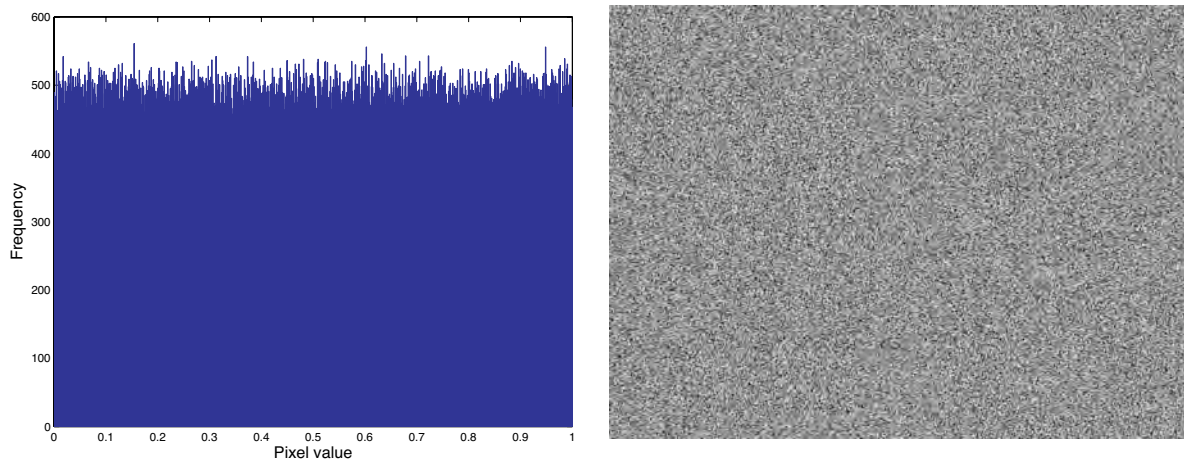


Figure 3-20. White noise pattern and histogram of its pixel values.

Base on the white noise pattern seven band-pass noise patterns were populated. Flowchart of stimuli generation is presented in Figure 3-21. In the first step Discrete Fast Fourier Transfer (DFFT) of the white noise image was computed and multiplied pixel by pixel with the low, medium, or high frequency cosine log filters, described in Section 3.2.2, to generate corresponding filtered image in the frequency domain. The filtered image was transferred back to spatial domain by computing its inverse DFFT. One could

linearly rescale a filtered image with a minimum and maximum values of L_A and L_B , respectively, to a range of $[L_C, L_D]$ using Equation (3-13):

$$L_o = (L_i - L_A) \cdot \frac{(L_D - L_C)}{(L_B - L_A)} + L_C \quad (3-13)$$

where L_i and L_o are pixel values before and after scaling, respectively. In this way the low, medium, and high frequency filtered images were scaled to the ranges of [0.41, 0.59], [0.325, 0.675], [0.15, 0.85], [0.16, 0.34], [0.075, 0.425], [0.66, 0.84], and [0.575, 0.925]. The resulting noise patterns for the ranges of [0.41, 0.59], [0.325, 0.675], and [0.15, 0.85] had a mean value of 0.5. The mean of patterns with ranges of [0.16, 0.34] and [0.075, 0.425] was equal to 0.25. The noise images with ranges of [0.66, 0.84] and [0.575, 0.925] had a mean of 0.75.

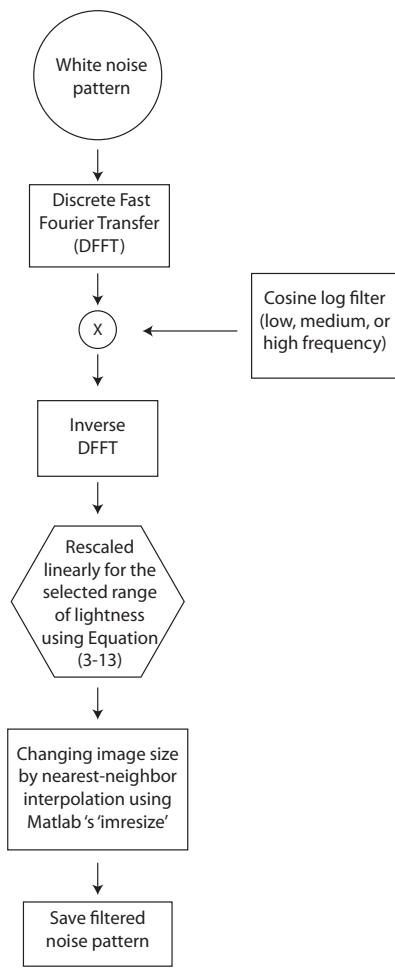


Figure 3-21. Flowchart of stimuli generation.

Each pixel value in a noise pattern was considered as a color coordinate in the CIE L*a*b* space, with CIE L* equal to the pixel value scaled by a factor of 100 and CIE a* and CIE b* values of zero. Using the DLP projector white point to equalize the maximum luminance level for both LCD and DLP displays, noise images were rendered by inverse characterization models of the LCD and DLP displays at three frequency bands. Table 3-3 summarizes the specification of the seven generated noise patterns for

one of the frequency bands. There were a total of 21 noise patterns, 3 bands \times 7 patterns = 21.

Table 3-3. Summary of specification of seven generated noise patterns for one of the frequency bands.

No	CIE L*			Y (cd/m ²)			Michelson Contrast
	Minimum	Lmean	Maximum	Ymin	Ymean	Ymax	
1	16.0	25.0	34.0	3.61	8.08	15.36	0.62
2	41.0	50.0	59.0	22.55	33.98	49.68	0.38
3	66.0	75.0	84.0	63.49	86.17	110.93	0.27
4	7.5	25.0	42.5	1.37	8.07	24.11	0.89
5	32.5	50.0	67.5	14.08	33.90	67.40	0.65
6	57.5	75.0	92.5	47.12	85.56	137.32	0.49
7	15.0	50.0	85.0	3.22	34.00	113.57	0.94

Please note that calculated Michelson contrast in Table 3-4, as expressed in Equation (3-4), was based on measured luminance value, Y (cd/m²), from the LCD using the PR650 spectroradiometer. Displayed image on the screen had a physical size of 105cm \times 105cm and subtended a visual angle of about 30°. As examples, the low,

medium, and high frequency noise images for ranges of $[0.41, 0.59]$, $[0.325, 0.675]$, and $[0.15, 0.85]$ and their corresponding histograms are shown in Figures 3-22 and 3-23.

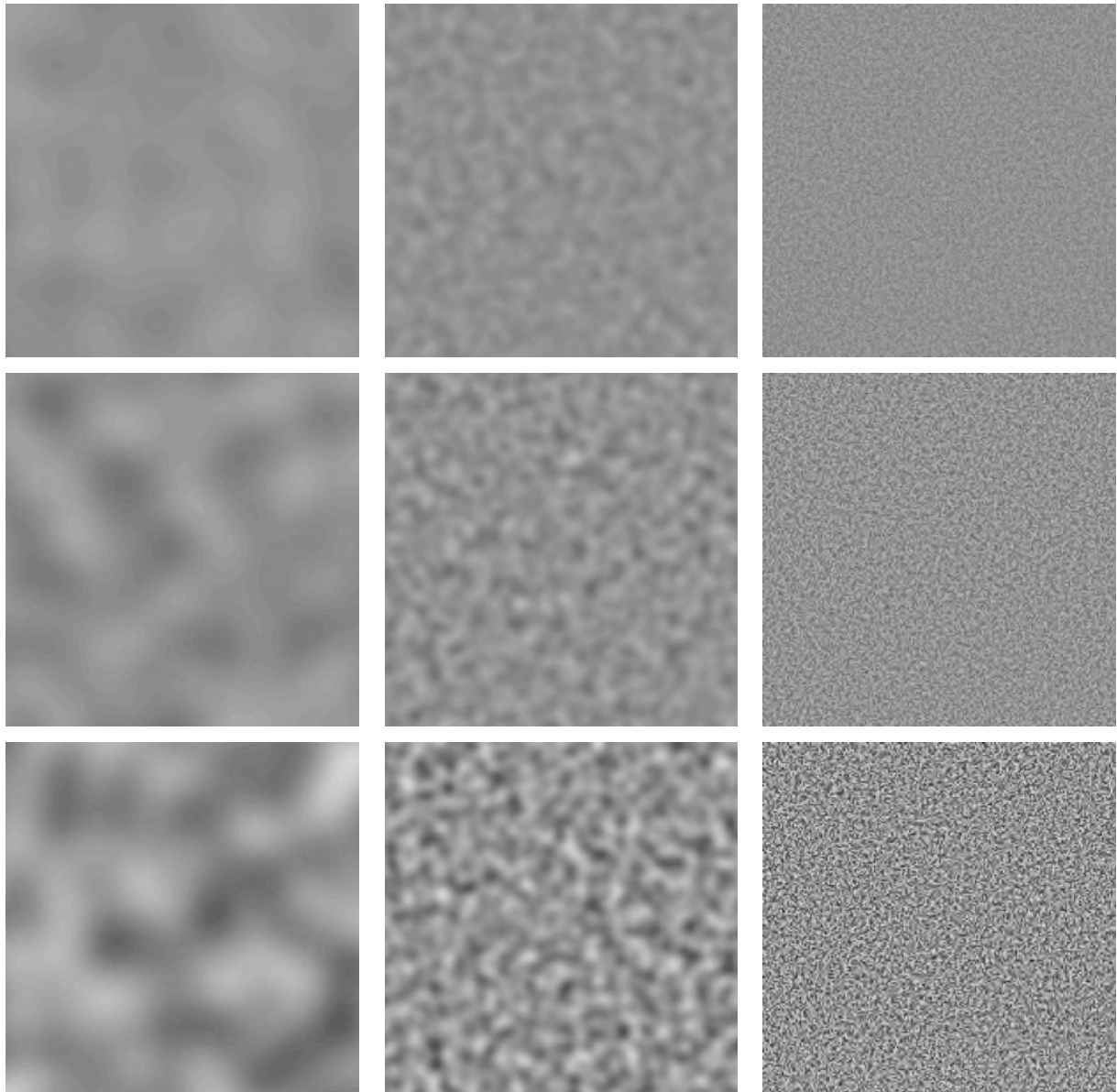


Figure 3-22. Examples of the noise images. Top, middle, and bottom rows corresponded to images numbered 2, 5, and 7 in Table 3-3, respectively. Left, middle, and right columns corresponded to low, medium, and high frequency, respectively.

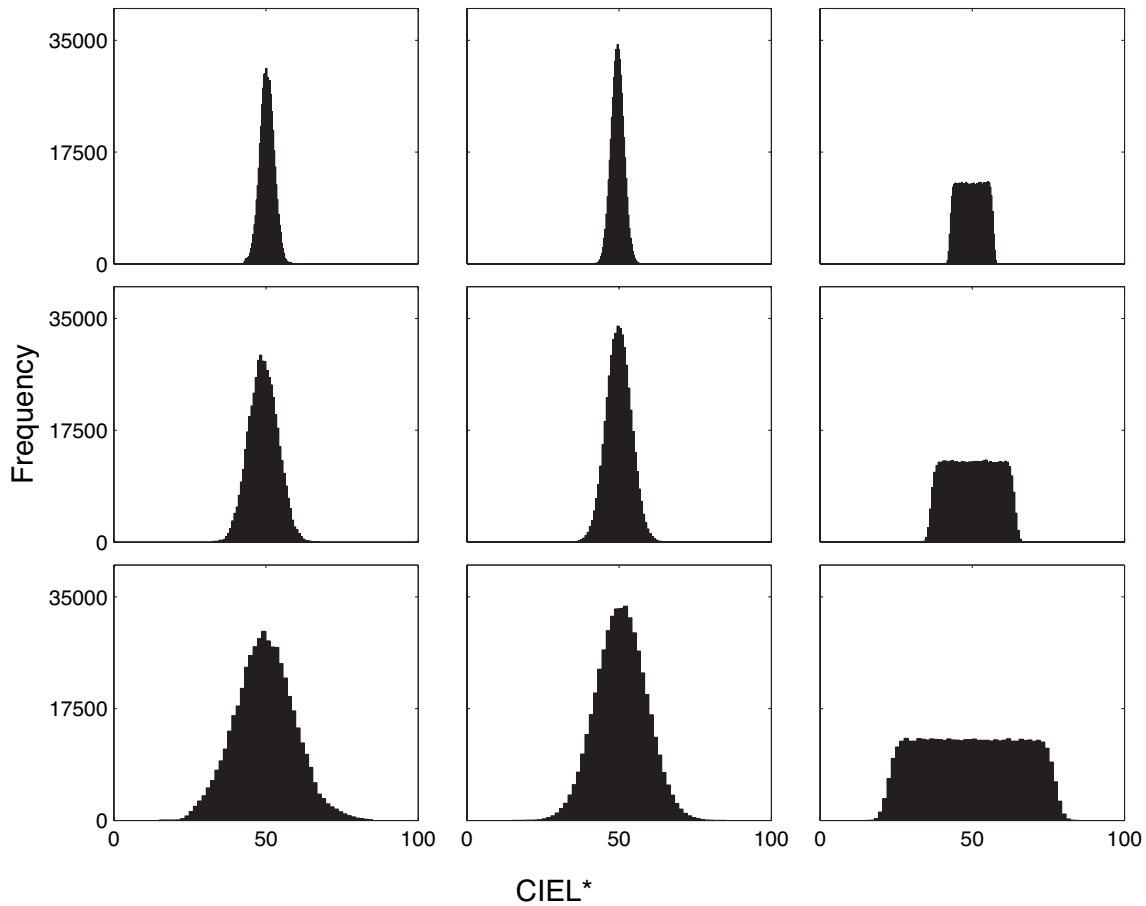


Figure 3-23. Histogram of the noise images presented in Figure 3-22.

Each of the noise patterns was rendered, using a nearest-neighbor interpolation technique, applied by the Matlab '*imresize*' function, for three resolutions of 701×701 , 1401×1401 , 2101×2101 , respectively. These three sizes corresponded to physical sizes of 87, 174, 288 mm on the LCD, respectively, which corresponded to magnification factors of 1/3X, 1/2X, and 1X, relative to the visual angle of the screen image. These

corresponded to retinal subtenses of approximately 10, 15, and 29 degrees of visual angle, although strict viewing distances were not fixed in order to approximate the natural viewing conditions in a museum setting. In this way a total of 63 images, 3 bands \times 7 patterns \times 3 sizes = 63, were prepared.

3.2.4 Characterization of Devices

An IBM T221LCD display, with an area of 478 x 299 mm and resolution of 3840x2400 at a refresh rate of 12 Hz was used in this experiment. In order to get better color uniformity across the projector screen an ASK Proxima M1 digital projector, driven by a dual 2-GHz PowerPC Apple G5 computer, was used to project rendered versions of the noise patterns. The ASK Proxima M1 projector used Digital Light Processing (DLP) technology and had a native resolution of 1024x768 and is called the DLP projector through the rest of this document. The LCD and DLP displays were characterized and evaluated in the same way as in the previous experiments, described in Sections 2.2 and 2.3. The colorimetric results for the LCD and DLP displays are listed in Table 3-4. The DLP projector was set to its factory standard mode during the experiment. Both colorimetric characterizations of the DLP and LCD had good performance.

Table 3-4. Summary of characterization results for the IBM T221 LCD display and ASK Proxima M1-DLP projector for the 1931 standard observer.

Display	Mean ΔE_{00}	Max ΔE_{00}	90 percentile ΔE_{00}
IBM T221 LCD Display	0.9	2.3	1.7
ASK Proxima M1 DLP projector	0.8	2.5	1.3

3.2.5 Psychophysical experiment

Fourteen observers, five females and nine males, in the range of 23-61 years old, participated in the contrast matching experiment conducted in a dark environment. The contrast matching experiment was performed using the method of adjustment in the same way as in the previous experiment, described in Section 3.1.3. The arrangement of equipment was also the same as in the previous experiments, shown in Figures 3-24. In other words, the LCD display and DLP screen were positioned at a 180° angle from one another. The observer was standing 55 cm from the LCD display and about 200 cm from the screen. The background and surround of the images on the screen and LCD display were set to a black color.

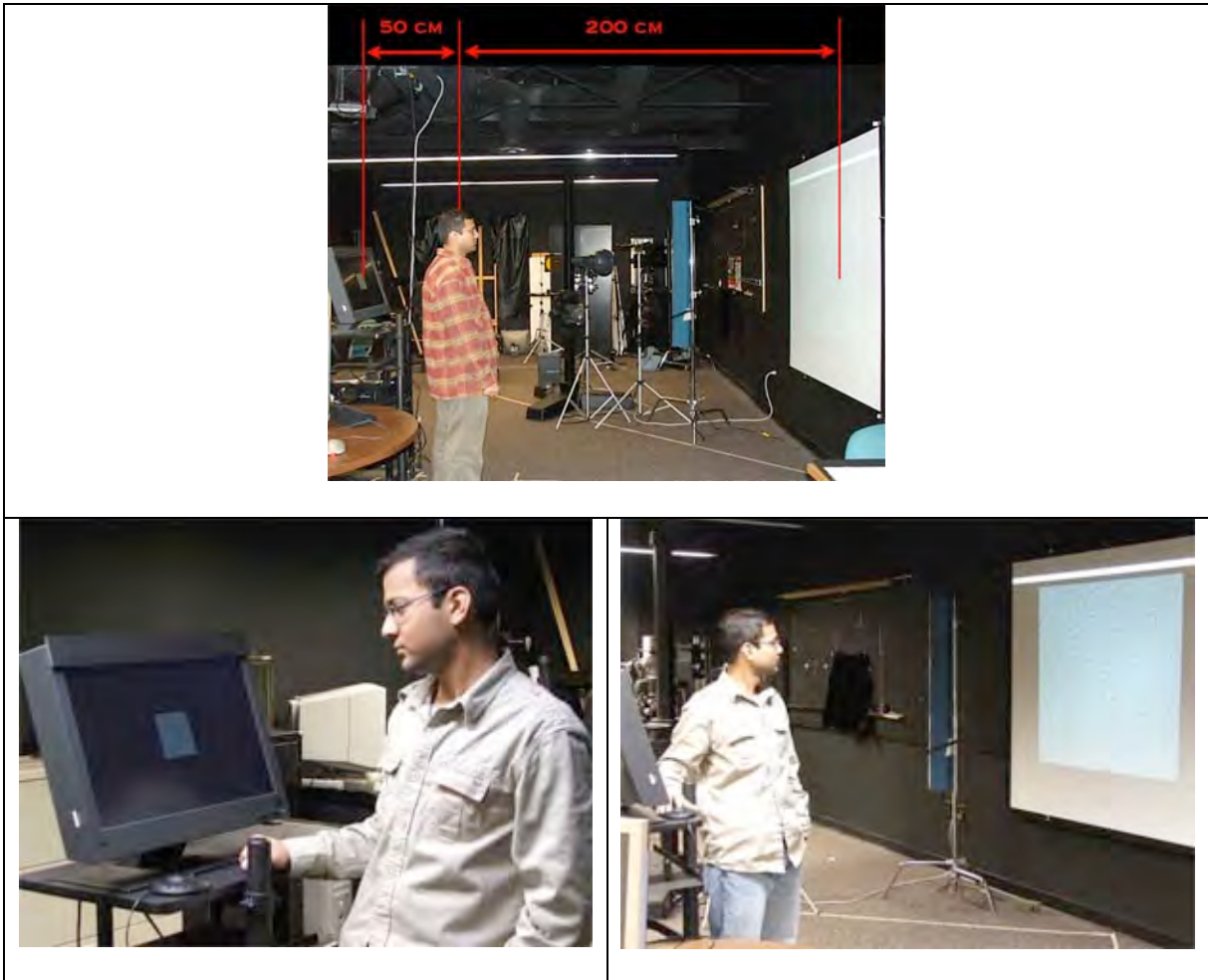


Figure 3-24. Experimental setup in contrast matching experiment.

Due to the specific experimental arrangement, an observer could not see both the LCD and screen at the same time and the adjustments were based on short-term memory matching. Observers were asked to match the appearance of images on the LCD and screen by adjusting the mean luminance level and contrast of the image displayed on the screen. As described in Section 3.1.3 observers adjusted the minimum and maximum of the test pattern on the DLP screen to match the appearance of the image displayed on the

LCD. The same ShuttleXpress dialer and adjustment mapping algorithms, described in Section 3.1.3 were used in this experiment. Each observer adjusted 21 noise patterns at three sizes, a total of 63 , $21 \times 3 = 63$. For example a medium frequency filtered pattern, image numbered 7 in Table 3-3, on the screen was compared and adjusted to three images of the same contrast and mean luminance but with sizes of 288, 174, and 87 mm on the LCD display, which corresponded to magnification factors of 1X, 1/2X, and 1/3X, respectively. For this example, the images displayed on the LCD and DLP screen are shown Figures 3-25 and 3-26, respectively.

Samples were presented to observers in a random order. The test image on the screen had an initial contrast and mean luminance level selected from a uniform random distribution within the range of [-20%, +20%] of their original values. There was an interval of 10 seconds between each adjustment, which was controlled by the data collection software. Observers were asked to ignore artifacts caused by aliasing. As described in Section 3.1.3 observers could adjust contrast and mean luminance of a test pattern, displayed on the screen, by changing its minimum and maximum; (changes were applied based on Equation (3-5) to (3-7).) Two examples of adjustments are presented in Figure 3-27 for a noise image with CIEL* in the range of [15, 85]. The mean luminance and contrast of the test image was decreased as shown in the middle and bottom rows of the Figure 3-27, respectively.

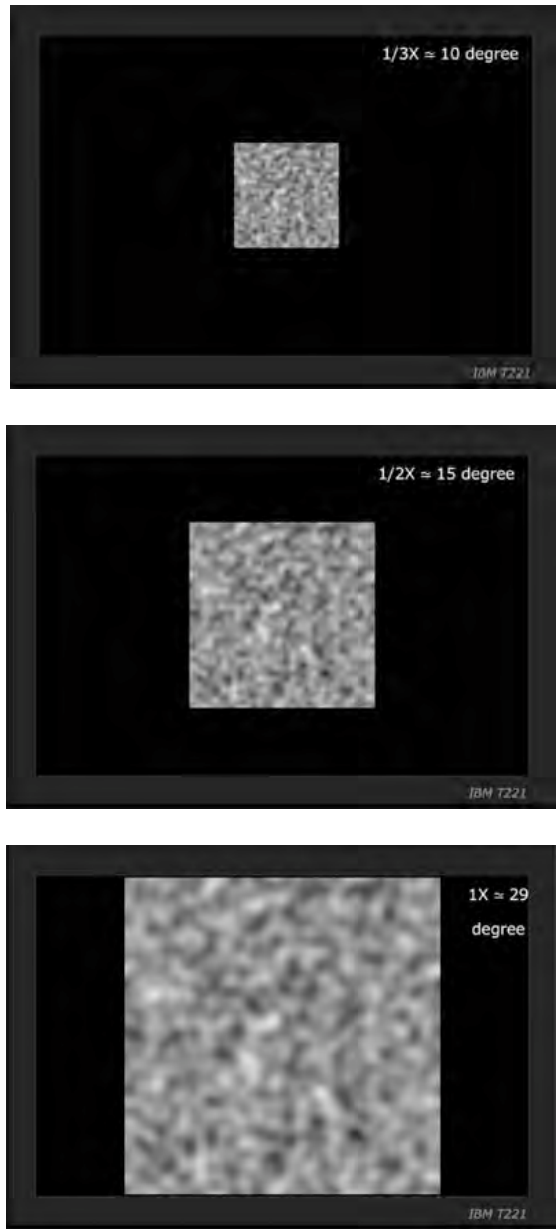


Figure 3-25. Examples of patterns displayed on the LCD. Medium frequency filtered pattern, image numbered 7 in Table 3-3, was displayed at magnification factors of 1X, 1/2X, and 1/3X on the LCD and compared to the image on the DLP screen (shown in Figure 3-26.)

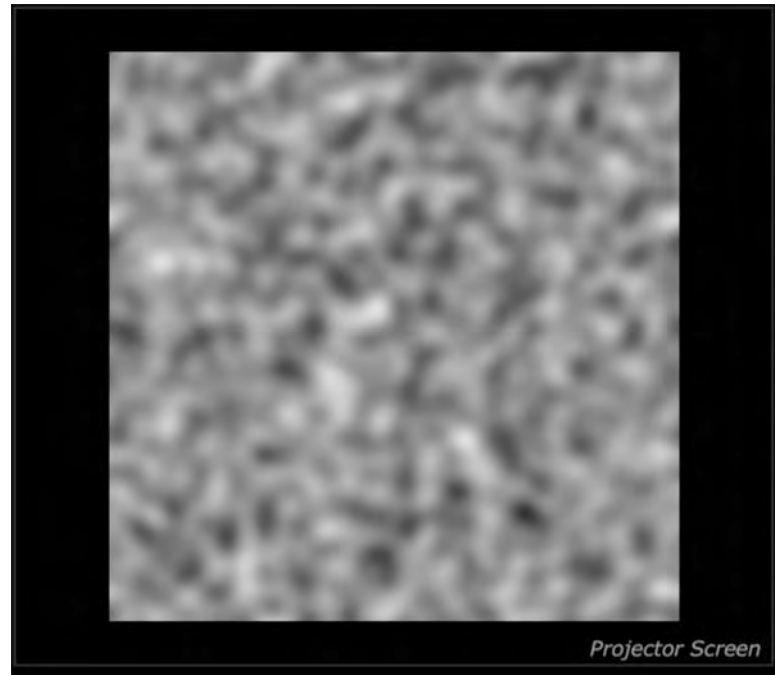


Figure 3-26. An example of noise pattern displayed on the DLP screen. Medium frequency filtered pattern, image numbered 7 in Table 3-3, was compared to the same pattern displayed at magnification factors of 1X, 1/2X, and 1/3X on the LCD.

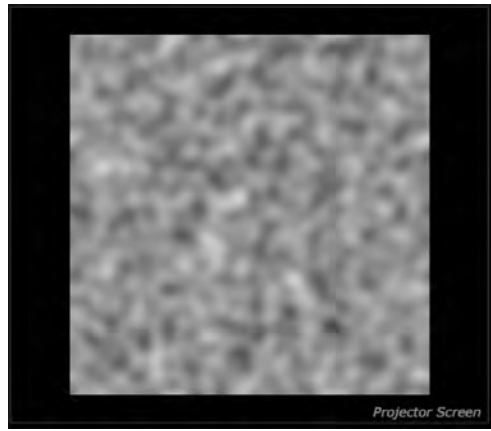
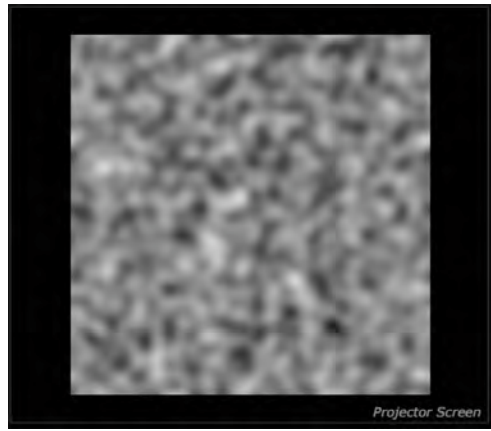
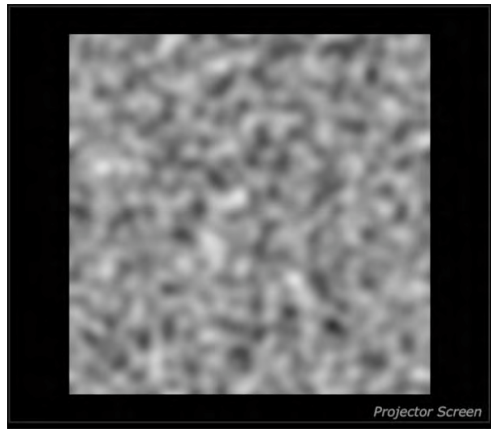


Figure 3-27. Top: original test image with $CIEL^*$ lightness of [15, 85]; middle: mean luminance was adjusted to $CIEL^*$ 45; bottom: contrast was decreased by adjustment of the $CIEL^*$ minimum and maximum to [30, 70].

3.2.6 Results and Discussion

For each observer, responses were saved as data files and used to redisplay and measure the minimum, maximum, and mean luminance values with the PR650 spectroradiometer. The mean luminance values of adjusted images were computed from the measured data for each observer. Furthermore, measured minimum and maximum luminance values were used to calculate Michelson contrast, using Equation (3-4), for each observer's adjustments. The mean of the adjusted contrast and mean luminance values were computed and corresponding 95% confidence intervals were computed for the 14 observers using Equation (3-11), described in Section 3.1.4.

The mean of contrast values and corresponding 95% confidence intervals are plotted in Figure 3-28. At each panel, the dashed line indicates the contrast of the LCD image, which was fixed for three different sizes. Observers were adjusting the contrast of DLP images compared to corresponding images on the LCD. Panels 3-28-A, 3-28-D, and 3-28-G correspond to noise patterns generated by the low frequency cosine log filter. A trend of increase of contrast versus decrease of image size is seen for the low frequency images as shown in panels 3-28-A, 3-28-D, and 3-28-G. An opposite trend is seen for the high frequency case, presented in panels 3-28-C, 3-28-F, and 3-28-I, where contrast was reduced for smaller images. In other words, the high frequency components were less perceivable when an image on DLP screen was scaled down on the LCD display. Conversely, low frequency noise patterns were perceived to have a higher contrast when they were scaled to a smaller size.

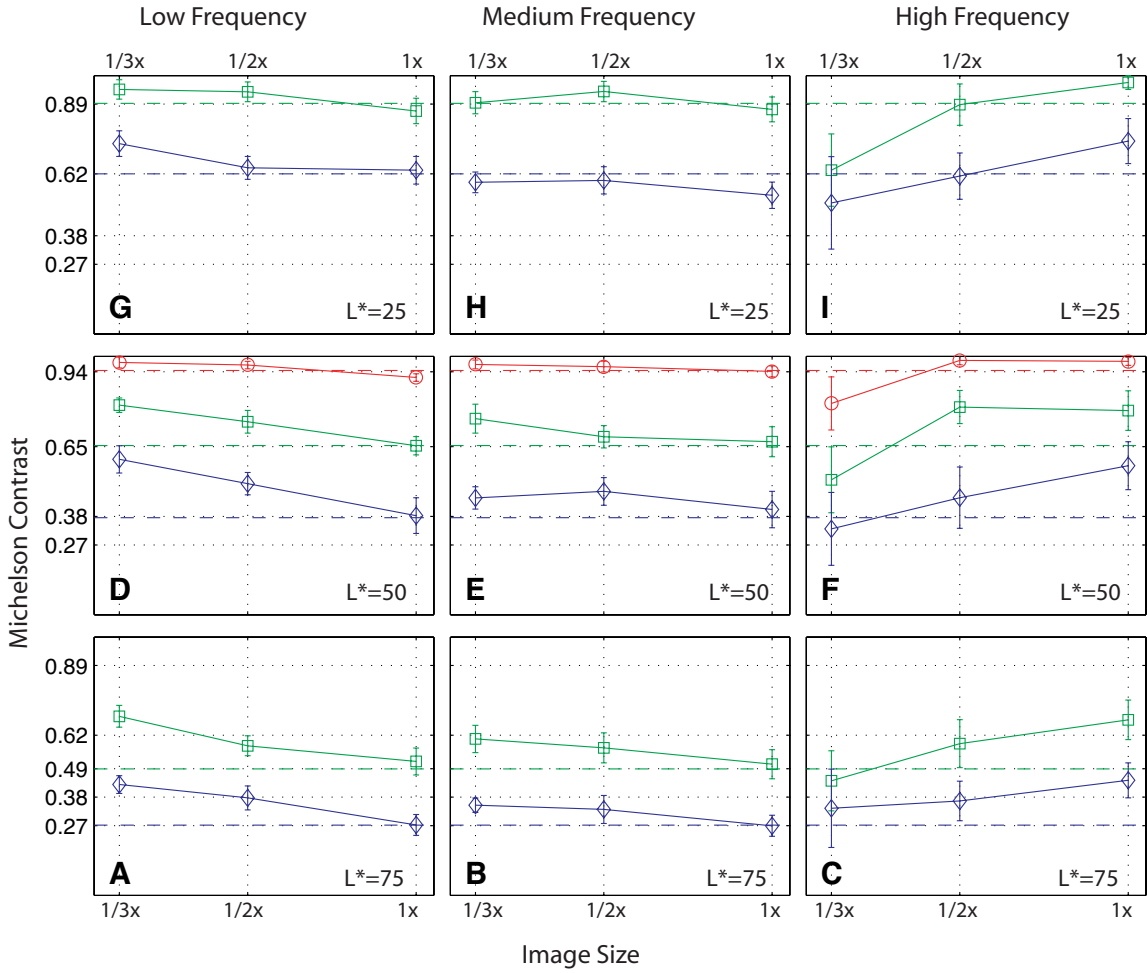


Figure 3-28. Contrast adjustment of DLP images versus LCD images for 14 observers. Panels A, D, G correspond to low frequency noise patterns, centered at 0.5 cpd, and CIEL values of 75, 50, and 25, respectively. Panels B, E, H correspond to medium frequency noise patterns. Panels C, F, I correspond to high frequency noise patterns, centered at 8 cpd. Dashed lines at each panel shows contrast of LCD images.*

An image of a sinusoid pattern of 1 cycles-per-degree scaled down to one third of its original size results in a sinusoid with 3 cycles-per-degree. In other words frequency

component of the image in the frequency domain would shift from 1 cycles-per-degree to the higher frequency of 3 cycles-per-degree. In the same way, the frequency components of complex images such as noise patterns or paintings shift toward higher frequency ranges when scaled down to a smaller size.

The visual cortex was considered as a spatial frequency analyzer [Maffei 1973], and the measured contrast sensitivity function was considered as the envelope to multiple mechanisms whose response characteristics were band-pass in the frequency domain [Wilson 1991, Losada 1994]. A qualitative representation of contrast sensitivity function is given in Figure 3-29-A. A low frequency pattern, located in the frequency range L, would shift to a higher frequency range, M, when scaled to a smaller size. The smaller and original images would be perceived based on the sensitivity of the visual mechanisms located in the range M and L, respectively. If the sensitivity of mechanism M was higher than L then one could expect the smaller image to have a higher perceived contrast than the original image. The results of contrast adjustment of low frequency noise patterns presented in panels 3-28-A, 3-28-D, and 3-28-G had a very similar trend; a trend of increase of contrast versus decrease of image size.

A high frequency image and corresponding smaller image are shown in Figure 3-29-C. Scaling the high frequency image shifted it from frequency range of P to a higher frequency range, Q. If mechanism Q had lower contrast sensitivity than P then the smaller image would be perceived to have a lower contrast than the original image.

Similarly, a trend of decrease of contrast versus decrease of image size was seen for the high frequency noise images presented in panels 3-28-C, 3-28-F, and 3-28-I.

If an image and its smaller version were located in the plateau area of the mechanism such as the case shown in Figure 3-29-C, then the smaller and original image would be perceived approximately by the same sensitivity. In such cases, the original and scaled image could have different or the same perceived contrast depending on the difference in sensitivity from area N to O. Results shown in panels 3-28-B, 3-28-E, and 3-28-H implies that scaling medium frequency noise images to smaller sizes did not change the perceived contrast significantly. The confidence intervals for the mean of the most of adjusted contrast values in panels 3-28-B, 3-28-E, and 3-28-H were overlapping; so they were not statistically different.

The results of contrast adjustment, shown in Figure 3-28, are in agreement with the concept of multiple mechanisms whose response characteristics are band-pass in the frequency domain. Actually, one could consider results presented in Figure 3-28 as another confirmation of the multiple mechanisms concept, suggested in previous research [Blackemore 1968, Maffei 1973, Wilson 1991, Losada 1994]. In chapter 5, a band pass filter, similar to an envelope to multiple mechanisms of the HVS, for a given mean luminance, was optimized. Those band-pass filters were able to adjust an image for the effect of scaling down and were used to render images of a few paintings for small size reproduction on the LCD.

There were a few other interesting observations to note. Although the experiments for contrast matching were in supra-threshold range, contrast constancy did not hold completely. However, in panels 3-28-D, 3-28-E, and 3-28-F, for images that initially had high contrast, the change in contrast before and after adjustments was not very significant. In other words, contrast constancy held for these very high contrast samples. For high frequency images for the same retinal angle, 1X, despite the equal initial contrast of DLP and LCD images, observers perceived LCD images to have higher contrast and adjusted DLP images to higher contrast levels to match appearance.

The error bars for contrast matching of high frequency noise patterns, Figures 3-28-C, 3-28-F, and 3-28-I, were larger than error bars for medium and low frequency bands. This was more pronounced for small images, at a magnification factor of 1/3X. This might be attributed to the lower sensitivity of the human visual system at high frequency range, which could result in the higher uncertainty in the perceived contrast and consequentially in contrast adjustment. This uncertainty would increase with lower sensitivity at higher frequency pattern for the lower signals, in other words, lower mean luminance values. The darkest image with the highest frequency content had the largest confidence interval since it had the lowest signal and was perceived with the lower sensitivity. (This corresponded to the high frequency image with CIEL* of 25 with a contrast of 0.62 shown in Figure 3-28-I.)

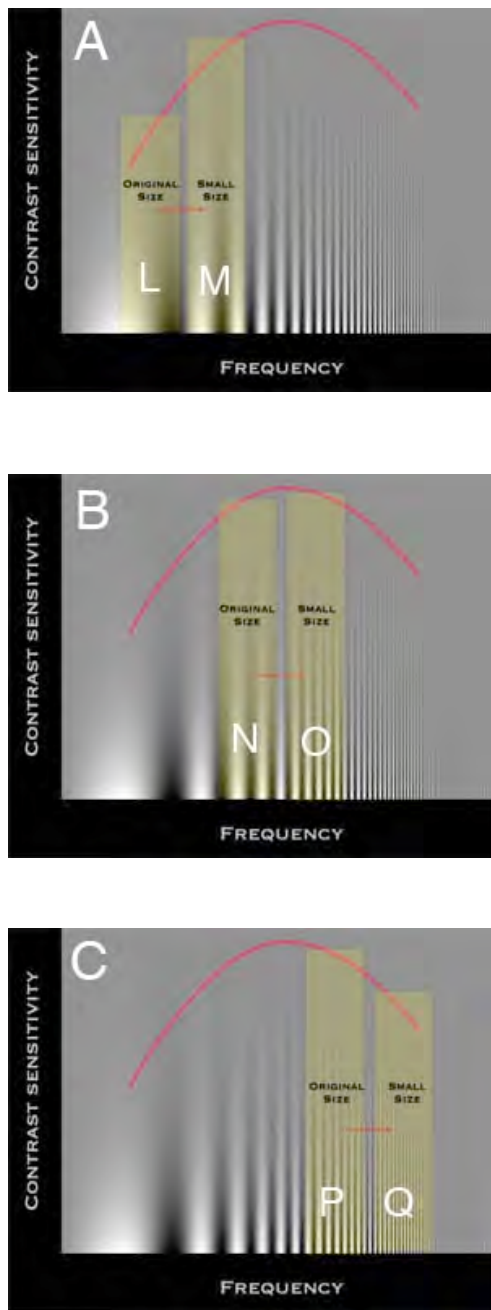


Figure 3-29. A band-pass filter in frequency domain similar to a contrast sensitivity function. Shift in frequency domain due to scaling down to smaller size for noise images of A: low frequency; B: medium frequency; C: high frequency.

The results of adjustment of mean luminance of the noise patterns versus image size are shown in Figure 3-30. A 95% confidence interval was computed for each mean luminance value using Equation (3-11), stated in Section 3.1.4. At each panel the dashed line shows the mean luminance level of the LCD image, which was fixed for three different sizes. Observers were adjusting luminance levels of the DLP images compared to the corresponding images on the LCD.

For low frequency images, panels 3-30-A, 3-30-D, and 3-30-G, mean luminance values of DLP images were adjusted to a lower or equal level compared to corresponding images on the LCD. The effect was more pronounced for medium and low contrast images at high luminance values, as shown in panels 3-30-D and 3-30-G at 86 (cd/m^2). The change of mean luminance was not very significant at the low luminance level, 8 (cd/m^2), for all frequency bands. Conversely, the change of mean luminance values before and after adjustments were significant at high luminance levels at all frequency bands, as shown in panels 3-30-D, 3-30-E, 3-30-F, 3-30-G, 3-30-H and 3-30-I at 86 (cd/m^2).

Observers perceived LCD images to be darker than DLP at the same retinal size, or 1X magnification, but perceived LCD images to be much darker for a magnification of 1/3X. Computed confidence intervals for high luminance images were relatively larger than those of low and medium luminance levels as seen in panels 3-30-D, 3-30-E, 3-30-F, 3-30-G, 3-30-H and 3-30-I at 86 (cd/m^2).

Two uniform patches of 50 (cd/m^2) with surfaces of 1 and 2 square meters need 50 and 100 (cd) of energy, respectively: the larger the surface the larger the amount of required energy. A subject observing the two patches with the same visual angle receives the same amount of energy from each patch. They have the same $\text{lum}/\text{sr} \cdot \text{m}^2$ and a radiometer reports the same radiance/luminance for the both patches regardless of their sizes or total energies. So, one could conclude that there would not be any difference in the perceived brightness versus surface area if the surfaces had the same luminance/radiance. However, based on the experimental results presented in this and the previous chapter, it seemed that observers were evaluating the brightness of images on the DLP and LCD based on both luminance and total energy. This might be attributed to cognitive visual mechanisms and complex processing in the human visual system. The luminance was the main criterion and had a much higher weighting in their judgment but the size of stimuli, which was in direct correlation with the total energy of the surface, affected the judgment, too. One could hypothesize that for LCD and DLP images with the same mean luminance, the DLP images are always perceive brighter regardless of the frequency and magnification factors, since they always have a greater total energy. For smaller images on the LCD, such as magnifications of 1/2X and 1/3X, this effect would be more pronounced. However with a decrease of mean luminance, the perceived difference in brightness would decrease. As shown in Figure 3-30, there was not a significant difference for the low lightness level, having a mean luminance of about 8 cd/m^2 .

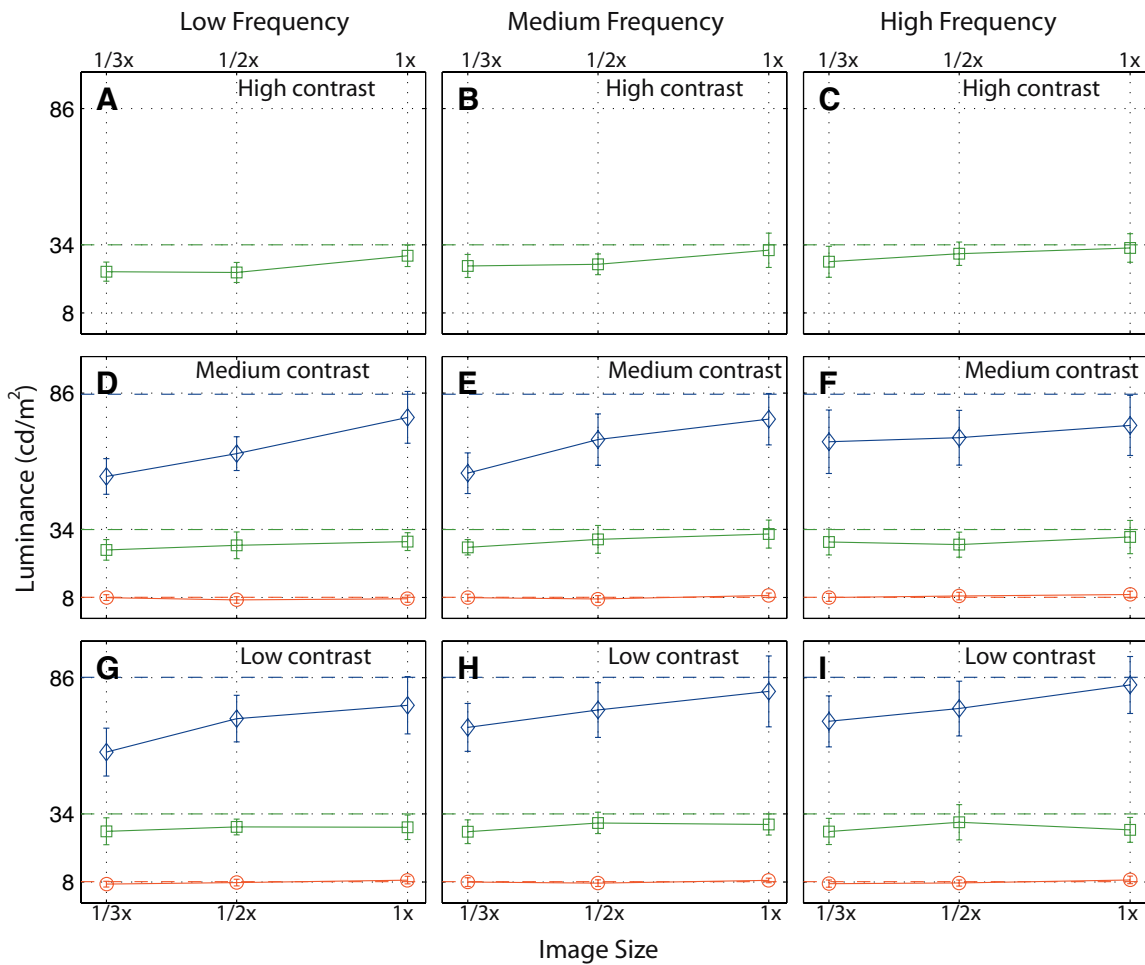


Figure 3-30. Luminance adjustment results for DLP images versus LCD images for 14 observers. Panels A, D, G correspond to low frequency noise patterns, centered at 0.5 cpd, and three levels of contrast levels. Panels B, E, H correspond to medium frequency noise patterns, centered at 2 cpd. Panels C, F, I correspond to high frequency noise patterns, centered at 8 cpd. Dashed line at each panel shows mean luminance of LCD images.

The adjustment of mean luminance values versus changes of image size had a similar trend for low, medium, and high frequency bands with overlapping confidence

intervals for all samples with the same initial mean luminance. Collected data for low, medium, and high frequency images were not statistically different. So, all data with the same initial mean luminance values were pooled together regardless of their frequency bands. Mean values at each luminance and size-scaling factor were computed. The three mapping curves for CIE L* from LCD to DLP for the 1X, 1/2X, and 1/3X magnification factors are presented in Figure 3-31. As an example, for 1/3X scaling factor, shown by the red line, a lightness of 60 on DLP screen was mapped to a value of 67 on the LCD display. As shown in Figure 3-31, DLP display was always perceived brighter than the LCD. Therefore, for any given image displayed on the DLP screen with a mean luminance value of L_{dlp} , an amount of ΔL should be added to the LCD image to make a match between LCD and DLP display lightness appearance. The ΔL can be calculated from curves in Figure 3-31:

$$\Delta L = L_{lcd} - L_{dlp} \quad (3-14)$$

where L_{dlp} and L_{lcd} are the CIEL* values on the ordinate and abscissa of the plot shown in Figure 3-31, respectively.

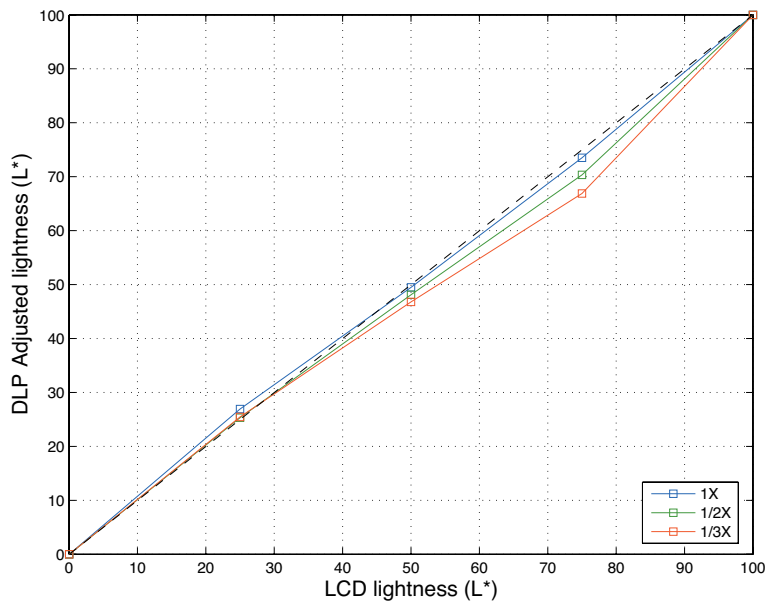


Figure 3-31. Adjusted mean lightness of noise patterns on the projector screen versus the mean lightness of corresponding images on the LCD for three magnification factors of 1/3X, 1/2X, and 1X.

In this experiment DLP images were adjusted to match the LCD images. It is a common practice to render an image of a large painting to a smaller size. The results of this experiment showed that for low frequency patterns one would need to reduce the contrast and increase the mean luminance of an LCD image to match the appearance of a reproduced image on the DLP screen. For high frequency patterns an increase in the mean luminance and a reduction of contrast for the LCD image would be needed. Two examples, a low and high frequency noise patterns adjusted and rendered for LCD, are presented in Figure 3-32 and 3-33, respectively. The same patterns colorimetrically rendered for the LCD display are shown also in the corresponding figures.

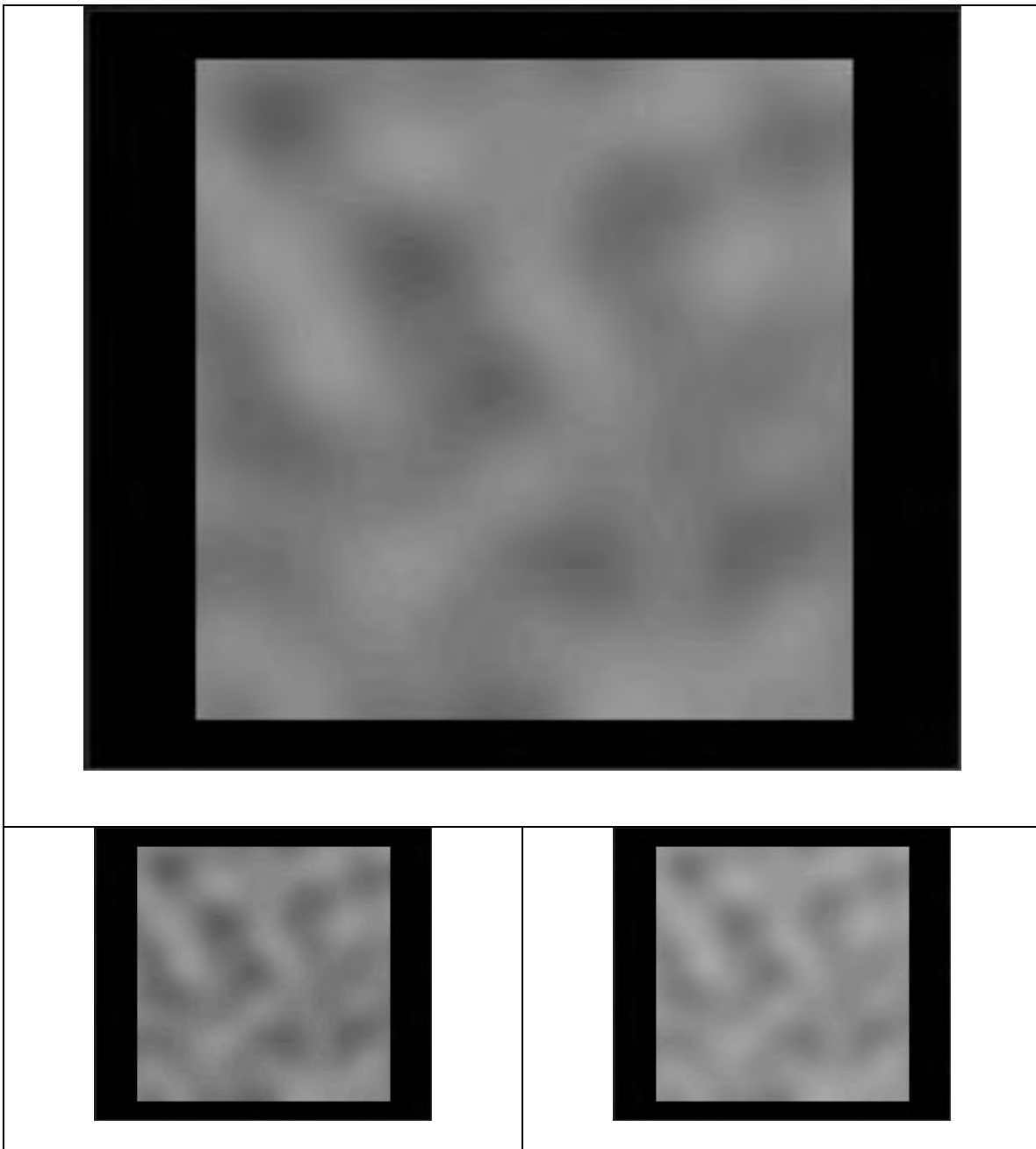


Figure 3-32. Top: low frequency noise pattern, image numbered 5 in Table 1-1, rendered for DLP display; Bottom left: same pattern colorimetrically rendered for LCD; Bottom right: same pattern colorimetrically rendered and also adjusted for the effect of 1/3X magnification for the LCD display.

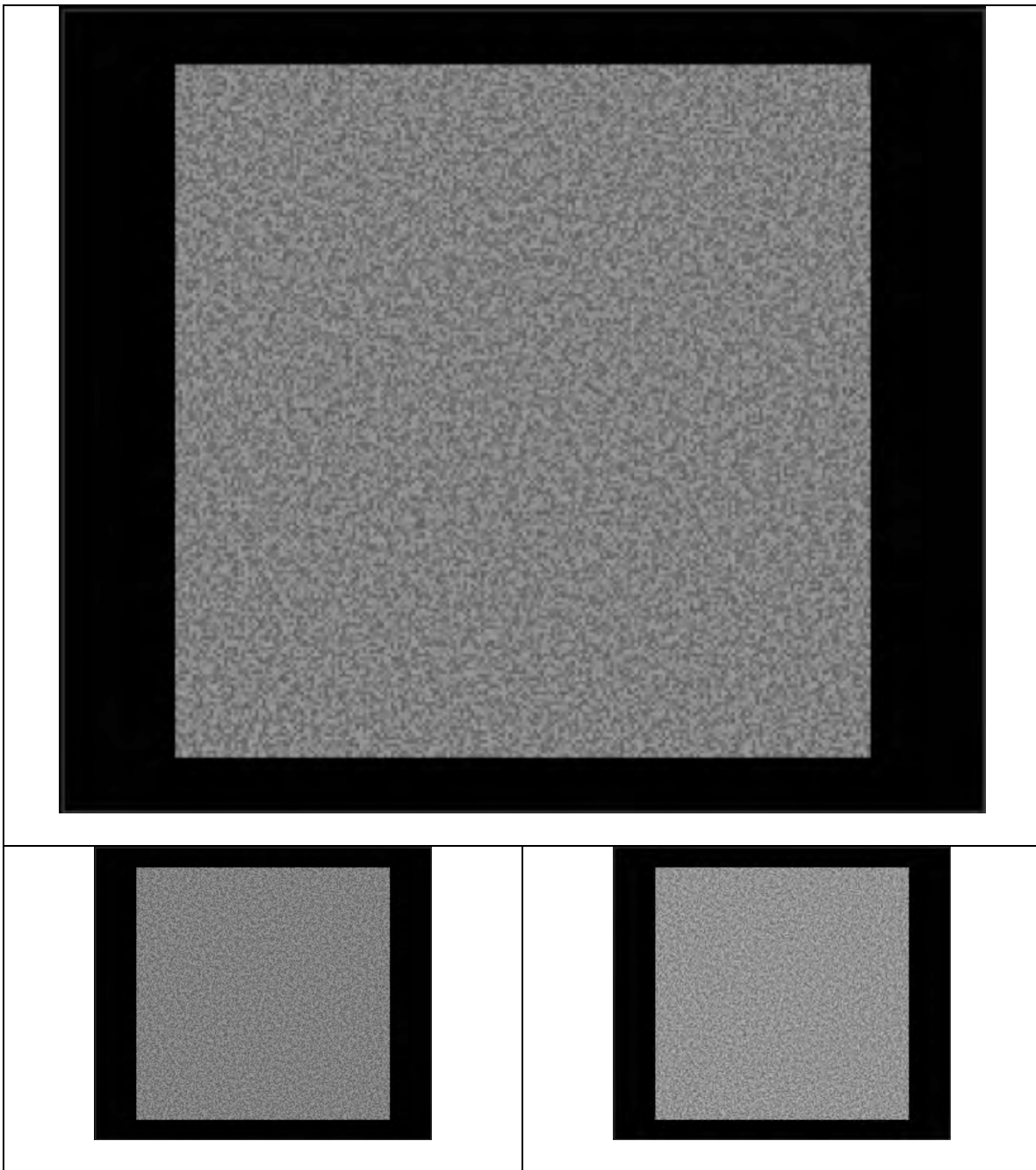


Figure 3-33. Top: high frequency noise pattern, image numbered 5 in Table 1-1, rendered for DLP display; Bottom left: same pattern colorimetrically rendered for LCD; Bottom right: same pattern colorimetrically rendered and also adjusted for the effect of 1/3X magnification for the LCD display.

3.2.7 Conclusions

The characterized LCD and DLP displays had good colorimetric accuracy in the reproduction of gray colors used in this research. Using the method of adjustment, it was shown that both mean luminance level and contrast were affected by image size. The method of adjustment utilized in this experiment successfully showed a trend of the increase of contrast in adjusted images versus the decrease of image size on the LCD display for low frequency band-pass noise patterns. Conversely, high frequency, small size images on the LCD were matched with images of low contrast on screen. This decrease in contrast was more pronounced for images with high mean luminance levels. Contrast constancy was observed for high contrast images. These results were consistent with the previous contrast matching experiment using Gabor patterns.

Compared to the mean luminance level of the LCD images, a decrease of the mean luminance level of the adjusted images was observed for all frequency noise patterns. This decrease was more pronounced for smaller images at. At low level of mean luminance, the change of luminance was not significant.

A similar trend was obtained for the previous experiment, described in Section 3.1, for mean luminance adjustment of Gabor patterns. In other words the larger images on DLP were perceived brighter than smaller images on the LCD. In previous experiments, [Xiao 2004], comparing small paint chips with painted walls, size enlargement caused an increase in perceived lightness which is consistent with the result of this experiment.

The dependency of the changes in mean luminance level and contrast to frequency content of images provided a better understanding for accounting the image size effect on image appearance.

4 CHROMATIC CONTRAST MATCHING

In order to develop a multiscale model accounting for the effect of image size on image appearance, both achromatic and chromatic attributes of an image should be considered.

In the Section 3.2 achromatic contrast matching using band-pass noise images was performed. In the following sections, a series of psychophysical experiments using chromatic patterns in IPT space are presented. The goal was to capture the effect of image size on the chromatic attributes of an image. Isoluminant band-pass noise patterns with varying chroma along a few selected hues were adjusted on a DLP screen to match corresponding images on an LCD display.

As described in Section 1.6.5, in the Helmholtz-Kohlrausch Effect, brightness of a color is dependent on both its luminance and chromaticity. Changes in chroma of a test pattern are accompanied by perceived changes in brightness. Experiments have shown that the Helmholtz-Kohlrausch Effect also holds for related colors [Fairchild 2005]. Hence a preliminary experiment to evaluate the magnitude of Helmholtz-Kohlrausch effect was conducted. In order to prevent interference of lightness changes with chromatic variations, the lightness of the noise images, used in the chromatic contrast matching, was adjusted based on the result of the preliminary experiment. The adjustments were applied to the test patterns in such a way that all noise patterns along a selected hue with variable chromatic contrast were perceived to have the same lightness.

4.1 Color Space

It was very important that the hue of the test patterns would not vary with changes in chroma in the chromatic contrast matching experiment. The most important attribute of the IPT color space is the linearity of constant perceived hue [Fairchild 1996]. So the IPT color space was selected and used in chromatic contrast matching to benefit from its constant hue lines. The IPT model was invertible and a simple model to implement. The input of the model was tristimulus values for the CIE 1931 standard observer and D₆₅ illumination. Therefore, in the first step, the XYZ of a color on an LCD or DLP display should be converted to the corresponding color under D₆₅. Conversion of tristimulus values of a pixel in an image, XYZ_{img} , to its corresponding color under D₆₅, $X_C Y_C Z_C$, is shown in equations (4-1) to (4-9).

$$M_{CAT02} = \begin{bmatrix} 0.7328 & 0.4296 & -0.1624 \\ -0.7036 & 1.6974 & 0.0061 \\ 0.030 & 0.0136 & 0.9834 \end{bmatrix} \quad (4-1)$$

$$\begin{bmatrix} R_{D65} \\ G_{D65} \\ B_{D65} \end{bmatrix} = M_{CAT02} \begin{bmatrix} X_{D65} \\ Y_{D65} \\ Z_{D65} \end{bmatrix} \quad (4-2)$$

$$\begin{bmatrix} R_{LCDw} \\ G_{LCDw} \\ B_{LCDw} \end{bmatrix} = M_{CAT02} \begin{bmatrix} X_{LCDw} \\ Y_{LCDw} \\ Z_{LCDw} \end{bmatrix} \quad (4-3)$$

$$\begin{bmatrix} R_{img} \\ G_{img} \\ B_{img} \end{bmatrix} = M_{CAT02} \begin{bmatrix} X_{img} \\ Y_{img} \\ Z_{img} \end{bmatrix} \quad (4-4)$$

$$R_{eq} = \left[\frac{100D}{R_{LCDw}} + (1 - D) \right] R_{img} \quad (4-5)$$

$$G_{eq} = \left[\frac{100D}{G_{LCDw}} + (1 - D) \right] G_{img} \quad (4-6)$$

$$B_{eq} = \left[\frac{100D}{B_{LCDw}} + (1 - D) \right] B_{img} \quad (4-7)$$

$$R_C = \frac{R_{eq} R_{D65}}{100} \quad G_C = \frac{G_{eq} G_{D65}}{100} \quad B_C = \frac{B_{eq} B_{D65}}{100} \quad (4-8)$$

$$\begin{bmatrix} X_C \\ Y_C \\ Z_C \end{bmatrix} = M_{CAT02}^{-1} \begin{bmatrix} R_C \\ G_C \\ B_C \end{bmatrix} \quad (4-9)$$

where X_{LCDw} , Y_{LCDw} , and Z_{LCDw} are tristimulus values of the LCD white point and X_{D65} , Y_{D65} , and Z_{D65} are tristimulus values of D_{65} light source, respectively. The X_C , Y_C , and Z_C are corresponding tristimulus values under D_{65} for the XYZ_{img} on the LCD. The parameter D is the degree of adaptation, which would be equal to 1.0 for a complete adaptation case. For all experiments performed in this research complete adaptation was assumed and D was assigned to 1.0. In the first step tristimulus values of the LCD white point, D_{65} light source, and image pixel were converted to an RGB response using the CIE Chromatic Adaptation Transform matrix (M_{CAT02}). The tristimulus values under D_{65} were transformed to the cone response space, LMS, using the Hunt-Pointer-Estevez transformation (M_{HPE}), described in Equation (4-10). Using exponential functions, the LMS signals were properly compressed and calculation was followed by another (3x3)

matrix multiplication, which resulted in the I, P, and T color coordinates. The parameters and computation process are shown in matrix form in Equations (4-10) to (4-17):

$$\begin{bmatrix} L \\ M \\ S \end{bmatrix} = \begin{bmatrix} 0.4002 & 0.7075 & -0.0807 \\ -0.2280 & 1.1500 & 0.0612 \\ 0.0 & 0.0 & 0.9184 \end{bmatrix} \begin{bmatrix} X_{D65} \\ Y_{D65} \\ Z_{D65} \end{bmatrix} \quad (4-10)$$

$$L' = L^{0.43}; L \geq 0 \quad (4-11)$$

$$L' = -|L|^{0.43}; L \leq 0 \quad (4-12)$$

$$M' = M^{0.43}; M \geq 0 \quad (4-13)$$

$$M' = -|M|^{0.43}; M \leq 0 \quad (4-14)$$

$$S' = S^{0.43}; S \geq 0 \quad (4-15)$$

$$S' = -|S|^{0.43}; S \leq 0 \quad (4-16)$$

$$\begin{bmatrix} I \\ P \\ T \end{bmatrix} = \begin{bmatrix} 0.4000 & 0.4000 & 0.2000 \\ 4.4550 & -4.8510 & 0.3960 \\ 0.8056 & 0.3572 & -1.1628 \end{bmatrix} \begin{bmatrix} L' \\ M' \\ S' \end{bmatrix} \quad (4-17)$$

where L, M, and S are cone responses and I, P, T are color coordinates in IPT color space. Chroma of a color is computed using P and T:

$$C = \sqrt{P^2 + T^2} \quad (4-18)$$

where C denoted chroma.

The same calculation can be used for the DLP display by replacing the LCD white point with the DLP white point. Therefore, one could compute IPT of a color on an LCD or DLP from its tristimulus values, XYZ, for an adapting white point such as XYZ_{LCDw} .

Furthermore, it was possible to calculate XYZ from an IPT color coordinates for a specific white point such as XYZ_{LCDw} , using Equations (4-1) to (4-17) in the reverse direction. The above calculation is briefly presented in a flowchart in Figure 4-1.

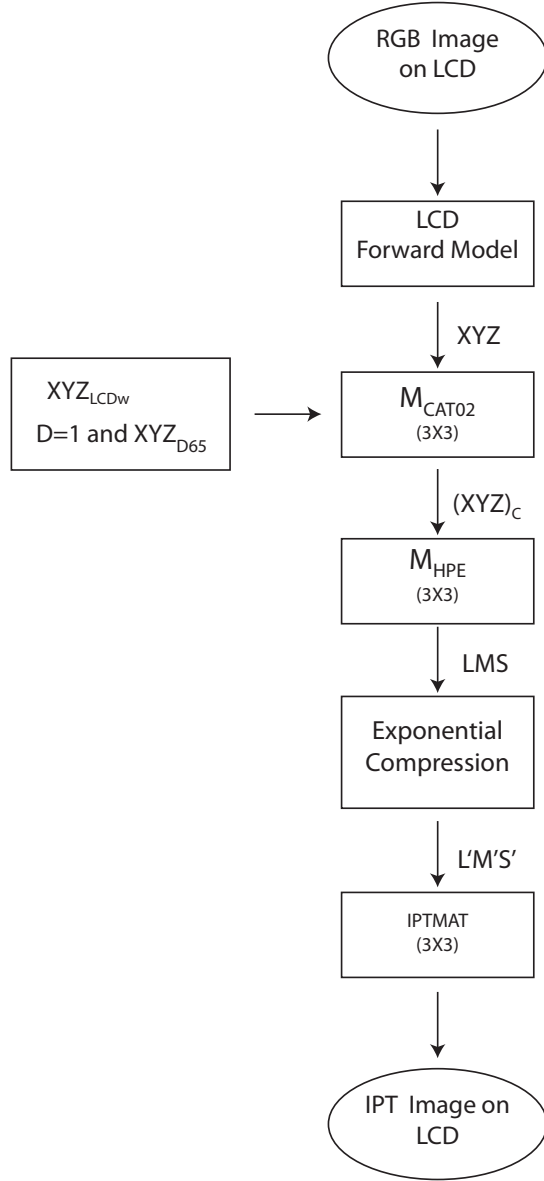


Figure 4-1. Forward model from RGB digital counts to IPT color coordinates.

4.2 Correction for the Helmholtz-Kohlrausch Effect

The goal of the chromatic contrast matching was to capture the effect of image size on the chromatic appearance of test patterns. One should use isoluminant test patterns to prevent the unwanted effect of lightness variation on the results of chromatic contrast matching. In this way the observers' judgments would be only based on the chromatic alteration due to changes in image size. In a preliminary experiment observers were asked to adjust lightness of chromatic patches, for a few hues, in comparison to a gray patch with the same lightness. The adjusted lightness values of the chromatic patches were used to correct lightness of the chromatic band-pass noise patterns and generate corresponding isoluminant noise images.

4.2.1 Stimulus and Experimental Setup

The same LCD, an IBM T221LCD, and characterization data used in the previous experiment, described in chapter 3, was used in this experiment. Five colors of red, green, blue, magenta, and yellow were selected. These colors corresponded to (R, G, B) digital counts of (255,0,0), (0,255,0), (0,0,255), (0,255,255), and (255,255,0), respectively. These five colors are called primary colors in the rest of this chapter. The tristimulus values for the CIE 1931 standard observer and corresponding IPT color coordinates of these colors are listed in Table 4-1.

Table 4-1. Tristimulus values, in cd/m^2 , for the CIE 1931 standard observer and IPT color coordinate of the selected five primary colors.

	Red	Green	Blue	Yellow	Magenta
X	97.6	68.3	42.1	165.3	139.1
Y	53.4	137.7	31.5	190.4	84.3
Z	4.5	24.5	210.1	28.2	213.8
I	0.4811	0.7180	0.5301	0.8306	0.7303
P	0.5916	-0.4130	-0.2791	-0.0416	0.4209
T	0.4710	0.4845	-0.6317	0.6340	-0.3128

Color coordinate of the primary colors projected onto the P-T plane are plotted in Figure 4-2.

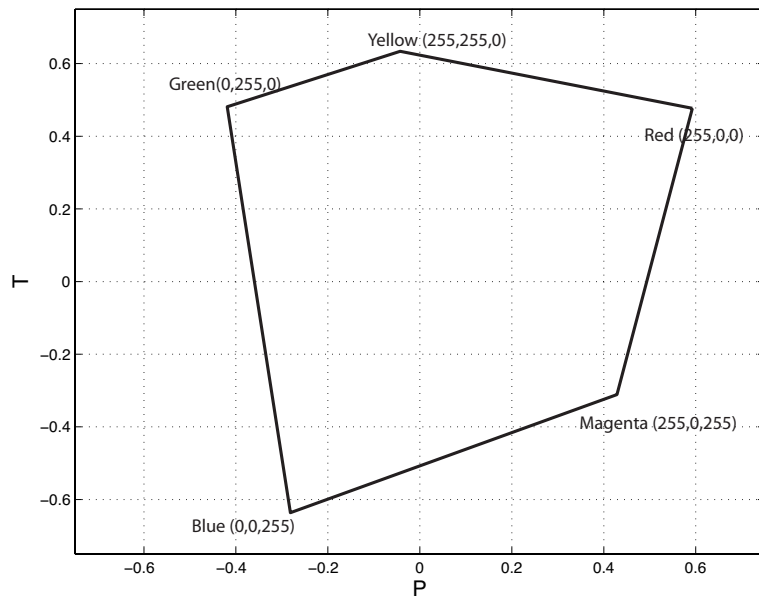


Figure 4-2. IPT color coordinates of the selected five hues for the IBM display.

In a psychophysical experiment, conducted in a dark environment, observers were asked to adjust perceived lightness of the primary colors compared to gray patches

displayed on the LCD at two lightness level of I=0.25 and I=0.75. It is important to note that the primary colors were at the edge of the LCD color gamut and there was no room for changes of lightness. Hence, chroma of the color patches was reduced to provide enough room for changes of lightness. The reduction of chroma for each primary color at each lightness level is given in Table 4-2. As an example, the chroma of the primary yellow was reduced to 85% of its original value at lightness level of I=0.75.

The tristimulus values for the CIE 1931 standard observer, XYZ, and corresponding IPT color coordinates for the reduced primary colors at two lightness levels of I=0.25 and I=0.75 are listed in Table 4-3. Color coordinates of the reduced primary colors, in IPT color space, are plotted in Figure 4-3. The red primary, corresponding to digital counts of (255,0,0) with (I, P, T) values of (0.4811, 0.5916, 0.4710) is also shown in Figure 4-3. The ‘I’ attribute was presented by the vertical axes and the two planes corresponded to the P-T surfaces at lightness levels of I=0.25 and I=0.75. The plane of constant hue encompassing the red primary and corresponding two reduced colors is shown by a pale red plane in Figure 4-3.

Sixteen observers, ten males and six females, adjusted lightness of 30 color patches ($30 = 5 \text{ hues} \times 2 \text{ lightness} \times 3 \text{ repetitions}$) in comparison to the two gray patches at I=0.25 and I=0.75. A screen shot of the LCD display is presented in Figure 4-4. Two rectangular patches, a gray and a primary color, were displayed on a gray background. The gray background had a lightness of I=0.5. The two patches were 17.5 cm wide and 20 cm high and there was a 2 cm gap between them. Observers were standing about 50

cm away from the LCD display. Two strips, 1cm wide, of black and white colors were displayed at the edge of the image. The black and white strips were presenting anchor points for minimum and maximum lightness in the scene and to induce the perception of the related colors.

Table 4-2. Reduction of chroma for each primary color at selected lightness levels.

		Hues				
		Red	Green	Blue	Yellow	Magenta
Lightness, I	0.25	0.45	0.25	0.25	0.35	0.30
	0.75	0.20	0.45	0.30	0.85	0.50

Table 4-3. IPT color coordinates and tristimulus values, in cd/m², for the chromatic colors used in lightness adjustment.

		Red	Green	Blue	Yellow	Magenta
I=0.25	X	19.2	6.5	6.8	10.7	11.1
	Y	11.3	11.0	7.0	12.2	7.2
	Z	1.6	3.6	21.4	1.1	16.6
	P	0.2662	-0.1033	-0.0698	-0.0146	0.1263
	T	0.2120	0.1211	-0.1579	0.2219	-0.0938
I=0.75	X	121.8	91.2	94.3	127.9	125.8
	Y	117.2	129.3	103.3	147.6	101.3
	Z	100.0	71.2	174.1	25.5	168.2
	P	0.1183	-0.1859	-0.0837	-0.0353	0.2105
	T	0.0942	0.2180	-0.1895	0.5389	-0.1564

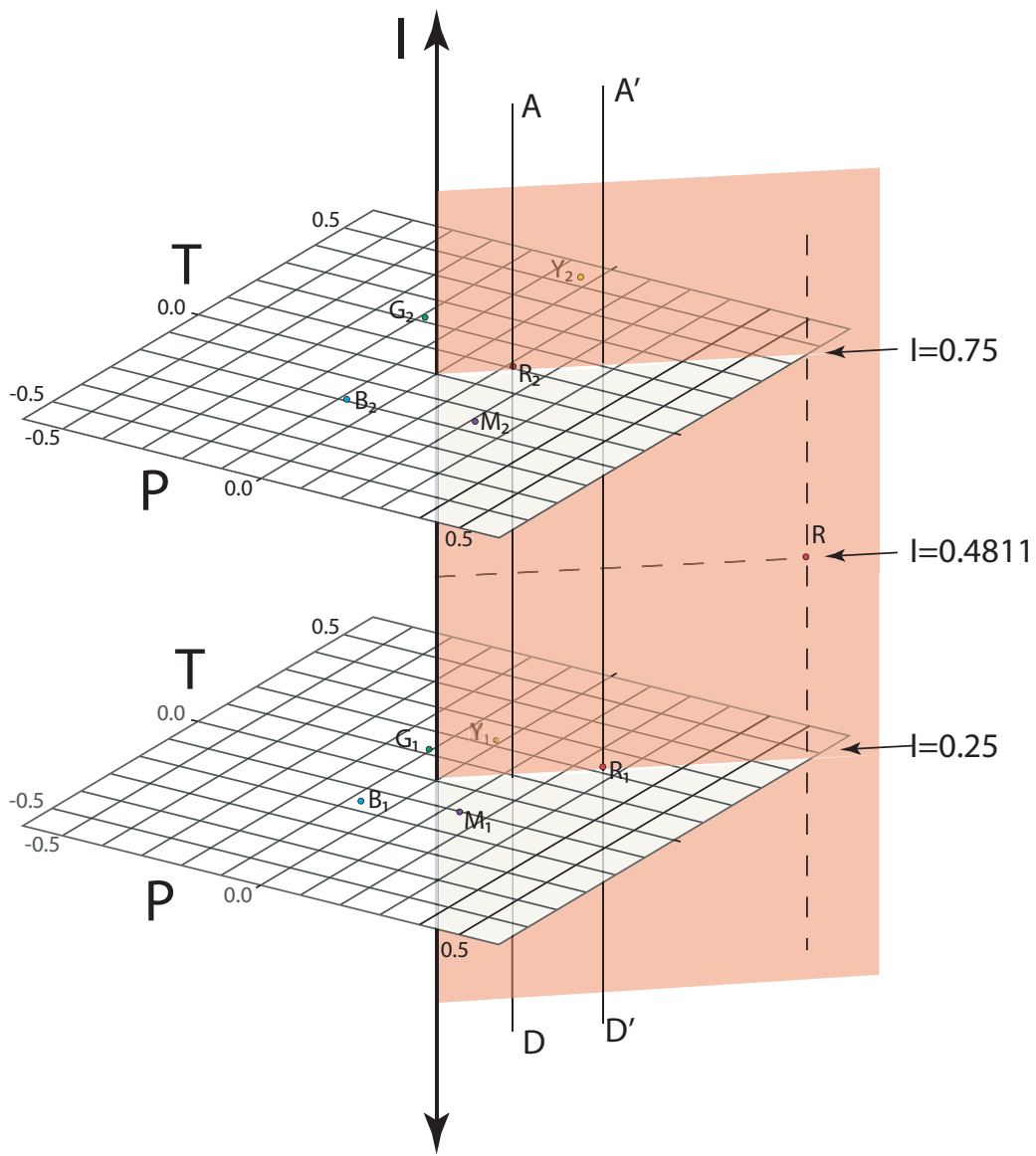


Figure 4-3. The red, green, blue, yellow, and magenta colors are tagged as R_1 , G_1 , B_1 , Y_1 , and M_1 at a lightness level of $I=0.25$. Symbols R_2 , G_2 , B_2 , Y_2 , and M_2 denote the same colors at a lightness level of $I=0.75$. The red color corresponding to digital counts of $(255, 0, 0)$ is shown by ‘ R ’ symbol. The plane of constant hue for the red color encompassed the R_1 , R_2 , and R colors.

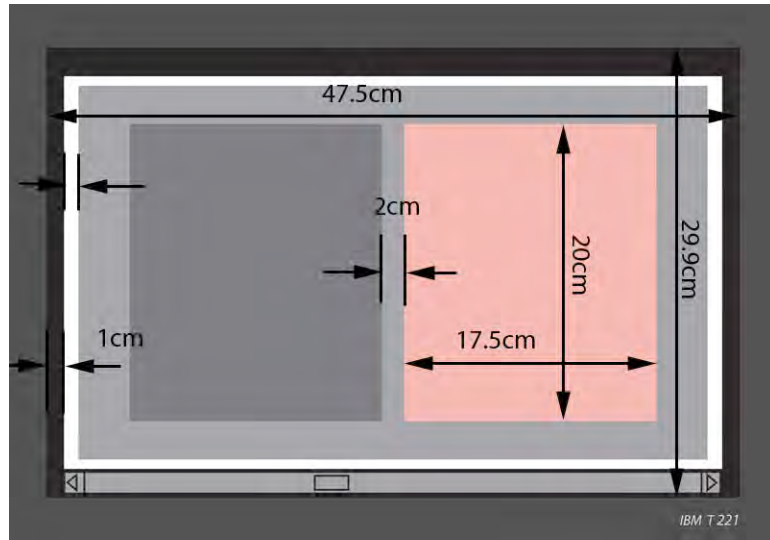


Figure 4-4. Lightness of the chromatic patch was adjusted to match the lightness of the achromatic patch. The instruction was: “Please adjust lightness of the color patch to the same lightness as of the gray patch using ShuttleXpress dialer. A clockwise turn increases lightness of the patch. You can decrease lightness by a counterclockwise turn.”

A screen shot of the IBM display for the psychophysical experiment is presented in Figure 4-4. Observers could adjust the lightness of the chromatic patch using a ShuttleXpress dialer (the same dialer used in the achromatic contrast matching.) A horizontal scroll bar ranging from [0 1], corresponding to lightness attribute, I, depicted the adjusted lightness value of the chromatic patch at each moment. Turning the dialer in clockwise direction could add an increment of $\Delta I=0.0025$ to the lightness value and shift the scroll bar to the right side. Conversely a counterclockwise turn would decrease lightness by $\Delta I=0.0025$ and shift the scroll bar to the left side. In each adjustment, the P and T color coordinates of the chromatic patch were kept constant and only lightness was

varying. For example, the red color with (I, P, T) coordinates of (0.25, 0.2662, 0.2120) was compared to a gray patch with (I, P, T) coordinates of (0.25, 0, 0) and could only move along an axis of constant P and T, the $A'D'$ axis shown in Figure 4-3. Similarly, for the same hue at lightness level of 0.75, the chromatic patch was compared to a gray patch of (0.75, 0, 0) and adjusted along a constant P and T axis, depicted by axis line AD in Figure 4-3.

Samples were presented to observers in a random order. There were intervals of 5 seconds between adjustments, controlled by the data collection software. A random noise pattern was also displayed between each adjustment. Color patches had initial lightness values selected from a uniform random distribution in the range of [-20%, +20%] of their original values.

4.2.2 Results and Discussion

Observers' adjustments at the two lightness levels for each color are presented in Figure 4-5. The two dashed lines at lightness levels of I=0.25 and I=0.75 corresponded to the lightness of the gray patches. For each color mean and corresponding 95% confidence interval were computed, as described in Section 3.1.4, using Equation (3-11). From Figure 4-5 one can see that all color patches were adjusted to darker or equal lightness in comparison to the corresponding gray patches. Primary colors with a lightness of I=0.75 were adjusted to lightness values lower than 0.75. Color patches were perceived lighter than the gray patch; so observers reduced lightness values of the color patches. The

Green and yellow colors had the largest lightness reduction. At lightness level of 0.25, the blue, yellow, and magenta patches were perceived the same lightness as the gray patch. But, the red and green primaries were perceived lighter than the gray patch and were adjusted to relatively darker colors.

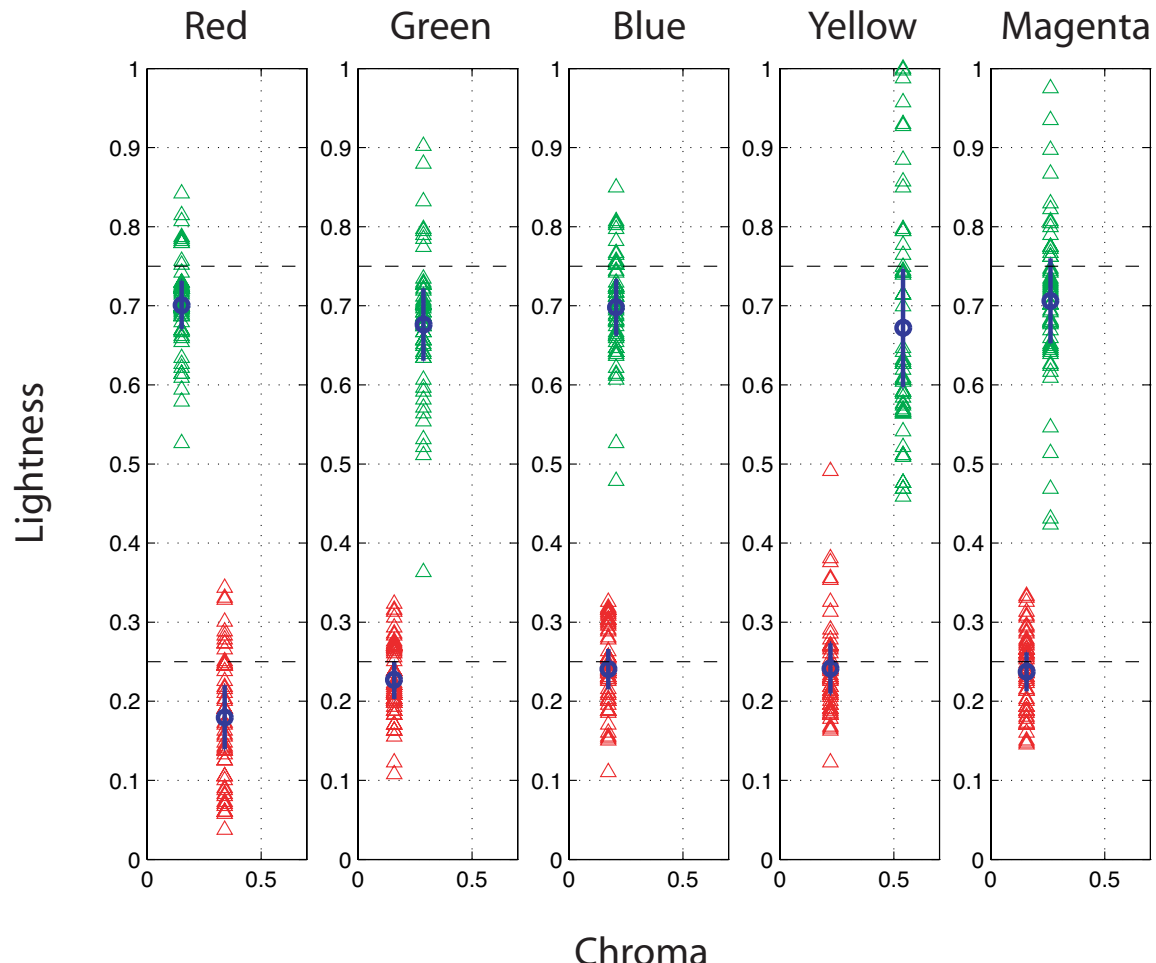


Figure 4-5. Observers' responses for the Helmholtz-Kohlrausch effect. Lightness of the gray patches are shown by dashed lines at $I=0.25$ and $I=0.75$.

Referring to Figure 4-3 and Figure 4-5, one can see that the all colors at lightness level of 0.75, except the red color, had higher chroma and were reduced in lightness more than corresponding colors at a lightness of 0.25. The more chromatic color the more reduction in lightness. These results were consistent with previous research [Fairchild 2005]. However the amount of reduction was dependent on the hue and initial lightness of the test patterns. The confidence interval of the green, blue, yellow, and magenta were overlapping with the dashed line at the lightness of 0.25; so their perceived lightness values were not statistically different from lightness of the gray patch.

Using the collected data, presented in Figure 4-5, it was possible to correct lightness of chromatic colors to account for the Helmholtz-Kohlrausch effect. Such a correction is presented below for the red color. The same calculation was performed for other colors.

Means of adjusted lightness for the red primary color, at the two lightness levels, are presented in Figure 4-6. The lightness differences between the original and adjusted primary colors are denoted by ΔL_1 and ΔL_2 for lightness values of 0.25 and 0.75, respectively. For a test color, denoted by 'A', with the same hue but different chroma and lightness, the reduction in lightness was calculated by Equation (4-19):

$$AA' = \left(1 - \frac{BA}{BD}\right)\left(\Delta L_2 \frac{CR}{CR_2}\right) + \left(1 - \frac{AD}{BD}\right)\left(\Delta L_1 \frac{CR}{CR_1}\right)$$

$$BD = 0.5 \Rightarrow AA' = \left(1 - \frac{BA}{0.5}\right)\left(\Delta L_2 \frac{CR}{CR_2}\right) + \left(1 - \frac{AD}{0.5}\right)\left(\Delta L_1 \frac{CR}{CR_1}\right) \quad (4-19)$$

where, CR_1 and CR_2 were chroma of the red primary color at lightness of 0.25 and 0.75, respectively. The CR denoted the chroma of the test color. The segment line AA' was the amount of reduction in lightness. Lightness correction shifted the test color from point A to point A'.

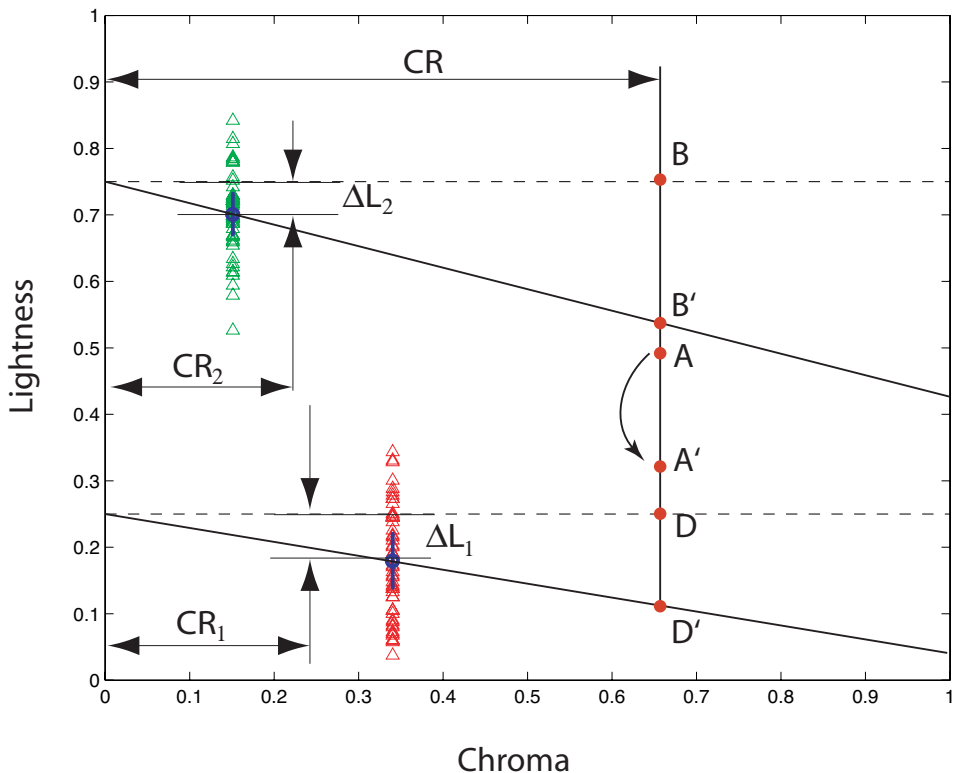


Figure 4-6. An example of perceived lightness reduction for the effect of Helmholtz-Kohlrausch for a red color denoted by A. Point A would be adjusted to A'.

The above correction method was used to generate isoluminant chromatic noise patterns used in a contrast matching experiment. The following sections describe noise pattern generation and the conducted psychophysical experiment.

4.3 Color Map Computation

The lightnesses of the primary colors were corrected based on the collected data from the preliminary experiment, described above in Section 4.2.2. The line connecting a corrected primary color and its corresponding gray was assumed to have a constant perceived lightness and hue, but varying chroma. The segment line KR' in Figure 4-7 depicts such a line with constant hue and perceived lightness in IPT space for the red primary color. The R and K denoted the primary red and corresponding gray colors and The R' was the red color corrected for the Helmholtz-Kohlrausch effect.

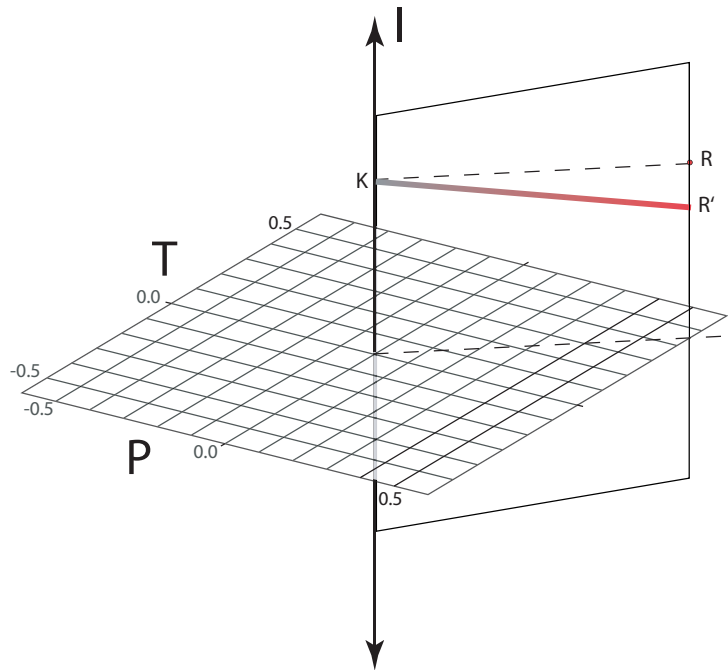


Figure 4-7. Primary red color, R, was corrected for the Helmholtz-Kohlrausch effect and denoted by R'. Segment line KR' was assumed to have a constant hue and perceived lightness.

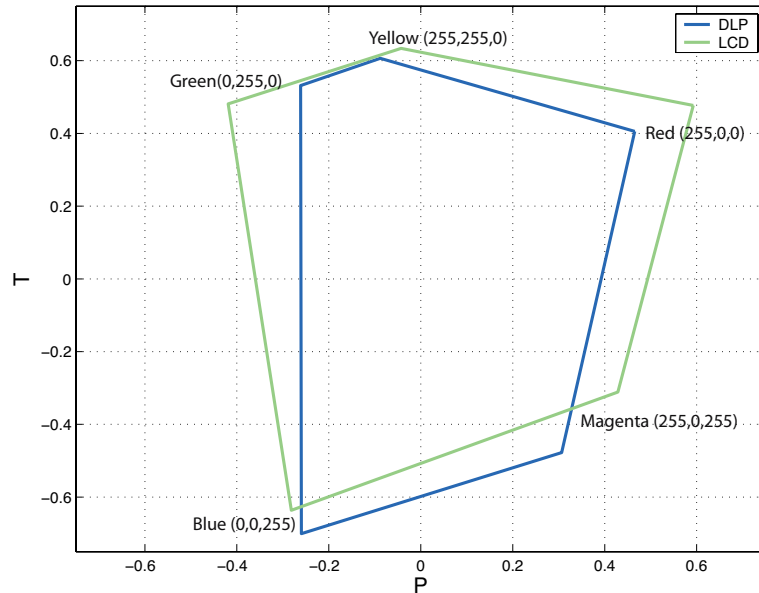


Figure 4-8. Color coordinates of the LCD and DLP primary colors projected on the P-T plane.

The LCD and DLP displays had different color gamuts, shown in Figure 4-9. In order to accommodate the primary hue lines in an overlapping area, where both LCD and DLP could accurately reproduce the hue lines, the chroma of the primary colors were reduced. Table 4-4 and 4-5 summarize the color coordinates of the start and end points of each hue line used to generate chromatic noise patterns. As an example, listed in Table 4-5, the red hue displayed on the LCD had (I, P, T) color coordinates of (0.5369, -.0037, 0.0017) and (0.4436, 0.3174, 0.2468) for the starting and ending points, the gray and primary red color, respectively. The line connecting each of the primary and corresponding gray color was divided to 400 equal steps and corresponding IPT and XYZ for the CIE 1931 standard observer were stored as proper arrays. The XYZ values were converted to RGB digital counts, using the LCD inverse characterization model, and

saved as color maps for LCD display. The same calculation was performed for the DLP projector. This is demonstrated in Figure 4-9.

Table 4-4. Tristimulus values, in cd/m², of start and end of each hue line for the CIE 1931 standard observer.

		Primary (end)			Corresponding Gray (start)		
		X	Y	Z	X	Y	Z
LCD	Red	20.19	12.47	1.75	18.24	19.55	20.86
	Green	13.11	22.60	4.47	22.34	23.83	25.23
	Blue	5.08	3.86	22.90	5.73	6.13	6.37
	Yellow	32.46	44.52	7.60	37.31	39.80	42.83
	Magenta	23.31	14.82	50.72	20.83	22.19	23.91
DLP	Red	18.46	11.55	1.38	16.36	19.42	20.01
	Green	12.89	22.34	4.13	20.15	23.98	24.57
	Blue	4.60	2.41	22.74	5.22	6.22	6.33
	Yellow	31.83	43.41	7.12	33.75	40.06	41.16
	Magenta	21.50	12.24	48.99	18.95	22.53	23.16

Table 4-5. IPT color coordinates of the start and end of each hue line for the tristimulus values listed in Table 4- 4.

		Primary (end)			Corresponding Gray (start)		
		I	P	T	I	P	T
LCD	Red	0.3986	0.3771	0.3344	0.5369	-0.0037	0.0017
	Green	0.5079	-0.2310	0.3311	0.5843	-0.0002	0.0045
	Blue	0.3231	-0.1331	-0.3528	0.3254	-0.0008	0.0057
	Yellow	0.6791	-0.1687	0.4824	0.7295	-0.0021	-0.0005
	Magenta	0.5443	0.1771	-0.3469	0.5676	-0.0009	-0.0007
DLP	Red	0.3895	0.3969	0.3438	0.5360	0.0001	-0.0009
	Green	0.5047	-0.1629	0.3352	0.5866	-0.0013	0.0007
	Blue	0.2895	-0.1199	-0.4154	0.3282	-0.0006	0.0016
	Yellow	0.6736	-0.0699	0.4827	0.7316	0.0002	0.0000
	Magenta	0.5219	0.2430	-0.3819	0.5712	-0.0007	-0.0003

Chromatic contrast was defined as the difference between the maximum and minimum values of chroma within an image. The chromatic contrast for an image with a minimum chroma value of zero would be equal to the maximum chroma in the image. Therefore, for an image with pixels ranging between a primary color and a corresponding gray, the chromatic contrast was determined by the chroma value of the primary color.

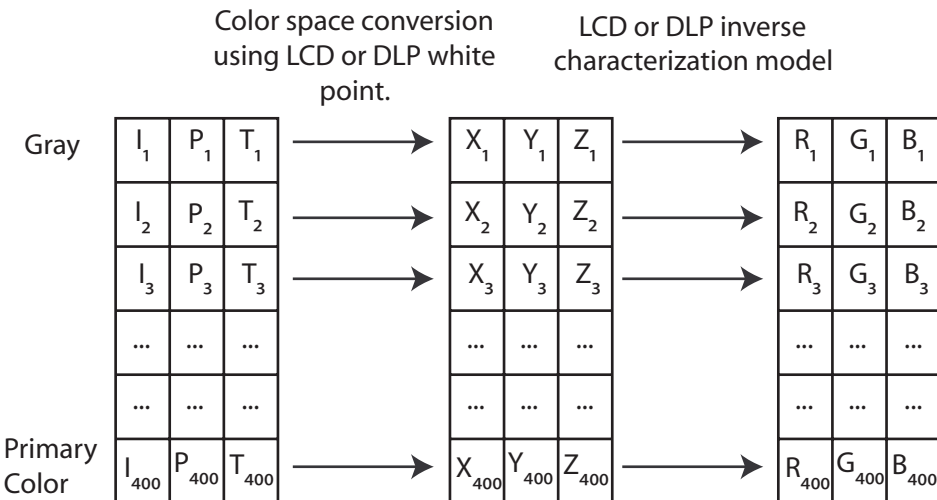


Figure 4-9. Color maps relating IPT to RGB values for LCD or DLP displays. All colors in a maps had the same hue and perceived lightness. A color map was generated for each hue. Chroma was zero for the first element and increased to the chroma of the primary color for the last element.

4.4 Chromatic Band-Pass Noise Patterns

The same white noise pattern, described in Section 3.2.3 and denoted by matrix N , was used to populate chromatic noise patterns at the five selected hues. Cosine log filters, discussed in Chapter 3, were utilized to filter the white noise image.

A typical example of contrast sensitivity functions for chromatic and achromatic contrast of the human visual system is presented in Figure 4-10. It is known that the chromatic mechanisms of the human visual system have lower cutoff frequencies than achromatic mechanisms [Fairchild 2005]. Therefore, lower center frequencies were selected for the cosine log filters for the chromatic noise generation than those used for the achromatic noise calculations. The cosine log filters were computed, using Equation (3-12), for three center frequencies of 0.1875, 0.75, and 3 cycles-per-degree, which are called low, medium, and high frequency filters, respectively. (The achromatic filters were centered at 0.5, 2, and 8 cycles-per-degree.) Frequency response of the low, medium, and high frequency filters are plotted in Figure 4-11.

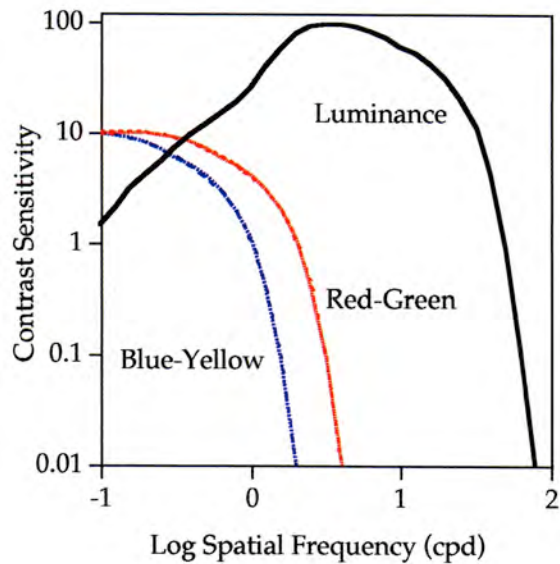


Figure 4-10. An example spatial contrast sensitivity functions for luminance and chromatic contrast of Human Visual System [Fairchild 2005].

Using the one-dimensional cosine log filters, the corresponding radially symmetric two-dimensional filters were constructed. The image of the octave cosine log filter, centered at 0.75 cycles-per-degree, is presented in Figure 4-12. The center of the two-dimensional filters corresponded to the zero frequency. Pixel by pixel multiplication of this image with the Fourier transfer of the white noise pattern would result in a band-pass noise image in the frequency domain. Images corresponding to the octave filters centered at 0.1875, 0.75, and 3 (cpd) are presented in Figure 4-13. Comparing achromatic and chromatic filter images, Figure 3-19 and 4-13, respectively, one can see that the chromatic filters had smaller bandwidth for low and medium frequency filters than the corresponding achromatic filters.

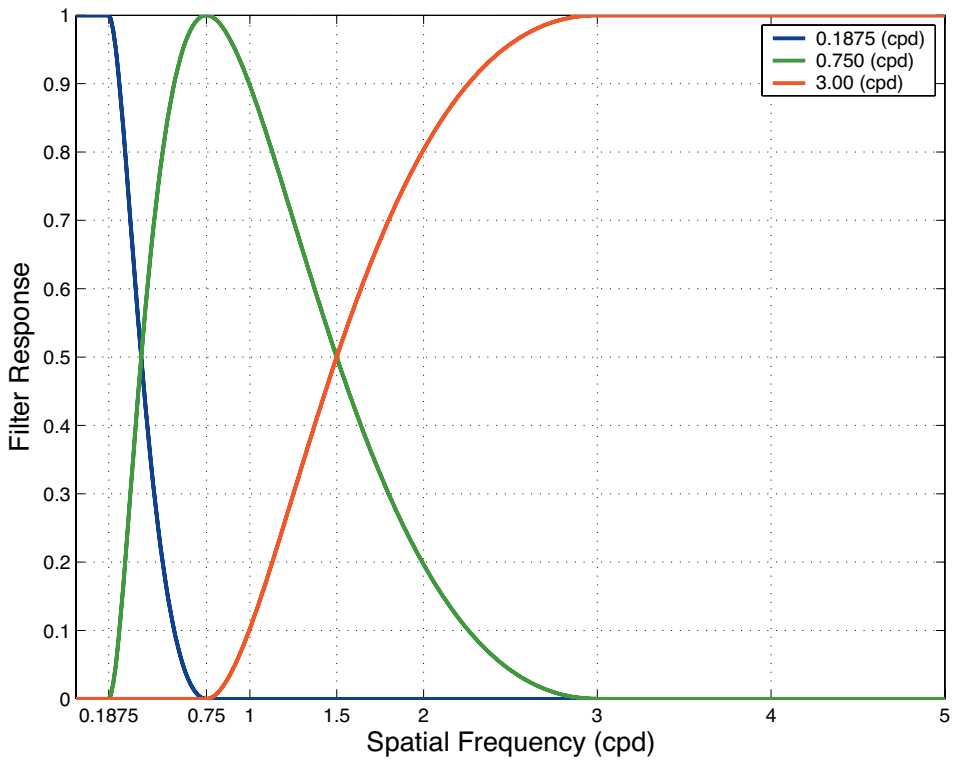


Figure 4-11. Frequency responses of octave filters centered at 0.1875, 0.75, and 3.0 cycle-per-degree, (cpd), of visual angle. For frequencies lower than 0.1875 cpd and higher than 3.0 cpd, filter responses were set to unity for filters centered at 0.1875 and 3.0 cpd, respectively.

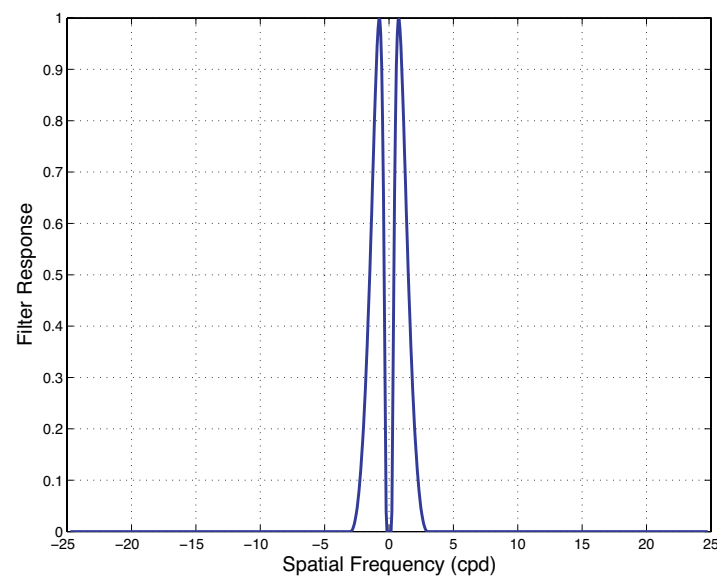
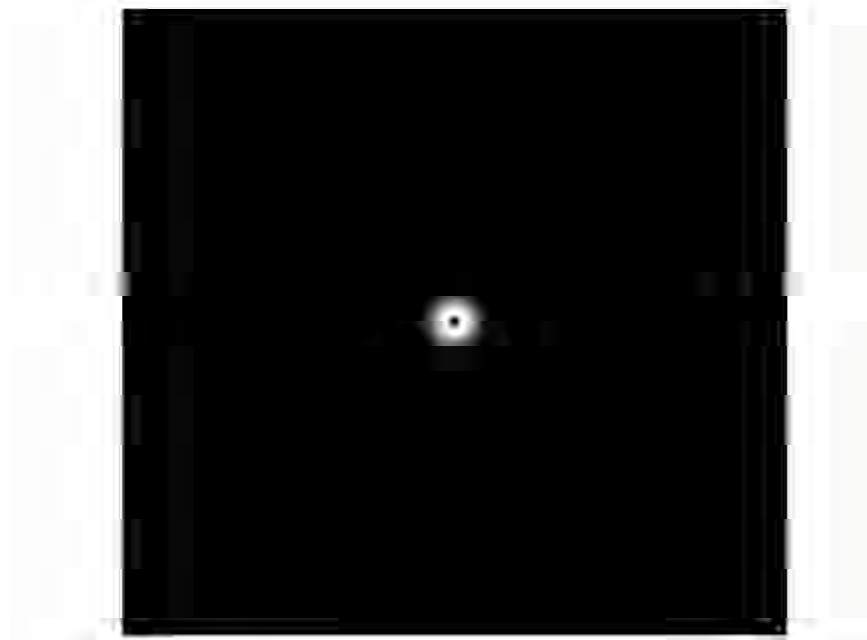


Figure 4-12. Octave cosine log filter centered at 0.75 cycles-per-deg. Response of the filter is plotted along its horizontal axis of symmetry.

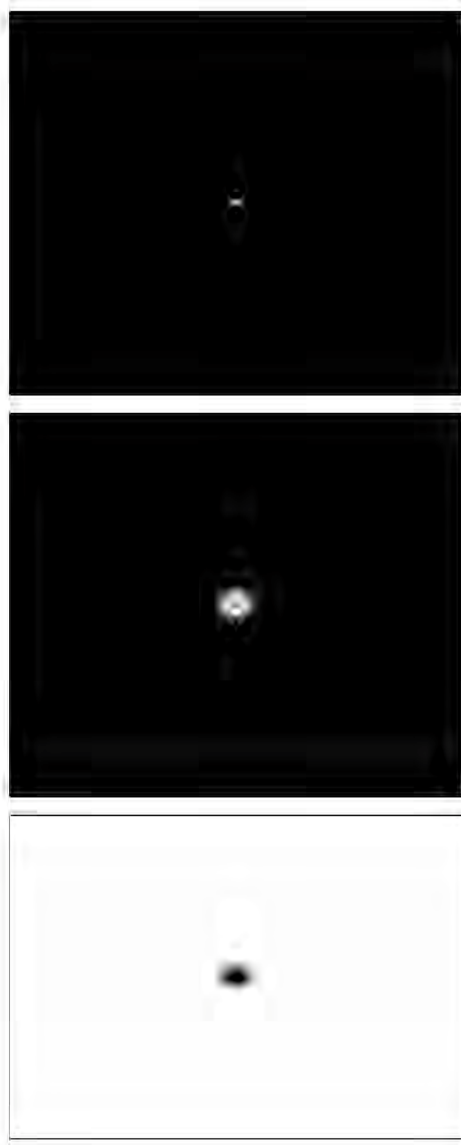


Figure 4-13. Images corresponding to low, medium, and high frequency octave cosine log filters centered at 0.1875, 0.75, and 3 (cpd), respectively. Top: low frequency; Bottom: high frequency; Middle: medium frequency. The center of each image corresponded to the zero frequency. Frequency range was [-35, 35] along the diagonal axis of each image.

Discrete Fast Fourier Transfer (DFFT) of the white noise image was computed and multiplied pixel by pixel with the low, medium, and high frequency cosine log filters, to generate corresponding filtered images in the frequency domain. The filtered noise patterns were transferred back to spatial domain by computing their inverse DFFT. Filtered images were linearly scaled to the range of [0, 0.7] using Equation (3-13), described in Chapter 3. The resulting low, medium, and high frequency noise images and their corresponding histograms are shown in Figure 4-14.

As explained in Section 4.3, the color map computed for each primary color had 400 elements ranging from zero chroma to the chroma of the primary color. Pixel values of the noise images were multiplied by a factor of 400 and used as the indices to the computed maps. Since the noise images were scaled in the range of [0, 0.7] they could address colors from 1 to 280 ($280=0.7\times400$) in the color map, which was 70% of the whole color map. Images could have a chroma as high as 70% of the chroma of the corresponding primary color. Please note that chromatic contrast was defined as the difference between the maximum and minimum values of chroma within an image. All images had a minimum value of zero. Therefore chromatic contrast values of the noise images were equal to their maximum chroma. Noise images, at low, medium, and high frequency bands for the selected five primary colors are presented in Figure 4-15. In the contrast matching experiment observers could increase or decrease chroma of the noise patterns by increasing or decreasing the maximum pixel values of the noise images.

Details on the adjustment of the chroma and conducted contrast matching experiments are given in the following section.

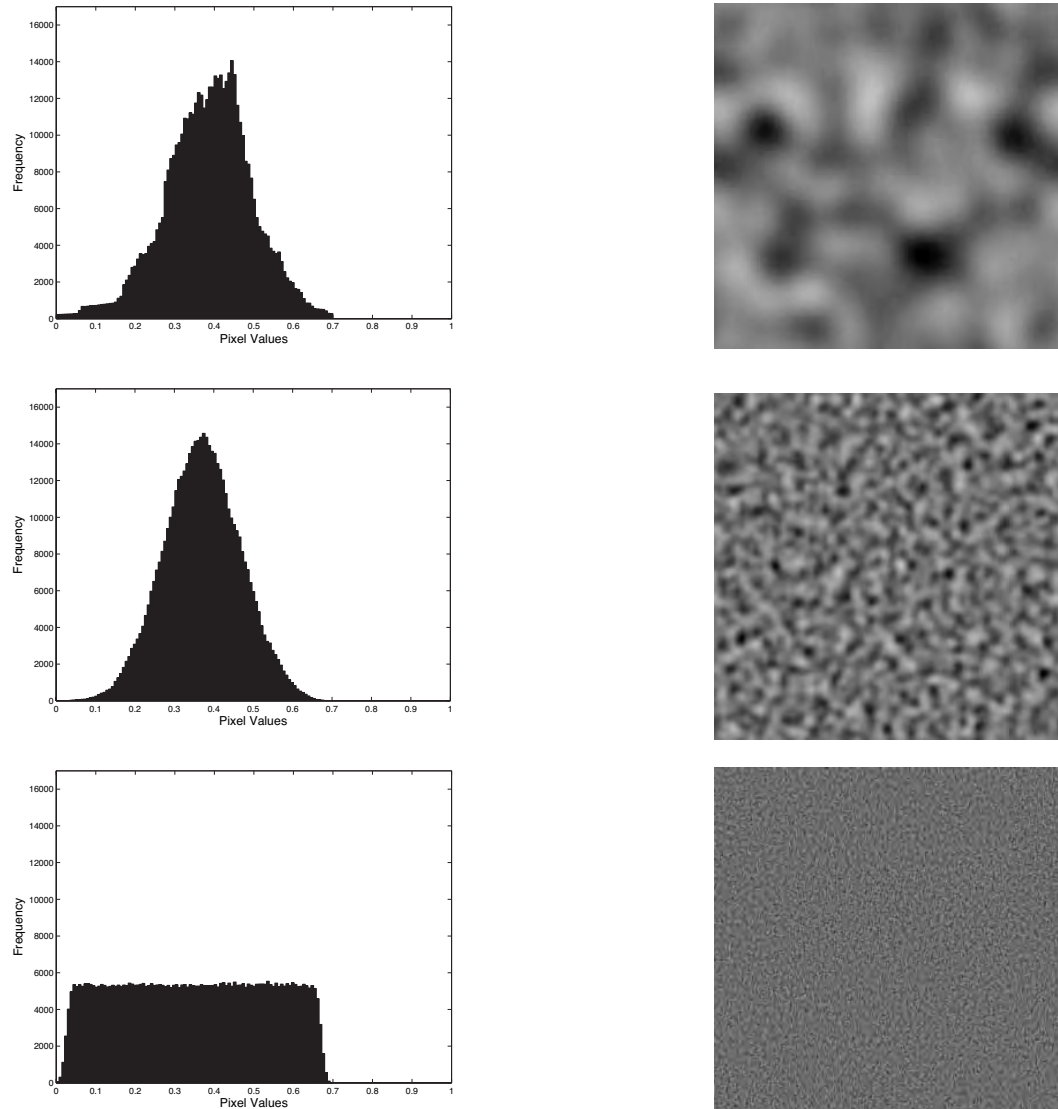


Figure 4-14. Low, medium, and high frequency noise images used to populate chromatic noise patterns at five hues. Pixel values were multiplied by 400 and used as indices to color map arrays.

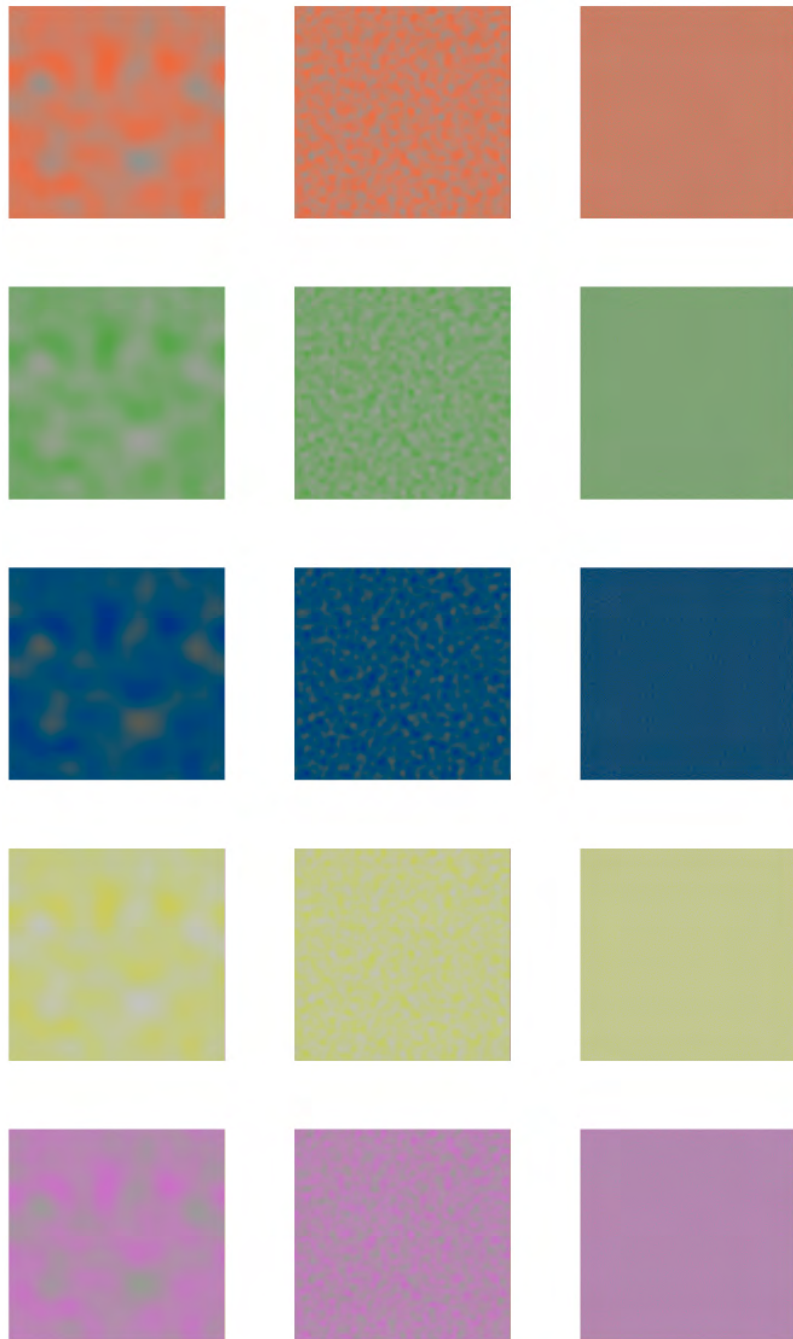


Figure 4-15. Low, medium, and high frequency noise patterns used in chromatic contrast matching. These noise patterns were populated based on the low, medium, and high frequency noise patterns presented in Figure 4-14.

Each of the noise patterns was rendered, using a nearest-neighbor interpolation technique, applied by the Matlab '*imresize*' function, for three resolutions of 701×701 , 1401×1401 , 2101×2101 , respectively. These three sizes corresponded to physical sizes of 87, 174, 288 mm on the LCD, respectively, which corresponded to magnification factors of $1/3X$, $1/2X$, and $1X$, relative to the visual angle of the screen image. These corresponded to retinal subtenses of approximately 10, 15, and 29 degrees of visual angle, although strict viewing distances were not fixed in order to approximate the natural viewing conditions in a museum setting.

4.5 Psychophysical experiment

The experimental setup was exactly the same as the achromatic contrast matching experiments described in Section 3.2.3. Experiments were conducted in the dark environment with the same LCD and DLP displays, calibrated by the analogous procedure, and displayed images subtended the similar visual angles as in the achromatic experiment. The equipment arrangement was also the same as the achromatic contrast matching, shown in Figure 3-24. The images on the LCD had magnification factors of $1X$, $1/2X$, and $1/3X$ in comparison to the images on the DLP display. The LCD display and DLP screen were positioned at a 180° angle from one another. The observers were standing 55 cm from the LCD display and about 200 cm from the screen. The background and surround of the images on the screen and LCD display were set to a black color.

Observers adjusted chromatic contrast of the image projected on the screen to match perceived chromatic contrast of the pattern displayed on the LCD. The chromatic contrast was equal to the maximum chroma in each image. Each observer adjusted 45 samples ($45 = 5 \text{ hues} \times 3 \text{ frequency bands} \times 3 \text{ sizes}$). Samples were presented to observers in a random order. The test image on the screen had an initial contrast selected from a uniform random distribution within the range of [-20%, +20%] of its original value. There were intervals of 5 seconds between adjustments controlled by the data collection software. Observers were asked to ignore artifacts caused by aliasing.

Ten males and six females, a total of sixteen observers participated in the chromatic contrast matching experiments. The chromatic contrast value was equal to the maximum chroma in the image. For each hue, observers could adjust chromatic contrast of the test image on the DLP screen by setting the maximum pixel value, corresponding to maximum chroma, of the image using a ShuttleXpress dialer. A clockwise turn would add an increment of 1/400 to the maximum pixel value and then the image was rescaled between the zero and the new maximum value. The minimum pixel value was always fixed at zero. Pixel values were multiplied by 400 and used as indices to the color map for the corresponding hue. An observer could decrease chromatic contrast of an image by turning the dialer in counterclockwise direction and subtracting a decrement of 1/400 from the maximum pixel value. It was possible to decrease the maximum value down to zero; this would result in a flat gray image with zero chromatic contrast. The maximum pixel value could be set to one, which would generate an image with maximum possible

chromatic contrast for the selected hue. Such a contrast value was equal to maximum chroma of the corresponding primary color.

A low frequency noise pattern for the green hue rendered for the LCD display is shown in the top row of Figure 4-16. Adjusted images to a higher and lower chromatic contrast for the same noise pattern are presented in the middle and bottom rows of Figure 4-16, respectively. The chroma mapping curves from LCD to DLP screen for these examples are plotted in of Figure 4-17 and 4-18. All chroma values were stated in percentage of the maximum possible chroma value, the chroma of the green primary. If there were no adjustment then line segment AB would map chroma values on the LCD to the same values on the DLP. The line segment AD in Figure 4-17, would map colors on the LCD with chroma values in the range of [0% 70%] to colors with chroma values in the range of [0%, 95%] on the DLP. A simple linear mapping, stated in Equation (4-20), was used:

$$C_o = C_i \cdot \frac{C_D}{C_B} \quad (4-20)$$

$$C_B = 0.7 \Rightarrow C_o = C_i \cdot \frac{C_D}{0.7}$$

where C_D is the adjusted maximum chroma by the observer and C_i and C_o are input and mapped chroma values, respectively. The C_D , C_i , and C_o were stated in percentage of the maximum possible chroma. The adjusted image and its histogram, corresponding to curve AD in Figure 4-17, are shown in the middle row of Figure 4-16. The adjusted image had higher chromatic contrast and had a wider histogram than the original image.

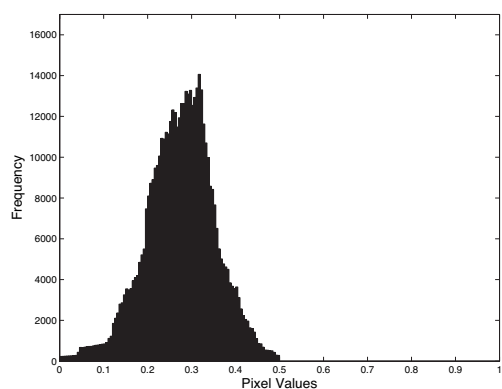
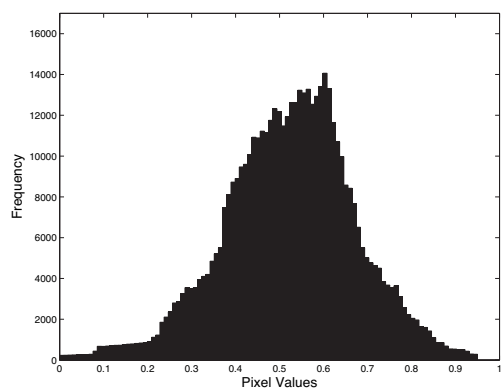
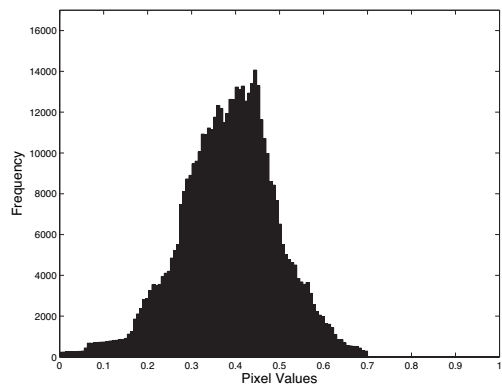


Figure 4-16. Top: original noise image; middle: 25% increase in chromatic contrast; bottom: 20% decrease in chromatic contrast. Histogram of the pixel values is plotted in the right column for each image. Pixel values were multiplied by 400 and used as indices to the corresponding color map.

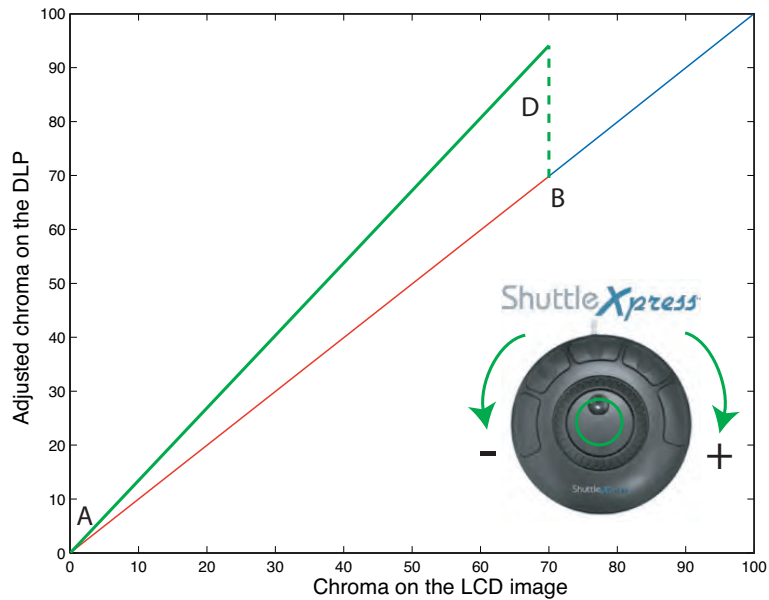


Figure 4-17. Contrast of a sample noise image was increased by adjusting the maximum value of the image to a higher value; so the indices to the color map would address a wider range of colors. In this example segment line AD map colors on the LCD from [0%, 70%] to a [0% 95%]. All values are expressed related to the chroma of the corresponding primary color.

Segment line segment AD, plotted in Figure 4-18, was used to map chroma of the image on the LCD to a narrower range on the DLP. The maximum chroma was adjusted to a lower value than the maximum chroma in the original image. The noise image mapped by the segment line AD is presented in the bottom row of Figure 4-16. Histogram of the adjusted image was narrower and was in the range of [0, 0.5].

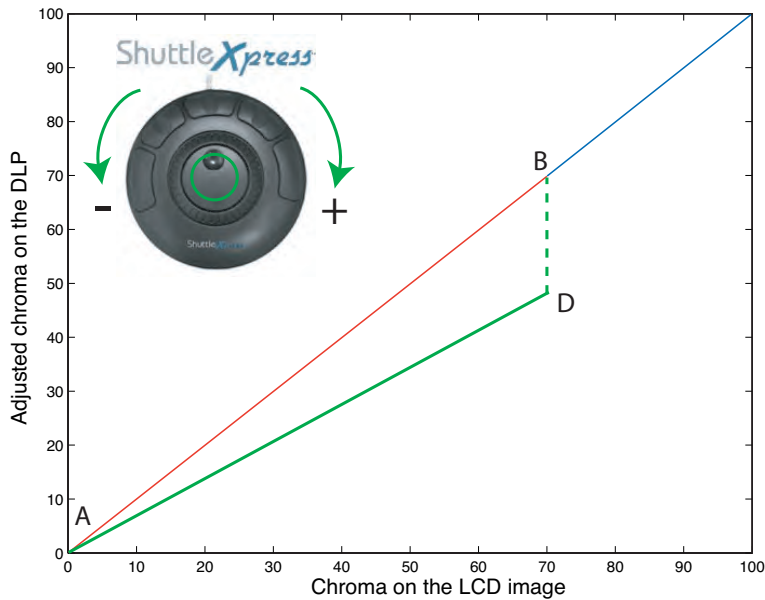


Figure 4-18. Contrast of a sample noise image was decreased by adjusting the maximum value of the image to a lower value.

4.6 Results and Discussion

Observers' responses were saved as data files and used to redisplay and measure the maximum pixel values of the adjusted image with the PR650 spectroradiometer on the LCD and DLP displays. The measured XYZ were converted to the IPT color coordinates and the maximum chroma values were calculated using Equation (4-18). Changes in maximum chroma/chromatic contrast versus image size for low, medium, and high frequency noise patterns are plotted in Figures 4-19 to 4-23. The means of the adjusted contrast and corresponding 95% confidence intervals were computed using Equation (3-11), described in Section 3.1.4, and also shown in each plot. The initial chromatic

contrast on the LCD was measured and shown by horizontal dashed blue lines in each graph.

Chromatic contrast decreased for smaller images with a magnification factor of 1/3X for high frequency noise patterns for most of the hues. The amount of decrease in chroma was dependent on the hue. For the high frequency patterns with the 1/3 X magnification factor, the most and least changes in perceived contrast were seen for the blue and magenta primary colors, respectively. The green, red, and magenta high frequency patterns were adjusted to higher contrast at the 1X magnification factor while yellow and blue were adjusted to lower contrast. For the high frequency patterns, the confidence intervals for all of the primary colors were overlapping for the collected results at 1X, 1/2X, and 1/3X. So one can argue that the contrast adjustment for different magnification factors were not statistically different. Most observers felt that contrast matching of the high frequency patterns were more difficult than others, especially for the yellow patterns. The adjusted high frequency noise patterns, for all hues, at 1/3X magnification factor, had the largest confidence intervals compared to the corresponding adjustment for other magnification factors and frequency bands. This is consistent with the fact that the human visual system has lower sensitivity at high frequencies and judgments would be more uncertain for those test patterns.

A trend of increase in chromatic contrast versus visual angle was seen for the low frequency patterns. Again, the difference in contrast was dependent on the hue of the test patterns. Magenta and red had the highest and lowest adjusted chromatic contrast for the

low frequency noise patterns. Although confidence intervals for the low frequency noise patterns were overlapping but they were relatively smaller than intervals computed for the high frequency patterns. The low frequency red noise images had almost the same chromatic contrast for all magnification factors.

The low and medium frequency noise patterns had the same trend of increase or decrease in chromatic contrast versus changes in image size at all hues.

Observers adjusted contrast of the chromatic patterns in a similar way as they did in achromatic patterns. In both chromatic and achromatic experiments, the low frequency images displayed on the LCD, with smaller visual angles, were perceived to have higher contrast than corresponding larger images on the DLP screen. Conversely, high frequency images on the LCD were perceived to have lower contrast than the corresponding images on the DLP. As discussed in chapter 3, this might be explained by multiple mechanisms whose response characteristics are band-pass in the frequency domain.

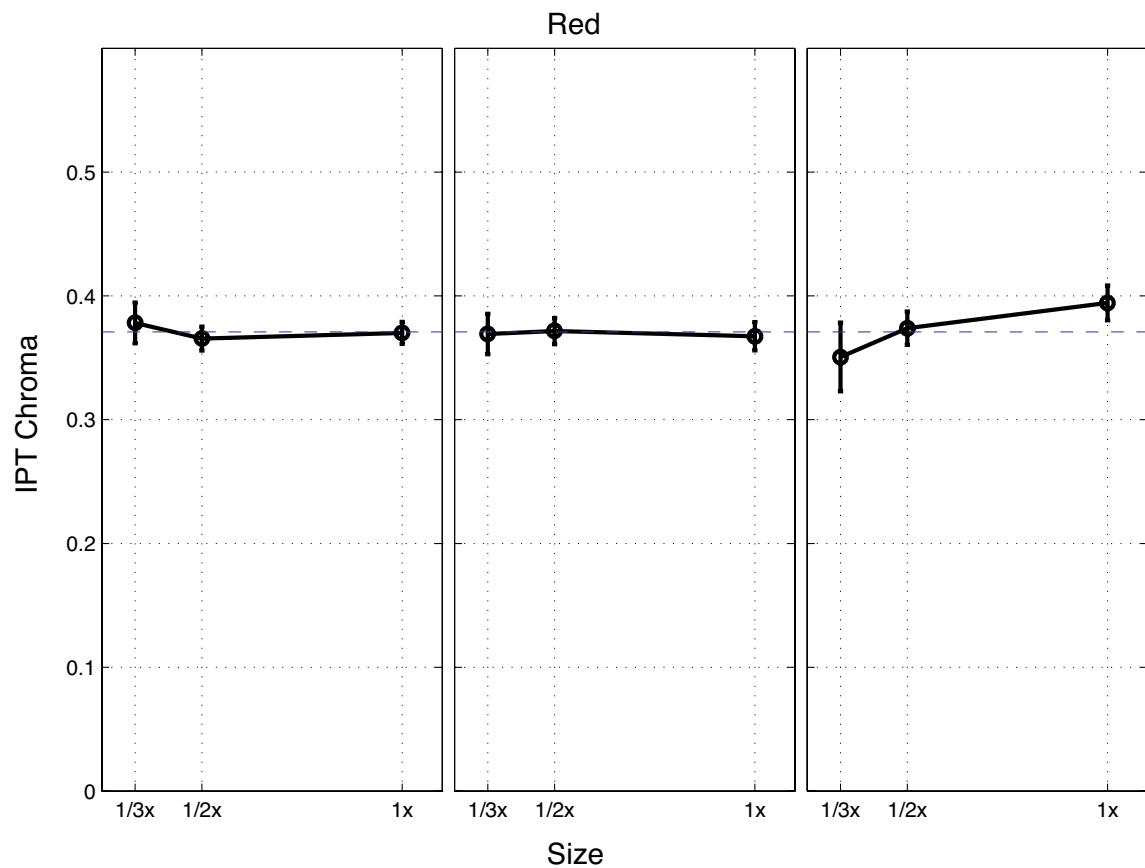


Figure 4-19. Adjusted chromatic contrast for red patterns displayed with different sizes on the LCD and compared to the DLP reproductions. Left: low frequency, Right: high frequency, Middle: Medium frequency. Dashed blue line is initial chroma of the images on the LCD.

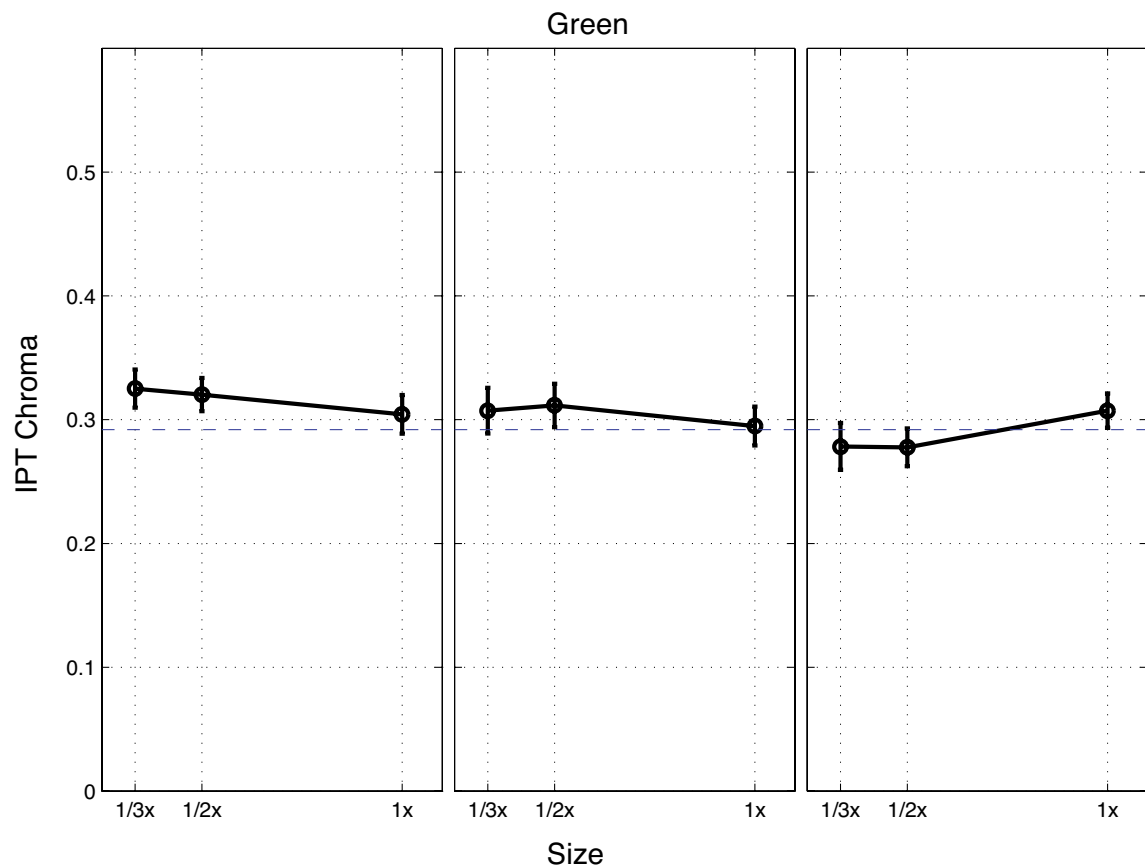


Figure 4-20. Adjusted chromatic contrast for green patterns displayed with different sizes on the LCD and compared to the DLP reproductions. Left: low frequency, Right: high frequency, Middle: Medium frequency. Dashed blue line is initial chroma of the images on the LCD.

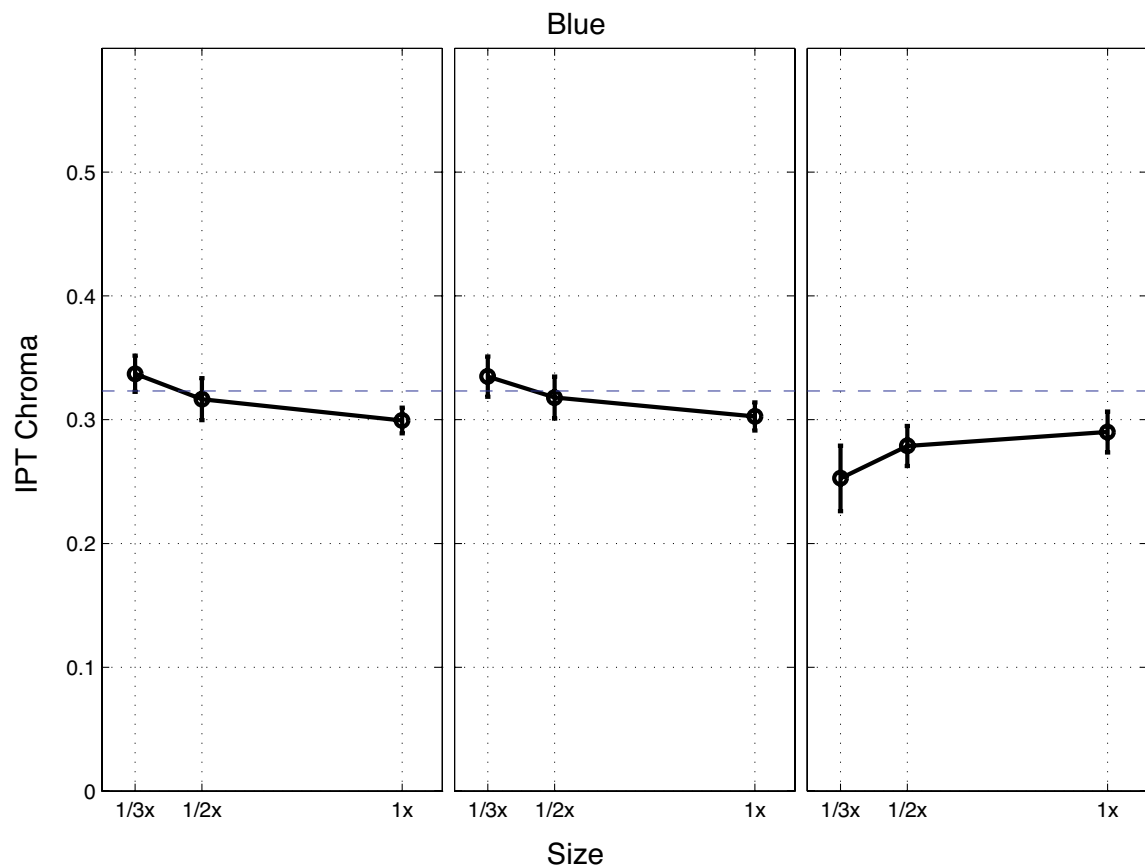


Figure 4-21. Adjusted chromatic contrast for blue patterns displayed with different sizes on the LCD and compared to the DLP reproductions. Left: low frequency, Right: high frequency, Middle: Medium frequency. Dashed blue line is initial chroma of the images on the LCD.

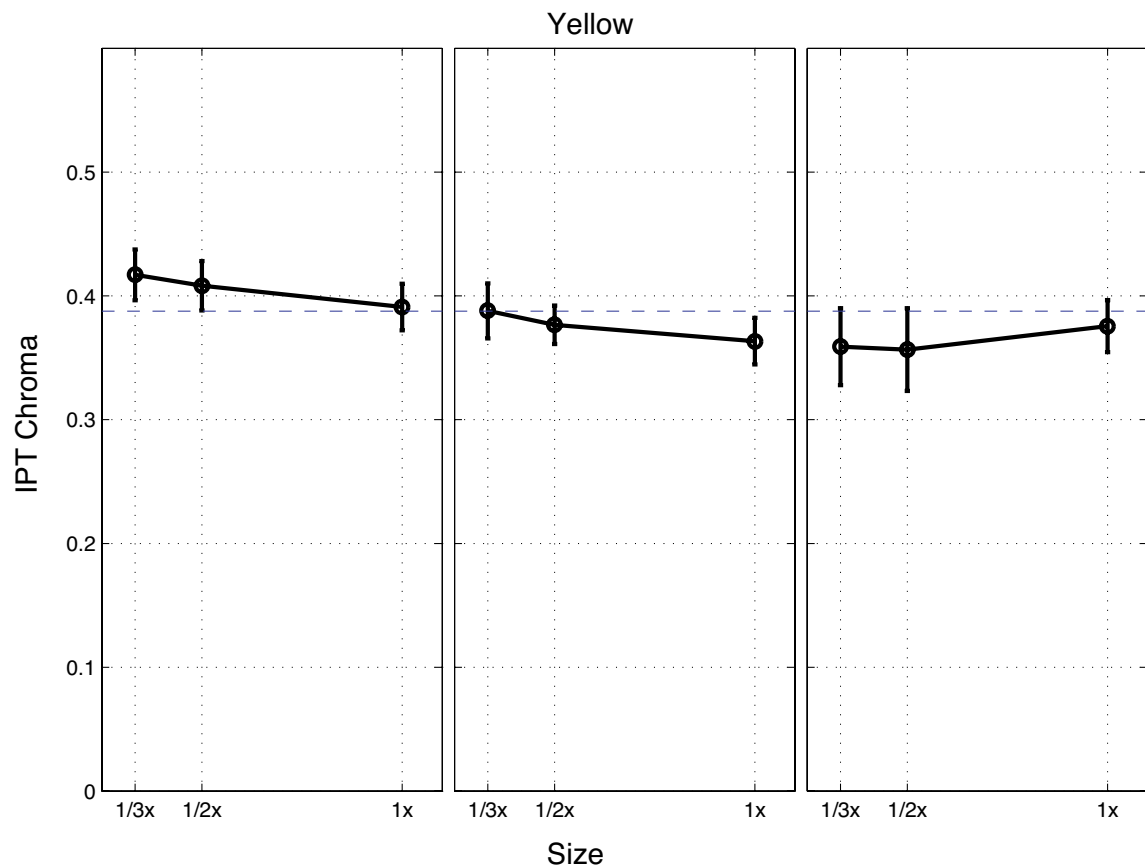


Figure 4-22. Adjusted chromatic contrast for yellow patterns displayed with different sizes on the LCD and compared to the DLP reproductions. Left: low frequency, Right: high frequency, Middle: Medium frequency. Dashed blue line is initial chroma of the images on the LCD.

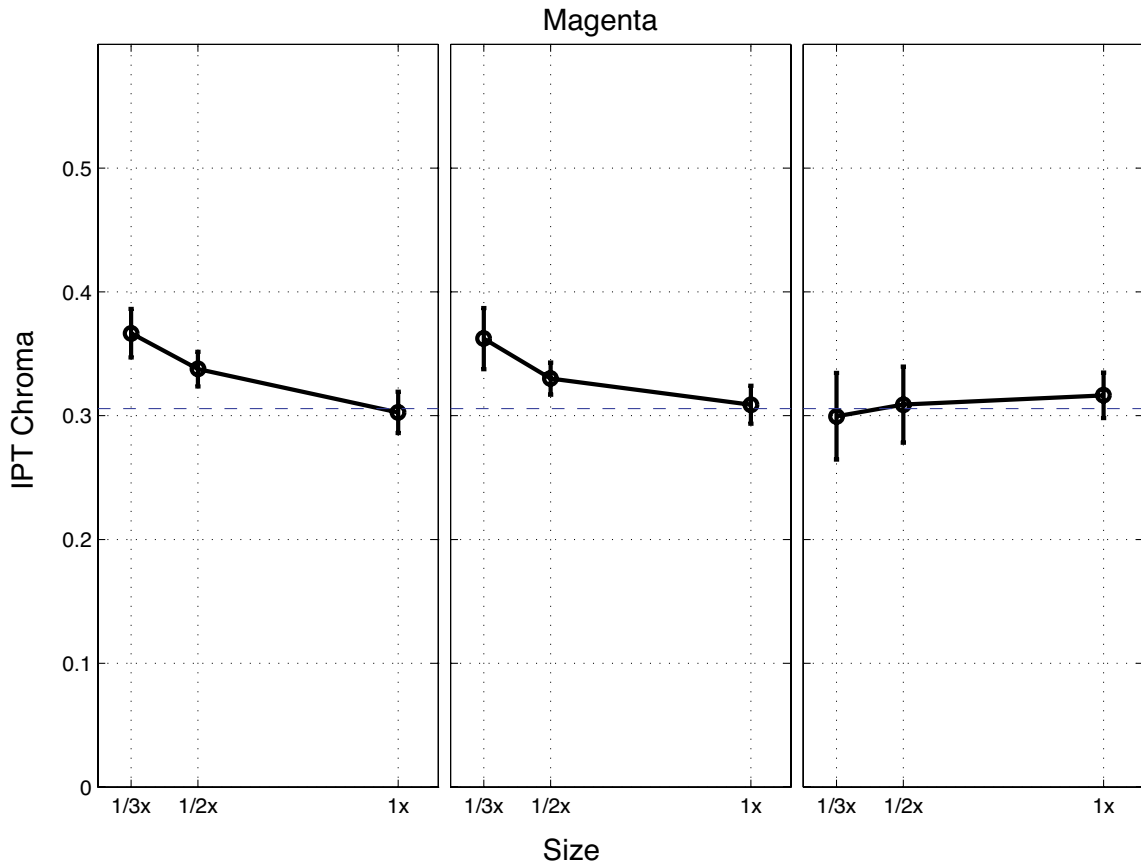


Figure 4-23. Adjusted chromatic contrast for magenta patterns displayed with different sizes on the LCD and compared to the DLP reproductions. Left: low frequency, Right: high frequency, Middle: Medium frequency. Dashed blue line is initial chroma of the images on the LCD.

Scaling down an image shifts it to higher frequency range. An example is presented in Figure 4-24, where an image in the frequency range denoted by 'A' is shifted to a higher frequency range 'B'. The chromatic channels have a low-pass rather

than a band-pass characteristics as shown in Figure 4-24. Sensitivity of a low-pass mechanism decreases monotonically versus frequency. Therefore, all images scaled to smaller sizes would be perceived based on mechanisms with lower sensitivities than the original larger image. The mechanisms located in the range ‘B’ have lower sensitivity than those located in the range ‘A’. Hence, for chromatic noise images, it was expected to observe a decrease in perceived contrast by a decrease in image size regardless of the frequency content of the images. However, a band-pass characteristic was observed. So one can hypothesize that image size has an effect on the image appearance that can be modeled by band-pass rather than low-pass mechanisms for both chromatic and achromatic channels. Such band-pass filters were optimized for each hue at different mean luminance values, to be described in Chapter 5.

The goal of the preliminary experiment was to decouple lightness and chroma and eliminate the effect of the lightness on image contrast by correcting chromatic noise patterns for the Helmholtz-Kohlrausch effect. If this correction was not effective enough to block the lightness contributions to appearance changes due to changes in image size then one could expect such a band-pass characteristics in the results.

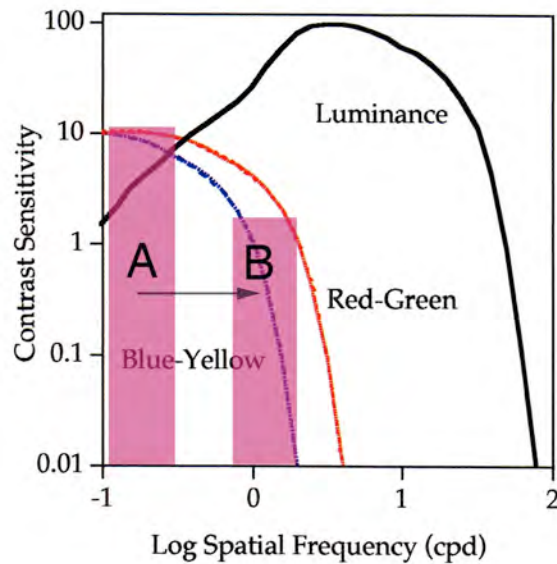


Figure 4-24. An example of spatial contrast sensitivity functions for luminance and chromatic contrast of Human Visual System [Fairchild 2005]. An image located in the frequency range ‘A’ would be shifted to range ‘B’ when scaled down to a smaller size.

Figures 4-25 and 4-26 show the same data presented in Figure 4-19 to 4-23 in another way. Means of adjusted maximum chroma values were computed for each hue. The corresponding P and T color coordinates were plotted for each frequency band. This formed a polygon in the P-T plane for each magnification factor. The larger the polygon, the more chromatic was the corresponding image on the DLP screen. One can see in Figure 4-25 that the area corresponding to 1/3X magnification is larger than 1/2X and 1X. In other words, the LCD images with 1/3X magnification factors were perceived to have higher contrast than 1/2X and 1X for low frequency; hence, the corresponding images on the DLP screen were set to higher contrast. Conversely, for high frequency

noise patterns, shown in Figure 4-26, the small images on the LCD were perceived to have lower contrast than larger images on the screen. Therefore contrast of the corresponding images on the DLP screen was reduced.

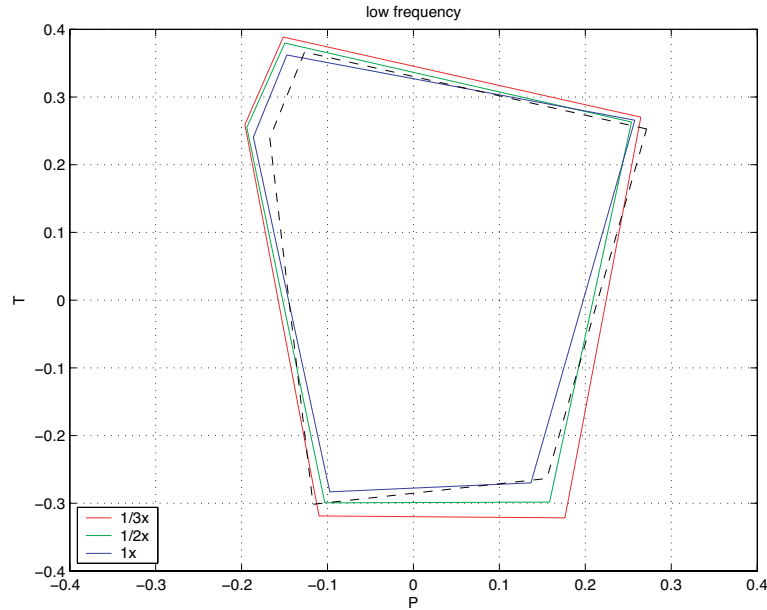


Figure 4-25. Adjusted chromatic contrast of the low frequency noise patterns on the DLP screen. The larger the polygon, the more chromatic corresponding images on the DLP screen. Dashed black line is initial chroma of the images on the LCD.

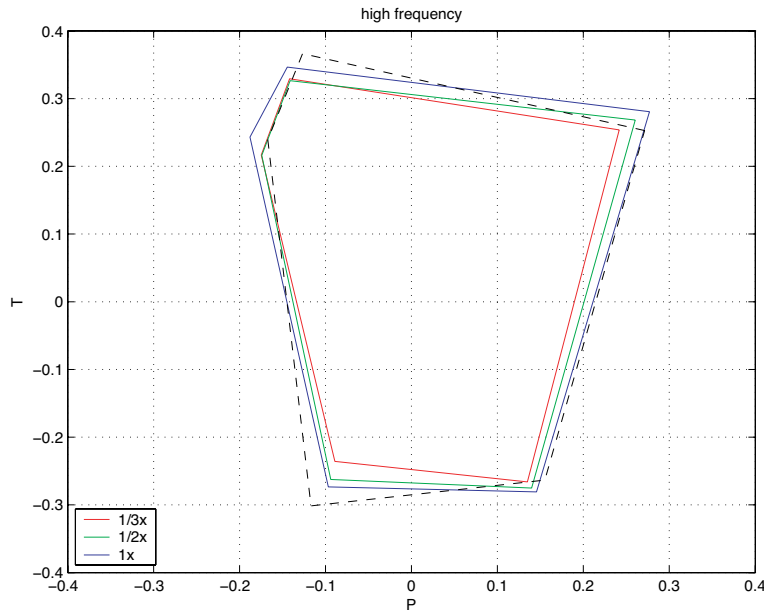


Figure 4-26. Adjusted chromatic contrast of the high frequency noise patterns on the DLP screen. The larger the polygon, the more chromatic corresponding images on the DLP screen. Dashed black line is initial chroma of images on the LCD.

In these contrast matching experiments DLP images were adjusted to match the LCD images. What if one should render a smaller size of a large test pattern? In order to render a smaller version of a low frequency chromatic noise pattern one would need to reduce the chromatic contrast. Conversely to render a high frequency chromatic noise pattern for a smaller size an increase in chromatic contrast is suggested. Two examples, a low and high frequency green noise patterns adjusted and rendered for LCD and DLP, are presented in Figure 4-28 and 4-29, respectively. The same patterns colorimetrically rendered for the LCD display are also shown in the corresponding figures.

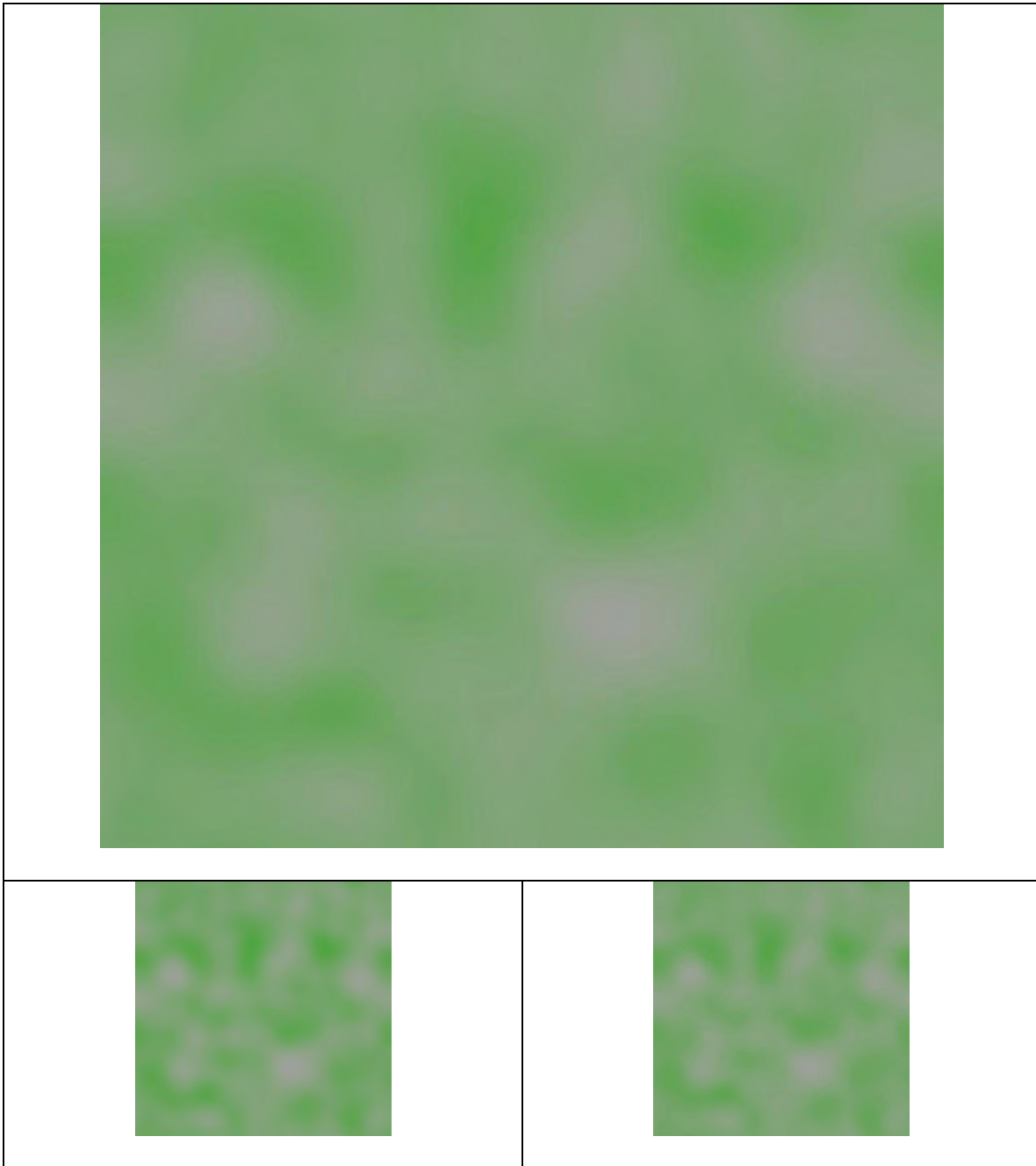


Figure 4-27. Top: Low frequency noise pattern rendered for DLP display; Bottom left: same pattern colorimetrically rendered for LCD; Bottom right: same pattern colorimetrically rendered and also adjusted for the effect of 1/3X magnification for the LCD display.

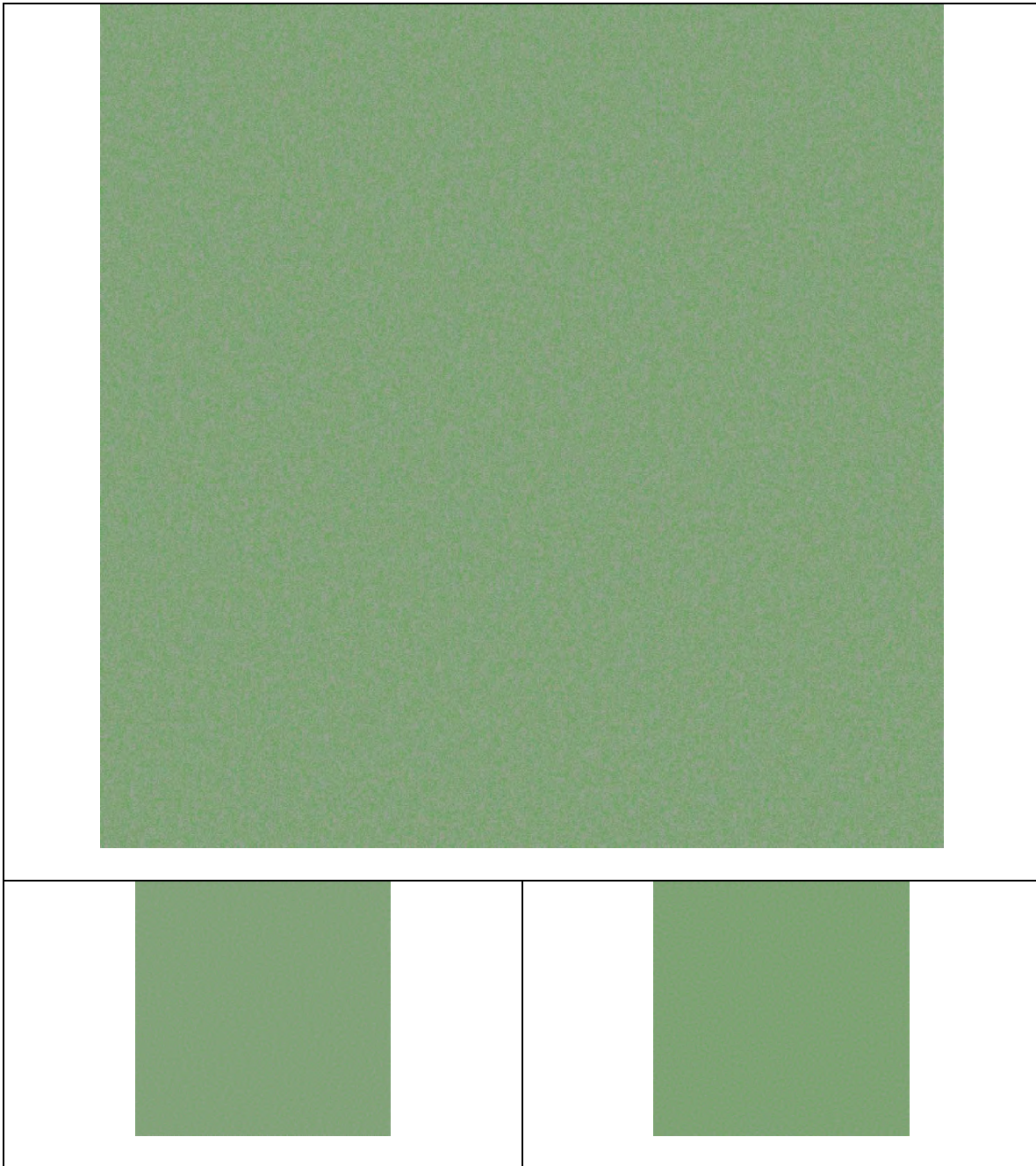


Figure 4-28. Top: high frequency noise pattern rendered for DLP display; Bottom left: same pattern colorimetrically rendered for LCD; Bottom right: same pattern colorimetrically rendered and also adjusted for the effect of 1/3X magnification for the LCD display.

4.7 Conclusions

Both achromatic and chromatic attributes should be considered in the design of image processing algorithms accounting for the effect of the image size. Chromatic contrast matching experiments using band-pass noise images at five selected hues were performed to investigate the effect of image size on image contrast.

Lightness of a color depended on both its luminance and chromaticity; changes in chroma of a test pattern were accompanied by perceived changes in their lightness. To prevent the unwanted effect of the lightness variation on the results of chromatic contrast matching, a preliminary experiment was performed to evaluate the magnitude of the Helmholtz-Kohlrausch effect. Lightness of color patches at five hues with lightness values of 0.75 and 0.25, in IPT space, were adjusted in comparison to gray patches with the same lightness.

All color patches were adjusted to darker or equal lightness in comparison to the corresponding gray patches. Primary colors with a lightness of $I=0.75$ were perceived lighter than the gray patch and adjusted to lightness values lower than 0.75. The green and yellow colors had the largest lightness reduction. At lightness level of 0.25, the blue, yellow, and magenta patches were perceived as light as the gray patch. But, the red primary was perceived lighter than the gray patch and was adjusted to relatively darker colors. The more chromatic the color, the more the reduction in lightness.

Proper lightness adjustments were applied to five sets of chromatic noise patterns. Pixels in each noise image were perceived to have the same lightness with variable chroma along an initial hue line.

Corrected noise patterns were used in a chromatic contrast matching experiment, where chromatic contrast was decreased for smaller images for high frequency noise patterns for all five hues. An opposite trend of an increase in chromatic contrast versus visual angle was seen for the low frequency patterns. These trends were similar to the results of achromatic contrast matching. In both experiments, the low frequency images with smaller visual angles were perceived to have higher contrast than corresponding larger images displayed on the DLP screen. Conversely, high frequency image on the LCD were perceived to have lower contrast than the corresponding larger images on the DLP. The amount of increase or decrease in perceived chromatic contrast versus image size was dependent on the hue of the test patterns.

Band-pass filters and collected results from chromatic and achromatic contrast matching were used to develop a color reproduction model, described in the next chapter, accounting for image size effect.

5 IMAGE REPRODUCTION MODEL ACCOUNTING FOR THE EFFECT OF IMAGE SIZE

As described in Chapter 4 and 5, two sets of achromatic and chromatic contrast matching experiments were conducted using band-pass noise patterns. Collected results from those relatively simple stimuli were used to develop a few image reproduction models capable of compensating for the effect of image size on more complex images. Three main correction algorithms as well as their combinations are described in the following sections. These models were used to correct image reproduction of five images of paintings at different visual angles/image sizes. The performances of the correction models were evaluated by psychophysical experiments using a paired-comparison method.

5.1 Painting Images

Images of five paintings were selected for the experiments performed in this chapter. These images were in LAB TIFF format. The mean of CIE L* values and a short description of each painting are presented in Table 5-1. Histograms of the CIE L* values for each image are shown in Figure 5-1. Furthermore, cumulative histograms are plotted with a solid red line in each figure. As seen in Figure 5-1, the distributions of CIE

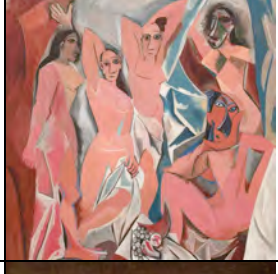
L^* values for the Rembrandt and Rousseau paintings are skewed toward lower values while they have a wide spread. In other words, they are relatively dark, high contrast images. The Renoir painting has a wide spread; it is a high contrast, medium lightness image. The CIE L^* value larger than 3% of the CIE L^* values in an image was selected as the effective minimum value. Similarly, the CIE L^* value less than 3% of CIE L^* values in an image was considered as the effective maximum value. Michelson contrast of each image was calculated using the effective minimum and maximum CIE L^* values:

$$M_c = \frac{L_{max} - L_{min}}{L_{max} + L_{min}} \quad (5-1)$$

where M_c is Michelson contrast and L_{min} and L_{max} are effective minimum and maximum CIE L^* values, respectively. The calculated Michelson contrast values for the five painting images are listed in Table 5-1.

The tristimulus values, XYZ, and IPT color coordinates for the D₅₀ illuminant, using Equations (4-1) to (4-17), were computed for each pixel. The image corresponding to lightness values, ‘I’ in IPT space, for the Seurat painting is shown in the top row left column of Figure 5-2. The same lightness separation was prepared for other painting images. As will be described in Sections 5.3 and 5.4, achromatic noise images at different lightness and contrast were used to develop algorithms for adjustment of mean lightness and lightness contrast for the image size effect. Therefore, one could apply the same adjustment algorithms to the lightness separation of a painting image and compensate for the image size effect.

Table 5-1. Mean CIE L* and calculated Michelson contrast for the five painting images.

No	Painting name	Mean CIE L*	Michelson contrast	
1	Auguste Renoir. (French, 1841 – 1919). Odalisque, 1870. Oil on canvas, 69.2 x 122.6 cm (27 1/4 x 48 1/4 in.). Chester Dale Collection, National Gallery of Art, Washington.	48.7	0.7699	
2	Georges Seurat (French, 1859 – 1891). Sunday Afternoon on La Grande Jatte, 1884–1886. Oil on canvas 207.6 x 308 cm. Art Institute of Chicago.	49.0	0.4472	
3	Pablo Picasso, (Spanish, 1881-1973). Les Demoiselles d'Avignon. Paris, June-July 1907. Oil on canvas, 243.9 x 233.7 cm (8' x 7' 8"). The Museum of Modern Art, New York.	61.4	0.4966	
4	Rembrandt van Rijn, (Dutch, 1606 – 1669). Self-Portrait. 1659. Oil on canvas, 84.5 x 66 cm (33 1/4 x 26 in.) Andrew W. Mellon Collection, National Gallery of Art, Washington.	16.3	0.8374	
5	Henri Rousseau. (French, 1844-1910). The Dream. 1910. Oil on canvas, 204.5 x 298.5 cm (6' 8 1/2" x 9' 9 1/2"). Gift of Nelson A. Rockefeller, The Museum of Modern Art, New York.	26.4	0.6022	

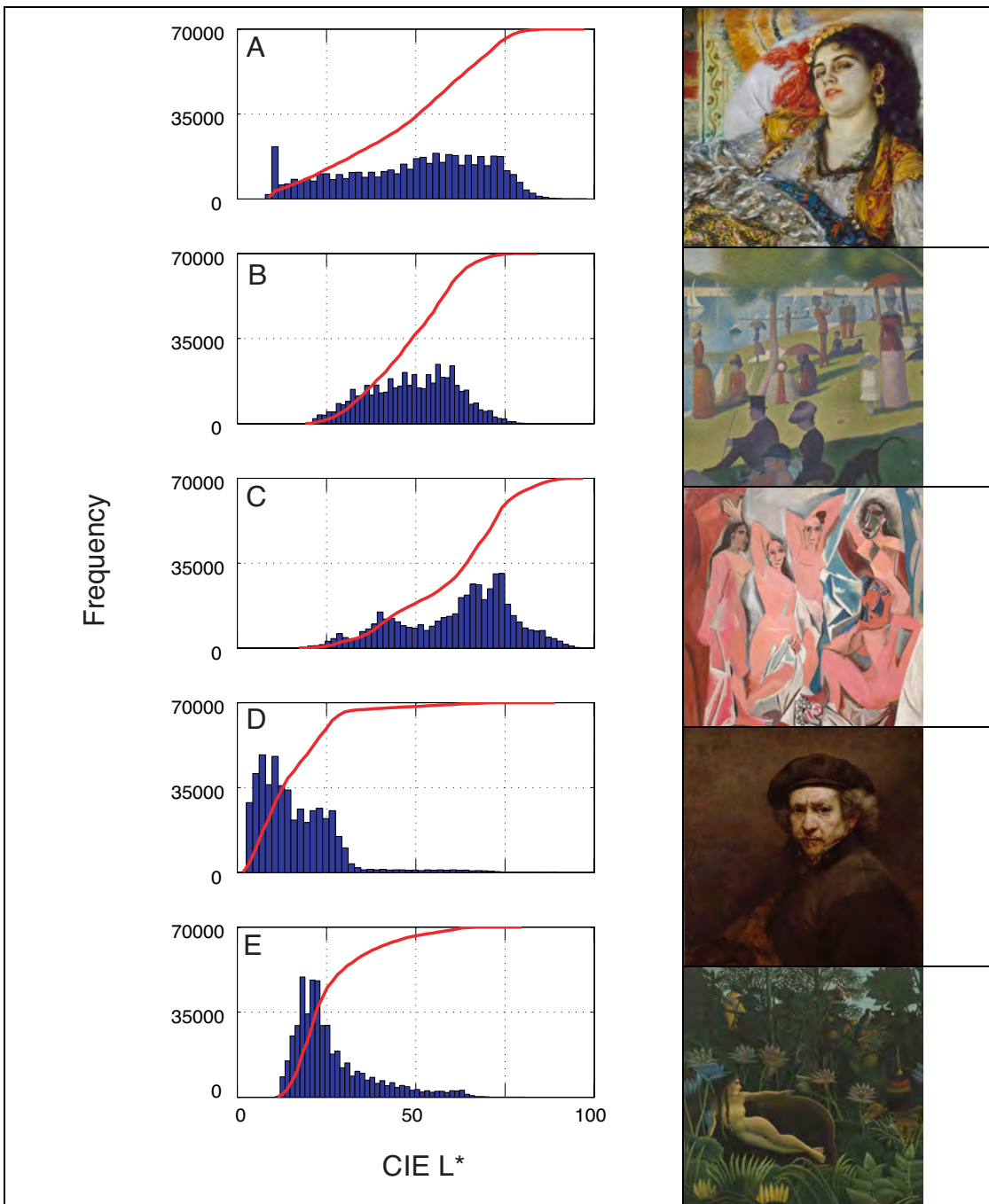


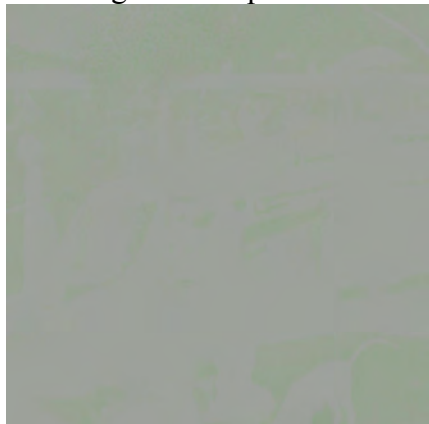
Figure 5-1. Histogram of CIE L^* of the selected paintings. The red lines plot the cumulative distributions. A: Renoir; B: Seurat; C: Picasso; D: Rembrandt; E: Rousseau.



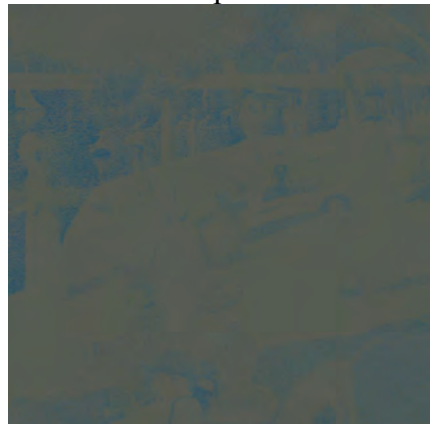
Lightness Separation



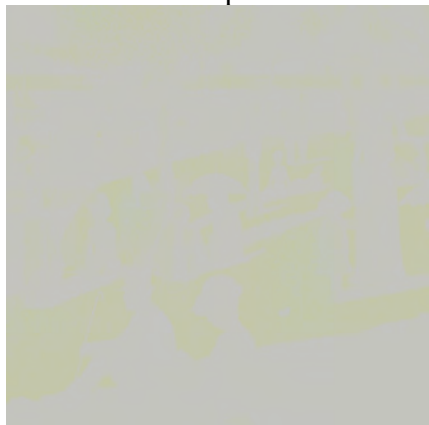
Red Separation



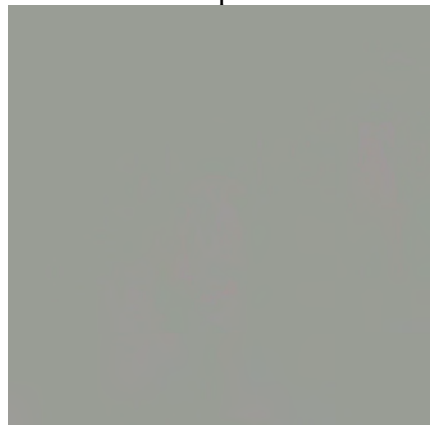
Green Separation



Blue Separation



Yellow Separation



Magenta Separation

Figure 5-2. Lightness and five color separations of the Seurat painting.

Similarly chromatic noise images were used to compute band-pass filters for chromatic contrast adjustment to compensate for image size effect. So, one could prepare five color separations of a painting image and apply corresponding optimized band-pass filter to each separation. The adjusted separations could be combined to reconstruct a final image, which was adjusted for the effect of image size on the chromatic contrast attribute. The computation of color separations of painting images is described in the following section.

5.2 Color Separations Computation

The chromatic contrast matching experiments, described in Chapter 4, were performed for five primary hues of red, green, blue, yellow, and magenta. For each painting image, the P and T of each pixel were used to compute five color separation images. The five primary colors, used in the chromatic contrast matching experiments, projected onto P-T plane are denoted by circle symbols in Figure 5-3. Unit vectors along the red, green, blue, yellow, and magenta primary hue lines are presented by \vec{R} , \vec{G} , \vec{B} , \vec{Y} , and \vec{M} , respectively. Any color, projected onto P-T plane, can be reconstructed by the weighted sum of any vector pairs of $\vec{R}\vec{Y}$, $\vec{Y}\vec{G}$, $\vec{G}\vec{B}$, $\vec{B}\vec{M}$ or $\vec{M}\vec{R}$. For example a color, represented by vector \vec{S} , in Figure 5-3, can be reconstructed by \vec{R} and \vec{Y} vectors using

positive values for ‘a’ and ‘b’ coefficients: $\vec{S} = a\vec{Y} + b\vec{R}$. The ‘a’ and ‘b’ coefficients, for this example, can be calculated by Equation (5-2):

$$\begin{aligned}\vec{S} &= \vec{S}_1 + \vec{S}_2 \\ \vec{S}_1 &= a\vec{Y} \\ \vec{S}_2 &= b\vec{R} \\ \vec{S} &= a\vec{Y} + b\vec{R} \\ \begin{bmatrix} a \\ b \end{bmatrix} &= \begin{bmatrix} R_p & Y_p \\ R_t & Y_t \end{bmatrix}^{-1} \begin{bmatrix} S_p \\ S_t \end{bmatrix}\end{aligned}\tag{5-2}$$

where \vec{R} and \vec{Y} are unit vectors along the red and yellow hues, respectively. The ‘P’ and ‘T’ subscripts denoted for the P and T coordinates, respectively. It was also possible to reconstruct \vec{S} using $\vec{G} \vec{B}$ vector pair, $\vec{S} = a\vec{B} + b\vec{G}$, which would require negative values for the ‘a’ and ‘b’ coefficients. Color coordinates corresponding to a pixel in an image in the P-T plane were decomposed using the very first vectors at the left and right side of it. The corresponding coefficients for such vector pairs would have positive values. The coefficients of the other vectors were set to zero. Therefore, a color point in the P-T plane with (S_p, S_t) coordinate would map to a coordinate of $(a, 0, 0, b, 0)$ for the (red, green, blue, yellow, and magenta), the five dimensional color coordinate system based on the selected five hues. As examples, five color separations corresponding to Seurat painting are shown in Figure 5-2.

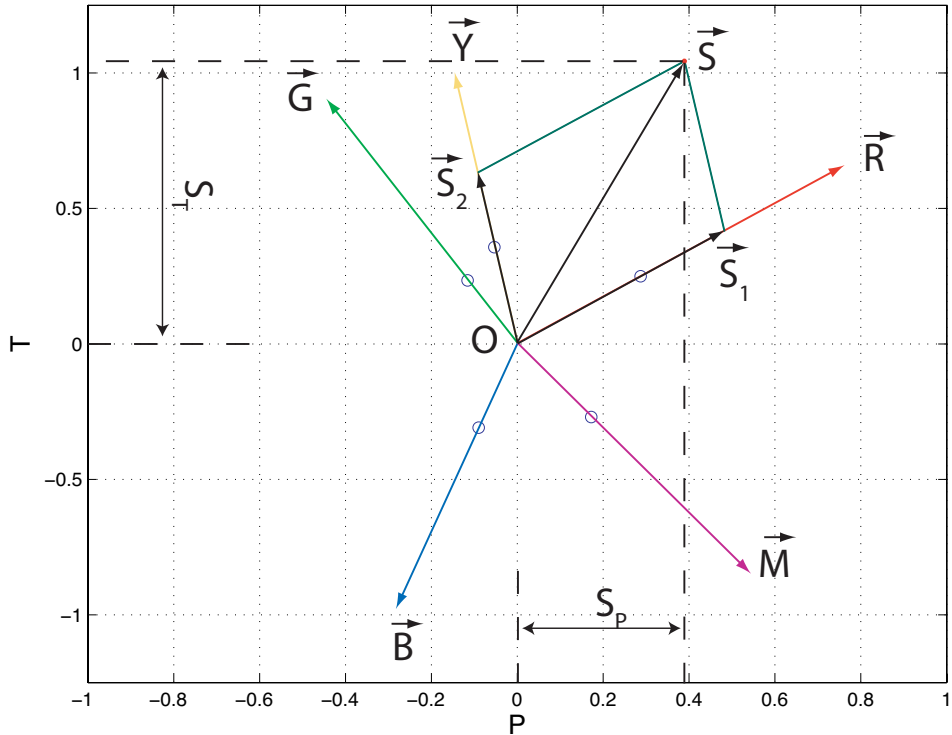


Figure 5-3. The circles show the DLP primary colors. The unit vectors along the five primary colors are represented by \vec{R} , \vec{G} , \vec{B} , \vec{Y} , and \vec{M} .

In a reverse process, the five separation images could be combined to generate the original P-T color coordinates. For each pixel only two vectors would have non-zero coefficient values:

$$\begin{bmatrix} R_p & Y_p \\ R_t & Y_t \end{bmatrix} \begin{bmatrix} a \\ b \end{bmatrix} = \begin{bmatrix} S_p \\ S_t \end{bmatrix} \quad (5-3)$$

Other vectors do not contribute to P and T since they have zero coefficient values. The five color separation images were used in a chromatic contrast adjustment, described in Section 5.4.

5.3 Adjustment of the Mean Lightness

Two uniform patches of 50 (cd/m^2) with surfaces of 1 and 2 square meters need 50 and 100 (cd) of energy, respectively: the larger the surface the larger the amount of required energy. However, they have the same $\text{lum}/\text{sr} \cdot \text{m}^2$ and a radiometer reports the same radiance/luminance for the both patches regardless of their sizes or total energies. As discussed in Chapter 3, it seemed that observers were evaluating the lightness of images on the DLP and LCD based on both luminance and total energy. This might be attributed to cognitive mechanisms and complex processing in the human visual system. Although the luminance was the main criterion and had a much higher weighting in observers' judgment, the size of stimuli, which was in direct correlation with the total energy of a surface, was also affecting their judgments. One could hypothesize that for LCD and DLP images with the same mean lightness, the DLP images are always perceived as lighter regardless of the frequency and magnification factors, since they always have a greater total energy.

The adjustment of mean luminance values versus changes of visual angle/image size had a similar trend for low, medium, and high frequency bands with overlapping confidence intervals for all samples with the same initial mean luminance. The low, medium, and high frequency results were not statistically different. So, all data with the same initial mean luminance values were pooled together regardless of their frequency bands and the mean values at each luminance and size-scaling factor were computed. The three mapping curves for CIE L* from LCD to DLP for the 1X, 1/2X, and 1/3X

magnification factors were presented in Figure 3-31, which is presented here again as Figure 5-4. For example, for the 1/3X scaling factor, shown by the red line, a lightness of 67 on the DLP screen was mapped to a value of 75 on the LCD display. The DLP display was always perceived lighter than the LCD, as shown in Figure 5-4. Therefore, for any given image displayed on the DLP screen with a mean lightness value of L_{dlp} , an amount of ΔL should be added to the LCD image to make a lightness appearance match between LCD and DLP display. The ΔL can be calculated from the curves in Figure 5-4:

$$\Delta L = L_{lcd} - L_{dlp} \quad (5-4)$$

where L_{dlp} and L_{lcd} are the CIEL* values on the ordinate and abscissa of the plot shown in Figure 5-4, respectively. For an image rendered for the DLP display, the lightness separation was converted to CIE L* and its mean lightness was calculated. An amount of ΔL , from Equation (5-4), was added to all pixels of the lightness separation image to get the adjusted image for the LCD display. This computation was performed for all five painting images. As an example, the colorimetrically rendered image of the Seurat painting and the corresponding adjusted image for 1/3X magnification factor are presented in Figure 5-5.

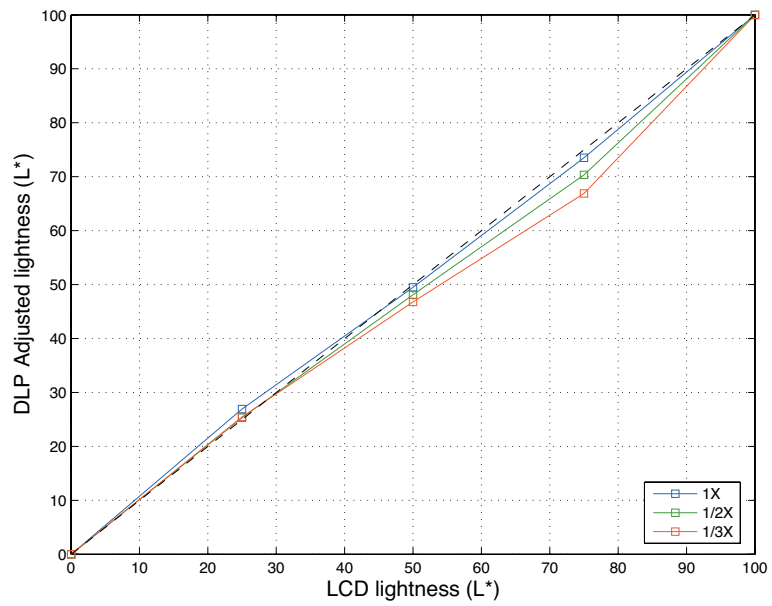


Figure 5-4. Adjusted mean lightness of noise patterns on the projector screen versus the mean lightness of corresponding images on the LCD for three magnification factors of 1/3X, 1/2X, and 1X.

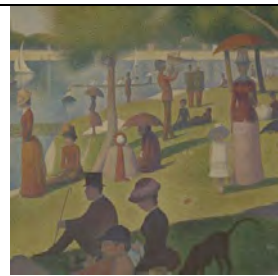
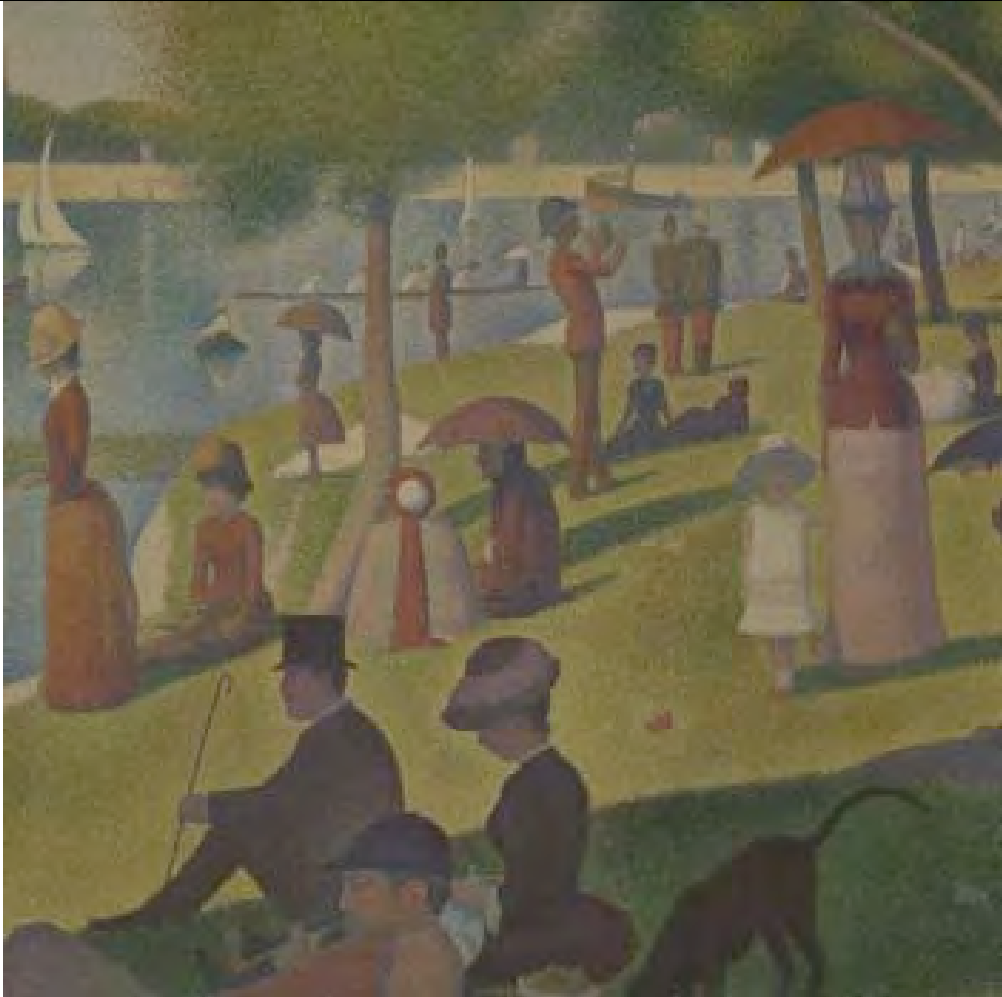


Figure 5-5. Top: Colorimetric rendered image of Seurat painting for the LCD. Bottom left: 1/3X magnification of the top image. Bottom right: Same image colorimetrically rendered and also adjusted for the mean lightness.

5.4 Contrast Adjustment in Frequency Domain

The frequency components of images shift toward higher frequency ranges when scaled down to a smaller size. As discussed in Chapter 3 and 4, adjustment of chromatic and achromatic contrast versus changes of image size were dependent on the frequency of the noise patterns. The method of adjustment showed a trend of the increase of contrast in adjusted images versus the decrease of image size on the LCD display for low frequency band-pass noise patterns. Conversely, high frequency, small size images on the LCD were matched with images of lower contrast on screen. The amount of increase or decrease in perceived chromatic contrast versus image size was also dependent on the hue of the test patterns.

The results of achromatic contrast adjustment, shown in Figure 3-28, were in agreement with the concept of multiple mechanisms, demonstrated in Figure 3-29, whose response characteristics are band-pass in the frequency domain. A band-pass rather than low-pass characteristic was observed for chromatic noise patterns, described in Chapter 4. So it was decided to model the effect of image size on the contrast of achromatic and chromatic images by band-pass filters. Seeking model simplicity, a simple three-parameter filter originally described by the Movshon and Kiorpes [Movshon 1988] was used. Johnson and Fairchild used Movshon filter in color image difference models and image difference metrics [Johnson 2001, 2002, 2003]. It has also been used for chromatic noise perception in digital photography [Xiaoyan 2004]. The Movshon filters were used for both achromatic and chromatic contrast adjustment.

The response function of the Movshon filter is shown in Equation (5-5):

$$fresp = \frac{(a.f^c.e^{-b.f})}{100} \quad (5-5)$$

where *fresp* is filter response at spatial frequency '*f*'. The 'a', 'b', and 'c' are filter parameters. A few examples of filter responses for different values of 'a', 'b', and 'c' are presented in Figure 5-6.

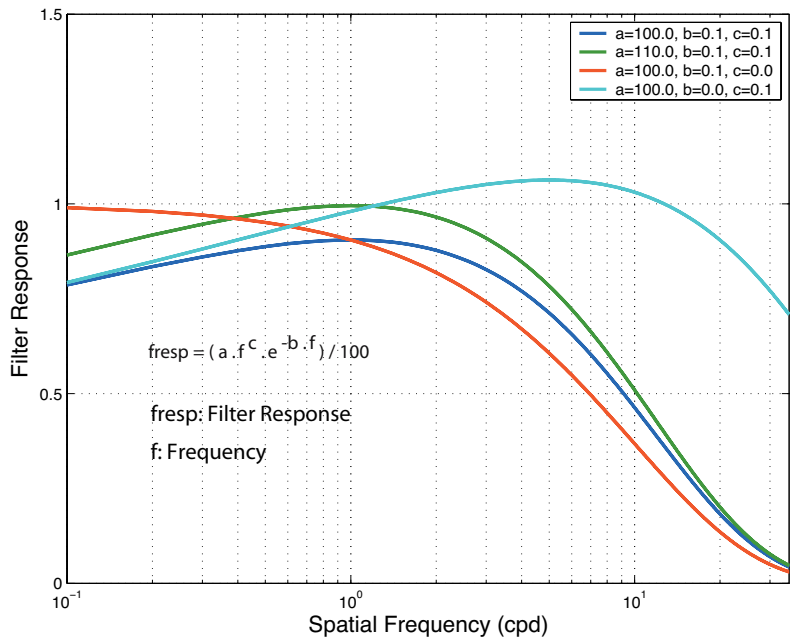


Figure 5-6. Samples of filter responses for different values of 'a', 'b', and 'c' parameters.

5.4.1 Achromatic Contrast Adjustment

Low, medium, and high frequency achromatic noise patterns rendered for the LCD display and corresponding adjusted images on the DLP screen were used to optimize

filter parameters for different lightness, contrast, and size scaling factors. The flowchart of filter parameter optimization is shown in Figure 5-7.

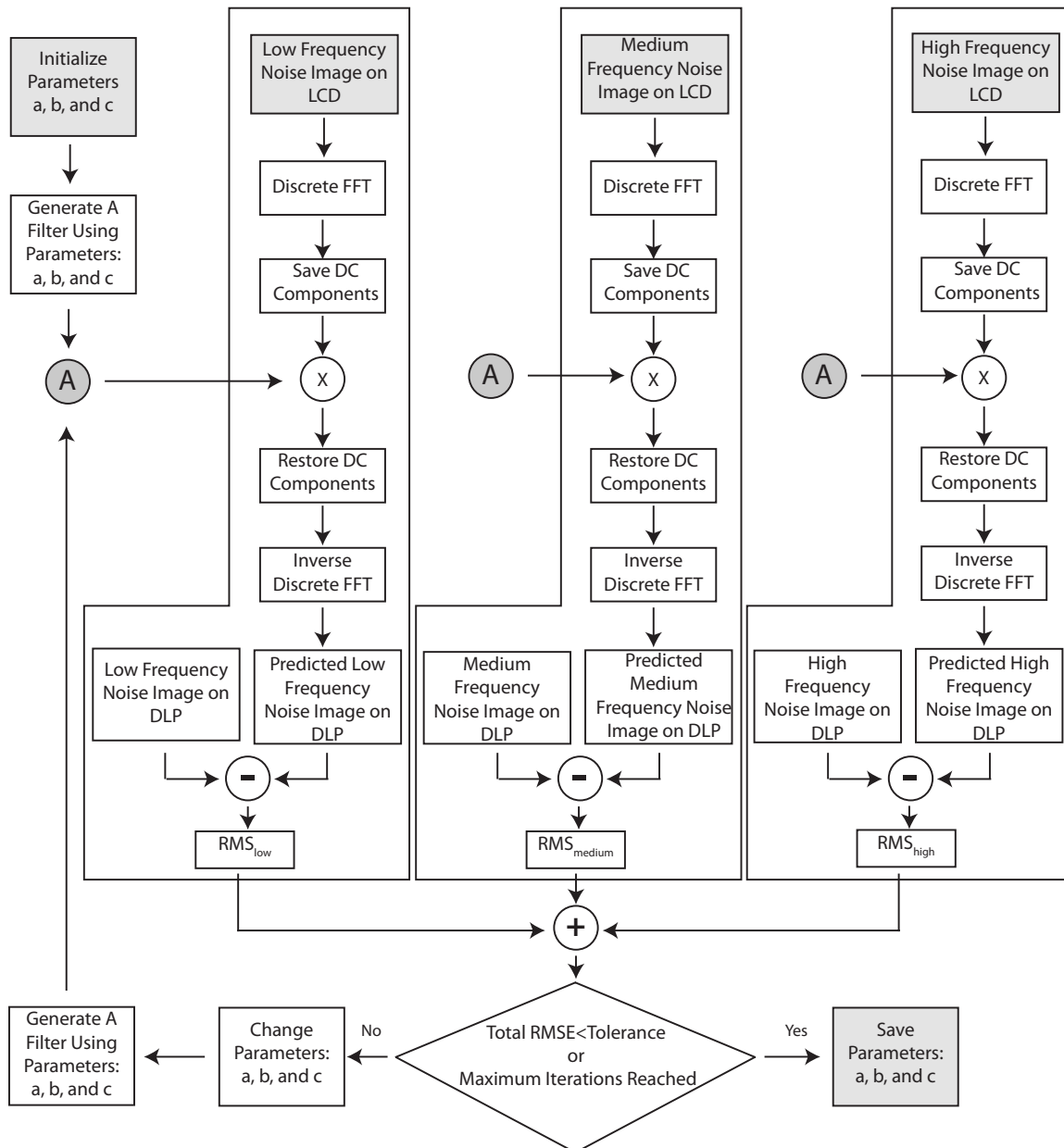


Figure 5-7. Optimization of three parameters of the Movshon filter.

The optimization was performed using the low, medium, and high frequency noise patterns for a magnification factor at a specific initial contrast. For example, low, medium, and high frequency noise images with mean luminance of CIE L*=50 and a Michelson contrast of 0.18 with a magnification factor of 1/3X on LCD and the corresponding images on the DLP were used to optimize three parameters of the filter. In the first step, The Discrete Fast Fourier Transfer (DFFT) of images displayed on the LCD were calculated and the corresponding DC components were saved. Three parameters ‘a’, ‘b’, and ‘c’ were set to initial values of 100, 0.02, and 0.03, respectively, and the corresponding filter was computed using Equation (5-5). The calculated filter was applied to the DFFT of images on the LCD. In the next step, the DC components of filtered images were restored to their saved values. Therefore, filtering would not change the mean lightness of images. Corresponding images in the spatial domain were computed by using the inverse DFFT. The adjusted images on the DLP screen and filtered images were compared and Root Mean Squared Error (RMSE) values were calculated for low, medium, and high frequency image differences. The three RMSE values were summed and compared to a small tolerance value. The tolerance value was set to zero. If the total error was more than zero and the maximum iteration count was not reached, then parameters were set to new values and corresponding filter was updated. Otherwise parameters were saved as the optimum values. The ‘*fmincon*’ function of Matlab was used to implement the optimization of parameters ‘a’, ‘b’, and ‘c’.

The optimized parameters for different lightness, magnification factors, and contrast are listed in Table 5-2.

Table 5-2. Optimized parameters for the achromatic noise patterns at different contrast and lightness levels for three magnification factors of 1/3X, 1/2X, and 1X. Contrast was calculated using Michelson formula and shown by Mc symbol.

	CIEL*	Mc	a	b	c
1/3X	0.25	0.18	106.0	0.0023	0.0000
	0.25	0.35	123.2	0.0114	0.0000
	0.5	0.18	120.1	0.0066	0.0000
	0.5	0.35	130.0	0.0093	0.0000
	0.5	0.7	109.5	0.0074	0.0093
	0.75	0.18	113.5	0.0003	0.0000
	0.75	0.35	111.3	0.0061	0.0000
1/2X	0.25	0.18	112.8	0.0000	0.0000
	0.25	0.35	112.2	0.0006	0.0203
	0.5	0.18	125.0	0.0005	0.0000
	0.5	0.35	113.7	0.0000	0.0390
	0.5	0.7	105.7	0.0000	0.0390
	0.75	0.18	117.4	0.0000	0.0000
	0.75	0.35	100.0	0.0003	0.0243
1X	0.25	0.18	130.0	0.0000	0.0390
	0.25	0.35	117.5	0.0000	0.0390
	0.5	0.18	100.0	0.0000	0.0390
	0.5	0.35	113.6	0.0000	0.0390
	0.5	0.7	100.0	0.0000	0.0390
	0.75	0.18	100.0	0.0000	0.0390
	0.75	0.35	115.6	0.0000	0.0390

Examples of filter responses for three magnification factors of 1/3X, 1/2X, and 1X for noise images with a contrast of 0.18 and CIE L*=50 are plotted in Figure 5-8. The corresponding filter images are shown in Figure 5-9.

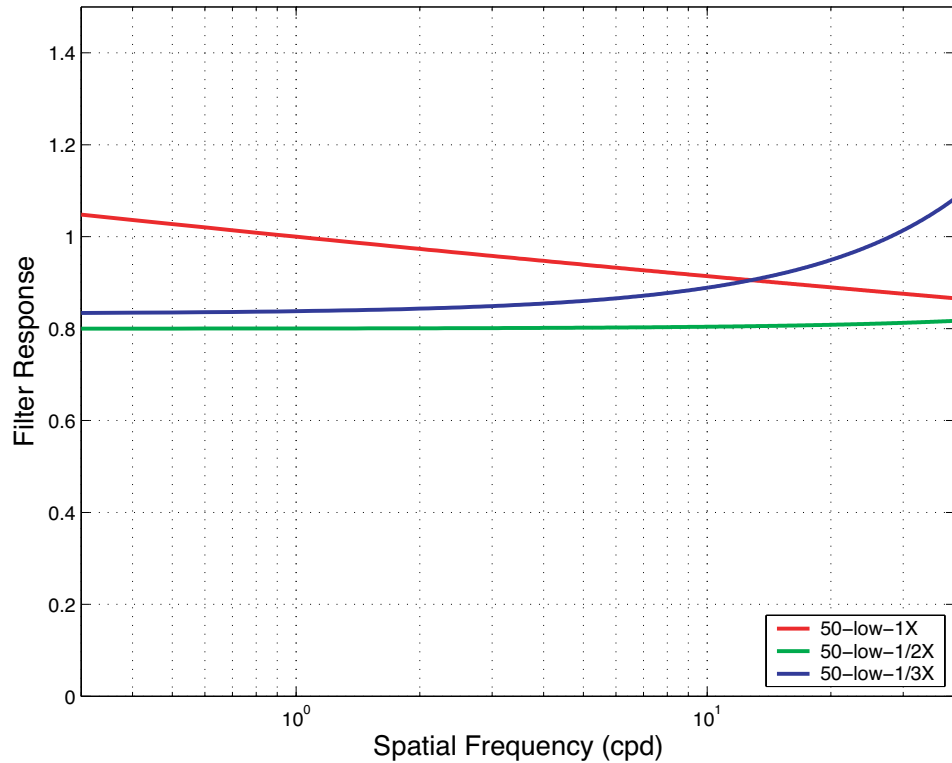


Figure 5-8. Filter responses of three modeled achromatic filters for adjustment of lightness contrast. Filters are modeled from noise patterns with mean lightness of CIEL=50 and Michelson contrast of 0.18.*

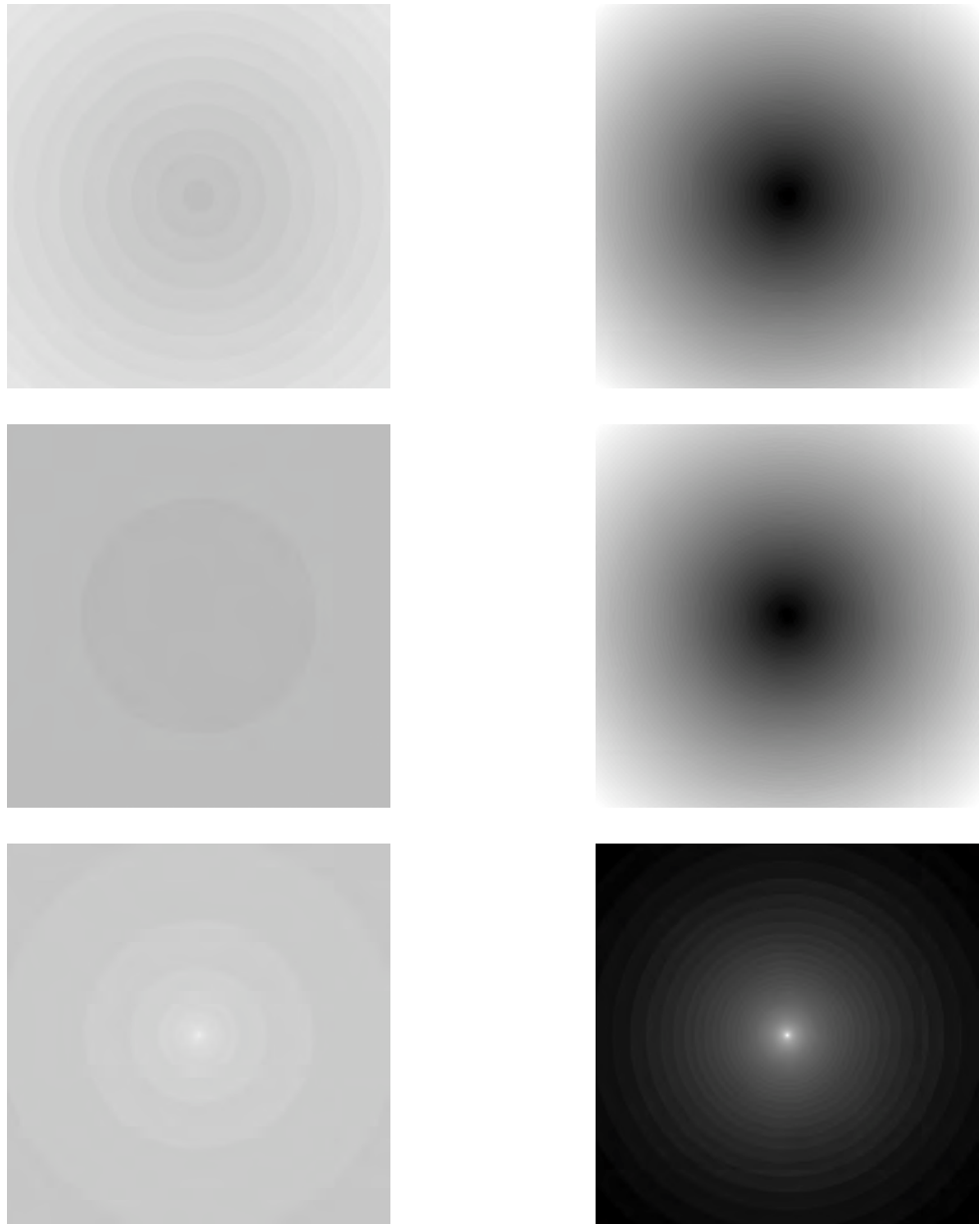


Figure 5-9. Achromatic filters presented in Figure 5-8. Top left: 1/3X; Middle left: 1/2X; Bottom left: 1X. images in the left column are color mapped between black and white and shown in the right column to amplify differences, visually. The center of each image corresponds to zero frequency.

As seen in Figure 5-8, the filter optimized for 1/3X magnification, had a frequency response that attenuates the low frequencies and boosts the high frequency components. In other words, for 1/3X magnification, low frequency components of images rendered for LCD using this filter would be attenuated compared to the same image displayed on the DLP screen. Conversely, the high frequency components of the smaller image on the LCD would be amplified in comparison to the larger image on the DLP. This is consistent with the trend of adjustment of noise images observed in the achromatic contrast matching experiments.

Linear interpolation, implemented by Matlab's '*interp1*', and parameters listed in Table 5-2 were used to compute the parameters for other mean luminance and contrast values. The image of Seurat painting had a mean lightness and Michelson contrast values of CIE L*=49 and 0.4472, respectively. For a 1/3X magnification, the interpolated parameters for this painting were 119.5, 0.0072, and 0.0012 for 'a', 'b', and 'c', respectively. The corresponding filter computed for this painting is plotted in Figure 5-10. The computed filter would amplify the high frequency components and attenuate low frequency range. The DFFT of the Seurat painting image was calculated and multiplied pixel by pixel with the computed filter image. The inverse DFFT of the resulting image was calculated and rendered for the LCD display using inverse characterization model of the LCD. Images of Seurat painting rendered colorimetrically for LCD and DLP display and the adjusted image for lightness contrast, using the computed filter for a magnification of 1/3X, are shown in Figure 5-11.

Similarly the optimized parameters were interpolated for the selected five paintings and corresponding filtered images were computed and rendered using inverse characterization models of the LCD and DLP displays. Those images were saved and used in the paired comparison experiment, to be described in Section 5.5.

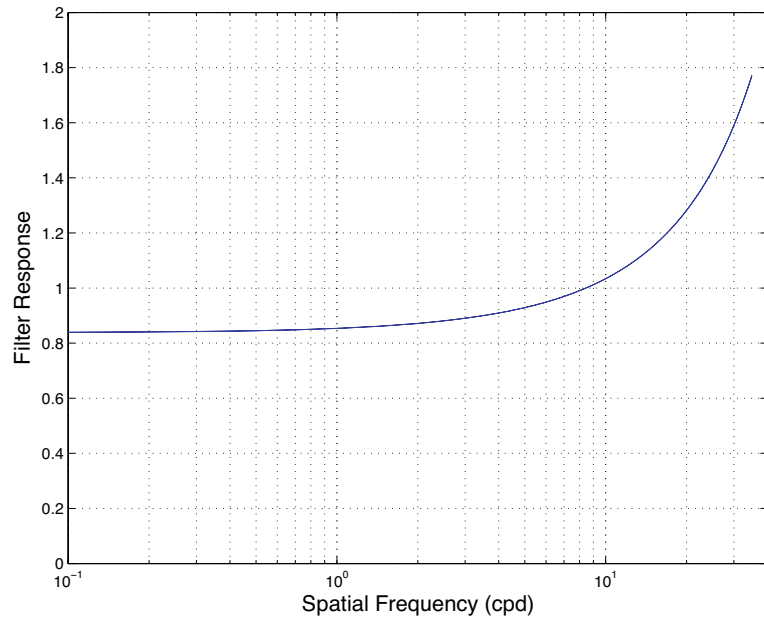


Figure 5-10. Optimized filter for adjustment of lightness contrast of Seraut painting for a magnification of 1/3X. The computed ‘a’, ‘b’, and ‘c’ parameters were 119.5, 0.0072, and 0.0012, respectively.

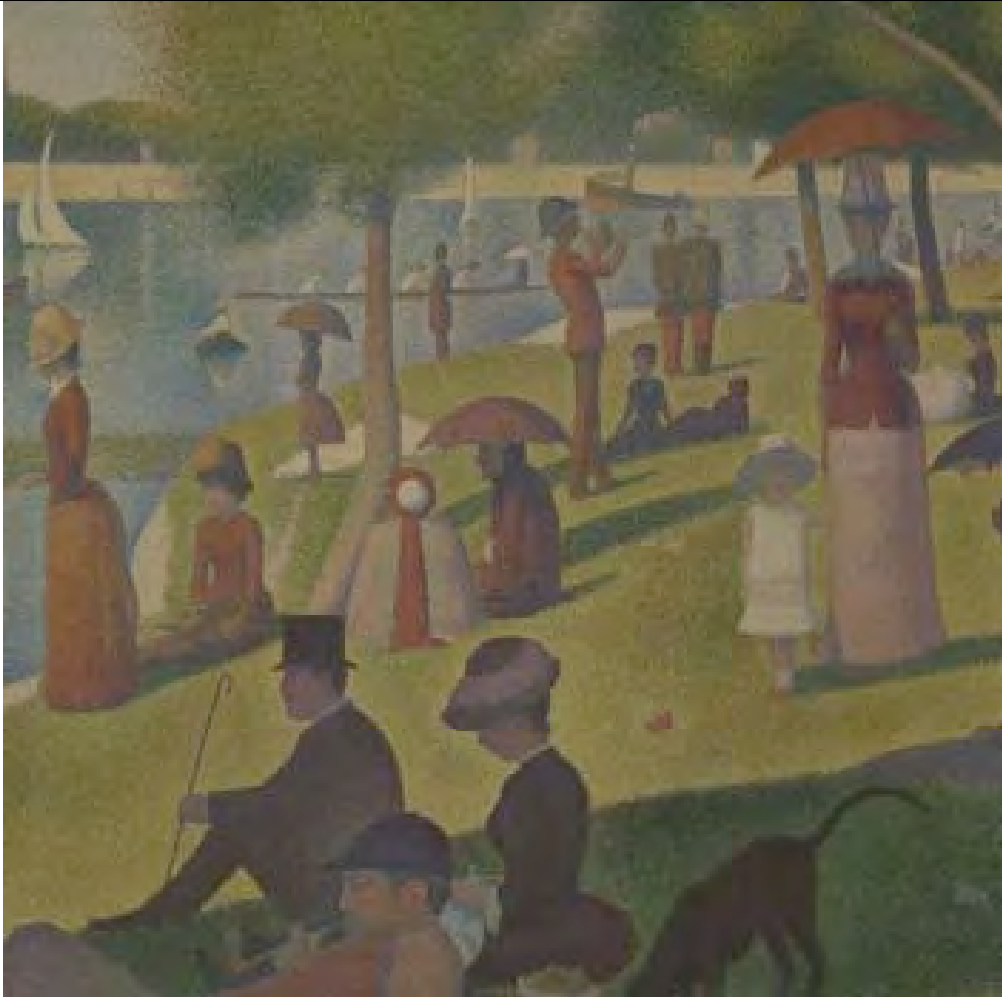


Figure 5-11. Top: Colorimetric rendered image of Seurat painting for the DLP. Bottom left: 1/3X magnification of the top image rendered for LCD. Bottom right: Same image colorimetrically rendered and also adjusted for achromatic contrast.

5.4.2 Chromatic Contrast Adjustment

The idea was to develop band-pass filters for each hue in such a way that they could adjust noise images display on LCD to match the corresponding image on the DLP.

Later, the optimized band-pass filters would be applied to corresponding color separations of a painting image.

The five primary noise patterns, used in chromatic contrast matching, had different lightness levels. However, a complex test image, such as a portrait, has the same lightness level for all five color separations. Therefore, lightness of the test image would be different from the noise images used in the experiments. As an example, the red noise patterns had lightness of $I=0.3986$ and the Seurat painting image had a mean lightness of $I=0.4737$. So, in the first step it was necessary to predict unadjusted and adjusted noise images on the LCD and DLP for a lightness level corresponding to a painting image.

Such predictions for the red noise patterns are presented below.

In Figure 5-12, ‘ I ’ and ‘ I_1 ’ denoted the original and required lightness of noise patterns, respectively, which for this example were 0.3986 and 0.4737. The maximum chroma of the noise image, R , was adjusted by observers to a value of R' at the original lightness of 0.3986. Assuming a linear relationship, one can calculate the maximum chroma of an unadjusted, R_1 , and adjusted, R'_1 , noise image at a lightness level of $I_1=0.4737$:

$$R_1 = R \frac{(1 - I_1)}{(1 - I)} \quad R'_1 = R' \frac{(1 - I_1)}{(1 - I)} \quad (5-6)$$

The original and adjusted red noise images at lightness level of $I=0.3986$ had chroma in the range of $[0, R]$ and $[0, R']$, respectively. These images were linearly scaled, using Equation (3-13), to the range of $[0, R_1]$ and $[0, R'_1]$, which were the corresponding noise images for a lightness of $I_1=0.4737$. If it was required to predict noise images for a lightness level, I_2 , lower than the original lightness I , then Equation (5-7) was used:

$$R_2 = R \frac{I_1}{I} \quad R'_1 = R' \frac{I_1}{I} \quad (5-7)$$

where R_2 , and R'_1 were unadjusted and adjusted predicted maximum chroma of the red noise images for a required lightness of I_2 .

The Renoir, Seurat, Picasso, Rembrandt, and Rousseau painting images had lightness values of 0.4709, 04737, 0.5954, 0.1922, and 0.2483, respectively. Predicted unadjusted and adjusted noise images were computed for the lightness of the selected five painting. Please note that the adjusted and unadjusted images corresponded to the LCD and DLP displays, respectively. Movshon filters, the same filters used for the achromatic images, were used to filter images on the LCD to match images on the DLP. For a magnification factor and lightness level, a set of filter parameters were optimized for each hue. In this way, fifteen sets of parameters ($15=5$ paintings' lightness \times 3 magnification factors) were optimized for each hue.

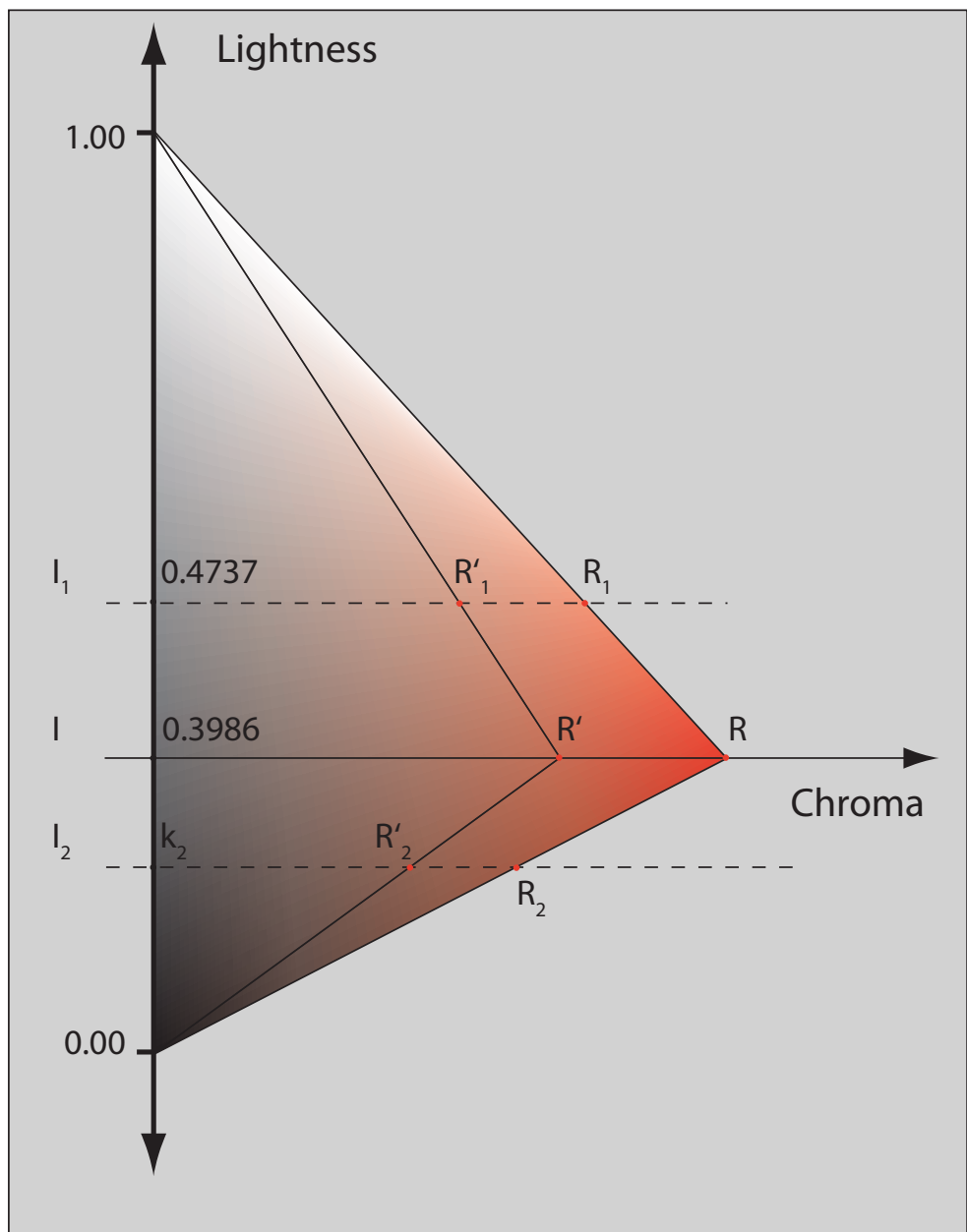


Figure 5-12. Unadjusted and adjusted noise images at lightness level ' I_1 ' and ' I_2 ' were predicted from the original and adjusted noise images at a lightness level of ' I '.

The parameter optimization flowchart for chromatic noise patterns was the same as the achromatic noise images, shown in Figure 5-12. The predicted noise images for the adjusted images on the DLP, the larger, and LCD, the smaller images, are called as the DLP and LCD images in the rest of this section. The same optimization process, described in Section 5.4.1, was performed for each hue using the low, medium, and high frequency noise images at mean lightness levels of the five selected painting images. Optimized parameters for the three magnification factors of 1/3X, 1/2X, and 1X for the five selected painting images are listed in Table 5-3. As an example, the filter responses for the Seurat painting for a 1/3X magnification is shown in Figure 5-13.

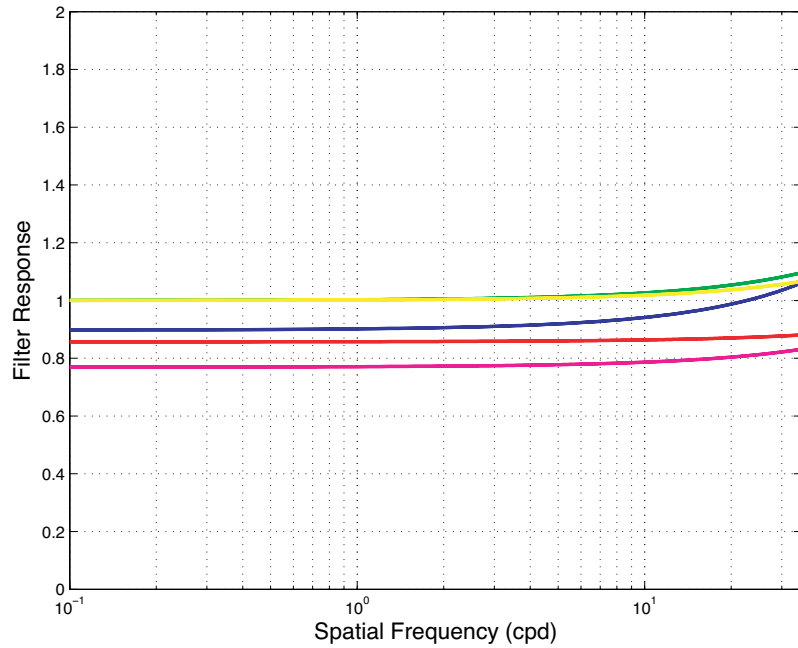


Figure 5-13. Optimized chromatic filters for Seurat painting image for a 1/3X magnification factor.

Table 5-3. Optimized parameters for the chromatic filters at five hues for the five selected paintings at three magnification factors of 1/3X, 1/2X, and 1X.

		1/3X			1/2X			1X		
		A	b	c	a	b	c	a	b	c
Renoir, I=0.4709	Red	118.9	0.000	0.013	116.0	0.000	0.006	116.7	0.001	0.000
	Green	94.8	0.000	0.002	100.0	0.004	0.000	100.0	0.003	0.000
	Blue	98.5	0.002	0.000	104.3	0.003	0.000	111.4	0.005	0.000
	Yellow	93.9	0.000	0.000	100.0	0.003	0.000	100.0	0.002	0.000
	Magenta	116.3	0.001	0.011	123.9	0.002	0.000	130.0	0.002	0.000
Seraut, I=0.4737	Red	118.9	0.000	0.013	116.0	0.000	0.006	116.7	0.001	0.000
	Green	94.8	0.000	0.003	100.0	0.004	0.000	100.0	0.003	0.000
	Blue	98.5	0.002	0.000	104.3	0.003	0.000	111.4	0.005	0.000
	Yellow	93.9	0.000	0.000	100.0	0.003	0.000	100.0	0.002	0.000
	Magenta	116.3	0.001	0.011	123.9	0.002	0.000	130.0	0.002	0.000
Picasso, I=0.5954	Red	118.9	0.000	0.013	116.0	0.000	0.006	116.7	0.001	0.000
	Green	94.8	0.000	0.003	100.0	0.004	0.000	100.0	0.003	0.000
	Blue	98.5	0.002	0.000	104.3	0.003	0.000	111.4	0.005	0.000
	Yellow	93.9	0.000	0.000	100.0	0.003	0.000	100.0	0.002	0.000
	Magenta	116.3	0.001	0.011	123.9	0.002	0.000	130.0	0.002	0.000
Rembrandt, I=0.1922	Red	118.8	0.000	0.013	116.0	0.000	0.006	116.7	0.001	0.000
	Green	94.8	0.000	0.003	100.0	0.004	0.000	100.0	0.003	0.000
	Blue	98.5	0.002	0.000	100.0	0.002	0.000	111.4	0.005	0.000
	Yellow	93.9	0.000	0.000	100.0	0.003	0.000	100.0	0.002	0.000
	Magenta	116.3	0.001	0.011	123.9	0.002	0.000	100.0	0.001	0.039
Rousseau, I=0.2483	Red	118.9	0.000	0.013	116.0	0.000	0.006	116.7	0.001	0.000
	Green	100.0	0.006	0.028	100.0	0.004	0.000	100.0	0.003	0.000
	Blue	98.5	0.002	0.000	104.3	0.003	0.000	111.4	0.005	0.000
	Yellow	93.9	0.000	0.000	100.0	0.003	0.000	100.0	0.002	0.000
	Magenta	116.3	0.001	0.011	123.9	0.002	0.000	130.0	0.002	0.000

As shown in Figure 5-13 low frequency components were attenuated and high frequency components were slightly amplified. The amount of attenuation and

amplification was dependent on the hue of the noise patterns. However, this was consistent with the expectation of a band-pass characteristic seen in the chromatic contrast matching experiments.

The image of Seurat painting rendered colorimetrically for LCD and DLP display and the adjusted image, using the filter shown in Figure 5-13, is presented in Figure 5-14. All five painting images for the 1/3X, 1/2X, and 1X magnification factors were rendered for the LCD display and saved. The rendered images were used in a paired-comparison experiment, to be described in Section 5.5.

Three algorithms of adjustment of the mean lightness, lightness contrast, and chromatic contrast were described in this chapter. In addition to the three main correction methods, one could apply any combinations of the two or three methods together. In this way, there would be seven color reproduction correction methods available for compensation of image size effect. Abbreviations used for the three correction methods and their combinations, which have been used in the rest of this chapter are listed in Table 5-4.

As examples, the Seurat painting image processed using the combined methods and rendered for the LCD display for a magnification factor of 1/3X are presented in Figures 5-15 to 5-18. A colorimetrically rendered image for the LCD and DLP displays are also presented in each figure.

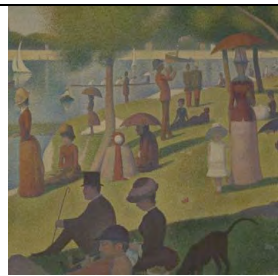
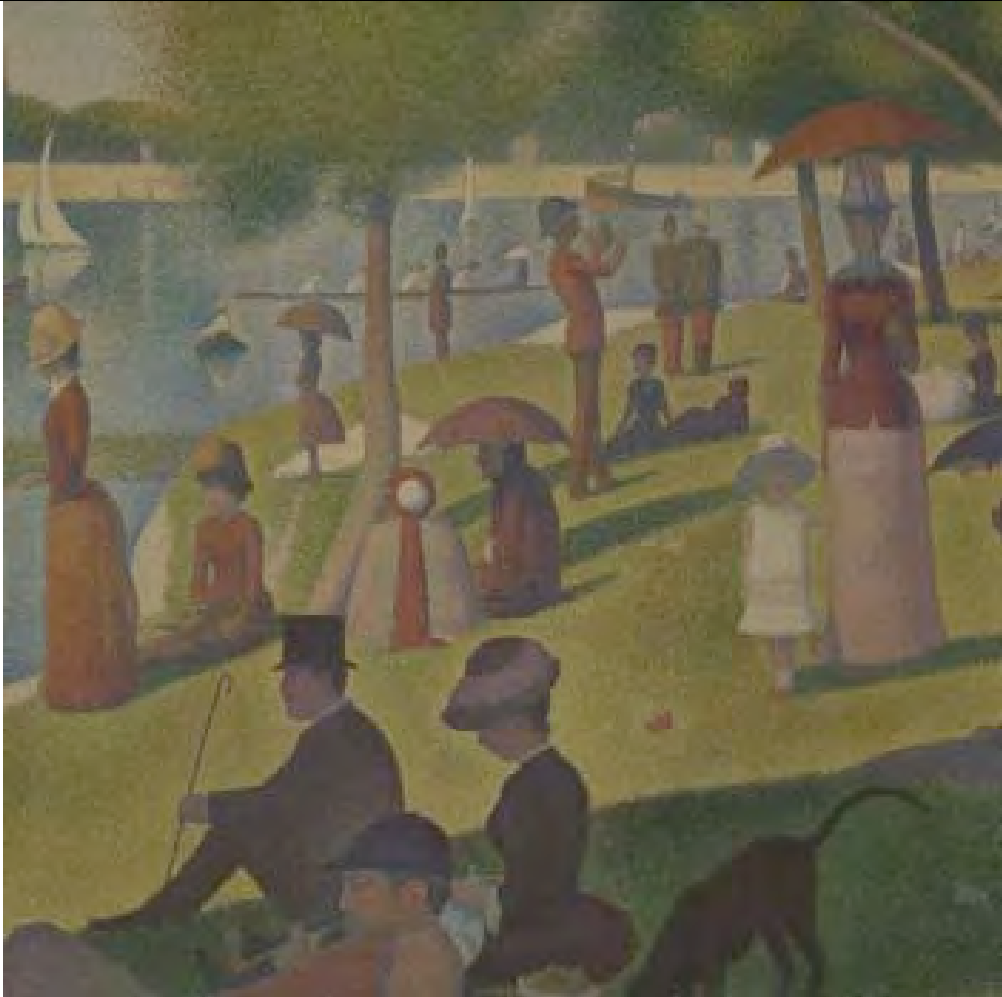


Figure 5-14. Top: Colorimetric rendered image of Seurat painting for the LCD. Bottom left: 1/3X magnification of the top image. Bottom right: Same image colorimetrically rendered and also adjusted for chromatic contrast.

Table 5-4. Eight methods of image rendering used in preparation of painting images and corresponding abbreviations.

No	Symbol	Model
1	A	Adjustment of mean lightness.
2	B	Correction of lightness contrast.
3	C	Adjustment of chromatic contrast.
4	AB	Compensating for mean lightness and lightness contrast.
5	AC	Adjustment of chromatic contrast and mean lightness.
6	BC	Correction of chromatic contrast and lightness contrast.
7	ABC	Adjustment of chromatic and lightness contrast followed by mean lightness adjustment.
8	COL	No adjustment; just colorimetric rendering of a painting image.

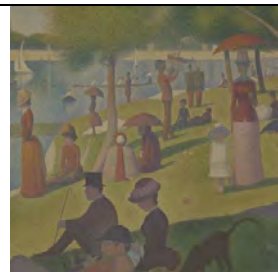
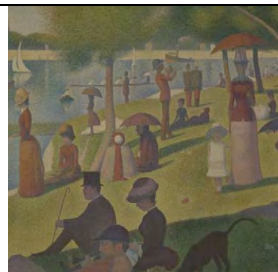
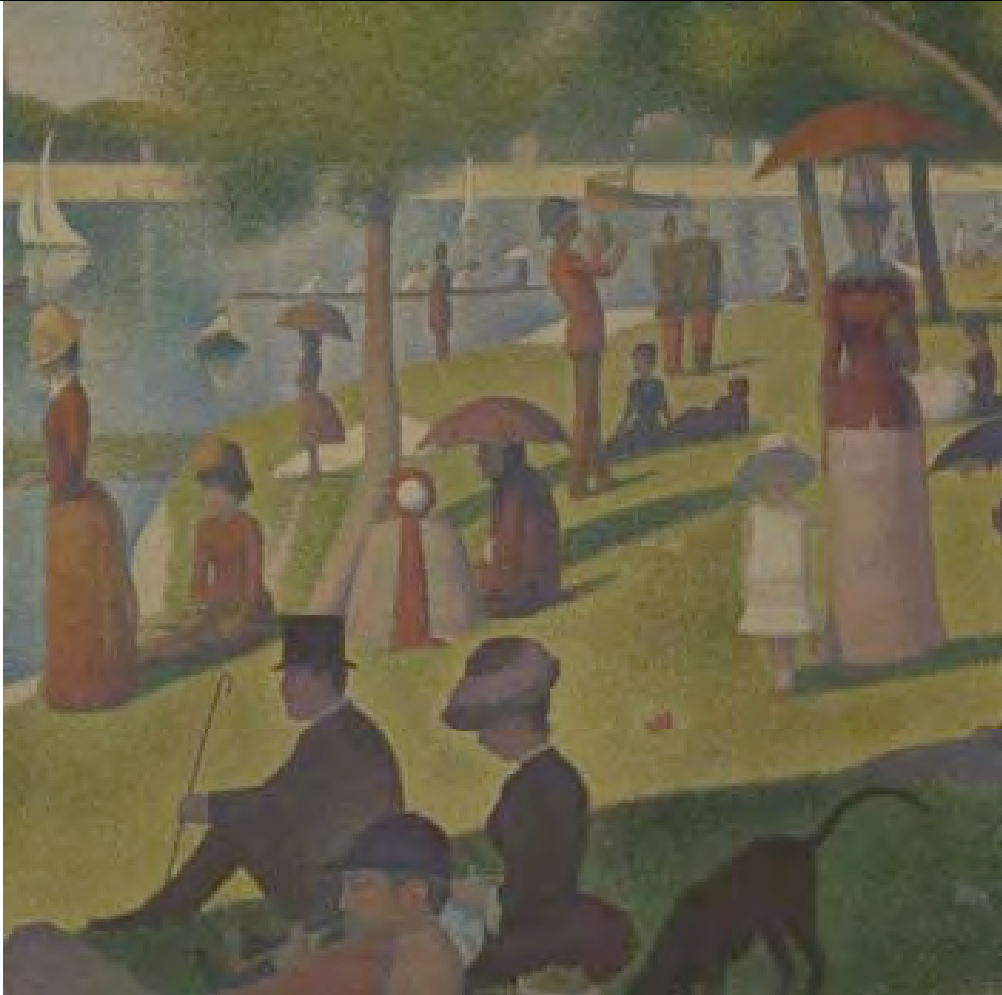


Figure 5-15. Top: Colorimetric rendered image of Seurat painting for the LCD. Bottom left: 1/3X magnification of the top image. Bottom right: Same image colorimetrically rendered and also adjusted for the mean lightness and achromatic contrast.

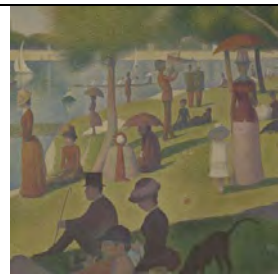
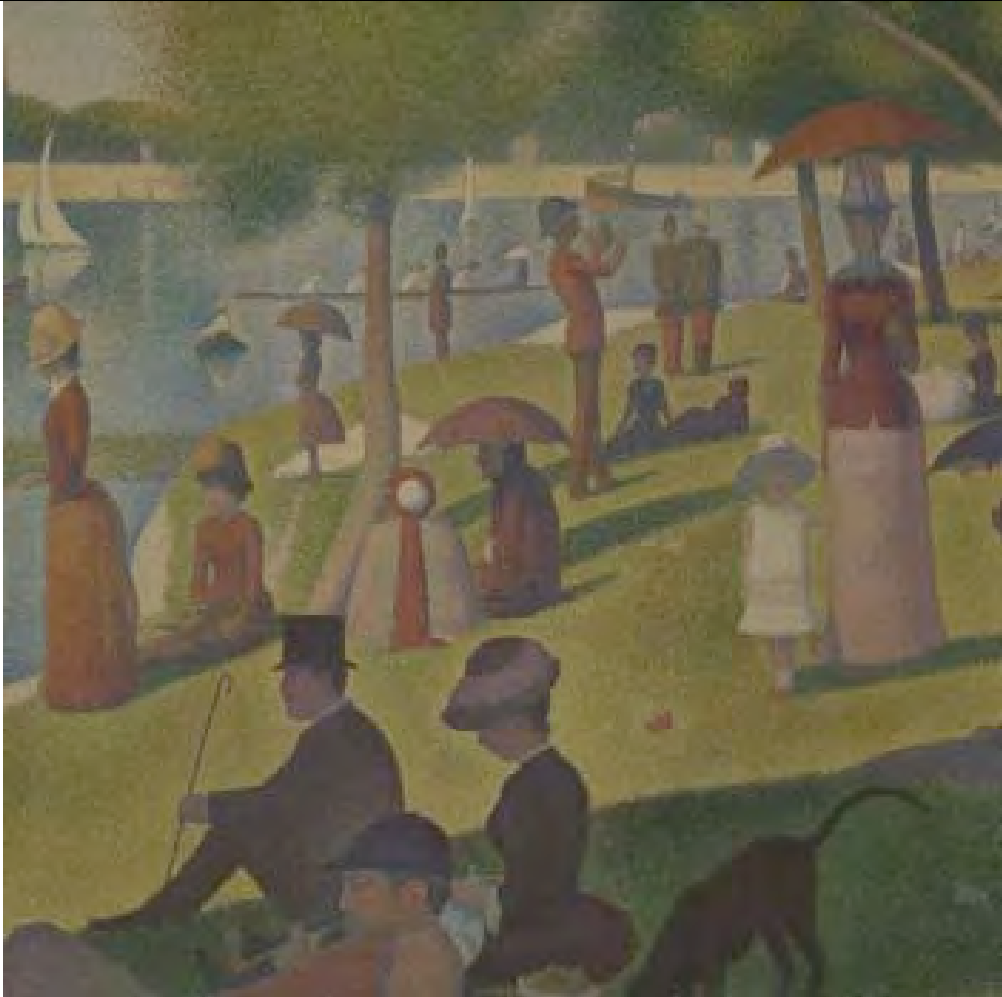


Figure 5-16. Top: Colorimetric rendered image of Seurat painting for the LCD. Bottom left: 1/3X magnification of the top image. Bottom right: Same image colorimetrically rendered and also adjusted for the mean lightness and chromatic contrast.

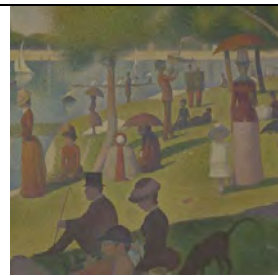
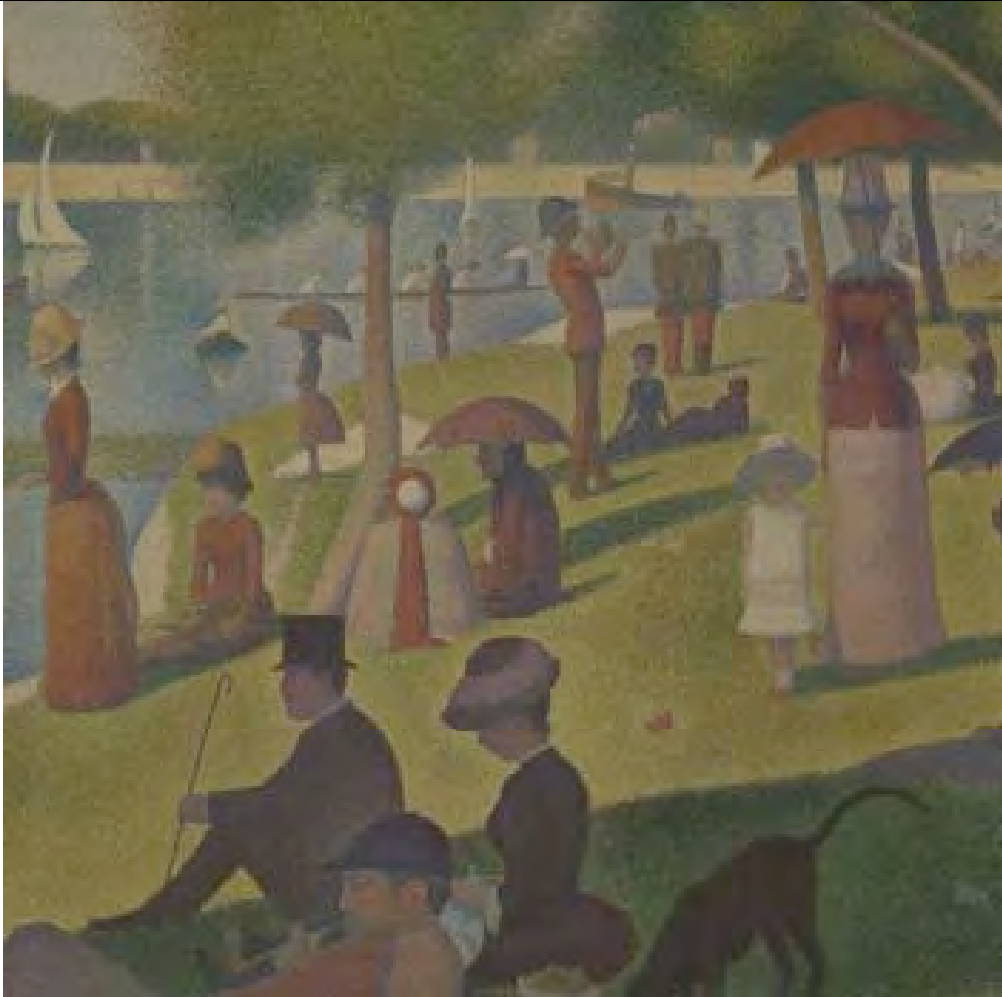


Figure 5-17. Top: Colorimetric rendered image of Seurat painting for the LCD. Bottom left: 1/3X magnification of the top image. Bottom right: Same image colorimetrically rendered and also adjusted for achromatic and chromatic contrast.



Figure 5-18. Top: Colorimetric rendered image of Seurat painting for the LCD. Bottom left: 1/3X magnification of the top image. Bottom right: Same image colorimetrically rendered and also adjusted for the mean lightness, chromatic and chromatic contrast.

5.5 Model Evaluation

In order to evaluate performance of the color correction methods, described in the previous sections, a series of psychophysical experiments were conducted using the paired-comparison method. As described in Table 5-4, eight methods were developed for image rendering of a painting image. For each painting all 28 possible pairs,

$$28 = \binom{8}{2} = \frac{8!}{2!(8-2)!}$$
, were displayed on the LCD and compared to a colorimetric

reproduction of the same painting projected on the screen. Images on the screen and LCD were called as the reference and test images, respectively, in the rest of this chapter.

The experimental setup was the same as contrast matching experiments described in chapter 3 and 4. Paired-comparison experiments were conducted in the dark environment using the same calibrated LCD and DLP displays utilized in the contrast matching experiments.

The test images were rendered for three magnification factors of 1/3X, 1/2X, and 1X in comparison to the reference images. Images on the screen had a resolution of (701 x 701) pixels and subtend approximately 30 degrees of visual angle. For the 1/3X, 1/2X magnification the LCD images had resolutions of (701 x 701) and (1401 x 1401) pixels and subtended 10 and 15 degree of visual angle, respectively. Images on the LCD and DLP screen should subtend the same visual angle for the 1X magnification. But it was not possible to accommodate two images, each subtending 30 degrees of visual angle, on the LCD simultaneously. Hence, images on the LCD and screen were reduced in size to

subtend a smaller visual angle. In this way, images on the screen were rendered for a visual angle of 20 degrees with a resolution of (571x 571) while the LCD images had a resolution of (1891x 1891) pixels corresponding to 20 degrees of visual angle. Table 5-5 summarizes specifications of images on the LCD and screen for the three magnification factors.

Table 5-5. Summary of subtending visual angles and resolutions for reference and test images for the three magnification factors in the paired-comparison experiments.

Magnification Factor	Visual angle on LCD (degrees)	Visual angle on DLP (degrees)	Resolution on DLP (pixels)	Resolution on LCD (pixels)
1/3 X	10	30	701x701	701x701
1/2 X	15	30	701x701	1401x1401
1 X	20	20	571x571	1891x1891

5.5.1 Visual Experiment

Seventeen, sixteen, and fifteen observers participated in three paired-comparison experiments for the magnification factors of 1/3X, 1/2X, and 1X. Observers were RIT student and staff with varying color experience and cultural background. As explained in the previous sections, five artwork images were rendered using eight methods. A total of 140 pairs, $28 \text{ pairs per painting} \times 5 \text{ paintings} = 140$, were presented to observers for each magnification factor. Observers were asked to select one image from each pair on the LCD that was the most accurate reproduction of the image displayed on the screen.

Observers were asked to ignore artifacts caused by aliasing. Pairs were presented to observers in a random order and an adapting noise pattern was shown between pairs. The background and surround of the images on the screen and LCD display were set to a black color. The LCD and DLP screen were positioned at a 180° angle from one another as shown in Figure 5-19. Observers were standing about 50 cm away from the LCD display and 200 cm from the screen.



Figure 5-19. Arrangement of scene and equipment in the paired-comparison experiment, observers could not see both the LCD and screen at the same time and the paired-comparisons were based on short-term memory matching.

5.5.2 Results and discussions

Observers' responses were saved as proper data files. All data were pooled together and the proportional number of times that a rendering method was chosen versus the other methods was recorded. Thurston's Law of Comparative Judgments, Case V, was used to calculate the interval scales from the proportionality data [Engeldrum 2000]. A 95% confidence limit was also calculated for each rendering method [Montag 2004]. The larger the interval scale value, the better performance of the method in image reproduction.

Abbreviations listed in Table 5-4 were used to address rendering methods in the rest of this chapter. Two methods with non-overlapping confidence interval values were interpreted as statistically different. In other words, observers could distinguish between images processed based on each method. As described in Section 1.14, the interval scale is an ordinal scale with equal intervals. There is no meaningful zero point on the interval scale axis. For better presentation purposes, all interval scales were shifted in such way that the colorimetric method, denoted by COL, always had a zero interval scale value. The interval scales and corresponding 95% confidence limits for each method at the three magnification factors are presented in Figures 5-20 to 5-22.

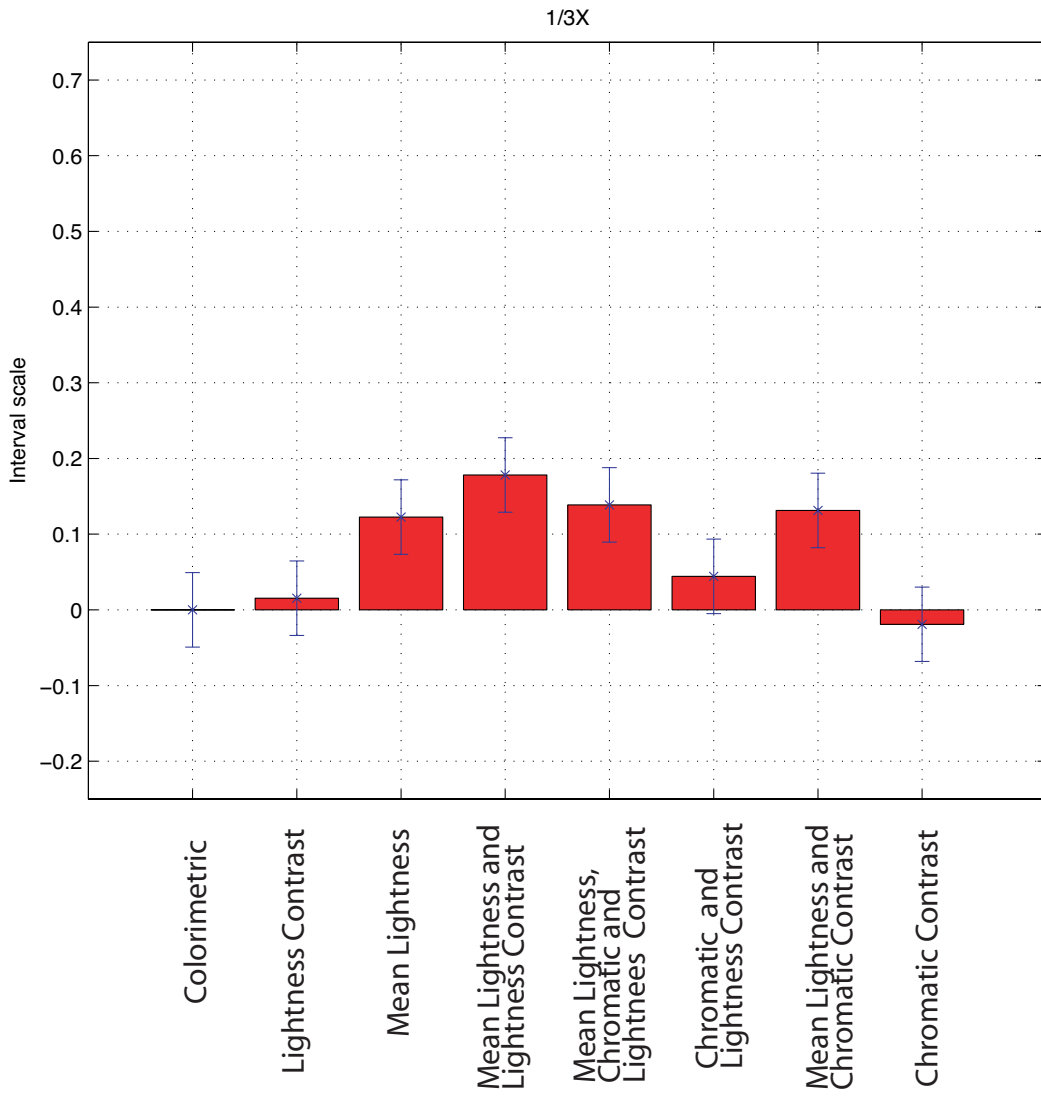


Figure 5-20. Overall results for different color rendering methods for the 1/3X magnification factor.

The AB method had the largest interval scale for 1/3X magnification factor, which is shown in Figure 5-20. The A, AC, and ABC had smaller scale values than the AB method. The confidence intervals of the A, AC, ABC, and AB methods were

overlapping with each other. Although the A, AC, and ABC methods had smaller scale values than AB method, they were not statistically different from each other. The A, AC, AB, and ABC had better performance than the colorimetric method, denoted by COL; they were statistically different from the COL method since their confidence intervals were not overlapping. From the results presented in Figure 5-20, a more accurate image reproduction of the reference images was made by adjustment of lightness contrast and mean lightness of test images, for a 1/3X magnification.

The overall results for a magnification factor of 1/2X are presented in Figure 5-21. The AC, BC, and C methods resulted in test images that were indistinguishable to observers and had the same interval scales with overlapping confidence intervals. These three methods had relatively larger scale than the COL method. In other words, observers could tell apart the better quality of appearance-matching of the test images on the LCD to the reference images on the DLP screen for the AC, BC, and C from the COL method. The ABC method had better performance than COL processing but not as good as the three methods of AC, BC, and C, which can be seen in Figure 5-21. The ABC was distinguishable from COL, AC, BC, and C methods. These results suggest that simultaneous adjustment of chroma and lightness attribute could make better image reproduction than traditional colorimetric image rendering for a 1/2X magnification factor. Except for the lightness contrast adjustment, each method alone also could make better image reproduction than colorimetric image rendering.

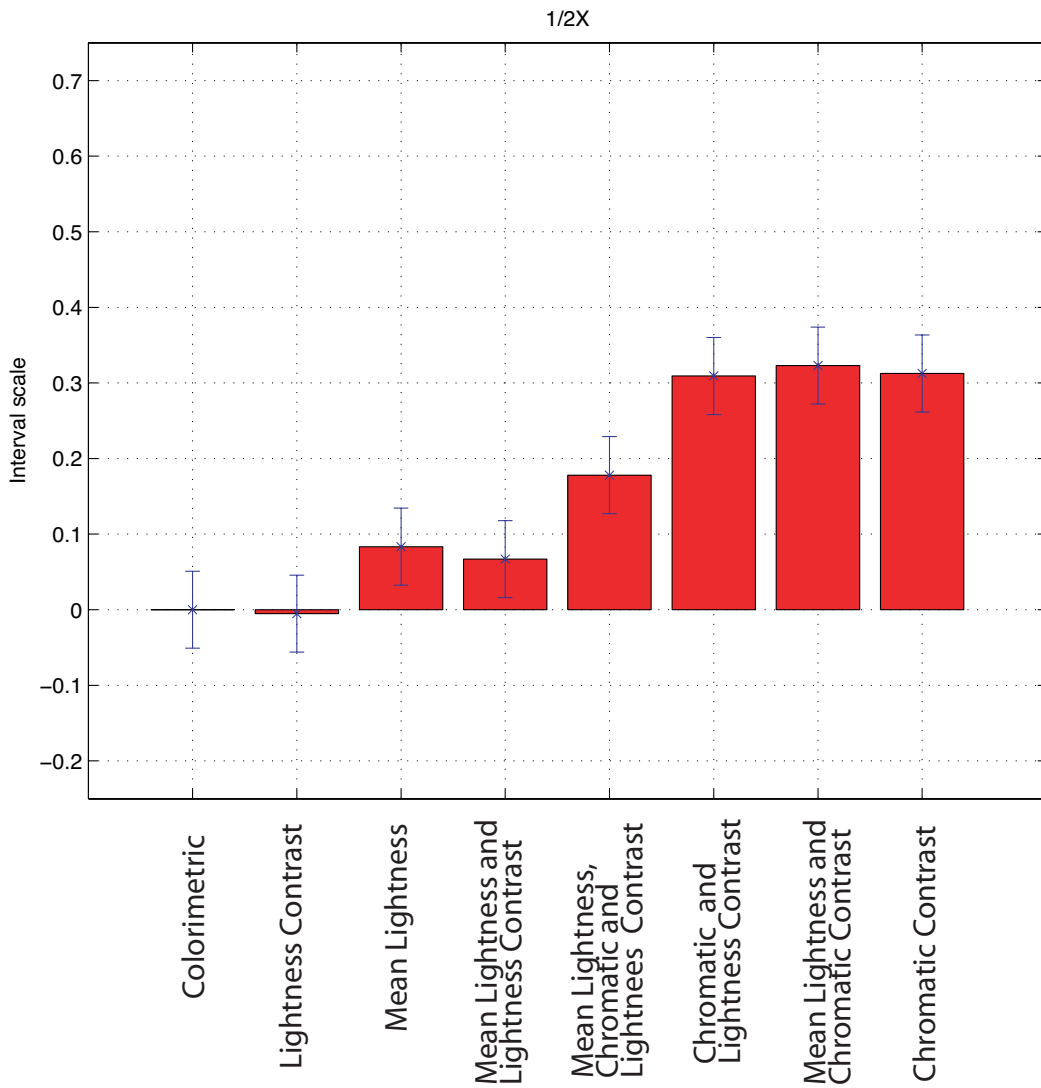


Figure 5-21. Overall results for different color rendering methods for the 1/2X magnification factor.

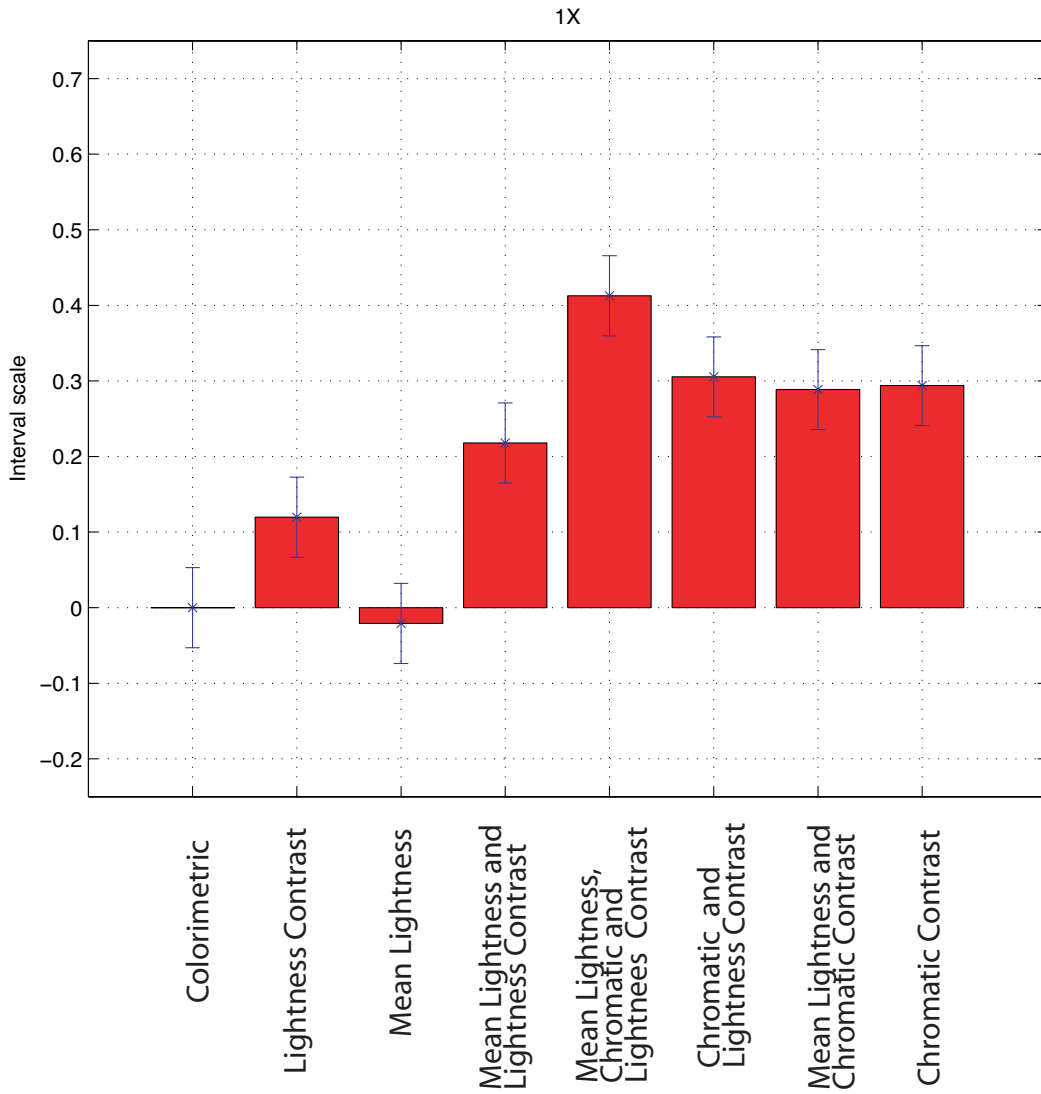


Figure 5-22. Overall results for different rendering methods for the 1X magnification factor.

The 1X magnification reproduction, the equal visual angle/image size, was an interesting case. Although both images on the LCD and DLP subtended the same visual angles, the collected data from contrast matching experiments, presented in Figures 3-28,

3-30, and 4-19 to 4-23, showed that the same patterns displayed on the LCD and DLP displays were perceived to have different appearance. The overall results presented in Figure 5-22 confirm that most of color reproduction methods developed in this research, for 1X magnification, had a better or equal performance in comparison to the traditional colorimetric method, COL. The ABC had the best color reproduction performance and was statistically different from other methods since its confidence interval was not overlapping with other methods' confidence intervals. The AC, BC, and C methods had the same scale values with overlapping confidence intervals. In the following three sections paired-comparison results for each magnification factor are discussed separately.

5.5.3 1/3X Magnification

Interval scales for the Seurat painting, rendered for 1/3X magnification factor, are shown in Figure 5-23. The two rendered images, AB and ABC, had higher interval scale values than the colorimetrically rendered image of the painting. Simultaneous modification of all three attributes of mean lightness, lightness contrast, and chromatic contrast, ABC, had slightly lower scale value than AB method. The confidence intervals for AB and ABC were overlapping and they were not statistically different. However the confidence interval of the colorimetrically rendered image did not overlap with intervals of AB and ABC. Observers could see the difference between COL and AB and ABC images and could tell them apart.

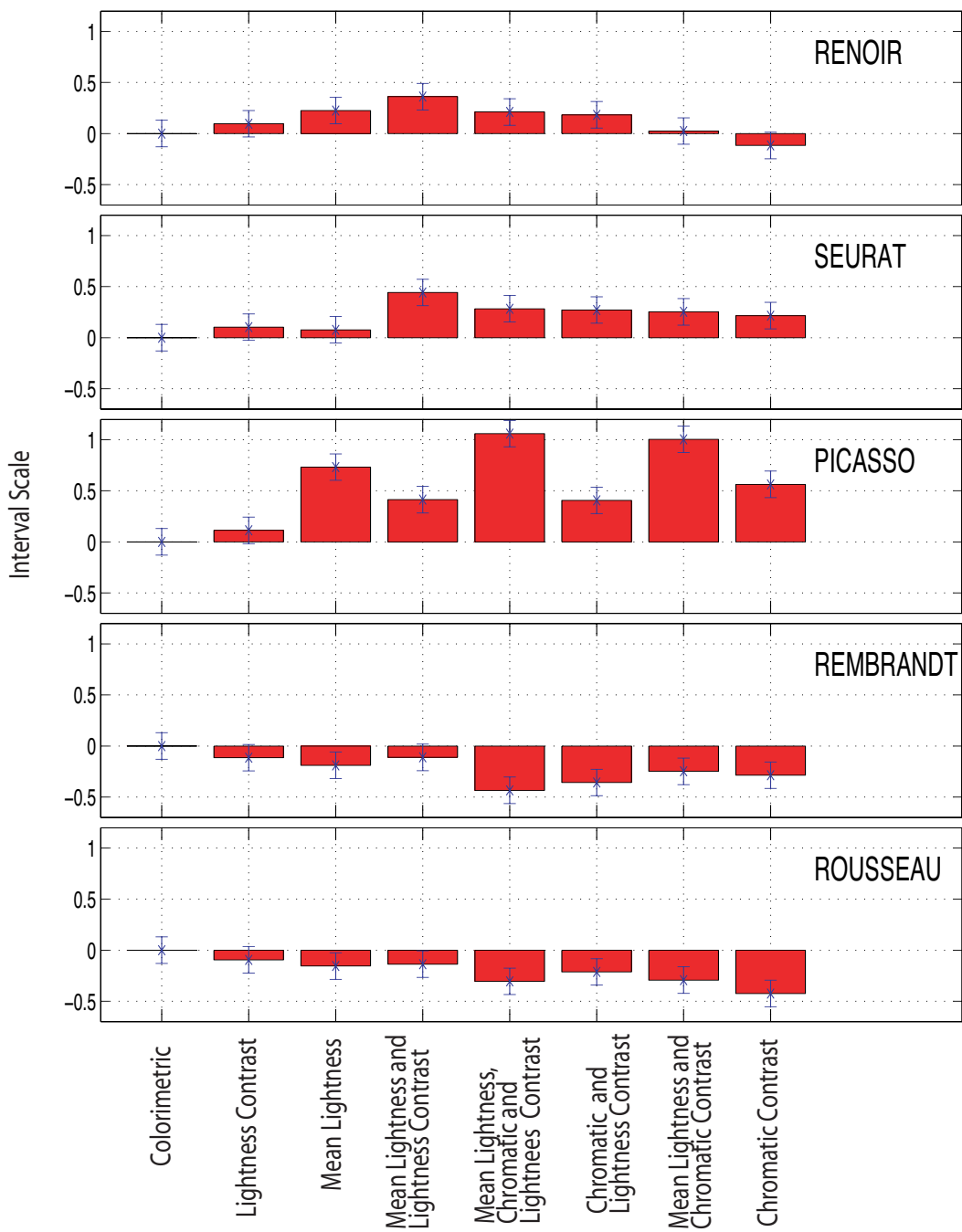


Figure 5-23. Interval scale values for different color rendering methods for the 1/3X magnification factor.

Paired-comparison results for Renoir painting is presented in Figure 5-23. The AB method had higher interval scale value than the other rendering methods; the AB method had a better image reproduction quality than other methods. The confidence intervals of COL and AB methods were not overlapping and observers could distinguish the quality of color reproduction; they were statistically different. Although B, BC, A, and ABC methods had higher interval scale values than COL, they were not statistically different; they had overlapping confidence intervals.

Figure 5-23 shows interval scales for the Picasso painting images. As shown in Figure 5-23, simultaneous correction for chromatic contrast, lightness contrast, and mean lightness of a test image, the ABC method, generated the best image reproduction of the reference image and had the highest interval scale value. The AC also could result in an image with about the same color reproduction quality as of ABC. Please note that confidence intervals corresponding to ABC and AC methods were overlapping. These two methods of image rendering had significantly higher interval values than colorimetric image rendering method. Furthermore interval scale values for A and C methods were also higher than the COL method. In other words, correction of mean lightness or chromatic contrast could also result in better color reproductions than the traditional colorimetric method.

Colorimetric image rendering of Rembrandt and Rousseau paintings had about the same or better interval scale values than other rendering methods as shown in Figure 5-23. It can be seen that the interval scale values for the B, A, and AB were slightly lower

than the COL method. However the corresponding confidence intervals for B, A, AB, and COL were overlapping which implies that observers could not tell them apart and were perceived to have the same image reproduction quality. As discussed in Chapter 3, the change of mean luminance was not very significant at the low luminance level for all frequency bands. Both Rembrandt and Rousseau images were relatively dark with mean lightness values of 26.4 and 16.3, respectively. So, the same interval scales for the mean lightness adjustment and colorimetric image rendering was expected. As shown in panels 3-28-D, 3-28-E, and 3-28-F, for images that initially had high contrast, the change in contrast before and after adjustments was not very significant. In other words, contrast constancy held for high contrast samples. The Rembrandt and Rousseau images were relatively high contrast images. So it was not surprising that neither B nor AB method could perform better than colorimetric rendering method.

Modification of chromatic contrast reduced the reproduction quality for Rembrandt and Rousseau and hence the interval scales for the C, AC, BC, and ABC images were lower than the other methods. Those images were not statistically different from each other since they had overlapping confidence intervals. All chromatic noise patterns used in the contrast matching experiments, except blue patterns, had lightness values higher than 40. However, the Rembrandt and Rousseau had mean lightness values of 26.4 and 16.3, respectively. The chromatic contrast filters corresponding to these two painting were optimized at lightness levels very different from the lightness of the original chromatic noise patterns. The linearity assumptions, presumed in Section 5.4.2,

might not hold for such large differences and the chromatic contrast filters optimized based on those assumptions would not be perfect. The reduction in reproduction quality for the C, AC, BC, and ABC might be attributed to this issue.

5.5.4 1X Magnification

Interval scales for 1X magnification for Seurat, Renoir, and Picasso paintings are shown in Figure 5-24. As can be seen, all the rendering methods had a higher interval scales than the colorimetric rendering method for the Seurat, Renoir, and Picasso paintings. However the range of interval scales were very different. Interval scales corresponding to Picasso painting had the widest range while those corresponding to Renoir had the narrowest.

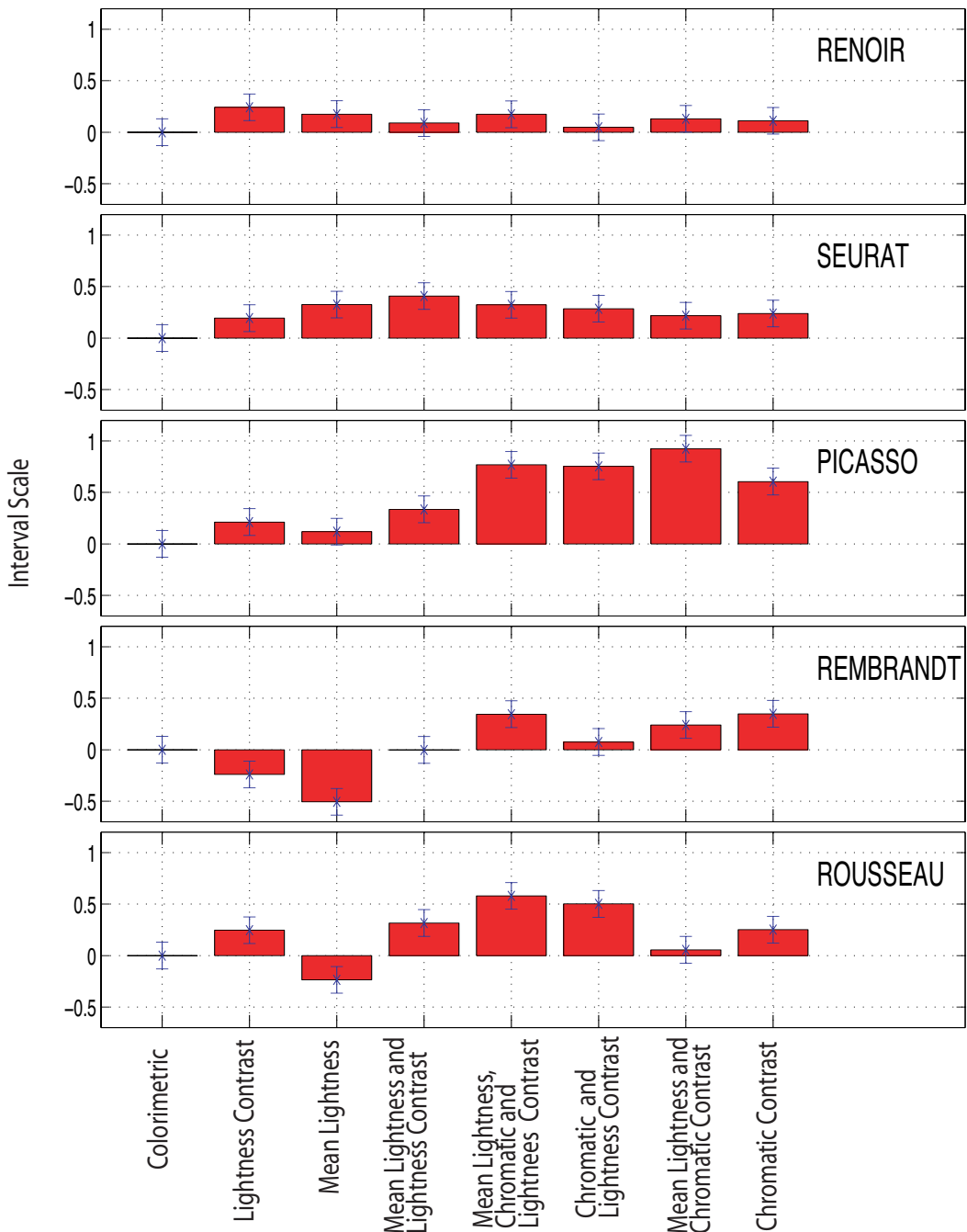


Figure 5-24. Interval scale values for different color rendering methods for the 1X magnification factor.

For the Picasso painting, shown in Figure 5-24, interval scales for ABC, BC, and AC methods were significantly larger than the COL method; observers perceived test images rendered using ABC, BC, and AC methods as better matches to the reference image than the colorimetric version for the same visual angle. Interval scales corresponding to A and B methods were higher than COL; however, the differences were not significant; observers could not differentiate images rendered based on COL, A, and B methods for the Picasso painting.

As presented in Figure 5-24, the Seurat painting rendered by the AB, ABC, and A methods were perceived as better color reproductions than the colorimetrically rendered image and were statistically different from it. Although, A, BC, AC, C methods had higher interval scales than COL method, they were not statistically different as shown by overlapping confidence intervals.

The first seven rendering methods of Table 5-4 had higher interval scale values than the colorimetric image rendering for 1X magnification factor for the Renoir painting, shown in Figure 5-24. The small range of interval scales and mostly overlapping confidence intervals suggest that all images of the Renoir painting appeared to have the same color reproduction quality and observers could not tell them apart. The A method has the highest interval scale and an almost non-overlapping confidence limit with interval of COL method; so one might consider them statistically different.

Interval scale values for Rembrandt and Rousseau painting for 1X magnification are also presented in Figure 5-24. Similar to Picasso, Seurat, and Renoir paintings, the

ABC method had interval scale value as high as, if not higher than other methods. So one could say that observers perceived the test images of Rembrandt and Rousseau paintings rendered by ABC method as a better image reproduction of the reference images than the colorimetric method. Furthermore, the non-overlapping confidence intervals of ABC and COL methods imply that the results of these two methods were statistically different. Observers were able to distinguish the color reproduction quality of those test images.

5.5.5 1/2X Magnification

Interval scale values for the five paintings, at 1/2X magnification factor, are shown in Figure 5-25. It was expected that scale values for 1/2X magnification would be located somewhere between interval scales of 1X and 1/3X magnification factors. As shown in Figure 5-23 and 5-24, for the Renoir painting, both 1X and 1/3X magnification had small interval scales. Furthermore most of the confidence intervals were overlapping. Therefore small interval scales with overlapping confidence intervals were expected for a 1/2X magnification factor. This was exactly what can be seen in Figure 5-25 for 1/2X magnification factor.

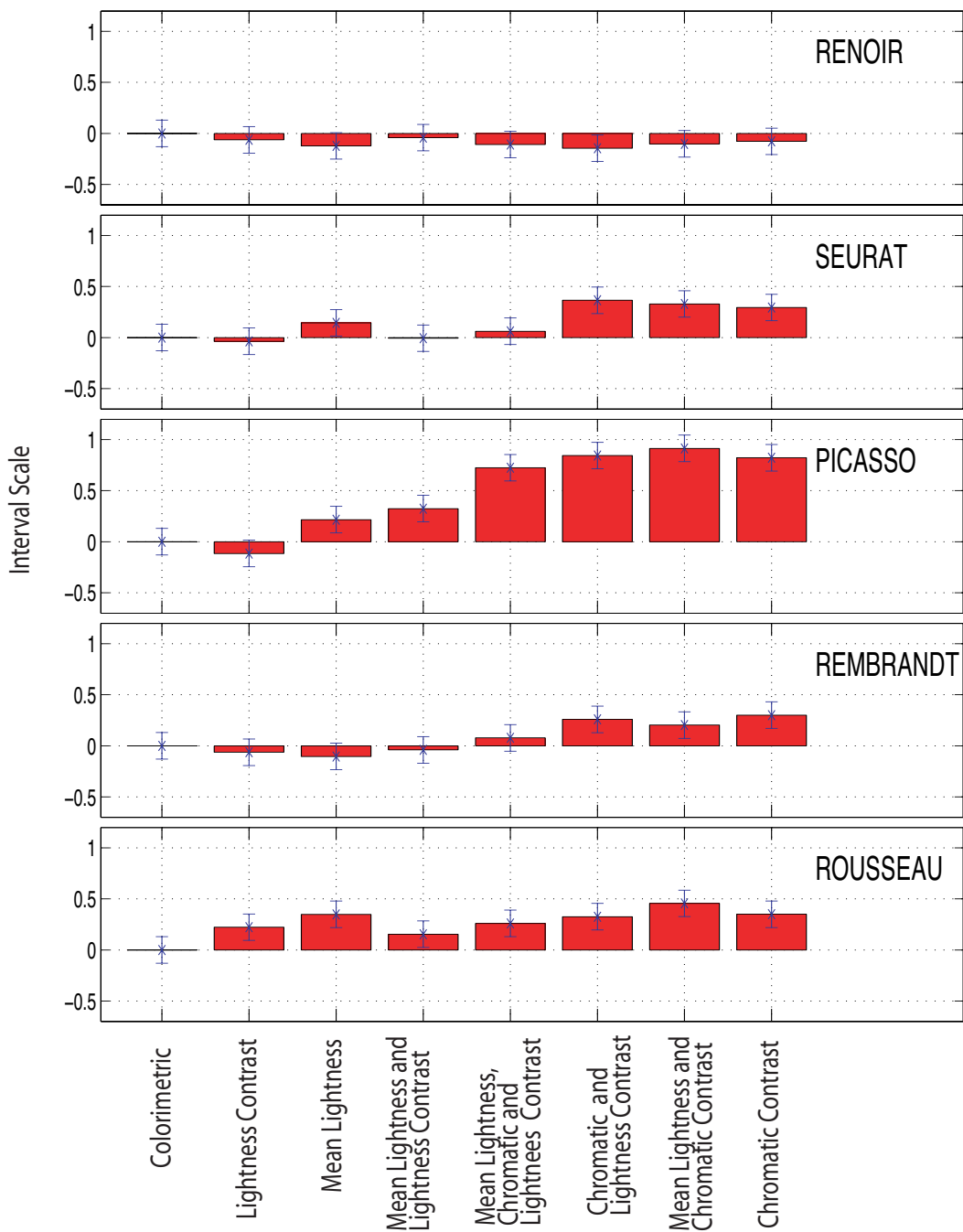


Figure 5-25. Interval scale values for different color rendering methods for the 1/2X magnification factor.

For the Picasso painting, if a method had scales at 1X and 1/3X significantly higher than interval scale of COL then corresponding scale for the 1/2X was also higher than scale of COL method for 1/2X magnification. This was true for most of rendering methods used for other paintings. However there were a few exceptions, such as AB method used in rendering of the Seurat painting image. Although, for 1X and 1/3X magnification, as shown in Figure 5-23 and 5-24, observers selected the AB method rather than COL the rendered images by AB and COL methods were not distinguishable for the 1/2X magnification, as presented in 5-25.

5.6 Conclusions

Seven algorithms accounting for the effect of image size on image appearance as well as a traditional colorimetric image rendering were designed and implemented. Contrast correction algorithms were based on filtering images in the frequency domain and simplicity was an important issue in the design of the filters. Filter parameters were optimized based on achromatic and chromatic noise patterns. Furthermore a method for adjustment of the mean lightness was developed.

Paired-comparison experiments were conducted to evaluate performance of each algorithm using rendered images of five selected painting. The implemented algorithms proved successful in compensating for the effect of image size on image appearance. There was enough difference between interval scale values of the traditional colorimetric

image rendering and the suggested rendering algorithms in this research; the confidence intervals were relatively small and indicating that observers could differentiate color reproduction quality for different methods. In other words, the experimental paradigm had enough accuracy in testing the different processing methods.

The overall results for the three magnification factors of 1/3X, 1/2X, and 1X confirmed that the suggested algorithms could reproduce a reference image with better or equal image reproduction quality than traditional colorimetric image rendering. No single rendering algorithm was performing consistently well for all painting and magnification factors; some image dependency was observed.

The image dependency was related to the mean lightness and contrast of the test images. As discussed in Chapter 3, the change of mean luminance was not very significant at the low luminance level for all frequency bands. Hence, the performance of the mean lightness adjustment was the same as the colorimetric rendering method for the dark images. The contrast constancy held in contrast matching experiments for high contrast noise images, as described in Chapter 3. For the painting images that initially had high contrast, the lightness contrast method could not perform better than colorimetric rendering method. Most of the chromatic noise patterns used in the contrast matching experiments had lightness values higher than 40. For the relatively dark images such as Rembrandt and Rousseau, the chromatic contrast adjustment had the same or lower interval scale values than the colorimetric method for 1/3X magnification factor.

The combined adjustment of mean lightness and lightness contrast had the best performance among the tested algorithms for a 1/3X magnification factor. This emphasized on the importance of the effect of image size on the lightness attributes of an image.

It was shown in Chapter 3 and 4 that patterns displayed on the LCD and DLP, subtending the same visual angle, were perceived to have different appearance. The simultaneous correction for mean lightness, achromatic and chromatic contrast suggested in this research could achieve better color reproduction quality than colorimetric image rendering for the 1X magnification. Except for few cases, interval scales for the 1/2X magnification factor were laying in the range of results obtained for the 1/3X and 1X magnification factors.

6 SUMMARY AND CONCLUSIONS

The main focus of this research was an investigation of the effect of image size on color perception of rendered images. This research had several goals. The first goal was to develop an experimental paradigm for studying the effect of image size on color appearance. The second goal was to identify the most affected image attributes caused by changes in image size. The final goal was to design and evaluate algorithms to compensate for the image size effect.

To achieve the first goal an exploratory experiment using a colorimetrically characterized digital projector and LCD was performed. The projector and LCD are light emitting devices and in this sense are similar soft-copy media. The physical sizes of the reproduced images on the LCD and projector screen could be very different. Additionally, one could benefit from the flexibility of soft-copy reproduction devices such as real-time image rendering, which was essential for adjustment experiments.

Both displays had good colorimetric characterization accuracy as shown in Table 6-1 and 6-2.

Table 6-1. Summary of colorimetric characterization results for LCD display for the 1931 standard observer.

	Mean ΔE_{00}	Max ΔE_{00}	90th percentile ΔE_{00}
All Samples	0.9	2.4	1.6
Primary ramps	0.4	0.8	0.6

Table 6-2. Summary of characterization results for DLP projector for the 1931 standard observer.

Display	Mean ΔE_{00}	Max ΔE_{00}	90th percentile ΔE_{00}
Plus Data Projector U4-232	1.0	8.4	1.6

The experimental approach proved successful in evaluating the effect of image size on color appearance. Furthermore, it was identified that lightness of an image was affected by the changes in image size. The observers found that colorimetrically matching images of different size could be made to more closely match in appearance by manipulation of the lightness. Interval scales for different images used in the exploratory experiment are shown in Figure 6-1. So a matching experiment using relatively simple stimuli, achromatic Gabor patterns, was performed to investigate the effect of image size on the mean luminance and achromatic contrast of the images.

In contrast matching experiment using Gabor patterns, the contrasts of the larger images on the projector screen were boosted while their mean luminance values were decreased relative to the smaller images on the LCD. For high contrast images this increase in contrast was insignificant (contrast constancy.) Compared to the mean luminance level of the LCD images, a reduction of the mean luminance level of the adjusted images was observed. This decrease was more pronounced for smaller images.

In building a model accounting for the effect of image size on the image appearance, a systematic way of collecting data and incorporating them into a proper image model is needed. A series of contrast matching experiments were conducted using achromatic and chromatic band-pass noise patterns, where one could study the effect of variation in visual angle (size) on the different frequency bands.

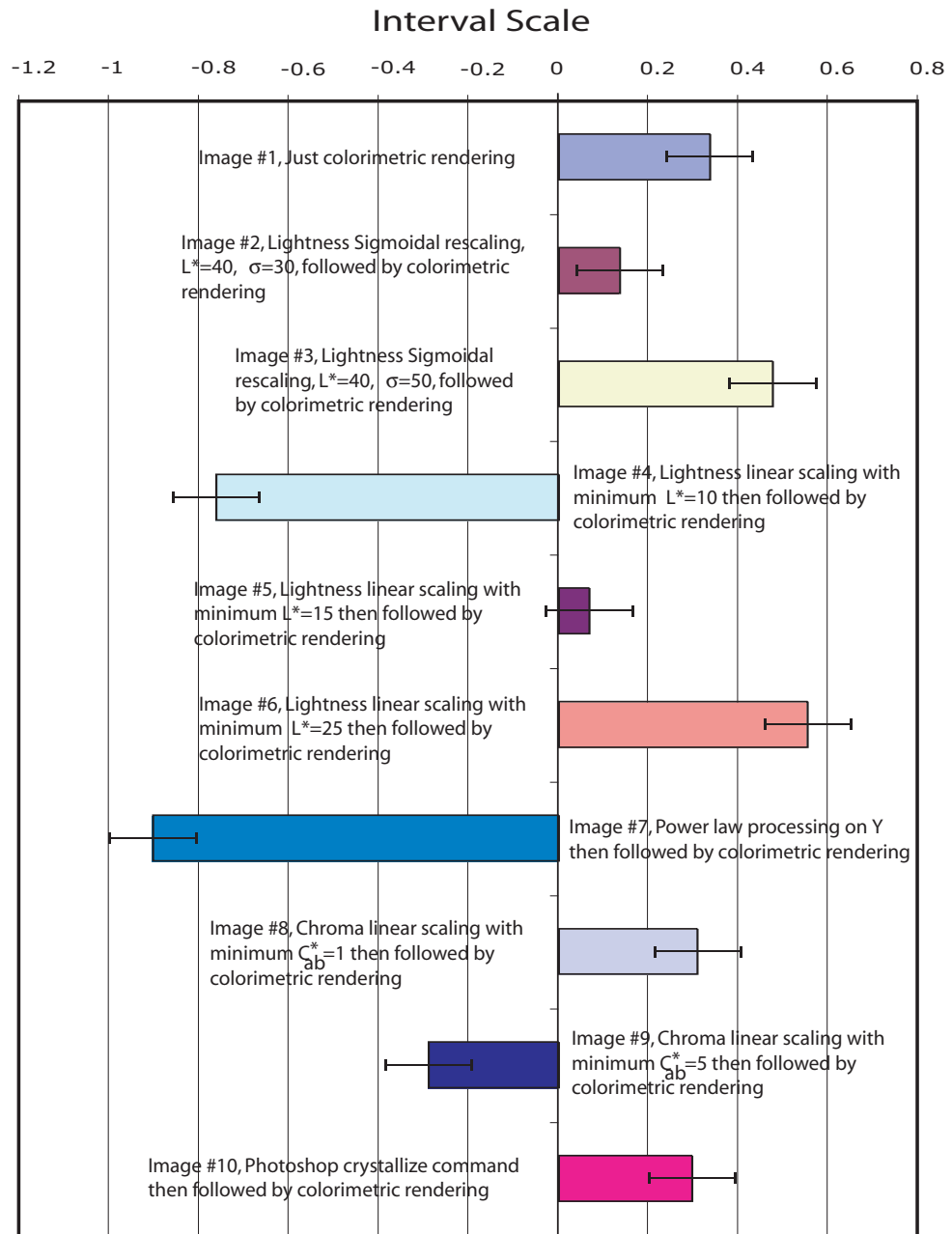


Figure 6-1. Interval scales and corresponding 95% confidence limits based on visual experiment.

The method of adjustment utilized in achromatic contrast matching experiment, discussed in Chapter 3, successfully showed a trend of the increase of contrast in adjusted images versus the decrease of image size on the LCD display for low frequency band-pass noise patterns. The contrast matching results for the achromatic noise patterns are shown in Figure 6-2. Conversely, high frequency, small size images on LCD were matched with images of low contrast on screen. This decrease in contrast was more pronounced for images with high mean luminance levels. Contrast constancy was observed for high contrast images.

Compared to the mean luminance level of the LCD images, a decrease of the mean luminance level of the adjusted images was observed for all frequency noise patterns, shown in Figure 6-3. This decrease was more pronounced for smaller images at low and medium contrast. The change of luminance was not significant at low mean luminance levels. The results of contrast matching using achromatic noise patterns were consistent with the previous experiment using Gabor patterns.

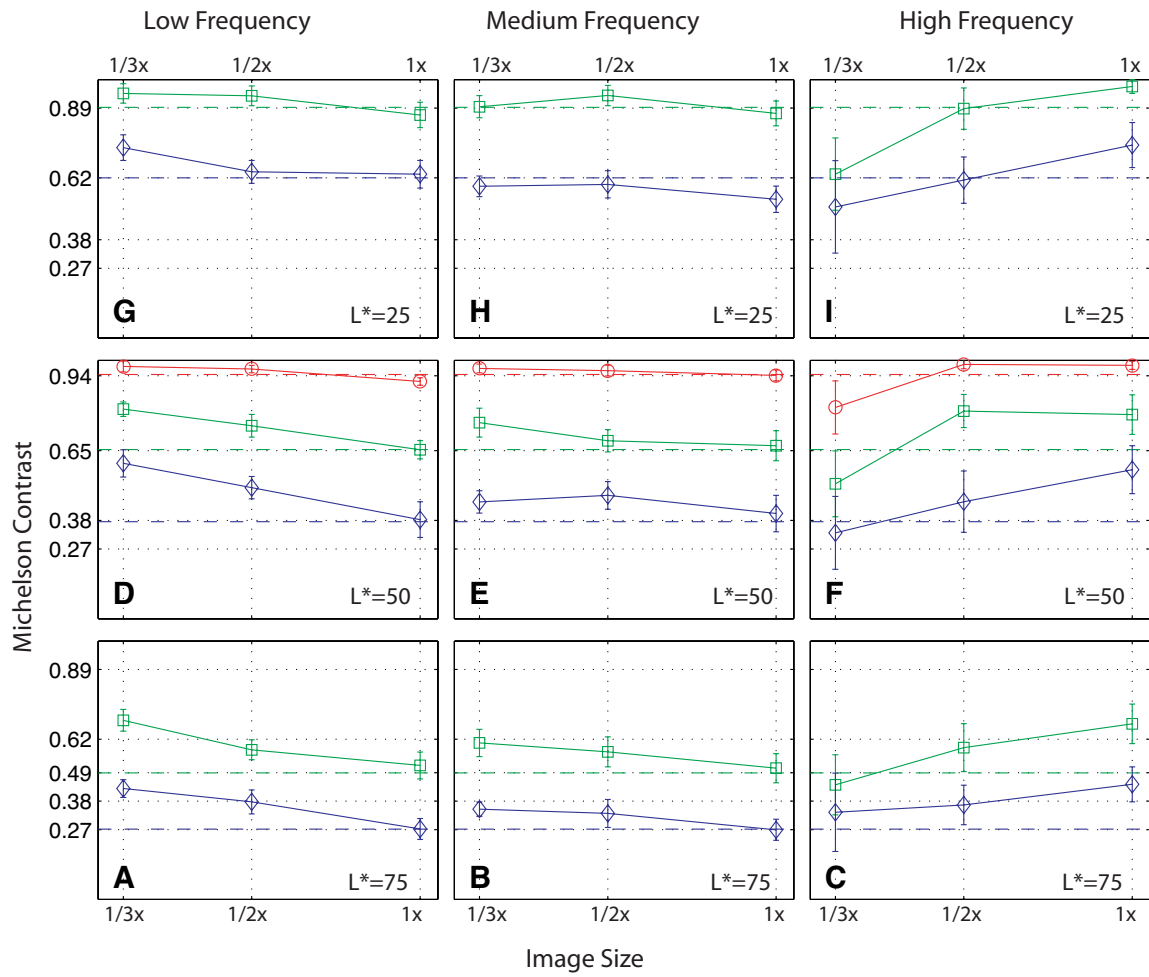


Figure 6-2. Contrast adjustment of DLP images versus LCD images for 14 observers. Panels A, D, G correspond to low frequency noise patterns, centered at 0.5 cpd, and CIEL values of 75, 50, and 25, respectively. Panels B, E, H correspond to medium frequency noise patterns. Panels C, F, I correspond to high frequency noise patterns, centered at 8 cpd. Dashed lines at each panel shows contrast of LCD images.*

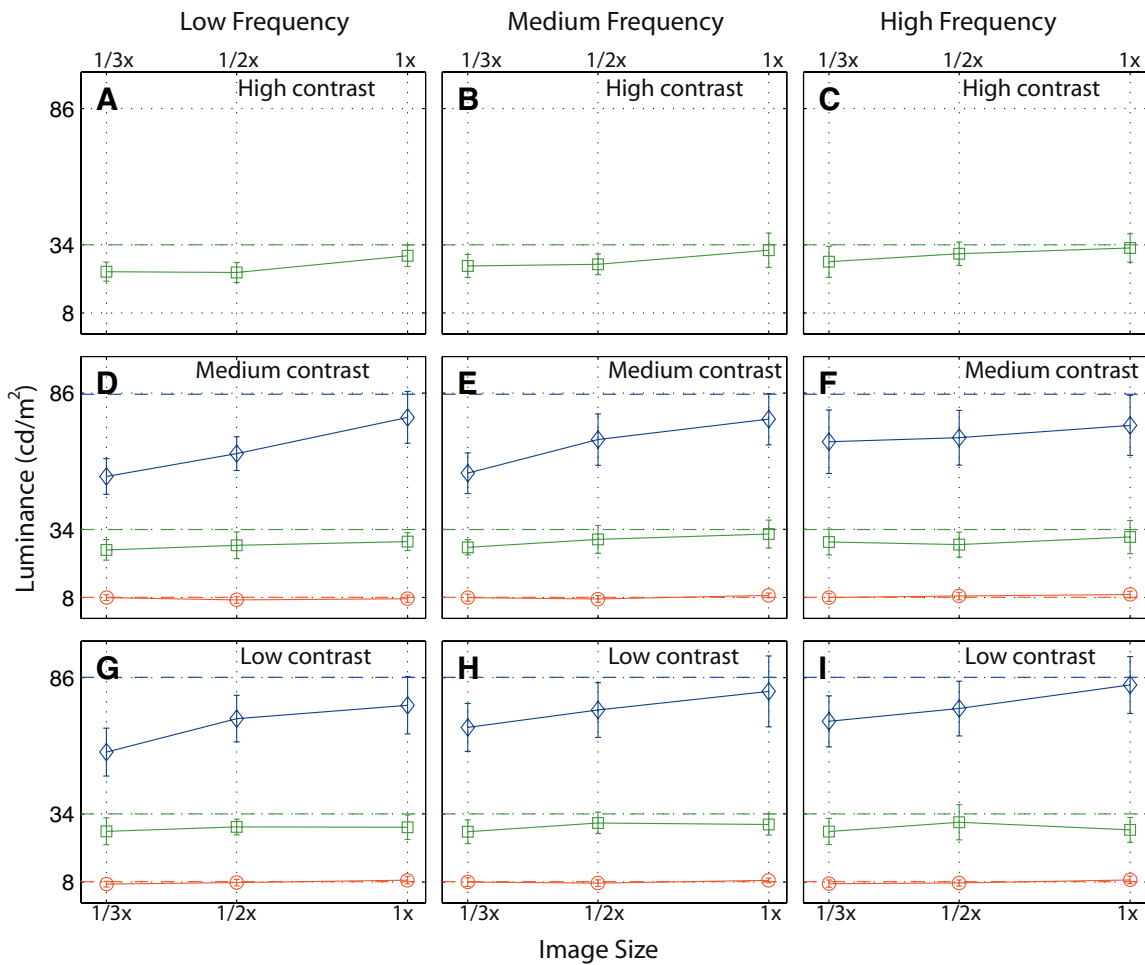


Figure 6-3. Luminance adjustment results for DLP images versus LCD images for 14 observers. Panels A, D, G correspond to low frequency noise patterns, centered at 0.5 cpd, and three levels of contrast levels. Panels B, E, H correspond to medium frequency noise patterns, centered at 2 cpd. Panels C, F, I correspond to high frequency noise patterns, centered at 8 cpd. Dashed line at each panel shows mean luminance of LCD images.

In order to capture the effect of the image size on the chromatic attributes of an image, isoluminant band-pass noise patterns with varying chroma along a few selected hues were adjusted on a DLP screen to match corresponding images on an LCD display.

The lightness of a color depends on both its luminance and chromaticity; changes in chroma of a test pattern are accompanied by perceived changes in their lightness. This is known as the Helmholtz-Kohlrausch effect. To prevent the unwanted effect of the lightness variation on the results of chromatic contrast matching a preliminary experiment was performed to evaluate the magnitude of the Helmholtz-Kohlrausch effect. Lightness of color patches at five hues with lightness values of 0.75 and 0.25, in IPT space, were adjusted in comparison to gray patches with the same lightness. All color patches were adjusted to darker or equal lightness in comparison to the corresponding gray patches. The more chromatic a color was, the more the reduction in lightness that was required to match perceived lightness. Proper lightness adjustments were applied to five sets of chromatic noise patterns. Pixels in each noise image were perceived to have the same lightness with variable chroma along an initial hue line.

Corrected noise patterns were used in a chromatic contrast matching experiment, where chromatic contrast was decreased for smaller images for high frequency noise patterns for all five hues. An opposite trend of an increase in chromatic contrast versus visual angle was seen for the low frequency patterns.

These trends were similar to the results of achromatic contrast matching. In both experiments, the low frequency images with smaller visual angles were perceived to have

higher contrast than corresponding larger images displayed on the DLP screen.

Conversely, high frequency image on the LCD were perceived to have lower contrast than the corresponding larger images on the DLP. It was shown that image size had an effect on the image appearance that could be modeled by band-pass filters for both chromatic and achromatic channels. The amount of increase or decrease in perceived chromatic contrast versus image size was dependent on the hue of the test patterns.

Band-pass filters and collected results from chromatic and achromatic contrast matching were used to develop color reproduction models accounting for image size effect. Seven algorithms as well as traditional colorimetric image rendering were designed and implemented. Contrast correction algorithms were base on filtering images in the frequency domain. The simplicity was an important issue in the design of the filters. Seeking for simplicity of the model, simple three-parameter filters originally described by Movshon and Kiorpes were used. Filter parameters were optimized based on achromatic and chromatic noise patterns used in contrast matching experiments. Furthermore a method for adjustment of the mean lightness was developed.

Paired-comparison experiments were conducted to evaluate performance of each algorithm using rendered images of the five selected painting. Overall results for different color rendering methods are shown in Figures 6-4 to 6-6. The implemented algorithms proved successful in compensating for the effect of image size on image appearance. There was enough difference between interval scale values of the traditional colorimetric image rendering and the suggested rendering algorithms in this research; the confidence

intervals were relatively small and indicating that observers could differentiate color reproduction quality for different methods. In other words, the experimental paradigm had enough accuracy in testing different processing methods.

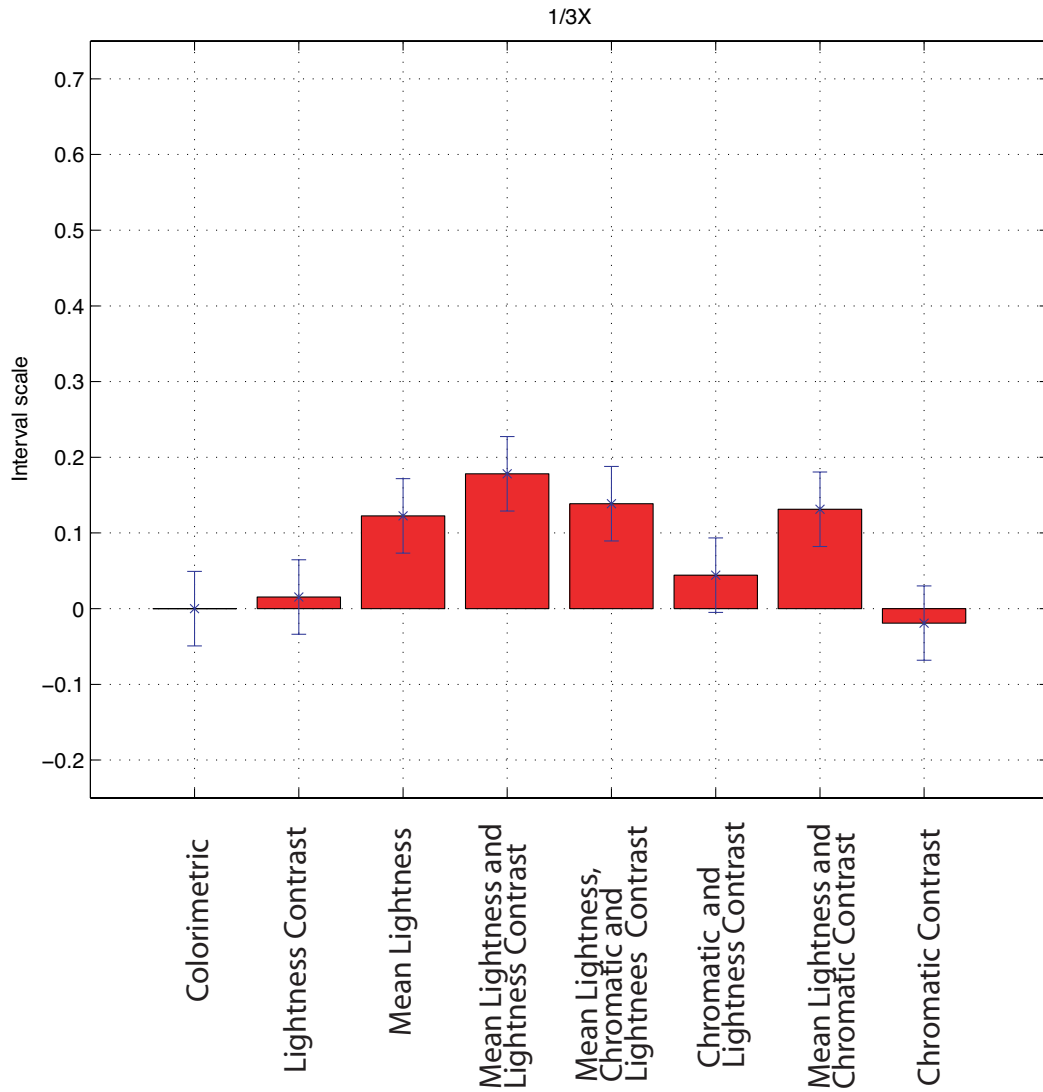


Figure 6-4. Overall results for different color rendering methods for the 1/3X magnification factor.

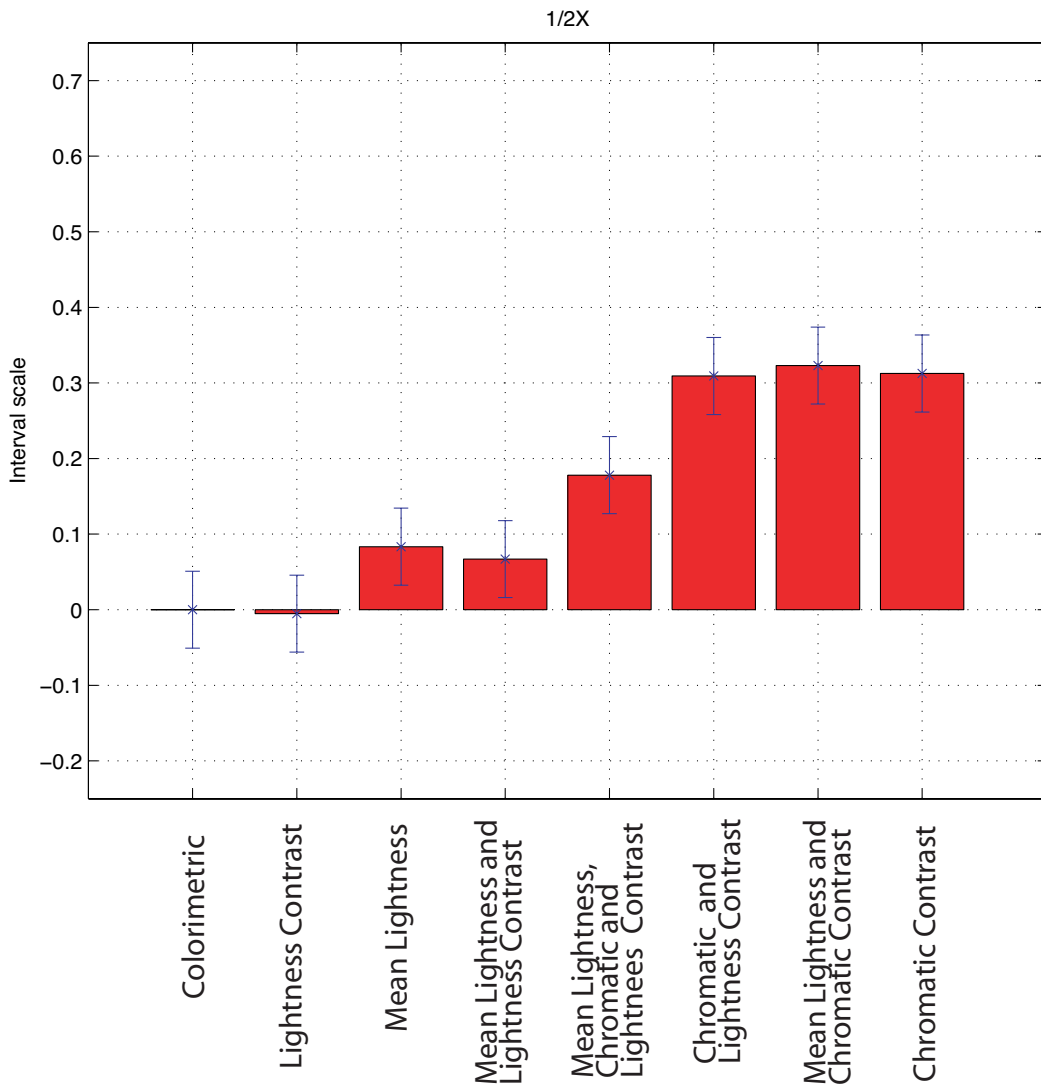


Figure 6-5. Overall results for different color rendering methods for the 1/2X magnification factor.

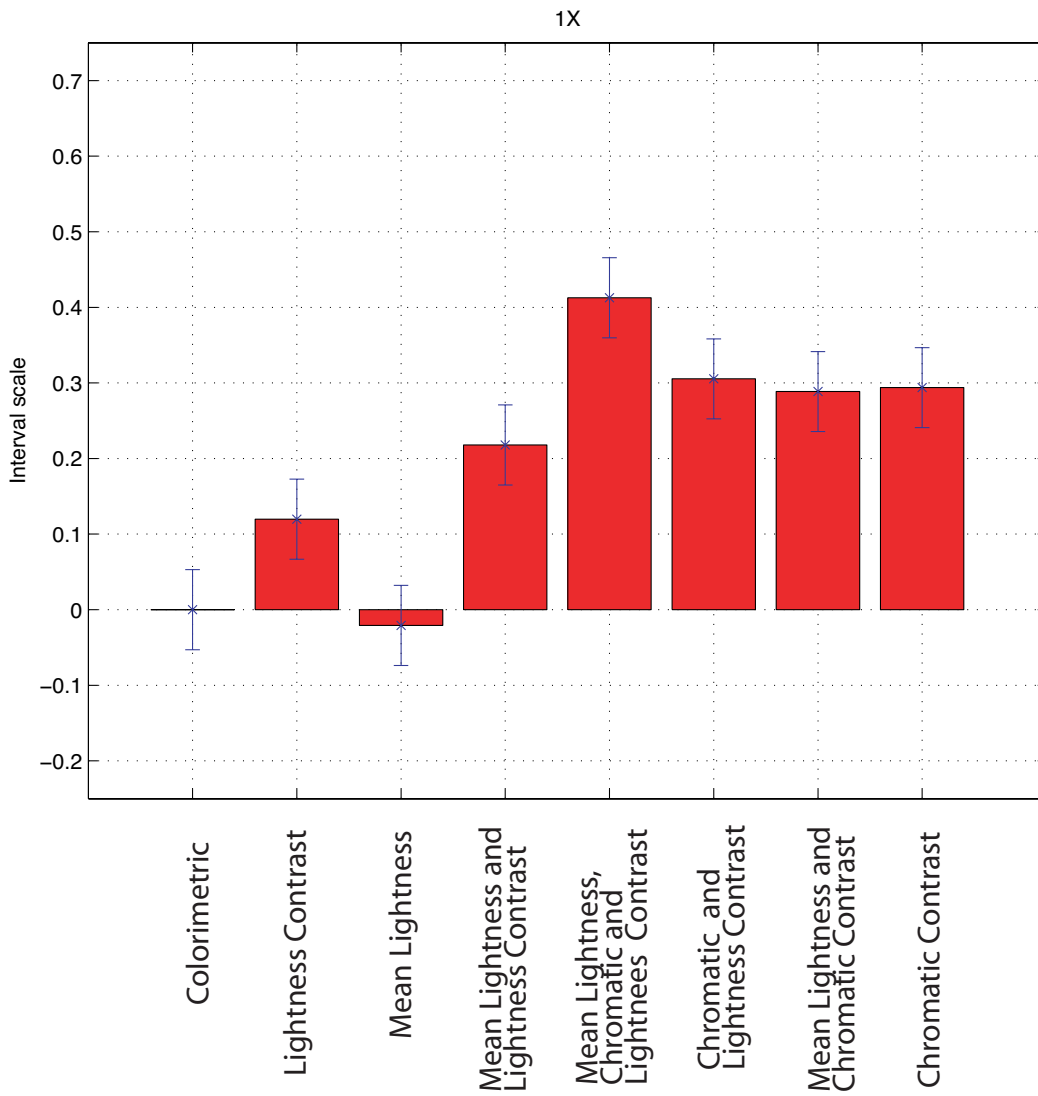


Figure 6-6. Overall results for different rendering methods for the 1X magnification factor.

The overall results for the three magnification factors of 1/3X, 1/2X, and 1X confirmed that the suggested algorithms could reproduce a reference image with better or equal image reproduction quality than traditional colorimetric image rendering. No single

rendering algorithm was performing consistently well for all painting and magnification factors; some image dependency was observed. The performance of the image rendering methods was dependent on the mean lightness and contrast of the test images.

The combined adjustment of mean lightness and lightness contrast had the best performance among the tested algorithms for a 1/3X magnification factor. This emphasized the importance of the effect of image size on the lightness attributes of an image. It was shown in Chapter 3 and 4 that patterns displayed on the LCD and DLP, subtending the same visual angle, were perceived to have different appearances. The simultaneous correction for mean lightness and achromatic and chromatic contrast suggested in this research could achieve better color reproduction quality than colorimetric image rendering for the 1X magnification. Except for few cases, interval scales for the 1/2X magnification factor were laying in the range of results obtained for the 1/3X and 1X magnification factors.

It is possible to perform quick and approximate compensation to adjust for image size effect using a graphic editing program. As an example, one can save an original image in CIELAB format and perform a few adjustments on the lightness attribute, CIEL, in Photoshop software. Although it is an image dependent issue, smaller images are usually perceived to have more lightness contrast than corresponding larger images. Furthermore they are perceived darker than a larger reproduction. Therefore it is recommended to decrease achromatic contrast and increase lightness of the small reproduction in comparison to the larger original image. This can be applied via

Brightness/Contrast command of the Photoshop software. Choosing *Image > Adjustments > Brightness/Contrast* command one can easily reduce contrast and increase lightness of a small reproduction of an original image. It is important to note that such adjustments are qualitative and their performance is limited.

6.1 Scientific Contributions

The scientific contributions of this research are summarized as the following:

- Development of an experimental paradigm for measuring the effect of image size on color appearance of soft-copy reproductions. Demonstrating the capability of the experimental paradigm in revealing the change of appearance for a change of visual angle (size). It was proved that image size affects color appearance perception and can be compensated by application of proper image rendering algorithms.
- Identification of the mean of lightness, achromatic and chromatic contrast as the affected attributes of an image for changes of image size through contrast matching experiments. Experimental measurement of the extent and trend of changes for each attribute.
- Design and evaluation of proper algorithms to compensate for the image size effect. The correction algorithms were tested versus traditional colorimetric image rendering using a paired-comparison technique. The paired-comparison results

confirmed superiority of the algorithms over the traditional colorimetric image rendering for the size effect compensation.

6.2 Directions for Future Study

Optimized chromatic and achromatic filters and the look up tables used for adjustment of mean lightness were populated based on relatively few experimental measurements.

Filters and look up tables optimized based on a larger experimental data set, for other contrast, hues, magnification factors, and mean luminance levels, are expected to generate better color reproduction of a reference image at different sizes.

Furthermore, it is suggested to investigate achromatic and chromatic contrast as well as mean luminance changes versus changes of image size for hard-copy reproductions. More efforts are needed to design and evaluate algorithms accounting for the image size effect for soft-copy versus hard-copy reproductions.

7 REFERENCES

[Anderson 1999] D. R. Anderson, D. J. Sweeney and T. A. Williams, Statistics for Business and Economics (South-Western College Publishing, Cincinnati, OH, 1999) pp. 375-376.

[Adelson 1993] Adelson, E.H., Perceptual organization and judgment of brightness, Science, 262, 2042-2044 (1993).

[Anter 2000] K. F. Anter, What color is the red house? Perceived color of painted facades. Doctoral Thesis. Royal Institute of Technology, Stockholm. (2000).

[Ashikhmin 2002] M. Ashikhmin. A tone mapping algorithm for high contrast images. In 13th Eurographics Workshop on Rendering. Eurographics, June 2002.

[Backhaus 1998] W.G.K Backhaus, R. Kligel, and J. S. Werner, Eds, Color Vision: Perspectives from Different Disciplines, Walter de Gruyter, Berlin, (1998).

[Bala 2002] R. Bala, Device Characterization, in G. Sharma, Digital Color Imaging Handbook, CRC Press, (2002).

[Barnard 1997] K. Barnard and B. Funt, Analysis and improvement of multi-scale Retinex, Proc. of IS&T/SID 5th Color Imaging Conference, 221-226 (1997).

[Bartleson 1967] C. J. Bartleson and E. J. Breneman, Brightness perception in complex fields, *J. Opt. Soc. Am.*, 57, 953-957 (1967).

[Bartleson 1975] C. J. Bartleson, Optimum image tone reproduction, *J. SMPTE* 84, 613-618 (1975).

[Berns 1987] R. S. Berns, F. Grum, Exhibiting artwork: consider the illuminating sources, *Col. Res. & Appl.*, 12, No. 2, 63-72 (1987).

[Berns 1996] R. S. Berns, Methods for characterizing CRT displays. *Displays*, 16, 173–182 (1996).

[Berns 1997] R. S. Berns, A generic approach to color modeling, *Col. Res. & Appl.* 22, 318-325 (1997).

[Berns 2000] R. S. Berns, Billmeyer and Saltzman's Principle of Color Technology, 3rd edition, New York, NY, 2000.

[Berns 2003] R. S. Berns, S. R. Fernandez,L. A. Taplin, Estimating black level emissions of computer-controlled displays. *Color Res Appl.*, 28, 379 –383 (2003).

[Berns 2004] R. S. Berns, "Rejuvenating Seurat's Palette Using Color and Imaging Science: A Simulation," in R. L. Herbert, *Seurat and the Making of La Grande Jatte*, Art Institute of Chicago and University of California Press, 214-227, 2004.

[Berns 2005a] R. S. Berns, L. A. Taplin, M. Nezamabadi, Y. Zaho, and Y. Okumura, High accuracy digital imaging of cultural heritage without visual editing, in Proc. IS&T Archiving Conference, IS&T Springfield, 91-95 (2005).

[Berns 2005b] R.S. Berns, Color accurate image archives using spectral imaging, Proc. (Sackler NAS Colloquium) Scientific Examination of Art: Modern Techniques in Conservation and Analysis, National Academies Press, 105-119 (2005).

[Blakemore 1968] C. Blakemore and F. W. Campbell, On the existence of neurons in the human visual system selectively sensitive to the orientation and size of retinal images, *J. Physiol. London*, 203, 237-260 (1968).

[Boynton 1979] R. M. Boynton, *Human Color Vision*, Optical Society of America, Washington D.C. (1979).

[Brainard 1986] D. H. Brainard and B. A. Wandell, Analysis of the Retinex theory of color vision, *J. Opt. Soc. Am., A* 3, 1651-1661 (1986).

[Braun 1999] G. J. Braun, and M. D. Fairchild, Image lightness rescaling using sigmoidal contrast enhancement functions, *J. Electronic Imaging*, 8, 380-393 (1999).

[Brog 1997] Brog and P. Groenen, *Modern Multidimensional Scaling*, Springer-Verlag, New York (1997).

[Cabral 1987] Cabral, B., Max, N., Springmeyer, R., Bidirectional Reflection Functions from Surface Bump Maps, *Computer Graphics (SIGGRAPH 87 Proceedings)*, 273-281 (1987).

[Campbell 1968] F. W. Campbell and J.G Robson, Application of Fourier analysis to the visibility of gratings, *J. Physiol. London*, 203, 237-260 (1968).

[CCIR 709] CCIR Recommendation 709, “Basic parameter values for the HDTV standard for the studio and for international programme exchange,” now, ITU-R BT. 709.

[Chiu1993] K. Chiu, M. Herf, P. Shirley, S. Swamy, C. Wang, and K. Zimmerman. Spatially non-uniform scaling functions for high contrast images. In *Graphics Interface '93*, pages 245–253, Toronto, Ontario, Canada, May 1993. Canadian Information Processing Society.

[CIE8-TC01] Please see: <http://www.colour.org/tc8-01/>

[CIE8-TC03] Please see: <http://www.colour.org/tc8-03/>

[Cohen 2001] J. Cohen, C. Tchou, T. Hawkins, and P. Debevec. Real-Time high dynamic range texture mapping. In 12th Eurographics Workshop on Rendering, pages 313–320. Eurographics, June 2002.

[Daly 1993] S. Daly, The Visible Difference Predictor: An Algorithm for the Assessment of Image Fidelity, in Digital Images and Human Vision, A. Watson, Ed., MIT, Cambridge, 179-206 (1993).

[Day 2004] E. A. Day, L. A. Taplin, and R. S. Berns, Colorimetric characterization of a computer-controlled liquid crystal display, *Color Res. Appl.* 29, 365-373 (2004).

[Debevec 1997] Debevec, P.E. and Malik, J. (1997) Recovering high dynamic range radiance maps from images. *Proceedings SIGGRAPH 97*, 369-378 (1997).

[Devlin 2002] K. Devlin, A review of tone reproduction techniques, Dep. of Computer Science University of Bristol, Nov. 2002.
[\(http://www.cs.bris.ac.uk/Publications/pub_info.jsp\).](http://www.cs.bris.ac.uk/Publications/pub_info.jsp)

[Durand 2000] F. Durand and J. Dorsey. Interactive tone mapping. In *Rendering Techniques 2000: 11th Eurographics Workshop on Rendering*, pages 219–230. Eurographics, June 2000. ISBN 3-211-83535-0.

[Durand 2002] F. Durand and J. Dorsey. Fast bilateral filtering for the display of high dynamic range image. In John Hughes, editor, SIGGRAPH 2002 Conference Graphics Proceedings, Annual Conference Series, pages 257–265. ACM Press/ACM SIGGRAPH, 2002.11.

[Ebner 1998] F. Ebner, M. D. Fairchild, Development and testing of a color space (IPT) with improved hue uniformity, The Sixth Color Imaging Conference: Color Science, Systems, and Applications, pp 8-13 (1998).

[Engeldrum 2000] P. Engeldrum, Psychometric Scaling: a Toolkit for Imaging Systems Development, Imcotek Press, Winchester, (2000).

[Evans 1948] R. M. Evans, An Introduction to Color, John Wiley & Sons, New York, N.Y. (1948).

[Fairchild 1993] M. D. Fairchild and R. S. Berns, Image color-appearance specification through extension of CIELAB, Col. Res. & Appl., 18, No. 3, 178-189 (1993).

[Fairchild 1996] M.D. Fairchild, Refinement of the RLAB Color Space, Col. Res. & Appl., 21, No. 5, 338-346, (1996).

[Fairchild 1998] M. D. Fairchild, D. R. Wyble, Colorimetric characterization of the Apple Studio Display (Flat Panel LCD). Munsell Color Science Laboratory Technical Report (1998), <http://www.cis.rit.edu/mcls/research/PDFs/LCD.pdf>

[Fairchild 2002] M.D. Fairchild and G.M. Johnson, Meet iCAM: A next-generation color appearance model, IS&T/SID 10th Color Imaging Conference, Scottsdale, 33-38 (2002).

[Fairchild 2003] M.D. Fairchild and G.M. Johnson, Image appearance modeling, SPIE/IS&T Electronic Imaging, Santa Clara, 149-160 (2003).

[Fairchild 2005] Fairchild MD. Color Appearance Models. 2nd edition, New York: Addison-Wesley, (2005).

[Fattal 2002] R. Fattal, D. Lischinski, and M. Werman. Gradient domain high dynamic range compression. In Proceedings of ACM SIGGRAPH 2002, Computer Graphics Proceedings, Annual Conference Series. ACM Press / ACM SIGGRAPH, July 2002.

[Fechner 1966] G. Fechner, Elements of Psychophysics (trans. by H. E. Adler), Holt, Rinehart and Winston, New York (1966).

[Ferwerda 1996] J. A. Ferwerda, S. Pattanaik, P. S. Shirley, and D. P. Greenberg. A model of visual adaptation for realistic image synthesis. In Proceedings of SIGGRAPH 96, Computer Graphics Proceedings, Annual Conference Series, pages 249–258, New

Orleans, Louisiana, August 1996. ACM SIGGRAPH / AddisonWesley. ISBN 0-201-94800-1.

[Field 1987] D. J. Field, Relations Between the Statistics of Natural Images and the Response Profiles of Cortical Cells, *J. Opt. Soc. Am., A* 4 2379-2394 (1987).

[Funt 2000] B. Funt, F. Ciurea, and J. J. McCann, Retinex in Matlab, Proc. of IS&T/SID 8th Color Imaging Conference, 112-121 (2000).

[Gegenfurtner 1999] K. R. Gegenfurtner and L. T. Sharpe, *Color Vision: From Genes to Perception*, Cambridge University Press, Cambridge (1999).

[Georgeson 1975] M. A. Georgeson and G. D. Sullivan, Contrast constancy: deblurring in human vision by spatial frequency channels, *J. Physiol.* 252, 627–656 (1975).

[Georgeson 1990] M. A. Georgeson, Over the limit: Encoding contrast above threshold in human vision, in *Limits of Vision*, J. J. Kulikowski, ed., Erlbaum London, pg. 106–119 (1990).

[Gibson 2000] J. Gibson and M. D. Fairchild, Colorimetric characterization of three computer displays (LCD and CRT). Munsell Color Science Laboratory Technical Report (2000), <http://www.cis.rit.edu/mcls/research/PDFs/GibsonFairchild.pdf>

[Granger 1993] E. M. Granger, Uniform color space as a function of spatial frequency, SPIE/IS&T Electronic Imaging Conference, SPIE Vol. 1913, San Jose, 449-457 (1993).

[Grum 1980] F. Grum and C. J. Bartleson, Optical Radiation Measurements, Academic Press, NY (1980).

[Hannah 1990] J. Hannah, An artist's experiments with color perception, SPIE Vol. 1250, 212-219 (1990).

[He 1991] X. He, K. Torrance, F. Sillion, D. Greenberg, A Comprehensive Physical Model for Light Reflection, Computer Graphics (SIGGRAPH 91 Proceedings), 175-186 (1991).

[Horst 1969] G. J. C. Van der Horst and M. A. Bouman, Spatiotemporal chromaticity discrimination, J. Opt. Soc. Am., 59(11), 1482-1488 (1969).

[Hunt 1952] R. W. G. Hunt, Light and dark adaptation and the perception of color, J. Opt. Soc. Am., 42, 190-199 (1952).

[Hunt 1995] R. W. G. Hunt. The Reproduction of Colour in Photography, Printing and Television, Fountain Press, England, 5th edition, (1995).

[Hunt 1989] R. W. G. Hunt, Hue shifts in unrelated and related colors, *Col. Res. & Appl.*, 14, No. 235-239, (1989).

[Hurvich 1981] L. M. Hurvich, *Color Vision*, Sinauer Associates, Sunderland, Mass. (1981).

[Jobson 1997] D. J. Jobson, Z. Rahman, and G. A. Woodell. A multiscale retinex for bridging the gap between color images and the human observation of scenes. *IEEE Transactions on Image Processing*, 6(7):965–976, July 1997.

[Johnson 2001] Garrett M. Johnson and Mark D. Fairchild, Darwinism of Color Image Difference Models, *Proc. of the IS&T/SID 9th CIC*, 108-112 (2001).

[Johnson 2002] Garrett M. Johnson and Mark D. Fairchild, On contrast sensitivity in an image difference model, *Proc. of the IS&T PICS Conf.*, Portland, OR, PP. 18-23 (2002).

[Johnson 2003] Garrett M. Johnson and Mark D. Fairchild. Measuring images: differences, quality, and appearance, *Human Vision and Electronic Imaging VIII*, *Proc. of SPIE*, 5007, PP. 51-60 (2003).

[Judd 1975] D. B. Judd, G. Wyszecki, *Color in Business, Science and Industry*, John Wiley & Sons, Inc., NY (1975).

[Katoh 2001a] N. Katoh, T. Deguchi, and R. S. Berns, An accurate characterization of CRT monitor (I) verifications of past studies and clarifications of gamma. *Opt Rev.*, 8, 305–314 (2001).

[Katoh 2001b] N. Katoh, T. Deguchi, and R. S. Berns, An accurate characterization of CRT monitor (II) proposal for an extension to CIE method and its verification. *Opt Rev.*, 8, 397– 408 (2001).

[Kelly 1994] D. H. Kelly, *Visual Science and Engineering Models and Applications*, Marcel Dekker Inc., New York, NY, chapter 7 (1994)

[Kruithof 1941] A. A. Kruithof, Tubular luminescence lamps for general illumination, *Philips Tech. Rev.*, 6, 65-73 (1941).

[Kruskal 1978] J. B. Kruskal and M. Wish, *Multidimensional Scaling*, Sage Publications, Thousand Oaks, Calif. (1978).

[Lafortune 1997] E. Lafourture, S-C. Foo, K. Torrance, D. Greenberg, Non-Linear Approximation of Reflectance Functions, *Computer Graphics (SIGGRAPH 97 Proceedings)*, 117-126(1997).

[Land 1986] E. H. Land, Recent advances in Retinex theory, *Vision Res.* , 26, 7-21 (1986).

[Land 1964] E. H. Land, The Retinex, American Scientist, 52, 247-264 (1964).

[Land 1971] E. H. Land and J. J. McCann, Lightness and the Retinex theory, J. Opt. Soc. Am., 61, 1-11 (1971).

[Larson 1998] G. W. Larson. Logluv encoding for full-gamut, high-dynamic range images. Journal of Graphics Tools, 3(1):15–31,1998. ISSN 1086-7651.

[Lennie 1988] P. Lennie and M. D'Zmura, Mechanisms of color vision, CRC Critical Reviews in Neurobiolog 3, 333-400 (1988).

[Livingstone 2002] M. Livingstone, Vision and Art: The Biology of Seeing, Harry N. Abrams, Inc., NY (2002).

[Li 2002] C. Li, M.R. Luo, R. W. G. Hunt , N. Moroney, M. D. Fairchild and T. Newma, , The Performance of CIECAM02, IS&T Tenth Color Imaging Conference, 28-32 (2002).

[Losada 1994] Losada, M.A. and K.T. Mullen, The spatial tuning of chromatic mechanisms identified by simultaneous masking. Vision Res., 34(3), 331-341 (1994).

[Lubin 1995] J. Lubin, A Visual Discrimination Model for Imaging System Design and Evaluation, in Vision Models for Target Detection and Recognition, E. Peli, Ed., World Scientific, Singapore, 245-283 (1995).

[MacDonald 1993] L.W. MacDonald, Gamut mapping in perceptual colour space, Proc. of IS&T/SID 1th Color Imaging Conference, Springfield, VA, 193-196 (1993).

[Maffei 1973] L. Maffei and A. Fiorentini, The visual cortex as a spatial frequency analyzer, *Vision Res.*, (13), 1255-1267 (1973).

[McCann 1976] J. J. McCann, S. McKee, and T. Taylor, Quantitative studies in Retiex theories: A comparison between theoretical predictions and observer responses to ‘Color Mondrian’ experiments, *Vision Res.*, 16, 445-458 (1976).

[McCann 1990] J. J. McCann, Psychophysical measurements of Hannah color/distance effects, SPIE Vol. 1250, 203-211 (1990).

[MCSL 2005], Please see: www.art-si.org.

[Miller 1984] N.J. Miller, P.Y. Ngai, and D.D. Miller. The application of computer graphics in lighting design. *Journal of the IES*, 14:6–26, 1984.

[Montag 2004] E. D. Montag, Louis Leon Thurstone in Monte Carlo: creating error bars for the method of paired comparison, IS&T/SPIE Symposium on Electronic Imaging: Science and Technology, SPIE Vol. 5294, 222-230 (2004).

[Moroney 2002] N. Moroney, M. D. Fairchild, R.W.G. Hunt, C.J. Li, M.R. Luo, and T. Newman, The CIECAM02 Color Apperance Model, IS&T/SID 10th Color Imaging Conference, Scottsdale, 23-27 (2002).

[Morovic 2000] J. Morovic and M. R. Luo, The fundamentals of gamut mapping: A survey, available at www.colour.org/tc8-03.

[Movshon 1998] T. Movshon and L. Kiorpes, Analysis of the development of spatial sensitivity in monkey and human infants, *J. Opt. Soc. Am. A*, 5, (1998).

[Nes 1967] F. L. van Nes and M.A. Bouman, Spatial modulation transfer in the human eye, *J. Opt. Soc. Am.*, 57, 401-406 (1967).

[Nezamabadi 2005] M. Nezamabadi and R. S. Berns, The Effect of image size on the color appearance of image reproductions, IS&T/SID 13th Color Imaging Conference, Scottsdale, AZ, Nov. 2005, pp. 79-84.

[Nezambadi 2006A] M. Nezambadi, R. S. Berns, and E. D. Montag, An Investigation of the Effect of Image Size on the Color Appearance of Softcopy Reproductions, *Proc. of*

the IS&T International Congress of Imaging Science, Rochester, NY, May 2006, pp. 126-129.

[Nezambadi 2006B] M. Nezamabadi and R. S. Berns, The effect of image size on the color appearance of image reproductions using colorimetrically calibrated LCD and DLP displays, Journal of the Society for Information Display, Volume 14, Issue 9, pp. 773-783 (2006).

[Nezambadi 2007] M. Nezamabadi, R. S. Berns, and E. D. Montag, An Investigation of the Effect of Image Size on the Color Appearance of Softcopy Reproductions Using a Contrast Matching Technique, SPIE/IS&T Electronic Imaging, San Jose, CA, Vol. 6493, pp. 6493091- 6493099 (2007).

[Oppenheim 1968] A. Oppenheim, R. Schafer, and T. Stockham. Nonlinear filtering of multiplied and convolved signals. In Proceedings of the IEEE, volume 56, pages 1264–1291, August 1968.

[Padfield 2005] J. Padfield, D. Saunders, T. Malzbender, Polynomial texture mapping: a new tool for examining the surface of paintings, 14th Triennial meeting the Hague preprints, Vol 1, 504-510 (2005).

[Palmar 1999] S. E. Palmar, Vision Science: Photons to Phenomenology, MIT Press, Cambridge (1999).

[Pattanaik 1998a] S. N. Pattanaik, M. D. Fairchild, J. A. Ferwerda, D. P. Greenberg, Multiscale model of adaptation, spatial vision and color appearance, The Sixth Color Imaging Conference: Color Science, Systems, and Applications, 2-7 (1998).

[Pattanaik 1998b] S. N. Pattanaik, J. A. Ferwerda, M.D. Fairchild, and D.P. Greenberg, A multiscale model of adaptation and spatial vision for realistic imaging. Proceedings SIGGRAPH 98, Orlando, 287-298 (1998).

[Pattanaik 2000] S. N. Pattanaik, J. E. Tumblin, Hector Yee, and Donald P. Greenberg. Time-dependent visual adaptation for realistic image display. In Proceedings of ACM SIGGRAPH 2000, Computer Graphics Proceedings, Annual Conference Series, pages 47–54. ACM Press / ACM SIGGRAPH / Addison Wesley Longman, July 2000. ISBN 1-58113-208-5.

[Peli 1990] E. Peli, Contrast in complex images, J. Opt. Soc. Am., Vol. 7, No.10, 2032-2040 (1990).

[Phong 1975] B-T. Phong, Illumination for Computer Generated Images, Communications of the ACM 18, 6, 311-317 (1975).

[Purdy 1931] D. M. Purdy, Spectral hues as a function of intensity, Am. J. Psych. 43, 541-559 (1931).

[Reinhard 2002] E. Reinhard, M. Stark, P. Shirley, and J. Ferwerda. Photographic tone reproduction for digital images. In Proceedings of ACM SIGGRAPH 2002, Computer Graphics Proceedings, Annual Conference Series. ACM Press / ACM SIGGRAPH, July 2002.

[Rosen 2000] M. R. Rosen, M. D. Fairchild, G. M. Johnson, D. R. Wyble, Color management within a spectral image visualization tool, IS&T/SID Eighth Color Imaging Conference, p 187-192 (2000).

[Rosen 2003] M. R. Rosen and N. Ohta, Spectral color processing using an interim connection space, IS&T/SID Eleventh Color Imaging Conference, 187-192 (2003).

[Scheel 2000] A. Scheel, M. Stamminger, and Hans-Peter Seidel. Tone reproduction for interactive walkthroughs. Computer Graphics Forum, 19(3):301–312, August 2000. ISSN 1067-7055.

[Schlick 1994] C. Schlick. High dynamic range pixels. In Graphics Gems IV, pages 422–429. Academic Press, Boston, 1994. ISBN 0-12-336155-9.

[Scuello 2004a] M. Scuello, I. Abramov, J. Gordon, S. Weintraub, Museum lighting: Optimizing the illuminant, Col. Res.& Appl., 29, No. 2, 121-127 (2004).

[Scuello 2004b] M. Scuello, I. Abramov, J. Gordon, S. Weintraub, Museum lighting: Why are some illuminants preferred?, *J. Opt. Soc. Am.*, 21, 306-311 (2004).

[Semerelroth 1970] C. C. Semerelroth, Prediction of lightness and brightness on different backgrounds, *J. Opt. Soc. Am.*, 60, 1685-1689 (1970).

[Sillion 1991] F. Sillion, J. Arvo, S. Westin, D. Greenberg, A Global Illumination Solution for General Reflectance Distributions, *Computer Graphics (SIGGRAPH 91 Proceedings)*, 187-196 (1991).

[Spencer 1995] Spencer, G., Shirley, P., Zimmerman, K., Greenberg, D. P. (1995), Physically-based glare effects for computer generated images. *Proceedings SIGGRAPH 95*, 325-334 (1995).

[Stam 1999] J. Stam, Diffraction Shaders, *Computer Graphics (SIGGRAPH 99 Proceedings)*, 101-110 (1999).

[Stevens 1963] J. C. Stevens and S. S. Stevens, Brightness functions: Effects of adaptation, *J. Opt. Soc. Am.*, 53, 375-385 (1963).

[Stevens 1966] S. S. Stevens, To honor Fechner and repeal his law, *Science* 133, pp 80-86 (1966).

[Stockham 1972] T. Stockham. Image processing in the context of a visual model. In Proceedings of the IEEE, volume 60, pages 828–842, 1972.

[Thomson 1978] G. Thomson, The Museum Environment, Butterworths, London, 1978.

[Thurston 1927] L. L. Thurstone, A law of comparative judgment, Psych. Review 34, 273-286 (1927).

[Tumblin 1993] J. Tumblin and H. E. Rushmeier. Tone reproduction for realistic images. IEEE Computer Graphics & Applications, 13(6):42–48, November 1993.

[Tumblin 1999a] J. Tumblin and G. Turk. Lcis: A boundary hierarchy for detail-preserving contrast reduction. In Proceedings of SIGGRAPH 99, Computer Graphics Proceedings, Annual Conference Series, pages 83–90, Los Angeles, California, August 1999. ACM SIGGRAPH / Addison Wesley Longman. ISBN 0-20148-560-5.

[Tumblin 1999b] J. Tumblin, J. K. Hodgins, and B. K. Guenter. Two methods for display of high contrast images. ACM Transactions on Graphics, 18(1):56–94, January 1999. ISSN 0730-0301.

[Upstill 1985] S. D. Upstill. The Realistic Presentation of Synthetic Images, PhD thesis, Computer Science Division, University of California, Berkeley, 1985.

[Wandell 1995] B. A. Wandell, Foundations of Vision, Sinauer Associates, Inc. Publisher, Sunderland, Massachusetts, (1995).

[Ward 1994] Greg Ward. A contrast-based scalefactor for luminance display, In Graphics Gems IV, pages 415–421. Academic Press, Boston, 1994. ISBN 0-12-336155-9.

[Watson 1987] A. B. Watson, The Cortex Transform: Rapid Computation of Simulated Neuro Images, Computer Vision Graphics, Image Processing, 39, 311-327 (1987).

[Watson 1997] A.B. Watson and J.A. Solomon, Model of visual contrast gain control and pattern masking. J. Opt. Soc. Am. A, 14(9), 2379-2391 (1997).

[Weintraub 2000] S. Weintraub, The color of white: Is there a preferred color temperature for the exhibition of works of art?, WACC Newsletter, Vol. 21, No.3 (Sep. 2000).

[Westheimer 1986] G. Westheimer, The Eye as an Optical Instrument. In K. Boff, L. Kaufman, and J. Thomas (Ed.), Handbook of Perception and Human Performance, New York: Wiley and Sons, (1986).

[Wilson 1991] H. R. Wilson, Psychophysical models of spatial vision and hyperacuity in D. Regan (Ed.) Spatial Vision, Vol. 10, Vision and Visual Dysfunction. Boca Raton, FL, CRC Press, 64-81 (1991).

[Wong 1997] T. Wong, P. Heng, S. Or, W. Ng, Image-based Rendering with Controllable Illumination, *Rendering Techniques 97: Proceedings of the 8th Eurographics Workshop on Rendering*, June 16-18, ISBN 3-211-83001-4, 13-22 (1997).

[Wyble 2000] D. R. Wyble, R. S. Berns, A critical review of spectral models applied to binary color printing, *Color Res. Appl.* 25, 4-19 (2000).

[Wyble 2003] D. R. Wyble, H. Zhang, Colorimetric characterization model for DLP projectors, *IS&T/SID Eleventh Color Imaging Conference*: 346 (2003).

[Wyble 2004] D. R. Wyble, M. R. Rosen, Color management of four-primary DLP projectors, *IS&T/SID Twelfth Color Imaging Conference*: 228 (2004).

[Wyszecki 1982] G. Wyszecki and W. S. Stiles, *Color Science: Concepts and Methods, Quantitative Data and Formulae*, 2nd edition, John Wiley & Sons, New York, 1982.

[Xiao 2003] K. Xiao, M. R. Luo, C. J. Li, P. A. Rhodes, C. Taylor, Specifying the color appearance of a real room, *IS&T/SID Eleventh Color Imaging Conference*: 308 (2003).

[Xiao 2004] K. Xiao, C. J. Li, M. R. Luo, C. Taylor, Color appearance for dissimilar sizes, *CGIV2004, Second European Conference on Color in Graphics, Imaging and Vision*, 12-16 (2004).

[Xiaoyan 2004] Xiaoyan Song, Garrett M. Johnson, and Mark D. Fairchild, Minimizing the Perception of Chromatic Noise in Digital Images. IS&T/SID 12th Color Imaging Conference, Scottsdale, AZ, Nov., 340-346 (2004).

[Zhang 1996] X. Zhang and B. A. Wandell, A spatial extension of CIELAB for digital color image reproduction, SID 96 Digest, (1996).